Advances in Science, Technology & Innovation
IEREK Interdisciplinary Series for Sustainable Development

Zhihua Zhang · Nabil Khélifi · Abdelkader Mezghani
Essam Heggy *Editors*

Patterns and Mechanisms of Climate, Paleoclimate and Paleoenvironmental Changes from Low-Latitude Regions

Proceedings of the 1st Springer Conference of the Arabian Journal of Geosciences (CAJG-1), Tunisia 2018

IEREK RESEARCH & KNOWLEDGE ENRICHMENT

Springer

Advances in Science, Technology & Innovation

IEREK Interdisciplinary Series for Sustainable Development

Advances in Science, Technology & Innovation (ASTI) is a series of peer-reviewed books based on the best studies on emerging research that redefines existing disciplinary boundaries in science, technology and innovation (STI) in order to develop integrated concepts for sustainable development. The series is mainly based on the best research papers from various IEREK and other international conferences, and is intended to promote the creation and development of viable solutions for a sustainable future and a positive societal transformation with the help of integrated and innovative science-based approaches. Offering interdisciplinary coverage, the series presents innovative approaches and highlights how they can best support both the economic and sustainable development for the welfare of all societies. In particular, the series includes conceptual and empirical contributions from different interrelated fields of science, technology and innovation that focus on providing practical solutions to ensure food, water and energy security. It also presents new case studies offering concrete examples of how to resolve sustainable urbanization and environmental issues. The series is addressed to professionals in research and teaching, consultancies and industry, and government and international organizations. Published in collaboration with IEREK, the ASTI series will acquaint readers with essential new studies in STI for sustainable development.

More information about this series at http://www.springer.com/series/15883

Zhihua Zhang • Nabil Khélifi
Abdelkader Mezghani
Essam Heggy
Editors

Patterns and Mechanisms of Climate, Paleoclimate and Paleoenvironmental Changes from Low-Latitude Regions

Proceedings of the 1st Springer Conference of the Arabian Journal of Geosciences (CAJG-1), Tunisia 2018

Springer

Editors
Zhihua Zhang
Climate Modelling Laboratory,
Department of Applied Mathematics
Shandong University
Jinan, China

Nabil Khélifi
Springer Nature
Heidelberg, Baden-Württemberg
Germany

Abdelkader Mezghani
Norwegian Meteorological Institute
Oslo, Norway

Essam Heggy
University of Southern California
Los Angeles, CA, USA

and

Jet Propulsion Lab, Caltech
Pasadena, CA, USA

ISSN 2522-8714 ISSN 2522-8722 (electronic)
Advances in Science, Technology & Innovation
IEREK Interdisciplinary Series for Sustainable Development
ISBN 978-3-030-01598-5 ISBN 978-3-030-01599-2 (eBook)
https://doi.org/10.1007/978-3-030-01599-2

Library of Congress Control Number: 2018958498

This Springer imprint is published by the registered company Springer Nature Switzerland AG
The registered company address is: Gewerbestrasse 11, 6330 Cham, Switzerland

Preface

The Mediterranean and Middle East region is located at a crossroad of global climate patterns. There is a convergence between various maritime conditions and different continental air masses from the adjacent extensive lands which leads to diverse climates over this region in view of the extreme differences in topographical features and atmospheric conditions. In spatial scale, various climate and environmental parameters vary considerably across the Mediterranean and Middle East and even within countries. In temporal scale, there are significant climate and environmental changes occurring over the past thousands of years. Generally, the Mediterranean and Middle East are characterized by hot and arid climate, already intolerable for human beings in many parts. Furthermore, global warming is causing serious water scarcity, heat waves, and other natural disasters across this region today and in the near future. In order to make suitable mitigation and adaptation measures, it is critically important to study how climate and environment in the Mediterranean and Middle East have changed across a wide range of timescales so that we can better assess the impacts of future climate and environmental changes across this region. Unfortunately, at present, the Mediterranean and Middle East have not been deeply investigated and assessed yet, compared with other regions of the world such as Europe and North America.

This proceedings volume is based on the best papers accepted for presentation during the 1st Springer Conference of the Arabian Journal of Geosciences (CAJG-1), Tunisia 2018. The book offers new climate and environmental studies by experienced researchers mainly from research institutes in the Mediterranean and Middle East region. Main topics include: paleoclimate, paleoceanographic, and paleoenvironmental evolutions, spatiotemporal patterns of climate change, sea level variabilities, and climate change impacts and migration schemes. This volume gives new insights into patterns, mechanisms, and impacts of past and future climate/environmental changes in the Mediterranean and Middle East region. Latest observation and proxy datasets included in this book fill some important gaps in the existing climate, paleoclimate, and paleoenvironmental records across the region. In particular, some various case studies are included to show how to use some state-of-the-art tools and algorithms to analyze local climate and environmental evolutions.

Jinan, China — Zhihua Zhang
Heidelberg, Germany — Nabil Khélifi
Oslo, Norway — Abdelkader Mezghani
Los Angeles/Pasadena, USA — Essam Heggy
July 2018

Acknowledgements

Our appreciation is extended to the authors of the papers for their hard and diligent work in producing high-quality contributions. We would like to thank the reviewers of the papers for their in-depth reviews and great efforts in improving the quality of the papers. Also, thanks are extended to Amjad Kallel who supervised and handled the evaluation process, to Sahbi Moalla who handled the submission and evaluation system for the ten conference proceedings volumes, and to the publishing staff of Springer headed by Nabil Khélifi, Senior Editor for their efforts and contributions in completing this conference proceedings volume. All the above-mentioned efforts were very important in making this book a success.

About the 1st Springer Conference of the Arabian Journal of Geosciences (CAJG-1), Tunisia 2018

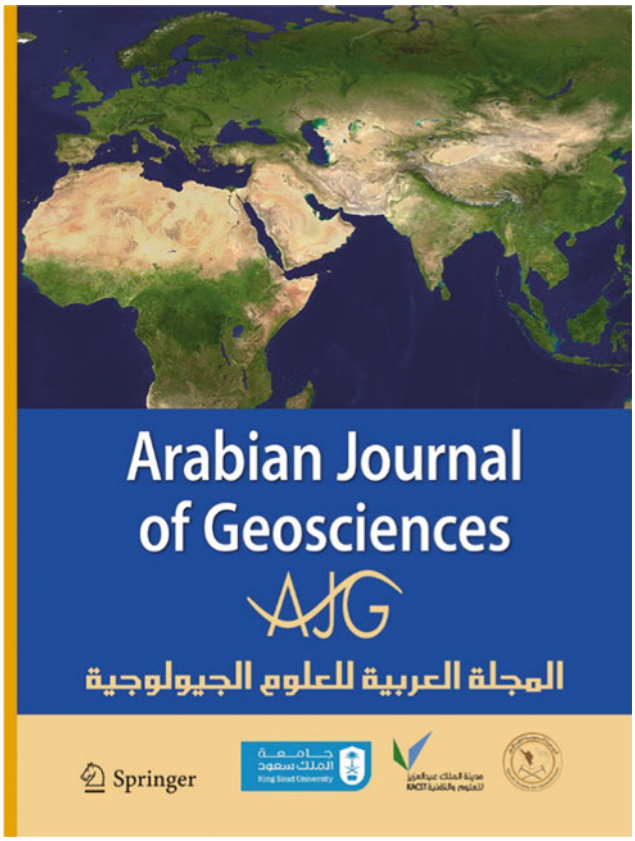

The *Arabian Journal of Geosciences (AJG)* is a Springer journal publishing original articles on the entire range of Earth sciences in partnership with the Saudi Society for Geosciences. The journal focuses on, but not limited to, research themes which have regional significance to the Middle East, the Euro-Mediterranean, Africa, and Asia. The journal receives on average 2000 submissions a year and accepts around 500 papers for publication in its 24 annual issues (acceptance rate 25%). It enjoys the participation of an editorial team of 100 international associate editors who generously help in evaluating and selecting the best papers.

In 2008, Prof. Abdullah Al-Amri, in close partnership with Springer, founded the Arabian Journal of Geosciences (AJGS). In this year, the journal celebrates its tenth anniversary. On this occasion and to mark this event, the Founder and Editor-in-Chief of the AJGS Prof. Al-Amri organized in close collaboration with Springer the 1st Conference of the Arabian Journal of Geosciences (CAJG-1) in Hammamet, Tunisia, from November 12th to 15th, 2018 (www.cajg.org).

The conference was an occasion to endorse the journal's long-held reputation for bringing together leading authors from the Middle East, the Euro-Mediterranean, Africa, and Asia who work in the wide-ranging fields of Earth sciences. The conference covered all cross-cutting themes of Geosciences and focused principally on the following ten tracks:

- Track 1. Climate, paleoclimate in the conference web page, without, and paleoenvironmental changes
- Track 2. Geoinformatics, remote sensing, geodesy
- Track 3. Geoenvironmental engineering, geomechanics and geotechnics, geohazards
- Track 4. Geography, geoecology, geoarcheology, geotourism
- Track 5. Geophysics, seismology
- Track 6. Hydrology, hydrogeology, hydrochemistry
- Track 7. Mineralogy, geochemistry, petrology in the conference web page, without, and volcanology
- Track 8. Petroleum engineering and petroleum geochemistry
- Track 9. Sedimentology, stratigraphy, paleontology, geomorphology, pedology
- Track 10. Structural/petroleum/mining geology, geodynamics, marine geology

The dynamic four-day conference provided more than 450 attendees with opportunities to share their latest unpublished findings and learn the newest geoscience studies. The event also allowed attendees to meet and discuss with the journal's editors and reviewers.

More than 950 short contributing papers to the conference were submitted by authors from more than 70 countries. After a pre-conference peer review process by more than 500 reviewers, 700 papers were accepted. These papers were published as chapters in the conference proceedings by Springer.

The conference proceedings consist of ten edited volumes, each edited by the following group of *Arabian Journal of Geosciences* (AJGS) editors and other guest editors:

Volume 1. Patterns and Mechanisms of Climate, Paleoclimate and Paleoenvironmental Changes from Low-Latitude Regions

Zhihua Zhang (AJGS Editor): Shandong University, Jinan, China
Nabil Khélifi (AJGS Editor): MENA Program, Springer, Heidelberg, Germany
Abdelkader Mezghani (Guest Editor): Norwegian Meteorological Institute, Norway
Essam Heggy (Guest Editor): University of Southern California and Jet Propulsion Laboratory, Caltech, USA

Volume 2. Advances in Remote Sensing and Geo Informatics Applications

Hesham M. El-Askary (Guest Editor): Schmid College of Science and Technology at Chapman University, USA
Saro Lee (AJGS Editor): Korea Institute of Geoscience and Mineral Resources, Daejeon, South Korea
Essam Heggy (Guest Editor): University of Southern California and Jet Propulsion Laboratory, Caltech, USA
Biswajeet Pradhan (AJGS Editor): University of Technology Sydney, Sydney, Australia

Volume 3. Recent Advances in Geo-Environmental Engineering, Geomechanics and Geotechnics, and Geohazards

Amjad Kallel (AJGS Editor): ENIS, University of Sfax, Tunisia
Zeynal Abiddin Erguler (AJGS Editor): Dumlupinar University, Kutahya, Turkey
Zhen-Dong Cui (AJGS Editor): China University of Mining and Technology, Xuzhou, Jiangsu, China
Ali Karrech (AJGS Editor): The University of Western Australia, Australia
Murat Karakus (AJGS Editor): University of Adelaide, Australia

Pinnaduwa Kulatilake (AJGS Editor): Department of Materials Science and Engineering, The University of Arizona, USA
Sanjay Kumar Shukla (AJGS Editor): School of Engineering, Edith Cowan University, Perth, Australia

Volume 4. Exploring the Nexus of Geoecology, Geography, Geoarcheology and Geotourism: Advances and Applications for Sustainable Development in Environmental Sciences and Agroforestry Research

Haroun Chenchouni (AJGS Editor): University of Tebessa, Algeria
Ezzoura Errami (Guest Editor): Chouaïb Doukkali University, El Jadida, Morocco
Fernando Rocha (Guest Editor): University of Aveiro, Portugal
Luisa Sabato (AJGS Editor): Università degli Studi di Bari "Aldo Moro", Bari, Italy

Volume 5. On Significant Applications of Geophysical Methods

Narasimman Sundararajan (AJGS Editor): Sultan Qaboos University, Muscat, Oman
Mehdi Eshagh (AJGS Editor): University West, Trollhättan, Sweden
Hakim Saibi (AJGS Editor): United Arab Emirates University, Al-Ain, Abu Dhabi, UAE
Mustapha Meghraoui (AJGS Editor): Université de Strasbourg, Strasbourg, France
Mansour Al-Garni (AJGS Editor): King Abdulaziz University, Jeddah, Saudi Arabia
Bernard Giroux (AJGS Editor): Centre Eau Terre Environnement, Québec, Canada

Volume 6. Advances in Sustainable and Environmental Hydrology, Hydrogeology, Hydrochemistry and Water Resources

Helder I. Chaminé (AJGS Editor): School of Engineering–ISEP, Polytechnic of Porto, Portugal
Maurizio Barbieri (AJGS Editor): University of Rome La Sapienza, Italy
Ozgur Kisi (AJGS Editor): Ilila State University, Tbilisi, Georgia
Mingjie Chen (AJGS Editor): Sultan Qaboos University, Muscat, Oman
Broder J. Merkel (AJGS Editor): TU Bergakademie Freiberg, Freiberg, Germany

Volume 7. Petrogenesis and Exploration of the Earth's Interior

Domenico Doronzo (AJGS Editor): Consejo Superior de Investigaciones Cientificas, Spain
Emanuela Schingaro (AJGS Editor): Università degli Studi di Bari Aldo Moro–UniBa, Italy
John S. Armstrong-Altrin (AJGS Editor): The National Autonomous University of Mexico, Mexico
Basem Zoheir (Guest Editor): Benha University, Egypt and University of Kiel, Germany

Volume 8. Advances in Petroleum Engineering and Petroleum Geochemistry

Santanu Banerjee (AJGS Editor): Indian Institute of Technology Bombay, Mumbai, India
Reza Barati (AJGS Editor): The University of Kansas, Lawrence, KS, USA
Shirish Patil (Guest Editor): Saudi Aramco and King Fahd University of Petroleum and Minerals, Dhahran, Saudi Arabia

Volume 9. Paleobiodiversity and Tectono-Sedimentary Records in the Mediterranean Tethys and Related Eastern Areas

Mabrouk Boughdiri (AJGS Editor): University of Carthage, Amilcar, Tunisia
Beatriz Bádenas (AJGS Editor): University of Zaragoza, Zaragoza, Spain
Paul Selden (AJGS Editor): University of Kansas, Lawrence, Kansas, USA
Etienne Jaillard (Guest Editor): University Grenoble Alpes, France
Peter Bengtson (AJGS Editor): University Heidelberg, Heidelberg, Germany
Bruno R. C. Granier (AJGS Editor): University of Bretagne Occidentale, Brest, France

Volume 10. The Structural Geology Contribution to the Africa-Eurasia Geology: Basement and Reservoir Structure, Ore Mineralisation and Tectonic Modelling

Federico Rossetti (Guest Editor): Università Roma Tre, Roma, Italy
Ana Crespo Blanc (Guest Editor): University of Granada, Spain
Federica Riguzzi (Guest Editor): National Institute of Geophysics and Volcanology, Roma, Italy
Estelle Leroux (Guest Editor): IFREMER, Unité Géosciences Marines, Plouzané, France
Kosmas Pavlopoulos (Guest Editor): Sorbonne University Abu Dhabi, Abu Dhabi, UAE
Olivier Bellier (Guest Editor): CEREGE, Aix-en-Provence, France
Vasilios Kapsimalis (Guest Editor): Institute of Oceanography, Hellenic Centre for Marine Research, Anavyssos, Greece

About the Conference Steering Committee

General Chair

Abdullah Al-Amri: Founder and Editor-in-Chief of AJGS, King Saud University, Saudi Arabia

Conference Supervisor

Nabil Khélifi: Senior Publishing Editor, Springer Middle East and North African Program Springer, a part of Springer Nature, Heidelberg, Germany

Scientific Committee Chair

François Roure: Guest of Editorial Board of AJGS, IFP—Energies Nouvelles, France

Walter D. Mooney: Guest of Editorial Board of AJGS, US Geological Survey Western Region, USA

Local Organization Chair

Mabrouk Boughdiri, Associate Editor of AJGS, University of Carthage, Bizerte, Tunisia

Evaluation Chair

Amjad Kallel: Assistant Editor of AJGS, ENIS, University of Sfax, Tunisia

Publication Chair

Biswajeet Pradhan: Associate Editor of AJGS, University of Technology Sydney, Sydney, Australia

Essam Heggy: Guest of Editorial Board of AJGS, University of Southern California and Jet Propulsion Laboratory, Caltech, USA

Program Chair

Hakim Saibi: Associate Editor/Assistant Editor of AJGS, United Arab Emirates University, Al-Ain, Abu Dhabi, UAE

Domenico Doronzo: Associate Editor/Assistant Editor of AJGS, Consejo Superior de Investigaciones Cientificas, Spain

Communication Chair

Mohamed Ksibi: Guest of Editorial Board of AJGS, ISBS, University of Sfax, Tunisia

English Language Advisory Committee

Abdelmajid Dammak: ENIS, University of Sfax, Tunisia
Chokri Khalaf: FMS, University of Sfax, Tunisia
Dhouha Mabrouk: FLSHS, University of Sfax, Tunisia
Mohamed Elbahi: ENIS, University of Sfax, Tunisia
Sami Shami: ENIS, University of Sfax, Tunisia
Yasmine Basha: FLSHS, University of Sfax, Tunisia

Conference Manager

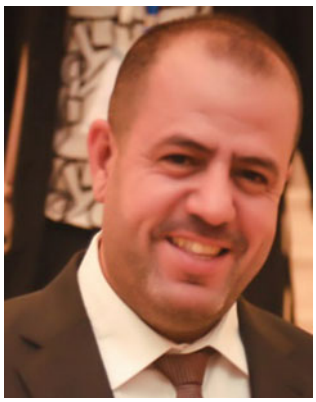

Mohamed Sahbi Moalla: Coordinator of AJGS, ISET, University of Sfax, Tunisia

Contents

About the Editors

Dr. Zhihua Zhang holds a Ph.D. (2007) from the University of California at Davis (USA). He is currently a Full Professor and Director of Climate Modelling Laboratory in the Department of Applied Mathematics at Shandong University, China. He has published more than 50 first-authored research articles and three first-authored monographes entitled *Multivariate Time Series Analysis in Climate and Environmental Research, Environmental Data Analysis: Methods and Applications, Mathematical and Physical Fundamentals of Climate Change*. He has served in the editorial board of several ISI-JCR journals including *International Journal of Global Warming*, *Journal of Cleaner Production*, *EURASIP Journal on Advances in Signal Processing*, and *Open Geosciences*. In 2013, he joined the AJGS as an Associate Editor responsible for evaluating submissions in the fields of Climate Change and Signal Processing.

Dr. Nabil Khélifi holds a B.Sc. in natural sciences and a M. Sc. in earth and environmental sciences from the University of Sfax in Tunisia (2004). He received fellowships from the global change System for Analysis, Research and Training (START) in 2005 and the German Academic Exchange Service (DAAD) from 2006 to 2010 to continue with his Ph.D. studies in marine geosciences at the University of Kiel in Germany. After his Ph.D. in 2010, he received a postdoctoral research grant from the German Science Foundation (DFG) to start his self-designed research projects at the GEOMAR—Ocean Research Centre in Kiel, Germany, on reconstructing past changes in oceanography and climate in the North Atlantic and the Mediterranean Sea using marine sediment samples retrieved by the International Ocean Drilling Program (IODP) and applying foraminiferal and geochemical proxy methods. He published his research work in some reputable journals. He also received funding from the European Science Foundation (ESF) and some European universities to co-organize two workshops on Pliocene climate in Bordeaux, France (2009) and Bristol, UK (2013). He also received the Swiss Government Excellence Scholarship (SGES) to continue with his research projects at ETH Zurich, Switzerland, in early 2014. However, he decided in March 2014 to pursue his career as a Publishing Editor with Springer, a part of Springer Nature in Heidelberg, Germany. He is mainly responsible for developing

the Springer's publishing program in the Middle East and North Africa (MENA). The program currently consists of developing 18 journals and publishing about 40 scientific books every year. In January 2017, he got promoted to Senior Publishing Editor with Springer. He also helps researchers in MENA countries publish their work by delivering educational seminars for authors, reviewers, and journal editors to help improve publication output and quality. He is also a Visiting Lecturer at the University of Carthage, Tunisia, and King Saud University, KSA, giving M.Sc. and Ph.D. courses in geocommunication/presentations and techniques of paper publishing, as well as career development training and professional development/soft skills workshops. Recently, he has been awarded with the 2016 Africa Green Future Leadership Award in recognition of work contributing to sustainable development through advancing science and promoting publications in Africa and Middle East.

Dr. Abdelkader Mezghani is a Research Scientist at the Climate and Model Analysis group, MET Norway. The main work at MET Norway has been on the development of new empirical-statistical climate downscaling methods and techniques that relates regional and global climate model results to local precipitation and temperature through generalized linear regression models. He acted as a MET Leader in CHASE-PL project (2014–2017). Currently, he is involved in the C3S DECM project by developing a prototype for COPENICUS services on how to evaluate Big Data from climate model simulations. He is also the co-developer of a the 'ESD' R package which contains a set of libraries to visualize and downscale climate variables and parameters using advanced methods such as empirical orthogonal function (EOF), principal component analysis (PCA), and canonical correlation analysis (CCA). His research expertise has addressed three different scales: synoptic, regional, and local scales with a particular interest on the interactions and associated uncertainties between them. Before joining MET Norway, he received his Ph.D. in environmental sciences from the Swiss Federal Institute of Technology (EPFL, 2009). Before joining MET Norway, he worked as a Postdoc at the French National Centre for Scientific Research (CNRS, 2009–2012) working on site at the Hydro-meteorology, Climate and Impact group at the University of Grenoble (LTHE, 2009). He had various international contributions in the CLIMAT project (Switzerland-Luxembourg, 2007), the European SWURVE project (Switzerland, 2005), RIWER2030 (France, 2009), OFEN (Switzerland, 2008), and CONSECRU (Switzerland, 2006). Key research areas include: Climate Change, Downscaling of Climate information, Statistical Analyses, R shiny web applications for climate models' evaluation.

Dr. Essam Heggy is a Research Scientist at the Microwave Systems, Sensors and Imaging Lab (MiXIL), the Viterbi School of Engineering at the University of Southern California and affiliate of the Rosetta Project at the NASA Jet Propulsion Laboratory. He obtained both his M.Sc. and Ph.D., respectively, in 1999 and 2002, with distinguished honors from the Paris VI University in France (UPMC-Sorbonne). His research focuses on understanding water evolution in Earth's arid environments as well as planetary surfaces using radar surface and subsurface characterization methods. His research particularly focuses on understanding volatile evolution in the North African Sahara and Arabian Peninsula, as well as Mars, the Moon, Jovian Icy satellites and Near-Earth Objects. His work involves probing structural, hydrological, and volcanic elements in terrestrial and planetary environments using different types of radar imaging and sounding techniques as well as measuring the electromagnetic properties of rocks in the radar frequency range. He is currently a member of the science team of the MARSIS instrument aboard the Mars Express orbiter (2003–present), the Mini-SAR experiment aboard Chandrayaan-1, the Mini-RF experiment on board the Lunar Reconnaissance Orbiter (2008–present), the CONSERT radar experiment aboard the Rosetta mission (2004–present), and the WISDOM GPR onboard ExoMars 2020 Rover (2008–present). He also edited a special JGR-Planets (AGU) volume on terrestrial and planetary radars. He is on the founding editorial board of the *Journal of Arctic Geoscience* ARKTOS (Springer), *Geosciences* (MDPI), *National Geographic* and co-chaired several sessions in international conferences and workshops on terrestrial and planetary radar subsurface imaging including AGU, LPSC, and IEEE meetings.

Part I
Keynote

Fifty Years of Paleoceanography: Major Achievements in Our Understanding of Past and Future Climate Change—Some Memories and Hearsay

Michael Sarnthein

Abstract

Paleoceanography quickly evolved into the first branch of historic geosciences that developed and employed strictly quantitative proxy data and a quantitative age scale to trace past ocean scenarios per analogy to the parameters used to study the modern ocean and to feed model simulations of modern, past, and future ocean scenarios. The present article outlined some milestones and 'heroes' that helped to promote the amazing evolution of this novel field of earth sciences.

Keywords

History of science • Major advances in paleoceanography • Quantitative tracers of ocean water masses • Major scientific pacemakers • Climatic change • Quaternary

1 Preliminary Note

This fairly incomplete resumé was focused on the (mostly empiric) reconstruction of Pleistocene scenarios of the ocean, on a period when plate-tectonic geometries were equal to those of today. A wealth of great findings also marked the pre-Quaternary to Mesozoic ocean. An adequate appraisal of these results, however, would require a separate small synthesis to do justice to the great scientific insights of pioneering colleagues like M. Cita, A.G. Fischer, B.U. Haq, W.W. Hay, A. Holbourn, J.P. Kennett, I. Premoli-Silva, W. Ruddiman, W. Ryan, N.J. Shackleton, J. Thiede, and T. van Andel.

M. Sarnthein (✉)
Institute of Geosciences, University of Kiel, 24098 Kiel, Germany
e-mail: michael.sarnthein@ifg.uni-kiel.de

2 Early Efforts

The actual onset of systematic efforts in paleoceanography occurred at the Lamont-Doherty Geological Observatory ('LDGO'; today: 'LDEO') of Columbia University, ~30 km north of Manhattan/New York in 1964. Colleagues of LDGO and the Scripps Institution of Oceanography (SIO) ended up in a heated discussion on the question, whether the glacial deep ocean was marked by enhanced dissolution (as originally observed by the Swede E. Olausson, 1949/1963 for the North Atlantic) or by increased preservation of calcium carbonate as proposed by some SIO data from the Pacific. The dispute lacked proper age control and finally culminated in a wild fight with chalk pieces. In the rear then quietly sat J. Imbrie (Brown University), gifted with special mathematical skills. He got a fancy idea how to rationalize the question of 'glacials' and 'interglacials' by means of quantitative sea surface temperature (SST) estimates that are based on census counts of planktic foraminifera species, the modern distribution patterns of which then were revealed by Weyl [1] and Bé and Tolderlund [2]. Imbrie named his strategy "transfer function technique", a catchy term created to solicit successfully funding from the U.S. National Science Foundation (NSF).

This technique formed the backbone and birth of a first great project on the quantitative reconstruction of past SST in the global ocean, named CLIMAP (Climate: Long-range Investigation, Mapping, and Prediction). The unique team efforts of CLIMAP project members resulted in the first empiric quantitative SST maps of the ocean for the last peak glacial [3, 4]. As major byproduct, CLIMAP also studied the record of sand deserts active in the subtropics during peak glacial and interglacial times, moreover, the record of changing dust deposits in the Atlantic [5, 6]. Most important, the new quantitative records of paleoceanography and paleoclimate induced—for the first time—a linkage between empiric scientists and the (then novel) community of climate modelers that tried to predict future climate change ([7];

Z. Zhang et al. (eds.), *Patterns and Mechanisms of Climate, Paleoclimate and Paleoenvironmental Changes from Low-Latitude Regions*, Advances in Science, Technology & Innovation, https://doi.org/10.1007/978-3-030-01599-2_1

GFDL Princeton) to identify potential sources of social unrest as a result of aridity and poor crops.

3 Sample Basis to Gain Empiric Proxy Data from Deep-Sea Sediments

Since Kullenberg [8], the piston corer formed the backbone for a successful, though in part somewhat distorted sampling of deep-sea sediments. In the early 1950s, M. Ewing, LDGO ("a piston corer brings up samples of the ocean floor just as a housewife cores an apple") ordered RV Vema and other vessels to take at least one piston core a day. After few decades this order resulted in the spectacular Lamont collection of thousands of sediment cores. Similar efforts were made in Miami/Florida. Also, the international DSDP/ODP/IODP project started to gain hundreds of (hydraulic piston and rotary) cores from well-selected hemipelagic sediment sites in the ocean since 1967. German vessels started to sample sediments in the East Atlantic and Indian oceans in the mid 1960s, later in the global ocean. 1995, French colleagues (Y. Balut) developed the new *Calypso* technique to retrieve most advanced long piston cores on board of N.S. *Marion Dufresne*, successfully employed by an international project called IMAGES.

4 Great Advances in the 1970s and 1980s

During these decades, four prominent colleagues especially marked the evolution of paleoceanography. W.H. Berger (SIO) established pioneering results on the productivity and preservation of calcareous-shelled planktonic foraminifera and their use for paleoceanographic proxies. He documented that differential shell preservation reflects the principles of deep-sea carbonate preservation, the calcite compensation depth (CCD), and the oceanic carbon cycle in general, a milestone in paleoceanography. He started to map Tertiary CCD shifts in the East Atlantic and developed the principles of Pacific versus Atlantic basin-to-basin fractionation in carbonate deposition. In the early 1980s, he outlined the joint role of denitrification, changes in the ratio of carbon/carbonate 'rain', and the buildup of shelf carbonates during the deglacial transgression that may have delivered considerable changes in atmospheric CO_2.

N.J. Shackleton (Cambridge, UK) shaped and dominated paleoceanography as a physicist, even though his father (a prominent petrologist) had tried to keep him away from geosciences, suggesting him to do 'something proper' in physics. So he developed a mass spectrometer for measuring stable oxygen and carbon isotopes ($\delta^{18}O$, $\delta^{13}C$) on minute mass samples of foraminifera tests, 10–100 times smaller than with conventional mass spectrometry, a technical milestone. On this basis, Shackleton further evolved the ingenuous approach of C. Emiliani (Miami) to generate records of foraminifera isotopes in deep-sea cores as a proxy of glacial-to-interglacial climate change. Most important, Shackleton found (and finally convinced Emiliani himself) that a major portion of the $\delta^{18}O$ signal was tied to past changes in global ice volume rather than to changes in ambient temperature and salinity.

In this way he created a novel tracer of past changes in global ice volume, a global tracer of sea level change and age control, soon a backbone of CLIMAP stratigraphy. Hays et al. [4] succeeded to tune past $\delta^{18}O$ records to Milankovitch orbital parameters, then just recalculated by Berger ([9]; Belgium), an effort that resulted in a first astronomical age scale of ocean and climate events, at the onset a truly utopic vision, shortly after proposed as age model for the last 100 My (U.S. SPECMAP project). As a clarinetist and genuine expert in music and its physical basics Shackleton first employed spectral theory and interferences in orbital cyclicity to derive the forcings of various climatic parameters over the Pleistocene. Prior to ice core records, a controversial question was focused on the amount of climate variability possibly controlled by orbital forcing: Hasselmann (MPI Hamburg) believed in zero (chaos), Imbrie estimated 65%, Herterich (MPI Hamburg) 38%.

A close friend of Imbrie, W.S. Broecker (LDEO) was the great pacemaker of ocean biogeochemistry, in particular, the carbon chemistry and its $\delta^{13}C$ and radiocarbon records (^{14}C) as tracers of past variations in the Ocean 'Salinity Conveyor Belt' or 'Meridional Overturning Circulation' (MOC) [10, 11]. Amongst his textbooks the 'Tracers in the Sea' (1982) [12] forms a standard reference that has endured in popularity up to today. His findings, definitions (e.g., of 'Heinrich Events'), and concepts were basic for the work of generations of paleoceanographers.

Like Shackleton, J.-C. Duplessy (LSCE near to Paris) started to analyze stable isotopes both in speleothems and in ocean waters and foraminifera as early as in the late 1960s. Especially, he defined $\delta^{13}C$ as tracer of the nutrient content in ocean deep waters and thus, of ocean MOC. In the early 1990s, E. Boyle, MIT Boston, compared these results with those of a second nutrient tracer of phosphorus, the Cd/Ca ratio of benthic foraminifera. Furthermore, Duplessy found a 'trick' to quantify the global ice volume effect in benthic $\delta^{18}O$ records (together with Labeyrie [13]). The authors deployed the present temperature of Norwegian Sea Deep Water near −1 °C as absolute minimum, constant over times, as reference value to assign the residual shifts in $\delta^{18}O$ in part to global ice volume and sea-level change, in part to temperature changes in different ocean basins over glacial-to-interglacial times. Also, a breakthrough was achieved by reconstructing a first LGM pattern of North Atlantic sea surface salinity, thereby locating potential sites

of LGM deep-water formation. Since 1985, Duplessy and E. Bard evolved as pacemakers of marine AMS-^{14}C stratigraphy, which involved a novel problem, the conversion of marine ^{14}C ages to the calendar age scale (in part, also led to heated discussions).

At the same time, various English colleagues contributed substantial new tools and insights to paleoceanography. G. Eglinton (Bristol) developed from biomarkers a whole 'shopping list' of new molecular tools, most important, 'Uk37', a new master tracer of SST (since 1986) [14]. I.N. McCave (Cambridge) recorded with current meters 'deep-sea storms' in the deep Atlantic and first defined 'sorted silt' as proxy to estimate past bottom current speeds. H. Elderfield (Cambridge) pioneered the links between seawater chemistry (e.g., defining Sr and rare earths as proxies of ocean water composition) and climate change. Also, he presented a diagram on three successive phases in assessing paleoceanographic proxies: An overly optimistic is followed by an overly pessimistic and finally, a pragmatic view. E. Rohling (Southampton) specified the long-term variations of global sea-level on the basis of δ^{18}O signals in the Red Sea.

5 Some Contributions of Kiel University (Germany)

The team of marine geology in Kiel was founded and oriented by E. Seibold, a most prominent German pioneer in this field, well known for the textbook of Seibold and Berger [4th ed., 15]. One of Seibold's last PhD students, H. Heinrich, later discovered tiny layers of dolomite debris in Late Pleistocene sediments of the East Atlantic, the basis for Broecker's idea to use his name for the term 'Heinrich Events' that record short events of melting iceberg armadas. In the late 1980s, the paleoceanographers' group Kiel University was enlarged significantly by the foundation of GEOMAR, a new research institution that implied both new laboratory facilities and many new positions for young scientists.

In the early 1980s, major progress was made in accelerating the analyses of stable isotopes of foraminifera by developing the 'Kiel Carboprep Device' that enables an automated carbonate preparation (H. Erlenkeuser in coop. with Finnigan MAT). On the basis of almost hundred epibenthic δ^{18}O and δ^{13}C records from the eastern and central Atlantic the group of Sarnthein first defined parameters that characterize coastal upwelling (G. Ganssen), Mediterranean Outflow Waters (R. Zahn), and in particular, three different states of Atlantic MOC for LGM-to-Holocene times [16]. Later, W. Curry (Woods Hole, US) continued this approach on the basis of West Atlantic δ^{13}C records [17]. Orbital-scale δ^{18}O stratigraphy of hundreds of sediment cores served as backbone for ocean-wide maps of glacial-to-interglacial changes in plankton productivity and, most important, for 'GLAMAP 2000', a joint project of Kiel, Bremen, and AWI Bremerhaven, that revised the SST patterns of CLIMAP for the LGM, now monitored at 275 sites in the Atlantic [18]. Later, the SST estimates were incorporated into an international MARGO project to assemble global SST maps (M. Kucera, Bremen). Moreover, Nürnberg ([19]; GEOMAR Kiel) re-assessed Mg/Ca in foraminifera as proxy of water mass temperatures, nowadays widely accepted as master tracer. Past SST patterns form an indispensable basis for the test of climate models, the importance of which for the prediction of future climate scenarios is ever increasing.

Important Kiel contributions were based on results of AMS ^{14}C dating (P.M. Grootes): Major ^{14}C excursions during Laschamp and other magnetic events helped to quantify the contemporaneous rise of ^{14}C radioactivity in the surface ocean [20]. Planktic ^{14}C plateaus were tuned to atmospheric ^{14}C plateaus, thus started to serve as novel tracer of centennial-scale age control. Benthic ^{14}C ventilation ages were revealed as tracer to quantify the carbon dissolved in ocean deep waters (Sarnthein).

Kiel paleoceanographers focused on past variations of the northern North Atlantic, a 'switchboard' of global MOC [21], but also provided first lines of evidence for North Pacific deep-water formation during the Late Pliocene [22] and early deglacials (Sarnthein; J. Rae, Saint Andrews), reflecting a current regime markedly different from that of today. Basic studies illuminated the short-term Pleistocene variability of Indian, SE Asian and, most recently, Australian monsoons (e.g., W. Kuhnt and A. Holbourn; in coop. with PX. Wang, Shanghai). Finally, the records provided proof for linkages between the Late Pliocene onset of major glaciation of Greenland and the final closure of Central American Seaways.

Since the mid-1980s, alumni of Kiel University started powerful groups of paleoceanographers at Bremen University (G. Wefer and W.H. Berger) and the Alfred-Wegener Institute (AWI) in Bremerhaven that developed with great success large-scale projects on the Plio-Pleistocene history of the South Atlantic and the polar oceans (e.g., R. Gersonde and R. Stein reconstructed past changes in sea ice cover on the basis of novel floral and biogeochemical proxy data).

6 Selection of Major Findings Over the Last 20 Years

Major progress was made in developing novel proxies such as TEX86 [23] and the 'clumped isotope method' [24] that allow us to monitor past SST further back in ocean history and independent of any faunal and chemistry changes.

Furthermore, εNd and Pa/Th were found suitable to reconstruct past changes in ocean MOC, finally, boron isotopes ($\delta^{11}B$) turned out as robust proxy to study past changes in ocean alkalinity [25]. Beyond orbital and millennial-scale forcings that dominate the periodicities in marine climate and polar climate records, Kennett and colleagues [26] identified a cosmic impact as prime forcing for the onset of the major cooling that initiated the abrupt climate setback of the Younger Dryas about 13 ka.

References

1. Weyl, P.K.: Micropaleontology and ocean surface climate. Science **202**(4367), 475–481 (1968)
2. Bé, A.W.H., Tolderlund, D.S.: Distribution and ecology of living planktonic foraminifera in surface waters of the Atlantic and Indian oceans. In: Funnel, B.M., Riedel, W.R. (eds.) The Micropaleontology of Oceans, pp. 105–149 (1971)
3. CLIMAP Project Members: Seasonal reconstructions of the earth's surface at the last glacial maximum. Geological Society of America, Map and Chart Series, MC-36 (1981)
4. Hays, J.D., Imbrie, J., Shackleton, N.J.: Variations in the earth's orbit: pacemaker of the ice ages. Science **194**(4270), 1121–1132 (1976)
5. Sarnthein, M.: Sand deserts during glacial maximum and climatic optimum. Nature **272**(5648), 43–46 (1978)
6. Sarnthein, M., Tetzlaff, G., Koopmann, B., Wolter, K., Pflaumann, U.: Glacial and interglacial wind regimes over the eastern subtropical Atlantic and NW Africa. Nature **293**, 153–157 (1981)
7. Manabe, S., Hahn, D.G.: Simulation of the tropical climate of an ice age. J. Geophys. Res. **82**, 3889–3911 (1977)
8. Kullenberg, B.: The pison core samples. Svenska Hydrogr. Biol. Komm. Skr. (Ser. 3: Hydrogr.) **1**(2), 46 (1947)
9. Berger, A.L.: Long-term variations of daily insolation and quaternary climatic changes. J. Atmos. Sci. **35**(12), 2362–2367 (1978)
10. Stommel, H.: Thermohaline convection with two stable regimes of flow. Tellus **13**, 224–230 (1961)
11. Stuiver, M., Quay, P.D., Östlund, H.G.: Abyssal water carbon-14 distribution and the age of the world oceans. Science **219**, 849–851 (1983)
12. Broecker, W.S., Peng, T.H.: Tracers in the Sea. ELDIGIO Press (1986)
13. Labeyrie, L.D., Duplessy, J.C., Blanc, P.L.: Variations in mode of formation and temperature of oceanic deep waters over the past 125,000 years. Nature **327**, 477–482 (1987)
14. Brassell, S.C., Eglinton, G., Marlowe, I.T., Sarnthein, M., Pflaumann, U.: Molecular stratigraphy: a new tool for climatic assessment. Nature **320**, 129–133 (1986)
15. Seibold, E., Berger, W.H.: The Sea Floor. An Introduction to Marine Geology, 4th edn, 316 pp. Springer, Heidelberg (2016)
16. Sarnthein, M., Winn, K., Jung, S., Duplessy, J.C., Labeyrie, L., Erlenkeuser, H., Ganssen, G.: Changes in East Atlantic deepwater circulation over the last 30,000 years—an eight-time-slice record. Paleoceanography **9**, 209–267 (1994)
17. Curry, W.B., Oppo, D.W.: Glacial water mass geometry and the distribution of $\delta^{13}C$ of ΣCO_2 in the western Atlantic Ocean. Paleoceanography **20** (2005). https://doi.org/10.1029/2004pa001021
18. Pflaumann, U., Sarnthein, M., Chapman, M., Funnell, B., Huels, M., Kiefer, T., Maslin, M., Schulz, H., Swallow, J., van Kreveld, S., Vautravers, M., Vogelsang, E., Weinelt, M.: The glacial North Atlantic: sea surface conditions reconstructed by GLAMAP-2000. Paleoceanography **18**(3), 1–28 (2003). https://doi.org/10.1029/2002pa000774
19. Nürnberg, D., Bijma, J., Hemleben, C.: Assessing the reliability of magnesium in foraminiferal calcite as a proxy for water mass temperatures. Geochim. Cosmochim. Acta **60**(5), 803–814 (1996)
20. Voelker, A., Sarnthein, M., Grootes, P.M., Erlenkeuser, H., Laj, C., Mazaud, A., Nadeau, M., Schleicher, M.: Correlation of marine 14C ages from the Nordic Seas with the GISP2 isotope record: implications for radiocarbon calibration beyond 25 kyr. Proc. 16th Int. 14C Conf. Radiocarb. **40**, 517–534 (1998)
21. Sarnthein, M., Stattegger, K., Dreger, D., Erlenkeuser, H., Grootes, P., Haupt, B., Jung, S., Kiefer, T., Kuhnt, W., Pflaumann, U., Schäfer-Neth, C., Schulz, H., Schulz, M., Seidov, D., Simstich, J., van Kreveld-Alfane, S., Vogelsang, E., Völker, A., Weinelt, M.: Fundamental modes and abrupt changes in North Atlantic circulation and climate over the last 60 ky—concepts, reconstruction, and numerical modelling. In: Schäfer, P., et al. (eds.) The Northern North Atlantic: A Changing Environment, pp. 365–410. Springer Verlag (2001)
22. Haug, G.H., Sigman, D.M., Tiedemann, R., Pederson, T., Sarnthein, M.: A biogenic silica record of the onset of halocline stratification on in the subpolar North Pacific 2.73 Ma. Nature **401**, 779–782 (1999)
23. Schouten, S., Hopmans, E.C., Schefus, E., Damste, S.: Distributional variation in marine crenarchaeotal membrane lipids: a new tool for reconstructing ancient sea water temperatures? Earth Planet. Sci. Lett. **204**, 265 (2002)
24. Eiler, J.M.: 'Clumped-isotope' geochemistry—the study of naturally-occurring, multiply-substituted isotopologues. Earth Planet. Sci. Lett. **262**, 309–327 (2007)
25. Klochko, K., Kaufman, A.J., Yao, W., Byrne, R.H., Tossell, J.A.: Experimental measurement of boron isotope fractionation in seawater. Earth Planet. Sci. Lett. **248**, 276–285 (2006)
26. Kennett, D.J., Kennett, J.P., West, A., Mercer, C., Que Hee, S.S., Bement, L., Bunch, T.E., Sellers, M., Wolbach, W.S.: Nanodiamonds in the Younger Dryas boundary sediment layer. Science **323**, 94 (2009)

Part II
Paleoceanographic Evolution

Orbital-Scale Paleoceanographic Response to the Indian Monsoon in the Laxmi Basin of the Eastern Arabian Sea

Boo-Keun Khim, Ji-Eun Kim, Keiji Horikawa, Minoru Ikehara, Yoshihiro Asahara, and Jongmin Lee

Abstract

International Ocean Discovery Program Expedition 355 performed a 1109.4 m penetration drill at Site U1456 in the Laxmi Basin of the Eastern Arabian Sea. The uppermost section (~121 m thick) was analyzed for the paleoceanographic change in response to the orbital-scale Indian monsoon. Correlation of $\delta^{18}O$ values of planktonic foraminifera (*Globigerinoides ruber*) to the LR04 stacks determined the age model (~1.2 Ma). The geochemical contents correspond to the sediment facies such that high TC contents correspond to the pelagic carbonates. High $\delta^{15}N$ values of bulk sediments coincide with the interglacial periods when denitrification was intensified. $^{87}Sr/^{86}Sr$ ratios and εNd values of detrital particles are controlled by the sediment sources (i.e., river sediments) as well as depositional processes. Mixed layer depth traced by $\delta^{18}O$ and $\delta^{13}C$ values between *G. ruber* and *G. sacculifer* varied in response to the monsoon activity. The sediments in the Laxmi Basin of the Eastern Arabian Sea record the orbital-scale variation of the Indian monsoon during the Pleistocene.

Keywords

Orbital scale • Indian monsoon • Paleoceanography • Arabian Sea

1 Introduction

The Arabian Sea is known to be a famous sediment repository, the Indus Fan. The Indus Fan covers 1.1×10^6 km^2, stretching 1500 km into the Indian Ocean, and the thickest point of the deposit is >7 km. Although the age of the Indus Fan remains a subject of debate, the initiation of the fan formation was linked to the uplift of the Himalayas, and associated with sea level lowering during the middle Oligocene to early Miocene [1]. During the International Ocean Discovery Program Expedition 355 in 2015, Site U1456 (16°37.28′N, 68°50.33′E, 3640 m of water depth) was drilled. Site U1456 is located offshore from the western margin of India, ~475 km from the Indian coast and ~820 km from the modern mouth of the Indus River in Laxmi Basin in the Eastern Arabian Sea (Fig. 1). The drilling penetration at Site U1456 attained ~1109.4 m below seafloor (mbsf), reaching 13.5–17.7 Ma (late early to early middle Miocene), with only a few hiatuses [2]. Using the various kinds of sediment properties, four lithologic units were defined onboard based on a compilation of Holes U1456A through U1456E at Site U1456, in which each lithologic unit was characterized by a different depositional environment [2].

In this study, we measured several paleoceanographic parameters which have responded to the orbital-scale Indian monsoon change during the last 800 kyrs.

2 Materials and Methods

A total of 260 samples, collected from a composite section of Unit I consisting of Holes U1456A and U1456C at Site U1456, were used in this study. TC content was measured using CHN Elemental Analyzer (Flash 2000 Model). The $\delta^{18}O$ and $\delta^{13}C$ values of planktonic foraminifera (*G. ruber* and *G. sacculifer*) with a test size between 250 and 355 μm were measured using IsoPrime at Center for Advanced Marine Core Research of Kochi University (Japan). Isotope

B.-K. Khim (✉) · J.-E. Kim · J. Lee
Pusan National University, Busan, 46241, Korea
e-mail: bkkhim@pusan.ac.kr

K. Horikawa
Toyama University, Toyama, 930-8555, Japan

M. Ikehara
Kochi University, Nankoku, 783-8502, Japan

Y. Asahara
Nagoya University, Nagoya, 464-8601, Japan

Z. Zhang et al. (eds.), *Patterns and Mechanisms of Climate, Paleoclimate and Paleoenvironmental Changes from Low-Latitude Regions*, Advances in Science, Technology & Innovation, https://doi.org/10.1007/978-3-030-01599-2_2

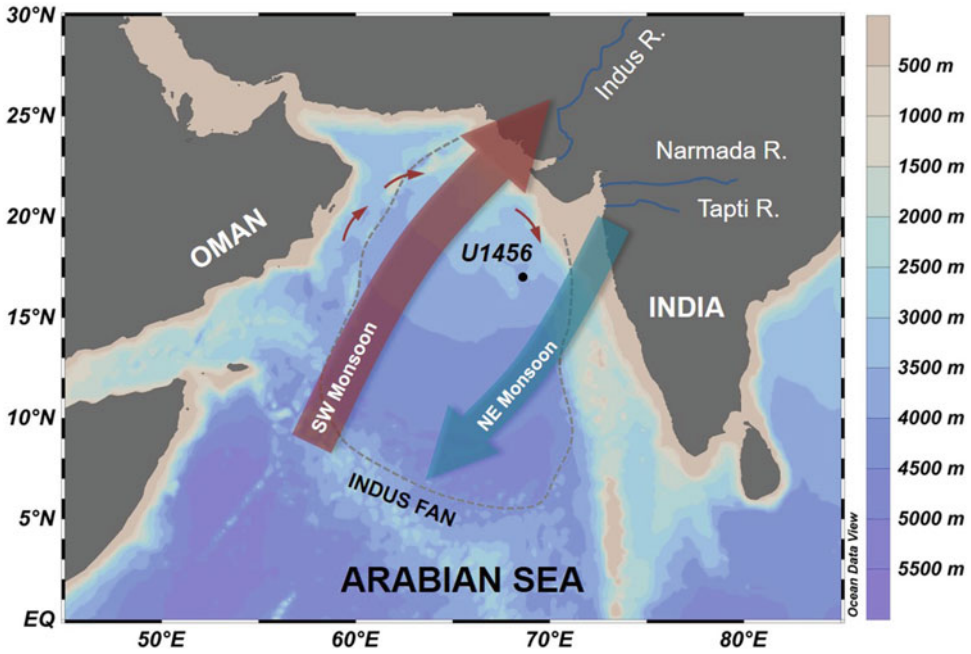

Fig. 1 IODP expedition 355 site U1456 in the Eastern Arabian Sea with seasonal wind patterns of the Indian monsoon. The grey dotted line represents the outline of the Indus Fan. The small red arrow symbolizes the Somali Current in the far north of the Arabian Sea that flows clockwise when the southwest monsoon is strong

ratios were calibrated to the V-PDB standard using international standard NBS19. The analytical precision of the $\delta^{18}O$ and $\delta^{13}C$ values is ±0.06‰ and ±0.05‰, respectively. The $\delta^{15}N$ values of bulk sediments were measured using EA-IRMS at Iso-Analytical Ltd. (UK). All $\delta^{15}N$ values were calibrated to $\delta^{15}N_{air}$ and the precision was about ±0.1‰. A total of 60 sediment samples were selected to measure the Sr and Nd isotopic compositions of the detrital fraction of the bulk sediments, using TIMS at Nagoya University.

3 Results and Discussion

3.1 Age Reconstruction at Site U1456

The preliminary age of the sedimentary sequence drilled at Site U1456 was estimated onboard [2]. The age of Unit I was mainly determined by the correlation of $\delta^{18}O$ values of planktonic foraminifera (*Globigerinoides ruber*) to the LR04 stack [3], in addition to the consideration of shipboard biostratigraphic and paleomagnetic data. The 37 tie points were determined by correlating $\delta^{18}O$ values to the LR04 stack, with an additional correlation of $\delta^{15}N$ values to ODP Leg 117 Site 722B [4] in the Western Arabian Sea. Although the age reference of Site 722B is different from the LR04 stack, the minor offset between them seems insignificant. As a result, the age of the study interval spans as old as 1.2 Ma, covering up to the Marine Isotope Stage (MIS) 36 [5]. The oxygen isotope stratigraphy shows that the quasi-cyclic pattern is characterized by 100-ka periodicity [5], which is prominently more visible since the Mid-Pleistocene Transition (Fig. 2).

3.2 Orbital-Scale Paleoceanographic Changes

Fluctuation of total carbon (TC) content, mainly contributed by total inorganic carbon, is not in coincident with the glacial and interglacial periods (Fig. 2). High TC content corresponds to the pelagic carbonate ooze whereas low TC content corresponds to the clay-rich turbidite layers. The occurrence of turbidite seems more frequent during the glacial periods. The $\delta^{15}N$ values of the bulk sediments, representing the degree of denitrification, range between 5.3 and 10.1‰ with an average of 7.5‰ during the last 800 kyrs (Fig. 2). The $\delta^{15}N$ variation is distinct following glacial-interglacial changes, being characterized by high $\delta^{15}N$ values during the interglacial periods indicating active denitrification and showing the opposite during glacial periods. Such data of $\delta^{15}N$ from Site U1456 shows the 100-ka periodicity that is displayed in glacial-interglacial variations that are possible to be correlated to the orbital-scale eccentricity cycle [5].

Variations in the pattern of $^{87}Sr/^{86}Sr$ ratios and εNd values appear to be quasi-cyclic during the last 800 kyrs (Fig. 2). Systematic variations in the $^{87}Sr/^{86}Sr$ ratios and εNd values are observed displaying a nearly symmetrical variation pattern throughout the core. However, these fluctuations are not clearly coincident with the

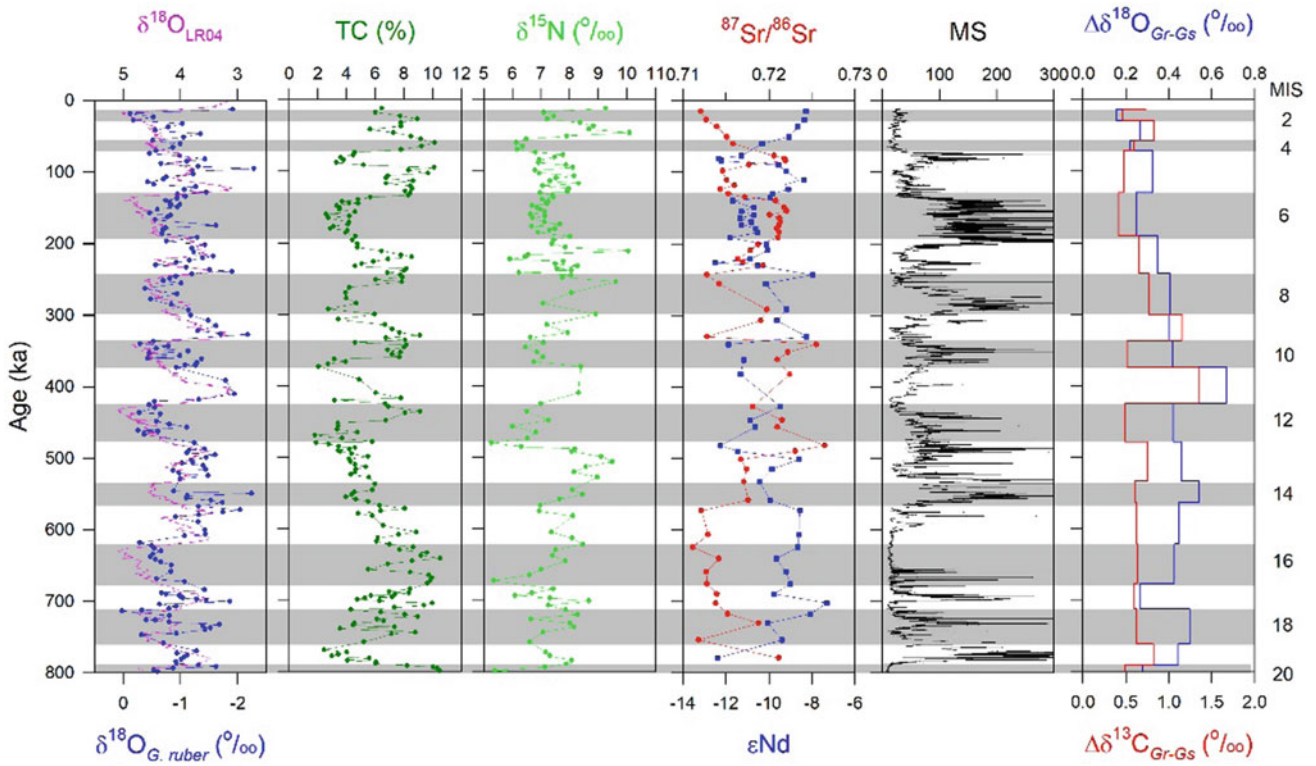

Fig. 2 Downcore profiles of $\delta^{18}O_{LR04}$ [3], $\delta^{18}O_{G.\ ruber}$ [5], total carbon (TC) content, $\delta^{15}N$ values [5], $^{87}Sr/^{86}Sr$ values and εNd ratios [6], magnetic susceptibility (MS), $\Delta\delta^{18}O_{Gr\text{-}Gs}$ and $\Delta\delta^{13}C_{Gr\text{-}Gs}$ values. Shading represents the glacial periods. MIS: Marine Isotope Stage

glacial-interglacial cycles. Instead, the fluctuations of these isotopes are more related to the variation of magnetic susceptibility. By considering the εNd and $^{87}Sr/^{86}Sr$ end-members of river sediment sources, the Tapi River is responsible for sediments with low $^{87}Sr/^{86}Sr$ ratios and high εNd values whereas the Narmada and Indus Rivers are the main contributors to sediments with high $^{87}Sr/^{86}Sr$ ratios and low εNd values [6]. However, depositional processes of pelagic sedimentation and turbidite deposition are important to affect these isotopes.

The difference ($\Delta\delta^{18}O_{Gr\text{-}Gs}$, $\Delta\delta^{13}C_{Gr\text{-}Gs}$) of $\delta^{18}O$ and $\delta^{13}C$ values between *G. ruber* and *G. sacculifer* provides information on the variation of mixed layer depth (Fig. 2). The mixed layer depth, estimated by the habitat depth of *G. ruber* and *G. sacculifer*, has been affected by the sea surface temperature and convection by wind mixing. $\Delta\delta^{18}O_{Gr\text{-}Gs}$ values (i.e., difference of $\delta^{18}O$ values between *G. ruber* and *G. sacculifer*) increased during the interglacial periods and $\Delta\delta^{13}C_{Gr\text{-}Gs}$ values did not change systematically between the glacial and interglacial periods (Fig. 2), despite the distinct orbital-scale Indian monsoon activity.

References

1. Clift, P.D., Shimizu, N., Layne, G., Blusztajn, J., Gaedicke, C., Schluter, H.-U., Clark, M., Amjad, S.: Development of the Indus Fan and its significance for the erosional history of the Western Himalaya and Karakoram. Geol. Soc. Am. Bull. **113**, 1039–1051 (2001)
2. Pandey, D.K., Clift, P.D., Kulhanek, D.K.: The expedition 355 scientists: site U1456. In: The Proceedings of the International Ocean Discovery Program 355, pp. 1–61 (2016). https://doi.org/10.14379/iodp.proc.355.103.2016
3. Lisiecki, L.E., Raymo, M.E.: A pliocene-pleistocene stack of 57 globally distributed benthic $\delta^{18}O$ records. Paleoceanography **20**, PA1003 (2005). https://doi.org/10.1029/2004pa001071
4. Altabet, M.A., Murray, D.W., Prell, W.L.: Climatically linked oscillations in Arabian Sea denitrification over the past 1 my: implications for the marine N cycle. Paleoceanography **14**, 732–743 (1999)
5. Kim, J.E., Khim, B.K., Ikehara, M., Lee, J.: Orbital-scale denitrification changes in the Eastern Arabian Sea during the last 800 kyrs. Sci. Rep. **8**, 7072 (2018). https://doi.org/10.1038/s41598-018-25415-7
6. Khim, B.K., Horikawa, K., Asahara, Y., Kim, J.E., Ikehara, M.: Detrital Sr–Nd isotopes and sediment provenance in the Laxmi Basin (IODP Exp. 355 Site U1456) of the Arabian Sea during the last 800 kyrs. Geol. Mag. (GEO-18-1943) (in review)

The 4.2 ka Event in the Euro-Mediterranean Region—A Study from the MISTRALS/ PALEOMEX Program

Bassem Jalali and Marie-Alexandrine Sicre

Abstract

High-resolution records documenting the 4.2 ka event (from 4200 to 3900 cal yr BP) are scarce. Archaeological and paleoenvironmental data from continental archives suggest that this event is coincident with a megadrought in the eastern Mediterranean basin. Here, we present an unprecedented high-resolution alkenone-based sea surface temperature (SST) record from the northwestern Mediterranean Sea showing a stepwise cooling of ca. 2 °C between 4400 and 3800 yr BP, which shares similarities with speleothem records from central Europe and the Mediterranean region. Our data suggest a reorganization of the North Atlantic atmospheric circulation during this event.

Keywords

Alkenone • SSTs • 4.2 ka event • Mediterranean Atmospheric circulation

1 Introduction

Holocene rapid climate changes (RCCs) are century-long time intervals of enhanced high-latitudes cooling and tropical dryness [1, 2]. One of the most widely documented RCC is the dry and cold period spanning from ca. 4200 to 3900 cal yr BP, known as the 4.2 ka event [3]. This time interval coincides with a megadrought in the eastern Mediterranean basin, which caused the collapse of the Akkadian Empire and the Old Kingdom in Egypt, and further to the far East of the Old Chinese cultures [4–6]. The 4.2 ka event is also considered as the boundary between the Middle and Late Holocene [7].

In this study, we used a recently published high-resolution alkenone-based sea surface temperature (SST) reconstruction from the northwestern Mediterranean Sea [8] and compared it to several speleothem isotope records where the 4.2 ka event was well developed to provide a climatic and environmental regional context to help understand the response of human societies as documented by archeological excavations.

2 Materials and Methods

The gravity core KSGC-31 (43°N; 3.29°E, 60 m water depth) was sampled and analyzed for alkenones. The unsaturation index $U^{k'}_{37}$ and the global calibration published by Conte et al. [9] were used to calculate SSTs. The age model of the core KSGC-31 between 5500 and 2500 cal yr BP is based on five AMS ^{14}C dates calibrated using the Calib 7.1 software and the MARINE 13 calibration data set.

3 Results and Discussion

Figure 1 shows the SST reconstruction for the Gulf of Lion [8] together with the air temperature/precipitation records derived from the oxygen isotope of stalagmites from Spannagel (Central Alps), Renella (Italy), Mavri Trypas (Southern Greece) and Jeita (Lebanon) caves (see references on Fig. 1). These records are indicative of precipitation changes in central and eastern Mediterranean and are thus used to explore the regional environmental patterns across the basin during the 4400–3800 cal yr BP interval and derive the role of atmospheric modes of variability in the observed changes.

SSTs in the GoL show a several-step cooling of ~2 °C starting at 4400 yr BP and culminating at 3800 yr BP that has never been described at this level of detail. Similar fingerprint is also seen in the air temperature from Central Alps

B. Jalali (✉)
Faculté Des Sciences de Sfax, GEOGLOB, Université de Sfax, Route de Soukra, Km 4, B.P. 802, 3038 Sfax, Tunisia
e-mail: bassemfss@gmail.com

B. Jalali · M.-A. Sicre
CNRS-IRD-MNHN, LOCEAN Laboratory, Sorbonne Universités (UPMC, Univ Paris 06), 4 place Jussieu, 75005 Paris, France

Z. Zhang et al. (eds.), *Patterns and Mechanisms of Climate, Paleoclimate and Paleoenvironmental Changes from Low-Latitude Regions*, Advances in Science, Technology & Innovation, https://doi.org/10.1007/978-3-030-01599-2_3

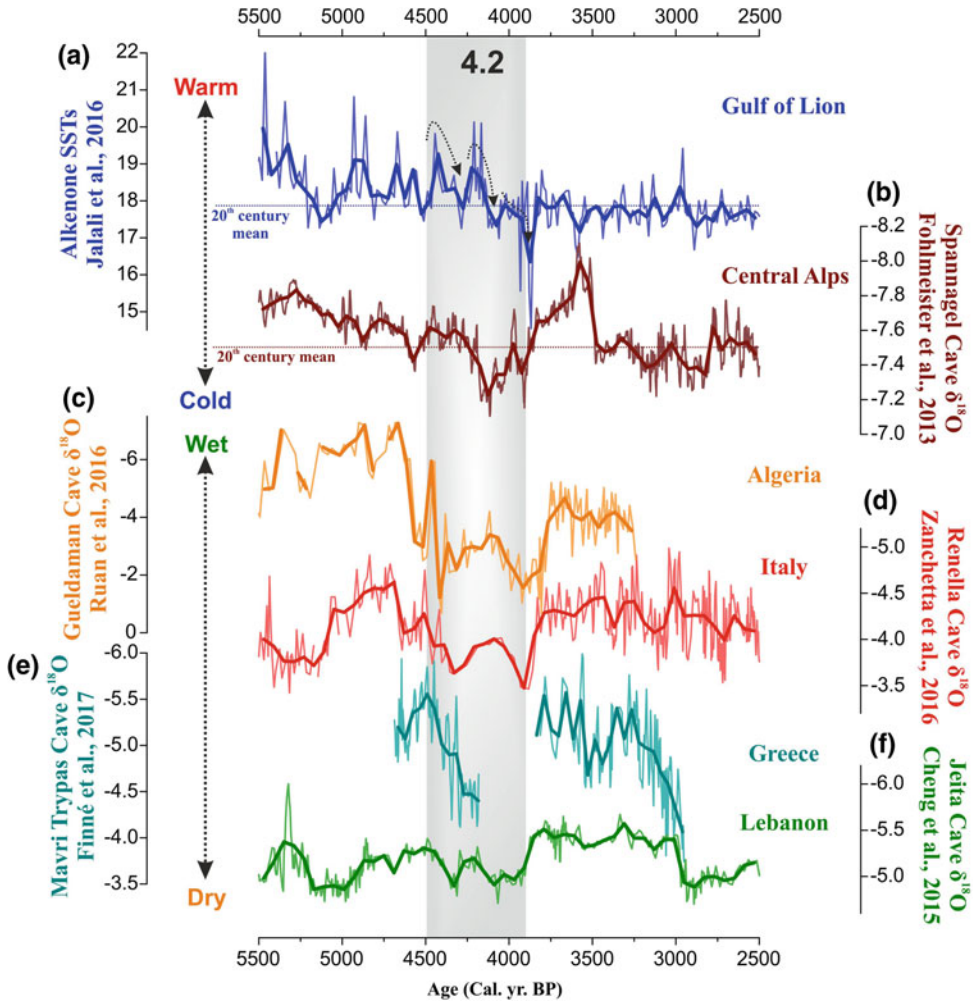

Fig. 1 Records of the 4.2 ka event used in this study

[10] (Fig. 1a, b). High-resolution speleothem records from western, central and eastern basins of the Mediterranean (Fig. 1c–f) highlight a drastic reduction of rainfall during the 4.2 ka event [11–13]. Cross-analyses of stable oxygen isotopes and archaeological layers from Gueldaman Cave in northern Algeria evidenced that dry conditions between 4400 and 3800 yr BP coincide with the abandonment of the cave [12] (Fig. 1c). According to Zanchetta et al. [13] drier conditions in the Renella cave record in central Italy between 4300 and 3800 yr BP would result from a long duration of summer drought (Fig. 1d). Proxy records from eastern Mediterranean (Mavri Trypas and Jeita caves; [11, 14]; Fig. 1e, f) further supports the occurrence of arid conditions during the 4.2 ka event. The presence of a hiatus in the speleothem record of southern Peloponnese Mavri Trypas Cave even witnesses the absence of stalagmite growth caused by insufficient rainfall. These proofs highlight that precipitations over several parts of the Mediterranean region were extremely low during the 4.2 ka event.

Today, the Mediterranean precipitations are controlled by frequency and intensity of the Mediterranean cyclones (Genoa Gulf, Gulf of Lion …) originating from the North Atlantic storm tracks [15]. The Mediterranean cyclogenesis is generally more active when westerlies are weak (weaker zonal flow) allowing cyclones from the North Atlantic to enter the Mediterranean basin and surroundings. However, several paleoreconstructions indicate a strong weakening of the westerly flow (negative North Atlantic Oscillation, NAO) during the 4.2 ka event [16–18]. Although the Mediterranean winters are expected to be wet under negative NAO, a reverse pattern is expected during North Atlantic atmospheric blocking. In fact, the anticyclonic cell associated with the North Atlantic blocking deflects the westerly wind flow to the North, returning to southern Europe and Mediterranean regions as colder and drier air masses [19]. Concomitantly coastal regions such as northern England, Ireland and northern Scandinavia would benefit from humid conditions [20–22]. This weather regime would thus account

for the observed dry conditions over the Mediterranean basins during the 4.2 ka event. Similar to the Little Ice Age (LIA), advection of cold northeasterly and northwesterly winds into the Western Europe and NW Mediterranean Sea would be responsible for the cold and dry conditions of the 4.2 ka event [23].

4 Conclusions

SSTs in the GoL together with air temperature records from central Alps both show colder conditions during the 4.2 ka event that can be explained by anticyclonic blocking over the North Atlantic as evidenced by the most recent severe climate period known as the LIA. Oxygen isotopes in speleothems indicate that precipitations during this time interval were below normal, reflecting drier continental air flow during this time period as opposed to the maritime westerlies flow that otherwise characterizes the northwestern European climate.

Acknowledgments We thank the MISTRALS/PALEOMEX program and ANR HAMOC (ANR-13-BS06-0003) for financial support.

References

1. Mayewski, P.A., Rohling, E.E., Stager, J.C., Karlén, W., Maasch, K.A., Meeker, L.D., Lee-Thorp, J.: Holocene climate variability. Quat. Res. **62**(3), 243–255 (2004)
2. Wanner, H., Mercolli, L., Grosjean, M., Ritz, S.P.: Holocene climate variability and change; a data-based review. J. Geol. Soc. London **172**, 254–263 (2014). https://doi.org/10.1144/jgs2013-101
3. Weiss, H.: Global megadrought, societal collapse and resilience at 4.2-3.9 ka BP across the mediterranean and west asia. PAGES **24**, 62–63 (2016)
4. Liu, F., Feng, Z.: A dramatic climatic transition at ~4000 cal. yr BP and its cultural responses in Chinese cultural domains. The Holocene **22**(10), 1181–1197 (2012)
5. Stanley, J., Krom, M., Cliff, R., et al.: Nile flow failure at the end of the Old Kingdom, Egypt: strontium isotopic and petrologic evidence. Geoarchaeology **18**, 395–402 (2003)
6. Weiss, H., Bradley, R.S.: What drives societal collapse? Science **291**(5504), 609–610 (2001)
7. Walker, M.J., Berkelhammer, M., Björck, S., Cwynar, L.C., Fisher, D.A., Long, A.J., Weiss, H.: Formal subdivision of the Holocene Series/Epoch: a discussion paper by a working group of INTIMATE (Integration of ice-core, marine and terrestrial records) and the subcommission on Quaternary Stratigraphy (International Commission on Stratigraphy). J. Quat. Sci. **27**(7), 649–659 (2012)
8. Jalali, B., Sicre, M.A., Bassetti, M.A., et al.: Holocene climate variability in the North–Western Mediterranean Sea (Gulf of Lions). Clim. Past **12**, 91–101 (2016)
9. Conte, M.H., Sicre, M.A., Rühlemann, C., Weber, J.C., Schulte, S., Schulz-Bull, D., Blanz, T.: Global temperature calibration of the alkenone unsaturation index (UK′ 37) in surface waters and comparison with surface sediments. Geochem. Geophys. Geosyst. **7**(2), (2006)
10. Fohlmeister, J., Vollweiler, N., Spötl, C., Mangini, A.: COMNISPA II: update of a mid-European isotope climate record, 11 ka to present. The Holocene **23**(5), 749–754 (2013)
11. Cheng, H., Sinha, A., Verheyden, S., Nader, F.H., Li, X.L., Zhang, P.Z., Ning, Y.F.: The climate variability in northern Levant over the past 20,000 years. Geophys. Res. Lett. **42**(20), 8641–8650 (2015)
12. Ruan, J., Kherbouche, F., Genty, D., Blamart, D., Cheng, H., Dewilde, F., Michelot, J.L.: Evidence of a prolonged drought ca. 4200 yr BP correlated with prehistoric settlement abandonment from the Gueldaman GLD1 cave, Northern Algeria. Clim. Past **12** (1), 1–14 (2016)
13. Zanchetta, G., Regattieri, E., Isola, I., Drysdale, R.N., Bini, M., Baneschi, I., Hellstrom, J.C.: The so-called "4.2 event" in the central Mediterranean and its climatic teleconnections. Alp Mediterr Quat **29**, 5–17 (2016)
14. Finné, M., Holmgren, K., Shen, C.C., Hu, H.M., Boyd, M., Stocker, S.: Late Bronze age climate change and the destruction of the Mycenaean Palace of Nestor at Pylos. PLoS ONE **12**(12), e0189447 (2017)
15. Reale, M., Lionello, P.: Synoptic climatology of winter intense precipitation events along the Mediterranean coasts. Nat. Hazards Earth Syst. Sci. **13**(7), 1707–1722 (2013)
16. Jackson, M.G., Oskarsson, N., Trønnes, R.G., McManus, J.F., Oppo, D.W., Grönvold, K., Sachs, J.P.: Holocene loess deposition in Iceland: evidence for millennial-scale atmosphere-ocean coupling in the North Atlantic. Geology **33**(6), 509–512 (2005)
17. O'brien, S.R., Mayewski, P.A., Meeker, L.D., Meese, D., Twickler, M.S., Whitlow, S.I.: Complexity of Holocene climate as reconstructed from a Greenland ice core. Science **270**(5244), 808 (1995)
18. Olsen, J., Anderson, N.J., Knudsen, M.F.: Variability of the North Atlantic Oscillation over the past 5,200 years. Nat. Geosci. **5**(11), 808 (2012)
19. Häkkinen, S., Rhines, P.B., Worthen, D.L.: Atmospheric blocking and Atlantic multidecadal ocean variability. Science **334**(6056), 655–659 (2011)
20. Hughes, P.D., Mauquoy, D., Barber, K.E., Langdon, P.G.: Mire-development pathways and palaeoclimatic records from a full Holocene peat archive at Walton Moss, Cumbria, England. The Holocene **10**(4), 465–479 (2000)
21. Korhola, A., Vasko, K., Toivonen, H.T., Olander, H.: Holocene temperature changes in northern Fennoscandia reconstructed from chironomids using Bayesian modelling. Quat. Sci. Rev. **21**(16–17), 1841–1860 (2002)
22. Plunkett, G.M., Whitehouse, N.J., Hall, V.A., Brown, D.M., Baillie, M.G.L.: A precisely-dated lake-level rise marked by diatomite formation in northeastern Ireland. J. Quat. Sci. **19**(1), 3–7 (2004)
23. Sicre, M.A., Jalali, B., Martrat, B., Schmidt, S., Bassetti, M.A., Kallel, N.: Sea surface temperature variability in the North Western Mediterranean Sea (Gulf of Lion) during the Common Era. Earth Planet. Sci. Lett. **456**, 124–133 (2016)

Record of Early Cretaceous Oceanic Anoxic Events in Adriatic Platform, Croatia

Antun Husinec and J. Fred Read

Abstract

The long (700 m) Hauterivian to Albian Adriatic Platform section mainly from Mljet Island, Croatia underwent little post-Mesozoic burial or little later diagenesis. Consequently its smoothed $\delta^{13}C$ and $\delta^{18}O$ record from calcite lime mudstone matrix provides one of the most continuous stable-isotope curves from an Early Cretaceous platform. This record captures the carbon isotope excursions (CIEs) and oceanic anoxic events (OAE1a, b, c) evident in published hemipelagic sections, with the added advantage of providing information on the shallow platform response to the OAEs. The platform facies appear to have been little affected by the OAEs, except for OAE1a when deposition of organic-rich laminated limestones occurred in local downwarps.

Keywords

Oceanic anoxic event • Carbon isotope excursion • Carbonate diagenesis • Early cretaceous • Adriatic platform

1 Introduction

Mesozoic carbon-isotope excursions were mainly documented from deep water facies and used to document major periods of oceanic anoxic events or OAEs as well as long- and short-term changes in carbon cycling [1–4]. In contrast, Mesozoic shallow carbonate platforms also may preserve a record of $\delta^{13}C$ excursions (albeit somewhat noisier), with the potential advantage that the history of relative sea-level changes on the platform are preserved in the facies successions and the platform response to the OAE can be ascertained [5–8]. We described a long duration, 30 m.y. Early Cretaceous, Hauterivian through Albian $\delta^{13}C$ and $\delta^{18}O$ record from the Adriatic Platform, southern Croatia, which underwent little post-Mesozoic burial or later diagenesis.

2 Methods

The $\delta^{13}C$ (and $\delta^{18}O$) stratigraphy is based on lime mudstone matrix generally sampled at 1 m intervals on Mljet Island, southern Croatia (Fig. 1). Dolomites and diagenetic cement-bearing packstones and grainstones were excluded [9, 10].

3 Results

The Adriatic Platform $\delta^{13}C$ curve captures the isotope excursions evident in the hemipelagic sections. The Faraoni OAE is evident as the negative excursion just below the top of the Barremmian. The OAE1a is well defined on the Adriatic Platform, as the major negative excursion followed by more positive $\delta^{13}C$ values. The major negative excursion of Niveau Fallot in the basin is subdued but present on the Adriatic platform. This is followed by the major negative excursion of the OAE1b set straddling the Aptian–Albian boundary. OAE1c is well developed on the Adriatic Platform as a major negative followed by a positive excursion. The oxygen isotope data proved unreliable as it was reset. Fischer plots were used to examine long-term accommodation and sea-level change but they proved to be of limited value due to common poorly cyclic subtidal intervals.

4 Discussion

Some diagenetic resetting of the platform lime mudstones is indicated by their $\delta^{13}C$ and $\delta^{18}O$ values which are only slightly lower (by ~2‰) than Early Cretaceous pelagic values [10, 11]. Although negative shifts in $\delta^{13}C$ and $\delta^{18}O$

A. Husinec (✉)
St. Lawrence University, Canton, NY 13617, USA
e-mail: ahusinec@stlawu.edu

J. Fred Read
Emeritus, Virginia Tech, Blacksburg, VA 24061, USA

Z. Zhang et al. (eds.), *Patterns and Mechanisms of Climate, Paleoclimate and Paleoenvironmental Changes from Low-Latitude Regions*, Advances in Science, Technology & Innovation, https://doi.org/10.1007/978-3-030-01599-2_4

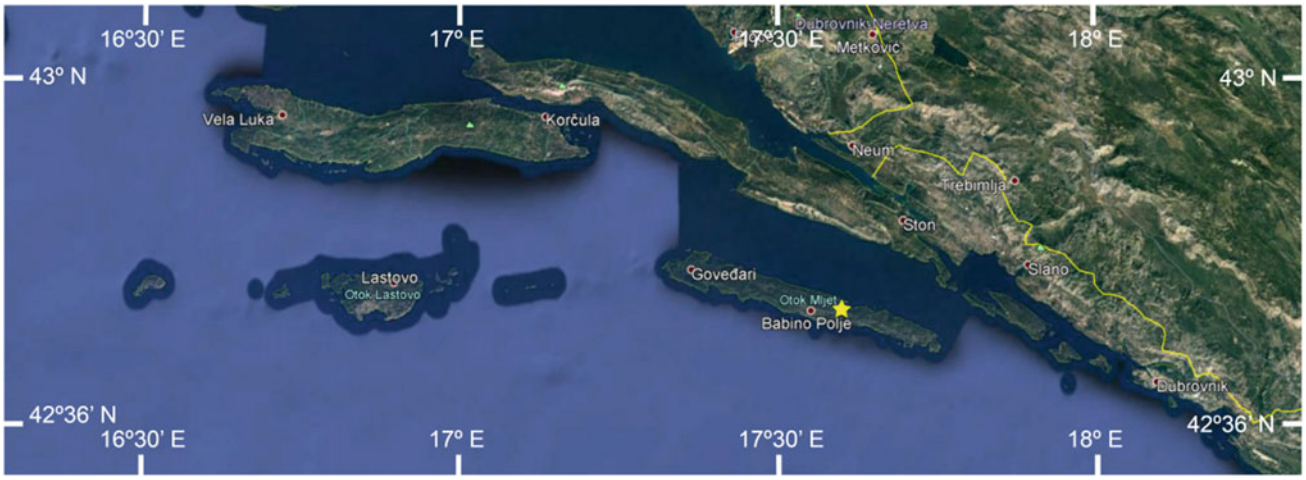

Fig. 1 Satellite image (© 2018 Google) of southern Croatia. Yellow star indicates location of the Mljet Island section

beneath unconformities are commonly observed, they only occur in sequence boundary zones, and affect very little of the stratigraphic succession [5, 6].

The negative excursions in $\delta^{13}C$ associated with the OAEs and CIEs have been attributed to input of ^{13}C into the oceans which caused warming, increasingly humid conditions. The positive CIEs resulted from the sequestration of C_{org}, resultant drawdown of atmospheric CO_2, and cooling [12–14]. We do not have usable oxygen data.

5 Conclusion

The Hauterivian to Albian Adriatic Platform section (Mljet and Korčula Islands), which for most intervals had predominantly calcite precursor mineralogies, underwent little post-Mesozoic burial or attendant diagenesis. It thus provides one of the most continuous Early Cretaceous platform $\delta^{13}C$ and $\delta^{18}O$ curves, including OAE1a, b and c. Although somewhat noisier than the hemipelagic/pelagic record, the Adriatic Platform recorded the major relative changes in $\delta^{13}C$ and $\delta^{18}O$ of platform waters over 30 m.y. at several time scales, in spite of periodic emergence, and thus provides an important repository of carbon cycling and relative sea-level changes.

References

1. Schlanger, S.O., Jenkyns, H.C.: Cretaceous oceanic anoxic events: causes and consequences. Geol. Mijnbouw **55**, 179–184 (1976)
2. Menegatti, A.P., Weissert, H., Brown, R.S., Tyson, R.V., Farrimond, P., Strasser, A., Caron, M.: High-resolution $\delta^{13}C$ stratigraphy through the early Aptian "Livello Selli" of the Alpine Tethys. Paleoceanography **13**, 530–545 (1998)
3. Luciani, V., Cobianchi, M., Jenkyns, H.C.: Albian high-resolution biostratigraphy and isotope stratigraphy: the Coppa della Nuvola pelagic succession of the Gargano promontory (southern Italy). Eclogae Geol. Helv. **97**, 77–92 (2004)
4. Föllmi, K.B.: Early Cretaceous life and anoxia. Cretac. Res. **35**, 230–257 (2012)
5. Grötsch, J., Billing, I., Vahrenkamp, V.: Carbon-isotope stratigraphy in shallow water carbonates: implications for Cretaceous black-shale deposition. Sedimentology **45**, 623–634 (1998)
6. Jenkyns, H.C., Wilson, P.A.: Stratigraphy, paleoceanography and evolution of Cretaceous Pacific guyots: relics from a greenhouse Earth. Am. J. Sci. **299**, 341–392 (1999)
7. Vahrenkamp, V.C.: Chemostratigraphy of the lower Cretaceous Shu'aiba formation: a δ^{13} reference profile for the Aptian stage from the southern Neo-Tethys Ocean. In: van Buchem, F.S.P., Al-Husseini, M.I., Maurer, F., Droste, H.J. (eds.) Barremian-Aptian Strat. Hydrocarbon Habitat East. Arab. Plate GeoArabia Spec. Publ. **4**(1), 107–137 (2010)
8. Husinec, A., Read, J.F.: Cyclostratigraphic and $\delta^{13}C$ record of the lower Cretaceous Adriatic platform, Croatia: assessment of Milankovitch-forcing. Sed. Geol. **373**, 11–31 (2018)
9. Husinec, A., Harman, C.A., Regan, S.P., Mosher, D.A., Sweeney, R.J., Read, J.F.: Sequence development influenced by intermittent cooling events in the Cretaceous Aptian greenhouse, Adriatic platform, Croatia. Am. Assoc. Petrol. Geol. Bull. **96**, 2215–2244 (2012)
10. Read, J.F., Husinec, A., Cangialosi, M., Loehn, C.W., Prtoljan, B.: Climate controlled, fabric destructive dolomitization and stabilization via marine- and synorogenic mixed fluids: an example from a large Mesozoic calcite-sea platform, Croatia. Palaeogeogr. Palaeoclimatol. Palaeoecol. **449**, 108–126 (2016)
11. Weissert, H., Erba, E.: Volcanism, CO_2 and palaeoclimate: a late Jurassic-early Cretaceous carbon and oxygen isotope record. J. Geol. Soc. **161**, 695–702 (2004)
12. Weissert, H.: Deciphering methane's fingerprint. Nature **406**, 356–357 (2000)
13. Jenkyns, H.C.: Evidence for rapid climate change in the Mesozoic-Palaeogene greenhouse world. Phylosophical Trans. R. Soc. Math. Phys. Eng. Sci. **361**, 1885–1916 (2003)
14. Robinson, S.A., Heimhoffer, U., Hesselbro, S.P., Petrizzo, M.R.: Mesozoic climates and oceans—a tribute to Hugh Jenkyns and Helmut Weissert. Sedimentology **64**, 1–15 (2017)

Sedimentological and Geochemical Records of Lower Cretaceous Carbonate Successions Around Trabzon (NE Turkey): Implications for Paleoenvironmental Evolution and Paleoclimatological Conditions of Tethys

Merve Özyurt, M. Ziya Kirmaci, İ. Ömer Yılmaz, and Raif Kandemir

Abstract

Upper Jurassic–lower Cretaceous carbonates (Berdiga Fm.) are widely exposed in the NE Turkey. An integrated study of sedimentological and geochemical analysis was carried out on the lower Cretaceous carbonates of Berdiga Fm. in Trabzon area in order to reveal the paleoenvironmental and paleoclimatological conditions of northern Tethyan Ocean. Three microfacies types were identified corresponding to inner to slope environments. Inner platform environment developed during the Hauterivian–Aptian interval. End of the Aptian, syn-sedimentary extensional tectonic regime might probably have caused the progressive deepening of the environment, so the inner platform environment evolved into an outer platform and then into slope during the late Aptian–Albian time. Additionally, $\delta^{18}O$ stable isotope values of the belemnites of studied section indicate that paleotemperature ranged between 25 and 26 °C during Aptian–Albian interval. Therefore warm Cretaceous climate conditions were recorded in the Eastern Pontides.

Keywords

Carbonates • Paleotemperature • Paleoenvironment NE Turkey

M. Özyurt (✉) · M. Ziya Kirmaci
Department of Geological Engineering, Karadeniz Technical University, 61080 Trabzon, Turkey
e-mail: merveyildiz@ktu.edu.tr

İ. Ömer Yılmaz
Department of Geological Engineering, Middle East Technical University, 06800 Ankara, Turkey

R. Kandemir
Department of Geological Engineering, Recep Tayyip Erdoğan University, 53100 Rize, Turkey

1 Introduction

The upper Jurassic–lower Cretaceous carbonates crop out extensively along with EW trending belt at the northern part of Turkey. They have the potential to serve as an excellent archive for paleoenvironment and paleoclimatic record of northern Tethyan Ocean (Fig. 1f). The carbonates successions in the western part of Turkey are well documented [1]. However, only a few studies studied the coeval carbonates that crop out in the eastern part of this belt [2]. Therefore, our study focused on the eastern part of Turkey (Fig. 1c, d) presenting new microfacies records of the lower Cretaceous carbonates, corroborated by detailed stable isotope analysis aimed at inferring paleoclimatic and paleoenvironmental conditions in NE Turkey.

2 Methods

Samples were collected from the studied stratigraphic section in Trabzon (NE Turkey) (Fig. 1a, c, d) and were examined under a polarizing microscope to determine the microfacies. Microfacies types were described and interpreted based on the textural and compositional characteristics [3, 4]. Stable isotope analyses ($\delta^{18}O$ and $\delta^{13}C$) of selected samples (belemnite) were conducted at the laboratories of the Friedrich-Alexander Universität Erlangen-Nürnberg (FAU). Carbonate powders were reacted with 100% phosphoric acid at 70 °C using a Gasbench II connected to a Thermo Fisher Delta V Plus mass spectrometer. All values are reported in per mil relative to V-PDB.

3 Results

3.1 Microfacies

In the study area comprising one of the rare typical exposures of the formation, the lower part is completely

Z. Zhang et al. (eds.), *Patterns and Mechanisms of Climate, Paleoclimate and Paleoenvironmental Changes from Low-Latitude Regions*, Advances in Science, Technology & Innovation, https://doi.org/10.1007/978-3-030-01599-2_5

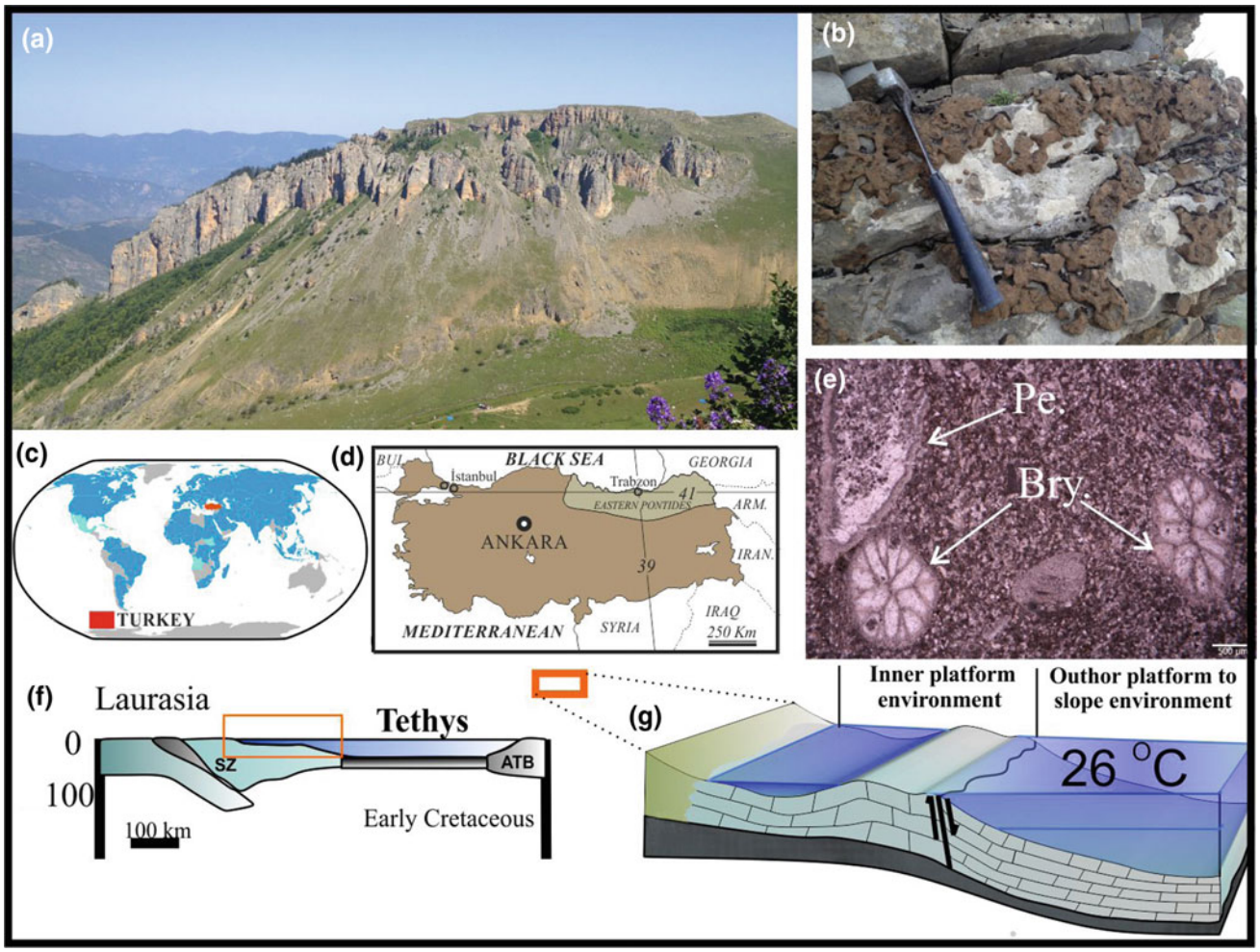

Fig. 1 **a** Field view of the section. **b** Limestone with chert nodules. **c** and **d** Location of study area. **e** Photomicrograph of the outer platform, Pe: pelecypoda, Bry: Bryozoa. **f** Schematic cross section of the NE Turkey (SZ) and **g** paleoenvironmental reconstruction of the study area

dolomitized. The middle and upper parts of the section are represented by grey-beige colored and medium-thick bedded limestone. General fauna community consists of benthic foraminifera. In addition, different facies contain echinoderm, belemnite, brachiopoda, pelecypoda, gastropoda, ostracoda, algae, sponge spicules and radiolaria with changing density. The middle and upper parts of the section are characterized by three different microfacies in time. (1) Benthic foraminiferal/peloidal packstone microfacies: The dominant carbonates are skeletal grains with an important amount of benthic foraminifera and pelloids. The fossil content of the facies indicates that these rocks were deposited in the interval of Hauterivian–Aptian times. (2) Allochtonous skeletal packstone microfacies: Almost all the entire carbonate component has been reworked, most of which are skeletal grains. Another important component is authigenic glauconite. (3) Sponge spicule packstone/wackestone microfacies: The carbonate components of these layers are generally represented by small benthic foraminifera and pelagic skeletal grains including radiolaria, calcisphere and Microhedbergellagi. The presence of *Microhedbergella rischi* indicates that the age of the facies is no older than late Albian [5].

3.2 Stable Isotope Analysis

Average $\delta^{13}C$ and $\delta^{18}O$ values of fossils are 1.47 and −3.57 respectively. The values agree well with early Cretaceous seawater, which enable us to reconstruct paleotemperature evidence. Paleotemperature calculations have been $14\ \Delta c + 0.13\ \Delta c^2$ [6]. $\delta^{18}O$ values for the non-glacial period were considered as −1.2 per mil (SMOW) [7]. The $\delta^{13}C$ curve of the whole sequence is sketched and correlated with published the $\delta^{13}C$ curve of the lower Cretaceous [8]. Moreover, the average temperature value for the fossil samples was taken as 26 °C.

4 Discussion

The middle part of the section is represented by benthic foraminiferal/peloidal packstone microfacies. According to benthic foraminifers, peloids, the lack of biodiversity and the muddy texture suggest that these beds were deposited on lagoon during the Hautrivian–Aptian. MF-1 corresponds to SMF18 [4]. Starting from the late Aptian, the inner platform environment changed into an outer platform with an abrupt transition to allochthonous facies. The predominance of bioclastic debris flow and local glauconitic grains imply that MF-2 deposited in the outer-platform to toe-of-slope (Fig. 1e, b). MF-2 corresponds to SMF 5-6 [4]. The gradual transition to the overlying MF-2, predominance of mud-rich texture, decrease in abundance of allochthonous fragments and presence of the planktonic organism indicate that the depositional environment was deeper and changed into a slope environment during the late Albian. MF-3 corresponds to SMF 3 [4] (Fig. 1g).

$\delta^{18}O$ values of the carbonates have widely been used to reconstruct the sea surface paleotemperature of the Tethyan Ocean and carbon isotope profiles were used for higher resolution stratigraphic correlations [9]. Therefore, carbon values derived from bulk rock samples and fossil shells were used to reconstruct paleoceanographic events and correlated with global and European carbon isotope profiles. Temperature value (26 °C) was conformable with the temperature interval recorded in the upper Barremian–lower Albian successions of the Caucasus and Russian basins [10]. Based on the paleotemperature analysis and carbon isotope profiles, a warm Cretaceous climate was characteristic of NE Turkey.

5 Conclusions

Microfacies analyses suggest that the inner platform environment existed during the Hauterivian–Aptian. However, the syn-sedimentary extensional tectonic regime might have caused the progressive deepening of the environment during the late Aptian–Albian time. So the inner platform evolved into an outer platform to a slope environment. Based on paleotemperature analysis and carbon isotope profiles a warm Cretaceous climate was characteristic of NE Turkey (Fig. 1f, g).

Acknowledgements The authors would like to thank Karadeniz Technical University (Project no.: FBA-2015-5160) and TUBİTAK (ÇAYDAG, Project no.: 115Y005 and International PhD Research Scholarship Program-2214-A-BIDEP) for their financial support. The authors wish to thank Prof. Dr. Ihsan Al-Aasm (University of Windsor, Canada) for his support and Prof. Dr. Kemal TASLI (Mersin University, Turkey) for the foraminifera determinations.

References

1. Yılmaz, C.: Platform–slope transition during rifting: the mid-Cretaceous succession of the Amasya region (northern Anatolia), Turkey. J. Asian Earth Sci. **27**(2), 194–206 (2006)
2. Vincent, S.J., Guo, L., Flecker, R., BouDagher-Fadel, M.K., Ellam, R.M., Kandemir, R.: Age constraints on intra-formational unconformities in upper Jurassic-lower Cretaceous carbonates in northeast Turkey; geodynamic and hydrocarbon implications. Mar. Petrol. Geol. **91**, 639–657 (2018)
3. Dunham, R.J.: Classification of Carbonate Rocks According to Depositional Textures (1962)
4. Flügel, E.: Microfacies Analysis of Carbonate Rocks. Analysis, Interpretation and Application. Springer, Berlin (2004)
5. Huber, B.T., Leckie, R.M.: Planktic foraminiferal species turnover across deep-sea Aptian/Albian boundary sections. J. Foramin. Res. **41**(1), 53–95 (2011)
6. Sharp, Z.D.: Principles of Stable Isotope Geochemistry, 2nd edn, p. 310. http://digitalrepository.unm.edu/unm_oer/1 (2017)
7. Vincent, B., Emmanuel, L., Houel, P., Loreau, J.P.: Geodynamic control on carbonate diagenesis: petrographic and isotopic investigation of the upper Jurassic formations of the Paris Basin (France). Sediment. Geol. **197**(3), 267–289 (2007)
8. Scott, R.W.: Barremian–Aptian–Albian carbon isotope segments as chronostratigraphic signals: numerical age calibration and durations. Stratigraphy **13**, 21–47 (2016)
9. Price, G.D., Passey, B.H.: Dynamic polar climates in a greenhouse world: evidence from clumped isotope thermometry of early Cretaceous belemnites. Geology **41**(8), 923–926 (2013)
10. Zakharov, Y.D., Kakabadze, M.V., Sharikadze, M.Z., Smyshlyaeva, O.P., Sobolev, E. S., Safronov. P.P.: The stable O- and C-isotope record of fossils from the upper Barremian-lower Albian of the Caucasus-paleoenvironmental implications. Cretac. Res. 1–19 (2017, in press)

Part III
Paleoclimate Evolution

Paleoclimate Evolution of the Kordofan Region (Sudan), During the Last 13 ka

Ahmed Dawelbeit, Etienne Jaillard, and Ali Eisawi

Abstract

The Kordofan region is located at the southern end of the present-day Sahara in Sudan. AMS ^{14}C dates and archeological findings allowed dating the latest Pleistocene–Holocene deposits in Kordofan. Several paleo-proxies (i.e., sedimentology, gastropod sub-fossil shells, pollens, stable isotopes, major element chemistry, and clay mineralogy) were used to reconstruct the climatic evolution for the past 13 ka. The region was subjected to an arid climate prior to 10 ka. Between 10 and 6 ka, the region experienced a wet climate marked by lacustrine/palustrine and fluviatile deposits. After ≈6 ka, the climate evolved to dry conditions, although the southern part remained more humid. Between 3 and 1 ka, a strong aeolian activity was recorded by a sedimentary hiatus and erosion features. From 1 ka to Present, the region became arid. This evolution can be correlated to the well-known evolution of Eastern Sahara during this time interval.

Keywords

Holocene • NE Africa • Stable isotopes
Climate • Kordofan region

1 Introduction

The period between 20 and 12 ka is well documented as a period of dune building in Northeast Africa [1]. This hyper-arid period was followed by a humid phase between ≈12 and 6 ka (African Humid Period, AHP) [2], marked by the occurrence of numerous lakes [2], locally exceptionally large [3]. The subsequent development of the Sahara Desert is recorded by the migration of prehistoric populations toward the present day Sahelian zone or the Nile valley in the last 10 ka [4].

The Kordofan region (Sudan) is located at the southern limit of the Eastern Sahara; however, its latest Quaternary climate evolution has never been studied. This paper is focused on the understanding of the climate evolution of central Kordofan during the latest Quaternary using several paleo-proxies of climate.

2 Methodology

Two field campaigns were carried out in Kordofan, complemented with short field works, which allowed us to perform a sedimentological study and a collection of 119 samples for further laboratory analyses. The latter includes AMS ^{14}C dating, paleo-biology of gastropods, palynology, stable isotopes of C and O, XRF of major elemental measurements and clay mineralogy.

3 Results

3.1 Sedimentology and Stratigraphy

The study of 24 sedimentological sections and 17 AMS ^{14}C dates from charcoal and organic-rich soils and limestone, allowed us to distinguish four main chronological units, corresponding to five main climatic periods (Fig. 1b).

A. Dawelbeit (✉)
Department of Geology, Faculty of Science,
Kordofan University, El Obeid, Sudan
e-mail: Ahmeddawelbeit69@gmail.com

E. Jaillard
Grenoble Alpes University, ISTerre,
IRD-CNRS-IFSTTAR-USMB, Grenoble, France

A. Eisawi
Faculty of Petroleum and Minerals, Al-Neelain University,
Khartoum, Sudan

Z. Zhang et al. (eds.), *Patterns and Mechanisms of Climate, Paleoclimate and Paleoenvironmental Changes from Low-Latitude Regions*, Advances in Science, Technology & Innovation, https://doi.org/10.1007/978-3-030-01599-2_6

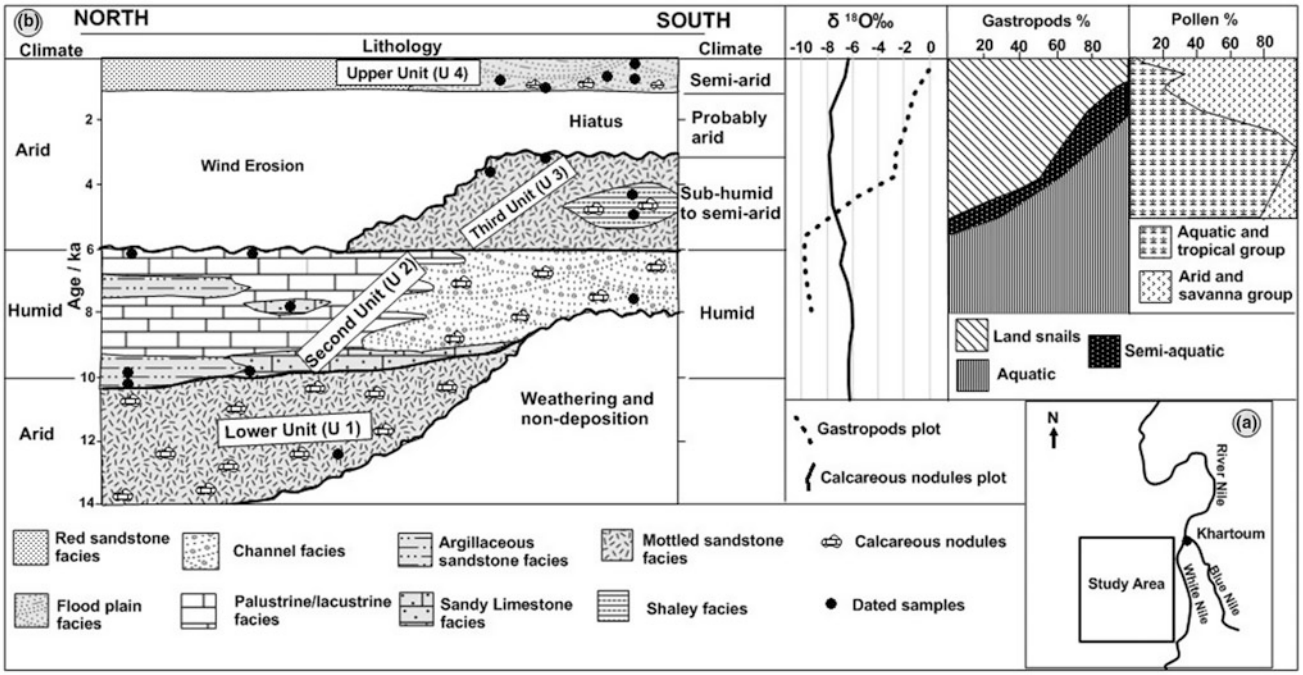

Fig. 1 **a** Location map, **b** summary of paleoclimate results

- The lowest unit (U1) is made of fine to coarse sands, subsequently pedogenetized (mottling, calcareous nodules), which yielded ages varying from ≈13 to 10 ka.
- The second unit (U2) consists of palustrine limestones in the northern and central part, and of fluviatile deposits in the southern part. ^{14}C ages vary from ≈10 to 6 ka in the North and from ≈8 to 6 ka in the South.
- The third unit (U3) is restricted to the southern part. It is formed of mottled sandstone and sandy shales. ^{14}C ages vary from ≈5 to 3 ka.
- A hiatus, detected between ≈6 and 1 ka in the North and between ≈3 and 1 ka in the South, and locally materialized by deflation surfaces, is interpreted as a period dominated by strong wind erosion, which occurred between ≈3 and 1 ka (Fig. 1b).
- The upper or fourth unit (U4) is formed of red sandstone in the North, replaced gradually by flood plain sediments to the South. Its maximum age is ≈1.1 ka.

In all units, grain size in sands decreases, and sorting increases, southward, suggesting deposition related to dominant southward blowing winds. Moreover, the South–North evolution of these units indicates that the southern area was more submitted to fluviatile influences than the northern ones during Holocene times.

3.2 Paleobiology

The vertical distribution of gastropod sub-fossil shells shows that aquatic and semi-aquatic gastropod species dominated in the palustrine limestone (U2), while land snails dominated in U4. This indicates that U2 was deposited under wetter conditions than U4.

22 samples from 3 sections from the southern area were analyzed for palynological investigation. 1213 counted pollens and spores were classified into 4 groups, representing aquatic, tropical, savanna and arid environments. Pollen assemblages from U3 are dominated by the aquatic, tropical and savanna groups indicating wet conditions, while those from the U4 are from the arid environments, reflecting dry conditions.

3.3 Stable Isotopes

49 samples of gastropod shells (3 sites) and calcareous nodules (2 sites) for oxygen and carbon isotopes. Gastropod shells of the U2 are depleted in ^{18}O, while those from the U4 show a rapid ^{18}O enrichment upward. Coeval depletion in δ^{18}O recorded in the Nile valley has been interpreted as due to high rainfall episodes [5]. The enrichment in ^{18}O in the

U4 can be interpreted as the result of a strong evaporation [6], reflecting drier conditions [5]. The calcareous nodules are generally depleted in ^{18}O, with little variability through time.

3.4 Geochemistry and Clay Mineralogy

23 samples from the U1 and U4 of two sections were analyzed for major elements. The calculated Chemical Index of Alteration (CIA) [7] is high for both the U1 and U4. High CIA values (76–100) in sedimentary rocks suggest intense chemical weathering in the source region [8].

8 samples from U1, U3 and U4 of one section show a remarkable predominance of smectite and kaolinite, while illite is less dominant. Smectite decreases upward, while kaolinite shows an opposite trend. These results suggest that the source areas were more submitted to chemical weathering than physical weathering, especially during the deposition of U4.

4 Discussion

The evolution of the Kordofan region can be summarized as follows. Aeolian deposition took place prior to ≈10 ka and covered most of the studied area. We correlate this arid period with the 20–12 ka interval, which is known as an arid period of dune building in northeastern Africa.

Palustrine–lacustrine limestone, pollens of humid vegetation, aquatic gastropods and depletion in $\delta^{18}O$ in the gastropods shells are recorded between 10 and 6 ka, and evidence a wet climate during the early to middle Holocene. This wet event is correlated with the AHP [2, 3], during which the present-day hyper-arid Sahara Desert was vegetated and covered by numerous lakes [9]. The exact start and termination dates of this wet phase could not be accurately determined, since part of the corresponding sediments were removed by subsequent aeolian erosion. According to previous works, this wet phase occurred between 11–9 and 6–4.5 ka in Northeast Africa [3, 10, 11].

The late Holocene period (≈6 ka to Present) recorded drier conditions in the northern part of the study area, while the southern part remained wetter. This aridification is well documented in Eastern Sahara [12]. As illustrations, we can mention northern Chad experienced a progressive drying out due to an abrupt hydrological change [13], palynological evidence from Lake Yoa (Chad) indicate a gradual shift from moist to arid condition during the last 6 ka [14], and desertification and aeolian deflation occurred during the Middle and Late Holocene in Egypt and northern Sudan [15].

5 Conclusion

The study of the sedimentary record of the Kordofan region allowed the reconstructions of the climate variability since 13 ka, based on the sedimentological, geochemical and paleontological analyses. The climate evolution can be summarized as follows: dry conditions prior to ≈10 ka, wet conditions between ≈10 and 6 ka, wet to dry conditions from ≈6 to 3 ka, dry from ≈3 to 1 ka associated with strong aeolian erosion, and dry after 1 ka, although wetter in the south. These climate changes can be correlated to the well-known climatic evolution of Eastern Sahara during this interval. These results highlight the climate changes along the still poorly known southern limit of Eastern Sahara.

References

1. Williams, M.A.J.: Late Pleistocene and Holocene environments in the Nile basin. Global Planet. Change **69**, 1–15 (2009)
2. deMenocal, P., Ortiz, J., Guilderson, T., Adkins, J., Sarnthein, M., Baker, L., Yarusinsky M.: Abrupt onset and termination of the African Humid Period: rapid climate responses to gradual insolation forcing. Quatern. Sci. Rev. **19**, 347–361 (2000)
3. deMenocal, P.B., Tierney J.E.: Green Sahara: African Humid Periods paced by Earth's orbital changes. Nat. Educ. Knowl. **3** (2012)
4. Kuper, R., Kröpelin, S.: Climate-Controlled Holocene Occupation in the Sahara: Motor of Africa's Evolution. Science **313**, 803–807 (2006)
5. Abell, P., Williams, M.: Oxygen and carbon isotope ratios in gastropod shells as indicators of paleoenvironments in Afar region of Ethiopia. Palaeogeography, Palaeoclimatology, Palaeo-ecology **74**, 265–278 (1989)
6. Leng, M.J., Marshall, J.D.: Palaeoclimate interpretation of stable isotope data from lake sediment archives. Quatern. Sci. Rev. **23**, 811–831 (2004)
7. Nesbitt, H.W., Young, G.M.: Early Proterozoic climates and plate motions inferred from major elements chemistry of lutites. Nature **299**, 715–717 (1982)
8. Madhavaraju, J., Ramírez-Montoya, E., Monreal, R., González–León, C.M., Pi-Puig, T., Espinoza-Maldonado, I.G., Grijalva–Noriega, F.J.: Paleoclimate, paleoweathering and paleoredox conditions of Lower Cretaceous shales from the Mural Limestone, Tuape section, northern Sonora, Mexico: Constraints from clay mineralogy and geochemistry: Revista Mexicana de Ciencias Geológicas **33**(1), 34–48 (2016)
9. Cole, J.M., Goldstein, S.L., deMenocal, P.B., Hemming, S.R., Grousset, F.E.: Contrasting compositions of Saharan dust in the eastern Atlantic Ocean during the last deglaciation and African Humid Period. Earth Planet. Sci. Lett. **278**, 257–266 (2009)
10. Pachur, H.J., Kröpelin, S.: Wadi Howar: Paleoclimatic evidence from an extinct river system in the Southeastern Sahara. Science **237**, 298–300 (1987)
11. Tierney, J.E., Lewis, S.C., Cook, B.I., LeGrande, A.N., Schmidt, G.A.: Model, proxy and isotopic perspectives on the East African Humid Period. Earth Planet. Sci. Lett. **307**, 103–112 (2011)

12. Tierney, J.E., deMenocal, P.B.: Abrupt shifts in Horn of Africa hydroclimate since the Last Glacial Maximum. Science **342**, 843–846 (2013)
13. Kröpelin, S., Verschuren, D., Lézine, A.-M., Eggermont, H., Cocquyt, C., Francus, P., Cazet, J.-P., Fagot, M., Rumes, B., Russell, J.M., Darius, F., Conley, D. J., Schuster, M., von Suchodoletz, H., Engstrom, D.R.: Climate-driven ecosystem succession in the Sahara: the past 6000 years. Science **320**, 765–768 (2008)
14. Lézine, A.-M., Zheng, W., Braconnot, P., Krinner G.: A late Holocene pollen and climate record from Lake Yoa, northern Chad. Clim. Past Discuss **7**, 2413–2444 (2011)
15. Nicoll, K.: Recent environmental change and prehistoric human activity in Egypt and Northern Sudan. Quatern. Sci. Rev. **23**, 561–580 (2004)

Use of Paleoclimate Rainfall Data to Detect Mega Drought Signals

Joo-Heon Lee, Chanyang Sur, and Seo-Yeon Park

Abstract

This study aimed to provide a historical mega drought information of Korea using the long-term precipitation for longer than 300 years that were observed by the Korean Meteorological Administration (KMA) during 1908–2015, and paleo-climate data by the Korea's ancient rain gauge (Chuk-Woo-Kee) during 1777–1907 and future climate change scenario from 2017 to 2099. The statistical analysis results showed that annual average precipitation were considerably different between records by the Chuk-Woo-Kee and records by the KMA. Precipitation data by the Chuk-Woo-Kee has seriously decreasing trends but KMA observed data show significant increasing trends because of climate change effect. Through the analysis of drought using paleoclimatic data observed by Chuk-Woo-Kee, mega drought on the Korean Peninsula lasting for 20 years at the end of the 19th century could be confirmed. It can also be concluded that extreme drought, which began in 2014, may be the beginning of another; the mega drought on the Korean peninsula based on the drought periodicity analysis.

Keywords

Mega drought • Chuk-Woo-Kee • Rainfall • Drought • Paleo climate

1 Introduction

Drought is a frequent occurrence that has overwhelmed civilization all over antiquity. It is one of the foremost natural reasons of extensive agricultural, socioeconomic, and environmental damage [2, 3]. Drought indices such as standardized precipitation index (SPI) and Palmer drought severity index (PDSI) are mainly used to analyze drought quantitatively and a great deal of research on drought using precipitation data have progressed continuously. However, long-term observation data for longer than few decades are required in order to quantitatively analyze mega droughts. For this reason, precipitation data from Chuk-Woo-Kee whose observed records are preserved since the late 1700s and the climate change scenarios in Seoul area will be very useful in analyzing the past, present, and future drought. In order to analyze the statistical characteristics of mega drought events in Seoul area, this study was carried out to investigate statistical characteristics of the precipitation in Seoul. Paleo precipitation data (1777–1907) restored through archives such as Seung-Jung-Won Diary and Ilseongrok, modern observed precipitation at Seoul (1908–1949, 1953–2015) for longer than 100 years by the automated weather station (AWS), RCP 8.5 scenario's precipitation data (2016–2099) from HadGEM2-AO were used for the analysis. We also aimed to quantitatively evaluate the mega droughts in Seoul area by analyzing their severity, duration, and magnitude.

2 Data and Methods

2.1 Chuk-Woo-Kee (Korean Ancient Rain Gauge)

The "Chuk-Woo-Kee", invented in 1441, the Joseon Dynasty of Korea, was recognized as one of the most significant inventions in hydrological history because it was the first scientific rain gage in the world. In Europe, in 1639,

J.-H. Lee (✉) · S.-Y. Park
Joongbu University, Goyang, Gyeonggi-do 10279, Republic of Korea
e-mail: leejh@joongbu.ac.kr

C. Sur
Drought Research Center, Joongbu University, Goyang, Gyeonggi-do 10279, Republic of Korea

Z. Zhang et al. (eds.), *Patterns and Mechanisms of Climate, Paleoclimate and Paleoenvironmental Changes from Low-Latitude Regions*, Advances in Science, Technology & Innovation, https://doi.org/10.1007/978-3-030-01599-2_7

B. Gustetelli of Italy observed rainfall for the first time with the invented rain gage. In France, rainfall has been observed since 1658 in Paris and from 1677 in England. In Korea, the rainfall was measured from May 1442, which is about 200 years earlier than Italy. In 1442 (King Sejong's 24th year), the observation system including Chuk-Woo-Kee's specifications and observation methods was established and a nationwide observation network was set up.

2.2 Precipitation

In this study, three different time window's precipitation data were used to perform drought research using long-term rainfall data for Seoul. Firstly, the rainfall data during Joseon dynasty (1777–1907) restored by Jun and Moon [1] by Chuk-Woo-Kee records in the Seung-Jung-Won Palace Diary and Ilseongrok were used. Secondly, the precipitation data of the Seoul rain gauge (1908–2015) by KMA (Korean Meteorological Agency) were used. Thirdly, we used future precipitation data (2016–2099) for Seoul based on the RCP 8.5 climate change scenario, which was obtained by ensemble the climate change prediction model HadGEM2-ES.

2.3 Drought Index

In order to quantitatively evaluate the drought at Seoul, the SPI (Standardized Precipitation Index) which is a representative meteorological drought index that can be estimated from rainfall data was conducted. Figure 1 shows the results of SPI (6) using the monthly precipitation data in Seoul during 1777–2099. The results were categorized into ancient (1777–1907), modern (1908–2010), and future (2011–2099) periods.

3 Results

3.1 Drought Periodicity

The Wavelet transform analysis was carried out using the SPI (6) for the estimated entire period to understand the periodicity of the droughts that occurred during the subjected period. Figure 2 shows that the periodicity analysis results and the overall drought period of 6 years is very strong for the paleo and modern climate.

3.2 Mega Drought

The following Table 1 shows the drought years that occurred over 3 consecutive years in the whole period by the drought spell analysis technique. Most extreme droughts occurred at the end of the Joseon Dynasty and lasted more than 10 years.

4 Conclusions

The following conclusions could be drawn from this study.

1. The long-term precipitation records analysis over 300 years to analyze Mega drought signal on the Korean

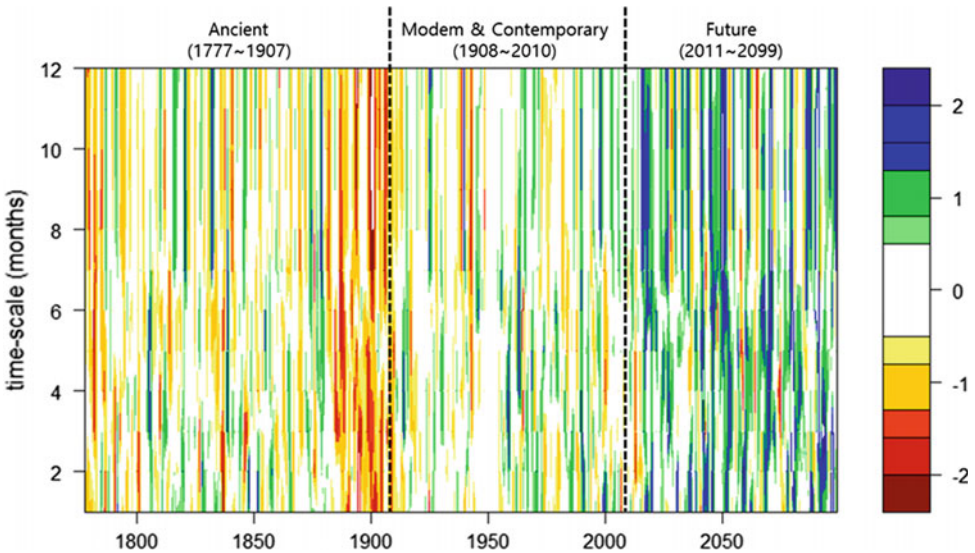

Fig. 1 SPI (6) of Seoul gaging station from 1777 to 2099

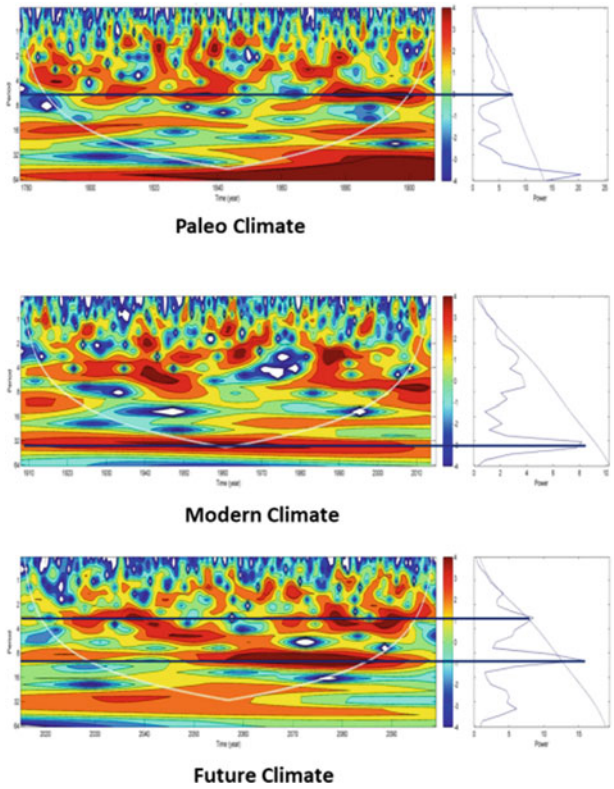

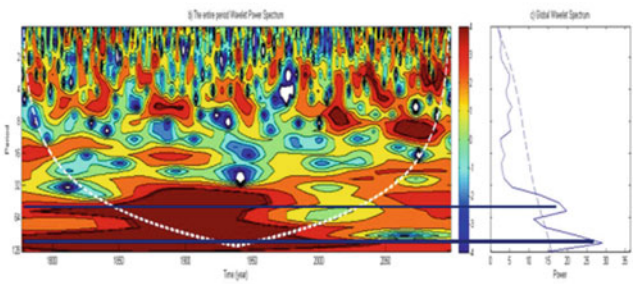

Era	Periodicity (year)
Paleo Climate	6
Modern Climate	4~6, 32
Future Climate	3, 8
Entire Period	6, 50, 120

Fig. 2 Wavelet analysis of SPI (6) for 3 different periods

Table 1 Extreme drought for consecutive multiyear droughts

Rank	Drought year	Successive year	Average severity	Drought duration (months)	Drought magnitude
1	1899–1902	4	−1.60	47	−75.15
2	1893–1895	3	−1.26	34	−42.99
3	1887–1889	3	−1.25	34	−42.64
4	1782–1783	2	−1.25	22	−27.59
5	2014–2015	2	−1.09	24	−26.15

Peninsula shows that the future (2016–2099) shows a significant increase in annual precipitation due to climate change.

2. Ancient precipitation observations recorded by Chuk Woo Kee revealed statistical characteristics such as the duration, severity, and magnitude of Mega drought, which lasted more than 10 years (1887–1902) at the end of Joseon Dynasty.
3. The recent observations recorded by the Korea Meteorological Administration (1908–2015) showed no mega drought and the most recent three-year drought in 2014–2016 was the most extreme.

Acknowledgements This research was supported by Basic Science Research Program through the National Research Foundation of Korea (NRF) funded by the Ministry of Education (NRF-2017R1D1A1A02018546).

References

1. Jun, J.G., Moon, B.K.: Restorations and analyses of rainfall amount observed by Chukwookee. J. Korean Meteorol. Soc. **33**(4), 691–707 (1997)
2. Lee, J.H., Kwon, H.H., Jang, H.W., Kim, T.W.: Future changes in drought characteristics under extreme climate change over South Korea. Adv. Meteorol. **2016**, 19 (2016)
3. Lee, J.H., Seo, J.W., Kim, C.J.: Analysis on trends, periodicities and frequencies of Korean drought using drought indices. J. Korea Water Res. Assoc. **45**(1), 75–89 (2012)

Paleoclimatology Evidence of Eocene from Jaddala Formation in Northwestern Iraq

Alaa Al-Zubaidi and Omar Al-Badrani

Abstract

Two hundred species of calcareous Nannofossils were identified from the Jaddala Formation from type section (stratotype) northwestern Iraq. The recorded of the calcareous nannofossils assemblages enables the recognition of the following four biozones which are (from older to younger):

Tribrachiatus orthostylus Interval Biozone (CP10) (Part)
Discoaster lodoensis Interval Biozone (CP11)
Discoaster sublodoensis Interval Biozone (CP12)
Nannotetrina quadrata interval Range Biozone (CP13).

On the basis of biocorrelation with previous works Early to Middle Eocene age was confirmed for the Jaddala Formation at the studied section (near Mosul, Iraq), and the paleoclimate was warm referred as tropical to subtropical at low latitude areas.

Keywords

Eocene • Paleoclimatology • Jaddala

1 Introduction

Jaddala Formation was first described by Hensen, 1040 in Bellen et al. [2], near Jaddala village at southern limb of Sinjar anticline Northwestern Iraq, and is about 342 m in thickness and consists of marly Limestone, chalky Limestone and Marlstone. The studied section (see Fig. 1) is situated in the stable shelf tectonic unit of Iraq, the same section (stratotype) as that in Buday and Jassim [3]. In most of the Tertiary, *Discoasters* are the most common solution-resistant taxa in low latitudes, whereas Prinsiaceae or Coccolith species are the most common solution-resistant taxa in high latitudes [7].

2 Materials and Methods

Fifty one samples were collected from Jaddala Formation at type section, Northwestern Iraq, and the calcareous nannofossils were extracted using the method (H) from Armstrong and Brasier [1].

3 Results

The studied classification which was based on Perch-Nielsen [7] and Young and Bown [8] assigned two handers species of Calcareous Nannofossils identified at the Jaddala Formation from the northwestern section (stratotype) of Iraq. The recorded calcareous nannofossils assemblages enabled the recognition of four biozones (see Fig. 2) organized from older to younger):

Tribrachiatus orthostylus Interval Biozone (CP10) (Part)
Discoaster lodoensis Interval Biozone (CP11)
Discoaster sublodoensis Interval Biozone (CP12)
Nannotetrina quadrata interval Range Biozone (CP13).

On the basis of biocorrelation with previous works [6], Early to Middle Eocene [4] was confirmed for the Jaddala Formation at the studied section, and the paleoclimate was worm water referred to as tropical to subtropical at low latitude areas (see Fig. 2).

A. Al-Zubaidi
Department of Geography, Education College, Hamdaniya, Mosul, Iraq

O. Al-Badrani (✉)
Department of Geology, Science College, Mosul University, Mosul, Iraq
e-mail: omarbadrani@yahoo.com

Z. Zhang et al. (eds.), *Patterns and Mechanisms of Climate, Paleoclimate and Paleoenvironmental Changes from Low-Latitude Regions*, Advances in Science, Technology & Innovation, https://doi.org/10.1007/978-3-030-01599-2_8

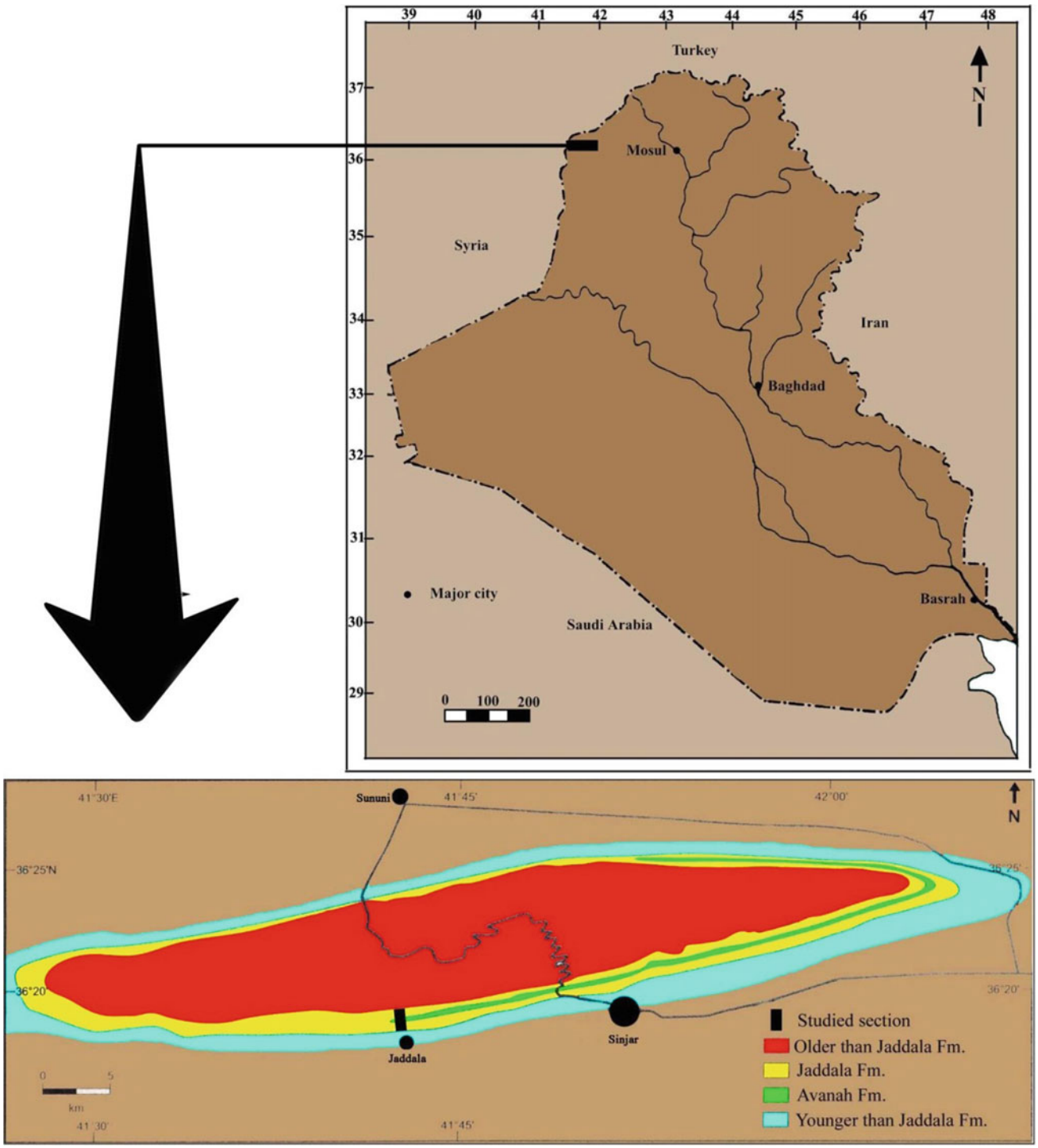

Fig. 1 Location map of the studied area (after Maala [5])

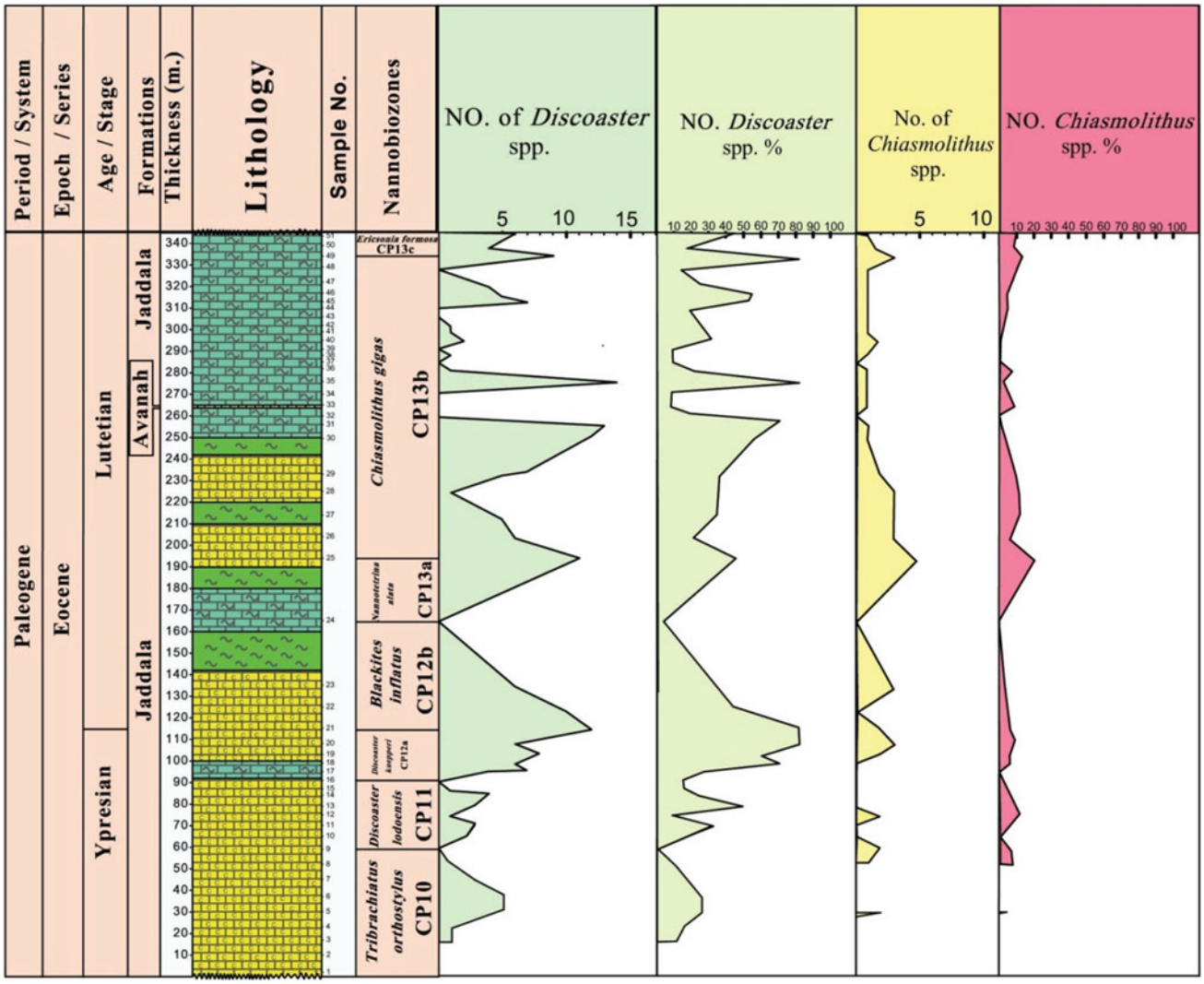

Fig. 2 The *Discoaster* and *Chiasmolithus* ratios in the studied section

References

1. Armstrong, H., Brasier, M.: Microfossils, p. 296. Black well publishing (2005)
2. van Bellen, R.C., Dunnington, H.V., Wetzel, R., Morton, D.M.: Lexique Stratigraphique International, Vol. III: Asie, Fascicule 10a, Iraq, p. 333 (1959)
3. Buday, R.T., Jassim, S.Z.: The Regional Geology of Iraq, Tectonism, Magmatism and Metamorphism, Baghdad, vol. 2, p. 352 (1987)
4. Gradstein, F.M., Ogg, J.G., Schmitz, M.D., Ogg, G.M.: The Geologic Time Scale 2012, vol. 2, 1144p. Elsevier (2012)
5. Maala, K.A.: Geology of Sinjar Area Part 1. No. 860. SOM Library (Unpubl. Rep), Baghdad (1977)
6. Molina, E., Alegret, L., Apellaniz, E., Bernoala, G., Caballero, F., Turell, J.D., Hardenbol, J., Clausen, C.H., Clarrasoana, J., Monechi, S., Ortiz, S., Orue-Etxebarria, X., Payros, A., Pujalte, V., Rodriguez-Tovar, F.J., Tori, F., Toaquella, J., Uchman, A.: The global stratotype section and point (GSSP) for the base of the Lutetian stage at the Gorrondatxe section, Spain. Episodes **34**(2), 87–108, Pl. 1 (2011)
7. Perch-Nielsen, K.: Cenozoic calcareous nannofossils. In: Bolli, H. M., Saundes, J.B., Perch-Nielsen, K. (eds.) Plankton Stratigraphy, pp. 427–554. Cambridge University Press, Cambridge (1985)
8. Young, J.R., Bown, P.R.: Cenozoic calcareous nannoplankton classification. J. Plankton Res. **19**, 36–47 (1997)

Holocene Paleoclimatic Variation Inferred from Study of Sediments in the Gulf of Tunis (North Africa)

Nizar Ouertani and Soumaya Yahyaoui

Abstract

The lithological study of sediments from a 30 m length core, taken at the western part of the lake of Tunis, combined with the study of benthic macrofauna, helped to identify the different stages of evolution of this ecosystem and the associated climatic fluctuations throughout the period spreading the Tardi Würm (about 42,000 years) to the Holocene. The sedimentological study allowed distinguishing six main facies characterizing different depositional environments. The identification of the mineralogical composition of the Holocene sediments of the upper part of the core, helped to note presence and dominance of two main minerals detected in all samples which are Quartz and Calcite. The determination of TOC contents in samples of Holocene sediments shows the existence of three levels: a surface level with high TOC values (reaching 5.1%), a second level at which values decrease gradually (around 1.1%) and the bottom level with sandy sediment record values <1%.

Keywords

Lake of Tunis • Holocene • Paleoclimatic fluctuation XRD • TOC

1 Introduction

Changes in deposition processes over thousands of years are recorded in sediments and will be revealed by lithological, geochemical and/or biological studies [1, 6]. The lithological study of the filling modes of the aquatic systems associated with the study of the rate of preservation of the organic matter in the sediments is an important tool in the reconstruction of the paleogeographic evolution of these environments [10].

The actual morphology of the Gulf of Tunis is the result of its evolution during Holocene Period [9, 7]. The aim of this study was the use of lithological and organic investigation to record paleoclimate evolution in this south Mediterranean zone (Gulf of Tunis) during Holocene and its impact on the morphological evolution of the lake and its filling mode.

2 Materials and Methods

"Tunis Lake" is a small ecosystem directly connected to the gulf of Tunis. Previous studies confirm that the sedimentation rate in the lake of Tunis, measured at 70, and 210 cm are respectively 28 cm/1000 years and 70 cm/1000 years [7, 9]. These results allow the estimation of core dating.

This study focused on the first ten meters (covering Holocene period) of the thirty-meter depth core (SC4). This core was taken from the inner side of the lake.

The lithology of the core was described (microscopic and macroscopic observation), different samples were collected for analysis and macro-fossils descriptions were undertaken. Coarse fraction consisting of shells was separated by sieving. Fine fraction (<63 μ) was taken for mineralogical analysis (X-ray analysis). The bulk composition of the total organic fraction (TOC) contained in the sediments was determined using a Ströhlein Coulomat 702 apparatus.

3 Results

3.1 Lithological Changes and Climatic Fluctuations

The top of the core is made up of 35 cm of black vase. In depth, the lithological variation along the core is

N. Ouertani (✉) · S. Yahyaoui
Faculty of Science of Tunis, University Tunis El Manar, Tunis, Tunisia
e-mail: nizar.ouertani@fst.rnu.tn

Z. Zhang et al. (eds.), *Patterns and Mechanisms of Climate, Paleoclimate and Paleoenvironmental Changes from Low-Latitude Regions*, Advances in Science, Technology & Innovation, https://doi.org/10.1007/978-3-030-01599-2_9

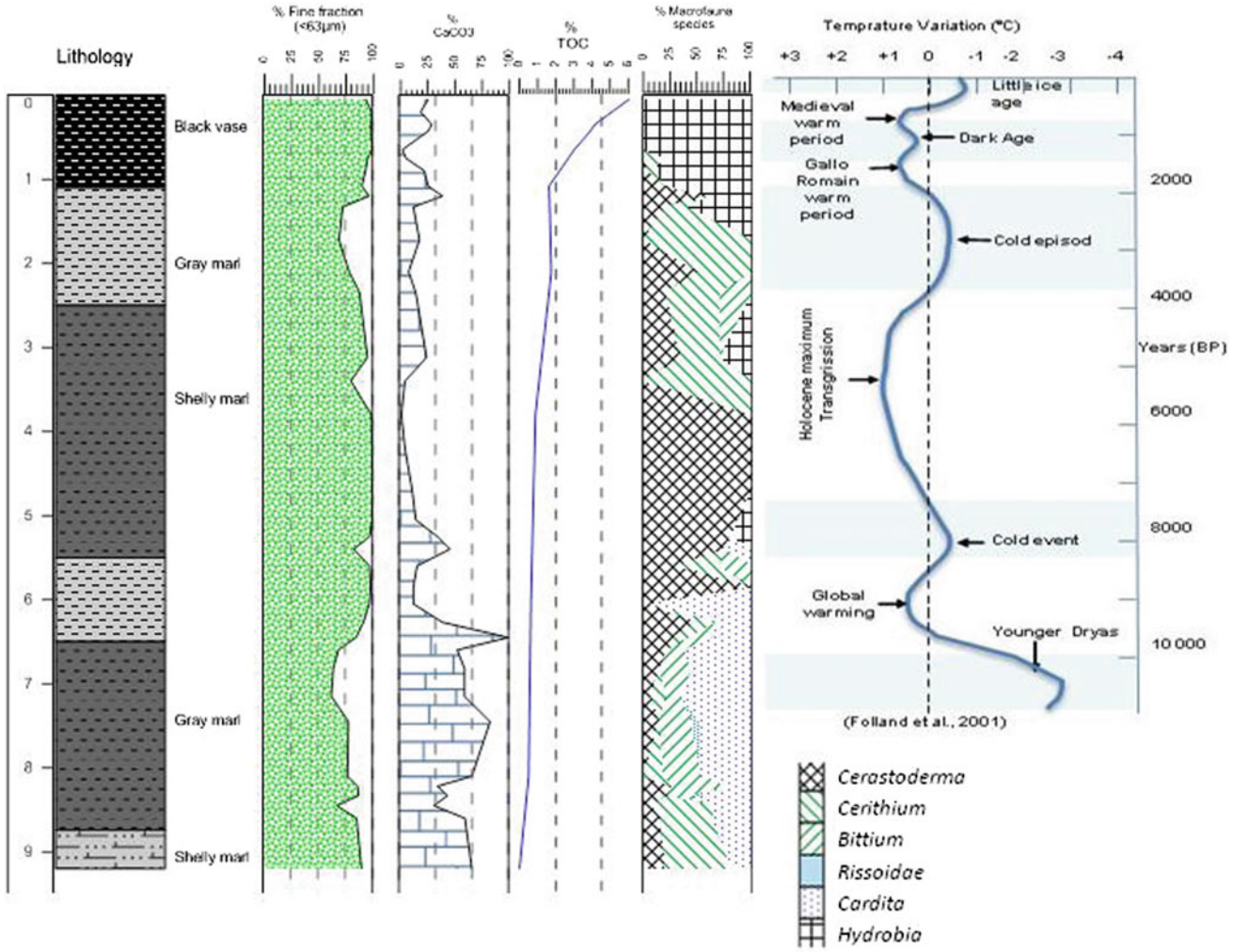

Fig. 1 A synthetic log representing the evolution of the filling in the lake during Holocene

characterized by alternating layers of gray sandy marl and layers of dark shelly marl. Compared to the diagram of temperature fluctuation during Holocene period [4] the cold events (early Holocene) are marked by sandy marly facies generally poor in shells. However the installation of warming episodes is always associated with the presence of shelly marl (Fig. 1).

3.2 Mineralogical Study of Holocene Sediments

Different diffractograms were used for the qualitative and quantitative characterization of minerals that form the Holocene deposits. Thus, it was observed that sediments crossed by the carrot, mainly consist of Quartz and Calcite, and a lesser amount of Aragonite and Dolomite.

In the upper part of the core, there is a predominance of quartz (around 50%). Calcite is present at a relatively low percentage (around 20%). This trend continues until about 6 m deep. Beyond this depth, sediments recorded relatively high percentages of calcite (reaching 95%).

3.3 Evolution of the Lake Environment Recorded by Macrofauna Study

Macro-fauna, representing the Holocene epoch [9, 3] shows a faunal association corresponding to three evolution stages (from bottom to top): closed lagoon environment, open lagoon environment and marine environment.

Species characterizing a closed lagoon environment are mainly represented by Hydrobia [5] and Cerastoderma [3]. These two species show a clear abundance in the upper part of the core.

Species indicating an open or semi-closed lagoon environment are mainly represented by Cerithium and Bittium [3]. These gastropods are abundant between 2 and 8.74 m and decrease in sandy sediments from 8.74 to 9.2 m.

Species of a marine environment which progressively replace the lagoon species are represented mainly by the Cardita species and by Rissoidae [8, 3].

3.4 Study of the Organic Content of the Holocene Sediments

The distribution of the TOC along the core shows an evolution directly related to lithological changes previously defined [2, 1, 6].

High TOC values reaching 5.1% in surface sediments are related to the evolution of the lake during the Little Ice Age (about 500 years BP).

Beyond 0.4 m, during the Flandrian transgression, the TOC contents showed a slight decrease (values are around 1.1%). During the Würmian phase (characterized by cold weather), TOC remains relatively low (around 0.5%). The episode of warming seems to be associated to relatively high levels of organic matter.

4 Results and Discussion

Different investigations and analyses have enabled identifying and understanding climatic fluctuations that influenced morphological changes in the gulf (Fig. 2), from the end of the last glaciation to the Holocene (last 40 ka).

During this period the sedimentary column in the gulf shows three distinct successive environments of deposition attested by changes in the lithology and the content of organic sediment.

The Younger Dryas (cold event: 12,700–10,000 years) is represented in the gulf by the deposition of sandy marl. The mineralogical composition of these sediments indicates the importance of detrital deposits.

The sedimentary filling of the lake, during the **Holocene**, consists essentially of marl (carbonates are systematically the dominant mineral: about 50% of abundance) or vase materials. Macrofauna, that dominated these deposits, consists mainly of mollusk characterizing an open lagoon. Global warming at this epoch promotes the primary of organic matter production, essentially near the surface.

In the little ice age (500 years BP), sediments were dominated by benthic macrofauna charactering a closed lagoon environment. During this period, the climate and especially morphological conditions favor deposits rich in organic matter.

5 Conclusion

The results obtained from the study of sedimentary column of the Gulf of Tunis allow reconstituting the morphological evolution of the basin. This is clearly expressed through the differentiation of the three distinct evolution stages within the sedimentary column during the Holocene period: closed lagoon stage, open lagoon and marine environment.

The present new results are of a significant interest since they demonstrate that the study of sediments accumulating in aquatic environments, combined with the study of organic matter, may act as a perfect tool to trace the sedimentary evolution of an aquatic system. Additionally, this should help in the reconstitution of the paleogeographic and

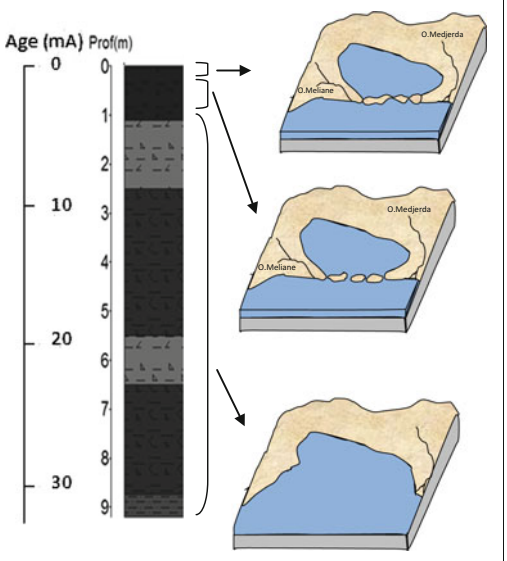

Stage1 : (600 years BP-present), closed Lake
Climate: cold climate tending to warming to 150 years BP.
Lithology: black mud deposits
Characteristic fauna: dominance of mollusk (Hydrobia, Cerastoderma)

Stage2: (2000 years -600 years BP), open lake
Climate: varies between cooling and warming
Lithology: marl deposits
Characteristic fauna: dominance of Bittium and Cerithium

Stage3:
Climate:
- Warm climate (8000 years- 2000 years BP)
- Varying temperatures between cooling and warming (42000 years- 8000 years BP)

Lithology: facies with madrepores, sandy facies, marl facies poor of shells.
Characteristic fauna: marin mollusk+ madrepores

Fig. 2 Schematic representation of the different stages of Lake of Tunis

morphological history, and in assessing even the subtle changes in the physico-chemical (oxic vs. anoxic) conditions that prevailed during the basin history and which are in close relationship with the global climatic changes.

References

1. Ariztegui, D., Chondrogianni, C., Lami, A., Guilizzoni, P., Lafargue, E.: Lacustrine organic matter and the Holocene paleoenvironmental record of Lake Albano (central Italy). J. Paleolimnol. **26**, 283–292 (2001)
2. Bourbonniere, R.A., Meyers, P.A.: Sedimentary geolipid records of historical changes in the watersheds and productivities of Lakes Ontario and Erie. Limnol. Oceanogr. **41**, 352–359 (1996)
3. Carbonel, P., Legigan, P.H., Pujos, M., Saubade, A.M., Bobier, C., Jouirou, M.: Evolution du lac de Tunis. Un modèle de passage du milieu littoral à un milieu lagunaire. Actes du 1er Congrès des sciences de la Terre, Tome 2, pp. 91–100 (1981)
4. Folland, C.K., Karl, T.R., Vinnikov, K.Y.: Observed climate variations and change. In: Intergovernmental Panel on Climate Change. University of Cambridge, Cambridge University Press, Cambridge, United Kingdom and New York, NY, USA, 881p (2001)
5. Harbridge, W.F., Pilkey, O.H., Whaling, P.J., Swetland, P.: Sedimentation in the lake of Tunis: a lagoon strongly influenced. Environ. Geol. **1**, 215–225 (1976)
6. Meyers, P.A.: Applications of organic geochemistry to paleolimnological reconstructions: a summary of exp from the Laurentian Great Lakes. Org. Geochem. **34**, 261–289 (2003)
7. Ouertani, N., Hamouda, R., Belayouni, H.: The use of organic matter study for the reconstitution of basin paleogeography and the record of global climate change. In: 4th North African/Mediterranean Petroleum and Geosciences Conference & Exhibition, EAGE, Tunis, 2–4 Mar 2009
8. Parenzan, P.: Un habitat marino di tipo subtropicale a Porto Cesareo. In: Scalera Liaci, L. (ed.) Atti del VI simposio nazionale per la conservazione della natura. Cacucci, Bari, pp. 151–157 (1976)
9. Thornton, S.E., Pilkey, O.H., Dayle, L.J., Xhaling, P.J.: Holocene evolution of a coastal lagoon, lake of Tunis, Tunisia. Sedimentology **27**, 79–91 (1980)
10. Van Welden, A.: Variations hautes résolution des apports terrigènes dans le golfe du lion pendant la dernière période glaciaire: caractérisation des événements climatiques rapides. DEA, 71p (2004)

Noble Gas Recharge Temperature of Sfax Deep Groundwater (Southeastern of Tunisia)

Rim Trabelsi, Mahdi Trabelsi, Kamel Zouari, and Takuya Matsumoto

Abstract

In the present context of climate change and increasing demand for water, it is crucial to identify the origin, groundwater flow dynamics and mean residence times for sustainable management of water resources. In this study, groundwater residence time and recharge conditions of the deep aquifer of Sfax were investigated using environmental isotopes and noble gases. The results show that Sfax deep groundwater was recharged during cooler period of Late Pleistocene. In broad agreement with evidence from other paleoclimate investigations, the estimated noble gas recharge temperature (NGT) is lower than the present by about 5.5 °C. Oxygen isotopes values of Late Pleistocene are also 1.5‰ lower than modern precipitation.

Keywords

Environmental isotopes • Noble gases • Paleoclimate Late Pleistocene • Tunisia

1 Introduction

As conservative tracers, the study of dissolved atmospheric noble gases (He, Ne, Ar, Kr, and Xe) in groundwater offers a powerful approach of paleo-climate reconstruction [1]. It is a tool to investigate the origin and the conditions during groundwater recharge, in particular the recharge or noble gas temperature (NGT). In fact, their concentrations in the recharge areas of groundwater systems are typically considered to be simply a function of temperature, altitude, excess air, and salinity [2]. However, the estimation of NGT requires a number of corrections and conditions to be satisfied. Different simplified models describing the formation of excess air and its fractionation [3, 4] have been used in diverse paleoclimatic studies. The most used models are the unfractionated air (UA) model [5], the continuous equilibration (CE) model in closed system [3] and the partial re-equilibration model (PR-model) [4]. The objective of this investigation was to determine the noble gas recharge temperature of Sfax deep groundwater located in southeastern of Tunisia using the most appropriate model in combination with stable isotopes (δ^2H and $\delta^{18}O$) and (^{14}C and ^{13}C) carbon isotopes.

2 Settings, Sampling and Analysis

Sfax region is located in south east of Tunisia; it represents the second largest urban area with 1.2 Million inhabitants. It is characterized by a semi-arid to arid Mediterranean climate with irregular and rare precipitations (an annual precipitation average of 239 mm) and mean annual temperature of 19 °C. The geology of the study area is made up of tertiary and quaternary sediments. The aquifer system of Sfax is defined as a multilayered aquifer system, consisting of three aquifers: the shallow aquifer (depth less than 50 m), the middle aquifer (from 60 to 240 m) and the upper Miocene deep aquifer (up to 750 m of depth) [6]. Several sampling campaigns were carried out during 2014–2015. A total of 11 samples were collected from deep groundwater (Fig. 1). Chemical, stables and radioactive isotopes parameters were measured in all the samples.

Samples for He, Ne, Ar, Kr, Xe and $^3He/^4He$ ratios analysis were typically collected by flushing the water sample through annealed copper tubes, which were then pinched off at either end to prevent atmospheric contamination.

R. Trabelsi (✉) · M. Trabelsi · K. Zouari
Radio-Analysis and Environment Laboratory, ENIS, Sfax University, Sfax, Tunisia
e-mail: trabelsi.rim01@gmail.com

T. Matsumoto
Isotope Hydrology Section, International Atomic Energy Agency, Vienna, Austria

Z. Zhang et al. (eds.), *Patterns and Mechanisms of Climate, Paleoclimate and Paleoenvironmental Changes from Low-Latitude Regions*, Advances in Science, Technology & Innovation, https://doi.org/10.1007/978-3-030-01599-2_10

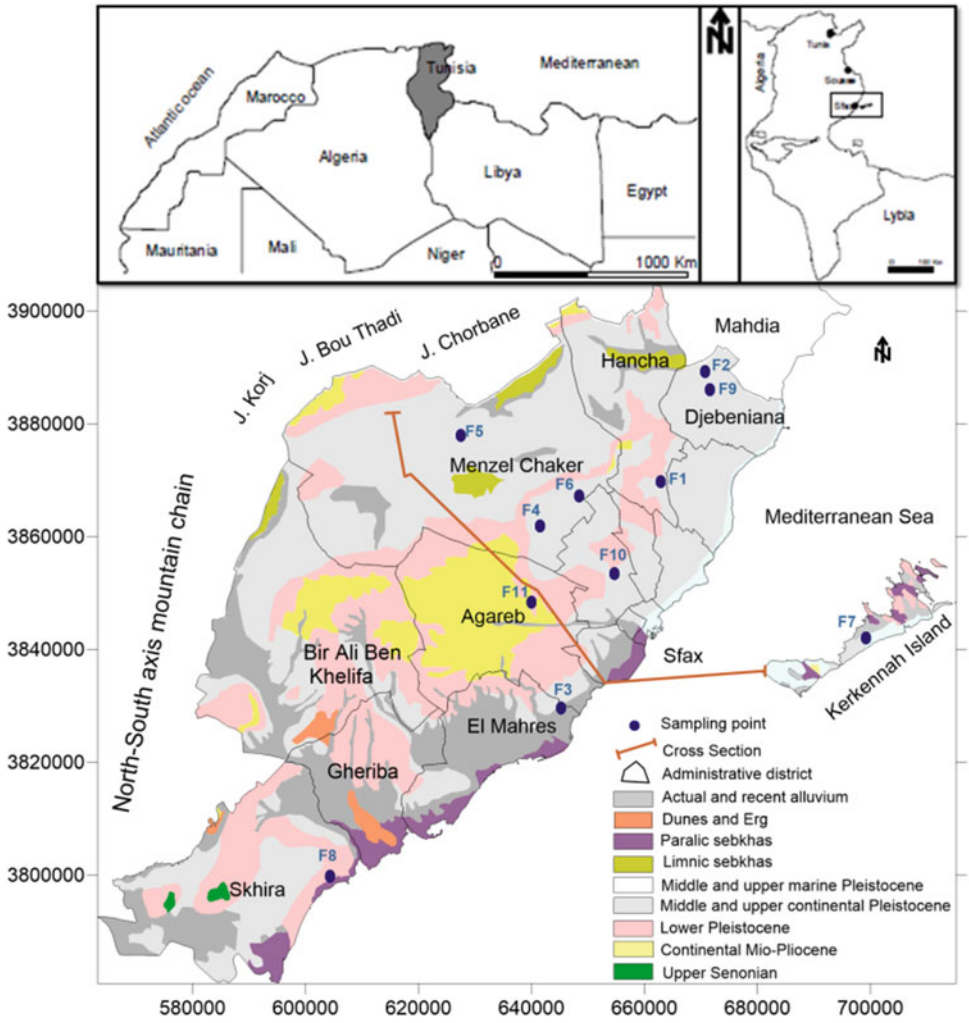

Fig. 1 Location and geological map of Sfax

3 Results

The measured stable isotopes of Sfax deep groundwater are homogenous; $\delta^{18}O$ changes from −6.4 to −6.0‰ with corresponding $\delta^{2}H$ values that vary between −42.3 and −40.5‰ Vs-SMOW. The noble gases concentrations are visualized using box-and-whisker plots (Fig. 2). The measured values were identified as outliers if the distance from the top or bottom 25th percentile was larger than one and a half time of the interquartile range represented by the box in box–whisker plots; the median is represented by a square mark. Outliers as determined by this method are plotted separately. Differences between measured concentrations in replicate tubes are noted in some samples which could be caused by sampling or measuring artifacts. Based on these data the different outliers were removed in order to investigate the recharge temperature.

4 Discussion

Compared to the weighted mean values of $\delta^{18}O$ and $\delta^{2}H$ for Sfax precipitation (−4.6 and −24.5‰) calculated from (1992 to 2016), the stable isotope contents of Sfax deep groundwater are depleted, which could reflect either recharge at higher altitudes and a palaeoclimatic effect (recharge under colder climatic conditions than at present). Further, the low carbon-14 activities measured in all the samples indicating high residence times support the palaeoclimatic groundwater recharge. Several geochemical correction models were applied to convert the measured carbon-14 activities into groundwater ages. For most of the samples, the calculated ^{14}C ages according to different correction procedures appear to be homogenous, providing fairly high confidence in ^{14}C ages. The mean residence times obtained from different correction models are systematically higher than 10 Ka confirming that most of this groundwater

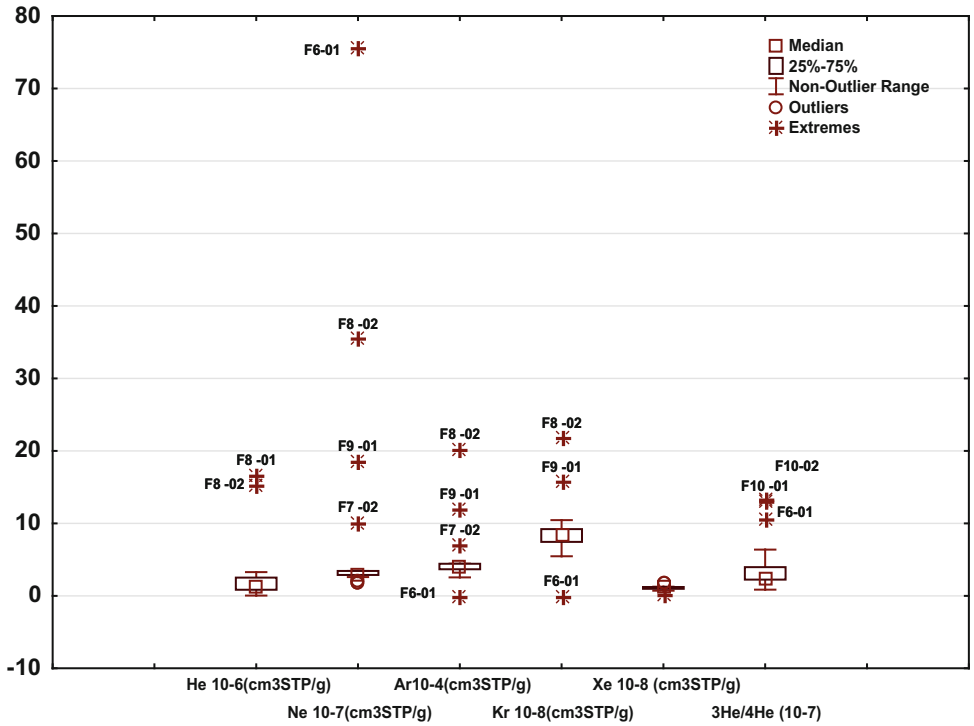

Fig. 2 Box–whisker plots for noble gases concentrations of Sfax groundwater

reserve was recharged before Holocene and the recent recharge of the Sfax aquifer system is very limited.

The analysis of noble gas data with respect to recharge temperature, excess air and its fractionation was performed using the program inoble2.5 by inverse fitting based on χ 2-minimization. According to this test, closed-system equilibration model (CE) [3] is the most appropriate and predicts Ne, Ar, Kr and Xe concentrations compatible with the measured data. The individual uncertainty (1σ) of the noble gas temperature determination varies between 0.1 and 0.2 °C. The calculated NGTs for all samples vary between 13.2 and 16 °C. Consequently, Sfax deep groundwater seems to have infiltrated during the cooler period of the Pleistocene. These palaeo-groundwaters are displaying a mean temperature decrease of 5.5 °C compared to the recharge temperature of modern groundwater in Sfax basin. Accordingly, the oxygen isotope values of Sfax deep groundwater are about 1.5‰ lower than modern precipitation. This transition Pleistocene–Holocene is well characterized in aquifers worldwide.

5 Conclusions

In this research study, environmental isotopes, noble gases, and carbon-14 dating were combined for a better understanding of groundwater flow dynamics and mean residence times of Sfax deep aquifer in southeastern Tunisia. ^{14}C age dating and noble gas data clearly confirm the presence of old groundwater that is recharged during cooler climate of Late Pleistocene. The closed-system equilibration model (CE) is proved to be the most adequate in the case of Sfax deep groundwater to estimate NGT. The calculated values show a decrease of recharge temperature by 5.5 °C compared to the present. Oxygen isotopes values of Late Pleistocene are also 1.5‰ lower than modern precipitation. All these results should be considered for the assessment of the renewability rates and the reliability of these groundwater resources as a major source of water supply in the region over the medium and long-terms.

References

1. Aeschbach-Hertig, W., Solomon, D.K.: Noble gas thermometry in groundwater hydrology. In: Burnard, P. (ed.) The Noble Gases as Geochemical Tracers. Advances in Isotope Geochemistry, pp. 81–122. Springer, Berlin (2013)
2. Heaton, T.H.E., Vogel, J.C.: Excess air in groundwater. J. Hydrol. **50**, 201–216 (1981)
3. Aeschbach-Hertig, W., Peeters, F., Beyerle, U., Kipfer, R.: Palaeotemperature reconstruction from noble gases in ground water taking into account equilibration with entrapped air. Nature **405**, 1040–1044 (2000)
4. Stute, M., Forster, M., Frischkorn, H., Serejo, A., Clark, J.F., Schlosser, P., Broecker, W.S., Bonani, G.: Cooling of tropical Brazil (5°C) during the last glacial maximum. Science **269**, 379–383 (1995)
5. Stute, M., Schlosser, P.: Principles and Applications of the Noble Gas Paleothermometer. INC (1993)
6. Maliki, A.: Etude hydrogéologique, hydrochimique et isotopique de la nappe profonde de Sfax (Tunisie), thèse. National School of Engineers of Sfax, Tunisia (2000)

Time Analysis of Emberger's Pluviothermic *Q* Index in the SW of the Iberian Peninsula

Leoncio García-Barrón, Julia Morales, and Arturo Sousa

Abstract

The annual Emberger's pluviothermic *Q* index is suitable for classifying the Mediterranean climate and drawing conclusions about the spatiotemporal behaviour from which environmental effects may derive. The *Q* index was calculated to analyse its temporal variability throughout the study period of 1901–2012 in the Southwest of the Iberian Peninsula. The results obtained show that the climate fluctuates between sub-humid Mediterranean and semi-arid Mediterranean. The Southwest of the Iberian Peninsula is characterized by the temporal irregularity of *Q*, with high variability. However, it is possible to detect sequences with differentiated behaviours.

Keywords

Emberger's *Q* index • SW Iberian Peninsula

1 Introduction

One of the potential effects of climate change, throughout the 21st century, is the progressive shortage of water resources in the Mediterranean area. This is mainly due to a possible rainfall decrease and the increase of evaporation associated with the scenarios of climate change predicted for the year 2100, which would increase the surface subjected to aridification. In this context, the Southwest of Europe is a potentially sensitive zone. This paper analyzed the evolution of the climatic behavior from the records of the meteorological variables of the early 20th century. Extrapolating the results can reveal potential risks if they show a decrease in water availability for vegetation, agriculture and human and industrial use, which can have a serious environmental, social and economic impact for the 21st century.

In order to quantify the phenomenon described the Emberger's pluviothermic *Q* index was selected. This index provides a staggered classification of the Mediterranean climate with its corresponding characteristic vegetation, as a function of meteorological variables. The study aimed to analyse, in the Southwest of the Iberian Peninsula, the temporal variability of an indicator related to the annual level of aridity/humidity. The analysis of the inter-annual series of *Q* values allowed detecting its evolution throughout the study period of 1901–2012.

2 Study Area and Method

The study area was the Southwest of the Iberian Peninsula. This region is predominated by a Mediterranean climate influenced by the regulatory effect of the Atlantic Ocean. Rainfall in this area is characterised by its irregularity, with large oscillations of the annual totals, including multi-annual drought periods [1]. In general, the intra-annual rainfall profile shows an asymmetric, unimodal curve, which increases in autumn and slowly decreases from the end of winter until the summer.

The temperature intra-annual profile is the opposite of that of rainfall: decreasing in autumn—until it reaches the minimum winter temperature—increasing in spring and maximum in summer [2].

The temperature and rainfall data used are from the *Global Climate Monitor* database and were provided by the Climate Research Group of the University of Seville. The study area had the Doñana Natural Reserve as the central geographical reference, given the importance and uniqueness of its wetlands which have been affected by changes in the

L. García-Barrón
Departamento de Física Aplicada II, Universidad de Sevilla, 41012 Seville, Spain
e-mail: leoncio@us.es

J. Morales · A. Sousa (✉)
Departamento de Biología Vegetal y Ecología, Universidad de Sevilla, 41012 Seville, Spain
e-mail: asousa@us.es

J. Morales
e-mail: jmorales@us.es

Z. Zhang et al. (eds.), *Patterns and Mechanisms of Climate, Paleoclimate and Paleoenvironmental Changes from Low-Latitude Regions*, Advances in Science, Technology & Innovation, https://doi.org/10.1007/978-3-030-01599-2_11

tendency of the climate and anthropogenic impact in the last centuries [3, 4].

The Annual Emberger's Pluviothermic Q Index [5] is formulated as:

$$Q = (100P)/\left(M_i^2 - m_i^2\right) \quad (1)$$

where

P = annual precipitations (mm); Mi = mean value of the maximum daily temperatures of the warmer month (°C); m_i = mean value of the minimum daily temperatures of the coldest month.

3 Results and Valuation

Given that the average temperature of the minimum temperatures of the coldest month is a limiting factor for vegetation, Emberger [5] generates a two-dimensional climograph (mi, Q) that classifies the climates according to m_i and Q. In the present study, we calculated the average of the complete observation period (m_i = 6.8 °C), which we used to characterize the study area. The cut-off points of the temperature vertical line with the corresponding climograph curves provide graphically the threshold values (33, 60, 108). Then we elaborated the classification Table 1 for the study area. The results are shown (Table 1), with the values of Q, the rate (%) of years corresponding to each class and the indication of characteristic vegetation.

Figure 1 shows the inter-annual evolution of Q, with the categories differentiated according to the aforementioned classification. The lineal tendency of the series is slightly ascendant (0.026 mm/°C•year) without climatic significance, since the variance explained is lower than 1% ($R^2 < 0.1$). The most relevant characteristic of the Q series is its irregularity. An example of this feature is the high coefficient of variation (V_N = 0.28). Therefore, the evolution of the central value is not enough to predict the temporal behaviour of the index. Figure 1 also includes the smoothing line of Q through a centered moving average of 11 years. This multi-annual grouping shows an epoch of pronounced sub-humid climate predominance between 1945 and 1975.

Despite the lack of a significant tendency, the relative cumulative deviations with respect to the limit value between the Mediterranean semi-arid and the Mediterranean sub-humid climate (Q = 60) allowed detecting differentiated multi-annual sequences. Figure 2a shows, overlapping the saw teeth, an initial descending segment until 1935, which indicates high frequency of semi-arid years. Then, there was a fluctuation period of two decades. Shortly before 1955, a phase change began with a predominance of sub-humid years, which lasted until 1970. In the last thirty years, there was a descending phase with a very pronounced slope, which the authors associate with a new semi-arid period.

Given the general variability detected during the study period, it is important to analyse its inter-annual evolution in detail. To this end, the authors calculated the coefficient of variation for the moving average by periods of 11 years (CV_{11}), defined as the coefficient of the standard deviation of the partial subseries made up of the reference year i and the previous 10 years, and the corresponding average (Fig. 2b). This figure shows an average value of 0.22 during the first third of the 20th century, which increases and stabilizes around 0.28 until 1985. In the last decades, there is a new increase, reaching values above 0.4.

The sensitivity of Q indicates its capacity to respond to the inter-annual alterations of thermal and pluviometric factors. To this end, the degree of simultaneity of the deviations was determined, through the Pearson's coefficient correlation (r), between the temporal series of Q and those of the corresponding meteorological variables P and ($M_i^2 - m_i^2$) for the study period. The obtained values were r_P = 0.96 with respect to rainfall and only r_T = 0.21 with respect to temperature. The authors deduce that the effect of precipitation P on the inter-annual behaviour of Q is much more intense, which they attribute to the greater temporal variability of P (V_N = 0.28) compared to the higher stability of the inter-annual thermic series (V_N = 0.08) throughout the entire analyzed period.

4 Conclusion

The results obtained confirm that the application of the Emberger's Q index is a suitable methodology for analysing the climatic evolution of geographical areas of the Mediterranean climate. The SW of the Iberian Peninsula is characterised by the temporal irregularity of Q, with high variability. However, it is possible to detect sequences with differentiated behaviours. Thus, during the first third and the last thirty years of the 20th century, there was a

Table 1 Classification of the Mediterranean climate in the Southwest of the Iberian Peninsula

Mediterranean climate	Arid	Semi-arid	Subhumid	Humid
Q index	17–33	33–60	60–108	>108
Average years (%)	7	52	51	–
Characteristic vegetation	Xerophytic scrub	*Pinus* spp.	Olive, Cork oak	Chestnut

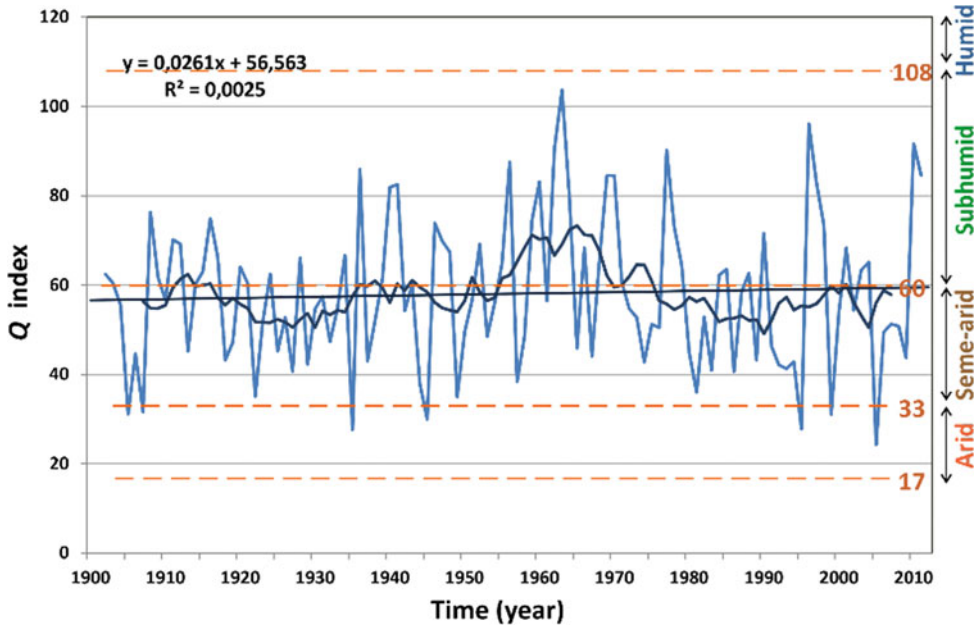

Fig. 1 Inter-annual evolution of the *Q* index, with intervals of category and centered moving average line, and linear tendency slope

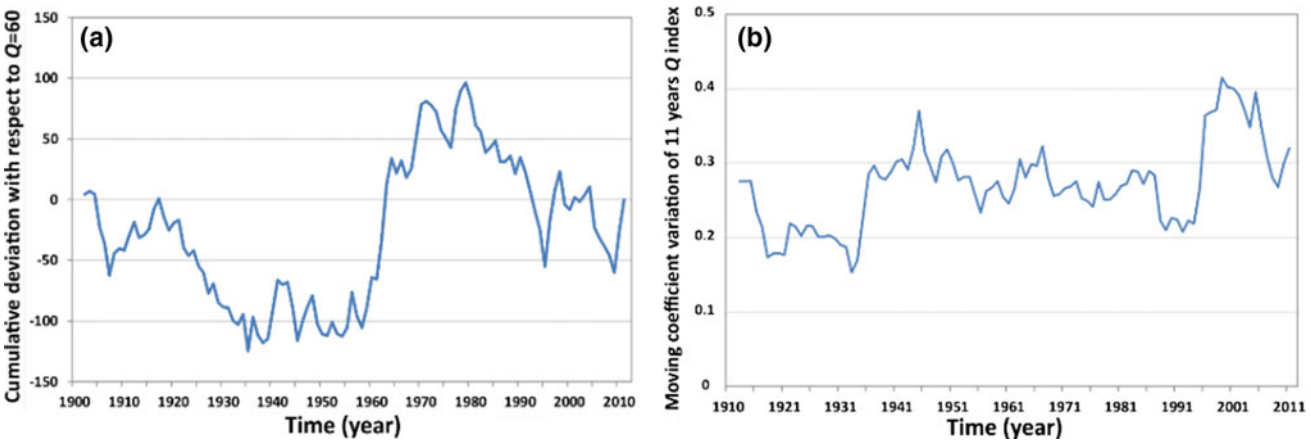

Fig. 2 **a** Cumulative deviations with respect to $Q = 60$, limit between Mediterranean semi-arid and sub-humid climates. **b** Moving variation coefficient using eleven-year periods

predominance of a Mediterranean semi-arid climate. On the other hand, during the period between 1950 and 1975, the study area was predominated by a Mediterranean sub-humid climate.

References

1. García Barrón, L., Pita, M.F.: Stochastic analysis of time series of temperatures in the South-West of the Iberian Peninsula. Atmósfera **17**(4), 225–244 (2004)
2. García-Barrón, L., Aguilar, M., Sousa, A.: Evolution of annual rainfall irregularity in the Southwest of the Iberian Peninsula. Theoret. Appl. Climatol. **103**, 13–26 (2011)
3. Sousa, A., Morales, J., García-Barrón, L., Garcia-Murillo, P.: Changes in the *Erica ciliaris* Loefl. ex L. peat bogs of Southwestern Europe from the 17th to the 20th centuries AD. The Holocene **23**(2), 255–269 (2013)
4. Sousa, A., García-Barrón, L., García-Murillo, P., Vetter, M., Morales, J.: The use of changes in small coastal Atlantic brooks in southwestern Europe as indicators of anthropogenic and climatic impacts over the last 400 years. J. Paleolimnol. **53**(1), 73–88 (2015)
5. Emberger, L.: Sur une formule climatique applicable en géographie botanique. C. R, Acad. Sci. **191**, 389–390 (1930)

Systematic and Palaeoclimatic Investigations of *Sivalhippus* from the Late Miocene Siwaliks (Pakistan)

Muhammad tahir Waseem, Abdul majid Khan, Rana Mansoor Ahmad, Ayesha Iqbal, and Muhammad Ameen

Abstract

A mandible and several isolated upper and lower teeth of a hipparionine horse were discovered and described from late Miocene localities of district Chakwal, Punjab, Pakistan. The morphometric analysis of the samples led to identify the genus *Sivalhippus*. *Sivalhippus* lived in the Siwaliks from 10.7 to 5.8 Ma. The stable isotope analysis of the carbon and oxygen was used as a palaeodietary and palaeoclimatic proxy. The enamel hypoplasia analysis of the samples revealed a moderate level of stress faced by the *Sivalhippus* as a result of seasonality and climate change. All the findings of our study represent that *Sivalhippus* endeavored a mosaic of woodlands and grasslands with increasing consumption of C4 grasses in their diet. Our study suggests that increase in hypsodonty index in *Sivalhippus* was due to the increasing dietary stress of coarser dietary material invading the region with a shift from C3 to C4 grasses.

Keywords

Stable isotopes • Enamel hypoplasia • Hypsodonty index • Middle Siwaliks • C4 vegetation

1 Introduction

The record of three toed horses is exclusively represented from the Middle Siwaliks of Pakistan spanning late Miocene to Pliocene [6]. The description of Neogene horses is chiefly based on their dental attributes while stable isotope analysis and enamel hypoplasia analysis represent palaeoeclogy, palaeodiet and stress faced by the animal during its life span. The *Sivalhippus* genus is represented by at least three species from the Siwaliks of Pakistan and these species are *S. nagriensis*, *S. theobaldi* and *S. perimense* [9].

The stable isotope analysis of carbon and oxygen has been considered best indicators of diet as well as ecological niche of animals and has been utilized by many scientists for the past three decades [3, 4]. The enamel hypoplasia is an excellent physiological and environmental stress marker which indicates the levels of stress that an animal face in its life span [8]. The current study included the morphometric analysis of dental material while the stable isotope analysis and the enamel hypoplasia studies have been used to reconstruct the palaeoecology and palaeodietary pattern of the genus *Sivalhippus*.

2 Materials and Methods

The samples were collected from late Miocene localities having an age from 8.6 to 7.6 Ma (after [1]) in district Chakwal, Punjab, Pakistan. The samples were thoroughly washed and cleaned in Environmental Biology Laboratory and housed at the Department of Zoology, University of the Punjab, Lahore. The dimensions of the teeth were measured in millimeter (mm), while W/L ratio was also taken into consideration for precise analyses. A complete mandible and other isolated teeth were used for the morphometric studies.

The enamel was extracted (15 mg) for the stable isotope analysis (n = 15) and subjected to pretreatment (see [7]) and for further analysis of oxygen and carbon isotope ratios. The samples were analyzed at PINSTIC Islamabad, Pakistan where IRMS (Isotope Ratio Mass Spectrometer) was used. For the studies of the linear enamel hypoplasia, a sum of 65 molars was used. Each tooth was examined under magnifying glass for the detection of enamel hypoplasia and description of enamel hypoplasia on the teeth on which there was a defect.

M. t. Waseem · A. m. Khan (✉) · R. m. Ahmad
A. Iqbal · M. Ameen
Department of Zoology, University of the Punjab, Lahore, 54590, Pakistan
e-mail: majid.zool@pu.edu.pk

R. m. Ahmad
University of Sargodha, Lyallpur Campus, Faisalabad, Pakistan

Z. Zhang et al. (eds.), *Patterns and Mechanisms of Climate, Paleoclimate and Paleoenvironmental Changes from Low-Latitude Regions*, Advances in Science, Technology & Innovation, https://doi.org/10.1007/978-3-030-01599-2_12

3 Results

3.1 Systematic Palaeontology

Order: Perissodactyla Owen, 1848
Sub-order: Hippomorpha Wood, 1937.
Family: Equidae Gray, 1837.
Genus: *Sivalhippus* Lydekker, 1877.
Holotype: GSI C153, Left Maxilla with DP 2-4.
Horizon: Middle Siwaliks.
Stratigraphic range: 10.7–5.8 Ma [1].
Geographic range: Ethiopia, Kenya, Pakistan and China.
Diagnosis: A large-bodied three-toed horse with pre-orbital facial fossa which is separated from orbit by a pre-orbital bone. Cheek teeth completely ornamented with thick fossettes, plication, bifid to trifid pre caballins [2, 5].
Description: The described and discussed specimens comprise a mandible and premolars and molars. Canines are not present in the mandible. The mandible is a well-preserved lower jaw having intermediate stage of wearing. It represents clear hypsodonty and teeth are highly extended and pillar like in appearance. A layer of thin cement is present around the sample. The basal part of the mandible was reconstructed by the help of Plaster of Paris. Incisors and canines were absent.
Premolars: PUPC 94/2000 is a well preserved mandible of *S. theobaldi*. Premolars are molariform. Stylids are well preserved. In LP_2 mesostlid is slightly damaged. Protoconid is extended in the form of parastylid. In LP_3 stylids are intact. Protoconid as well as hypoconid are broad. The rounded metaconid is somehow fused with isthmus. LP_4 has a smaller entoconid as compared to other conids. The mesostylid is partially damaged. Entoflexid is longer in size as compared to metaflexid. The enamel of right P_2 is thick and rugose due to which dentine cannot be seen. A thin coating of cement is present on buccal side. RP_3 follows the same pattern as in RP_2. The upper premolar PUPC 09/15 represents some striking features. It is a well-preserved tooth at an early stage of wear. It is highly elongated and represents a pillar like appearance. Major cusps are highly developed and in a good preserving stage. The isolated protocone is somewhat rounded. It is covered by a moderately thick layer of cement. The paracone is deep and almost equal to the metacone in antero-posterior length. The lower premolars PUPC 8/15 and PUPC 11/15 are well preserved but slightly damaged. The metaconid is united with isthmus and almost rounded in general appearance. Both premolars are in middle wearing stage.
Molars: All the molars either right or left are intact and represent an excellent preserving stage. Anteroposterior part of metaflexid represent complicated enamel in LM_1. The LM_2 represent a pointed metastylid and have a wavy outline. Protostylid and parastylid is pillar like in general appearance. The rugosity of enamel is high and it is thick in LM_3. The crown is not much broader but narrower and represents extreme hypsodonty. Mesostylid is narrow. The depression on lingual side is plihypoconid. Two prominent foldings, metaflexid and entofelxid are present. However, entoflexid is a little elongated and curved. Right M_2 represents middle stage of wearing, so all the conids and stylids were well preserved. Protoconid is less broad than hypoconid. Protoconid of RM_3 is also rounded and smaller as compared to hypoconid. PUPC 06/15 and PUPC 07/15 are both isolated upper molars in which all the lophs viz. ectoloph, metaloph and protoloph are prominent and in a good preserving stage. Complex enamel foldings are represented in fossettes. Both pre and post-fossettes display many plications with thick enamel. The cusps are highly developed and a thin coating of cement covers all over the crown.

a. Stable Isotope Analysis:

Insignificant differences were found for both carbon and oxygen ($p = 0.106$) when one sample t-test was applied. C13 values range from −11.03 to 4.94‰ and the difference was found to be 6.09‰. Oxygen isotope values also revealed insignificant differences of a range of −10.38 to −6.89‰ with the difference of 3.49‰. The average values for $\delta^{13}C$ and $\delta^{18}O18$ are −7.682 and −8.520‰ respectively.

b. Enamel Hypoplasia Analysis:

A total of 65 samples were studied for the enamel hypoplasia and linear enamel hypoplasia was found on 17 samples, which indicate a moderate stress in late Miocene (8.6–7.6) hipparionines (Fig. 1 and Table 1).

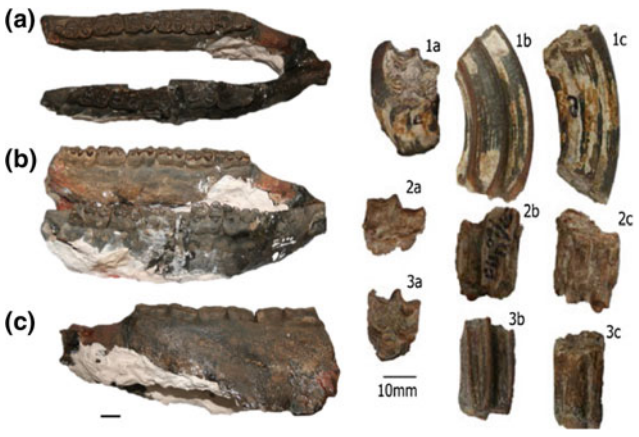

Fig. 1 Some of the dental material used in the study including a mandible and isolated molars of *Sivalhippus*. **a–c** indicates the occlusal, lingual and buccal view respectively. Scale is equal to 10 mm

Table 1 The comparison of cheek teeth measurements of *Sivalhippus theobaldi* with its own members as well as with other sister species in mm

Taxa	Specimen number	Position	Length (mm)	Width (mm)
S. theobaldi (Studied)	PUPC 10/15	M_2	25	14
	PUPC 08/15	P_4	24	19
	PUPC 11/15	P_3	26	13
	PUPC 06/15	M^3	25	22
	PUPC 07/15	M^2	24.5	22
	PUPC 09/15	P^2	29.5	19
	PUPC 94/2000	R&LP_2	24.2	16.2
		R&LP_3	24.2	16.3
		R&LP_4	24.3	16.3
		R&LM_1	23.9	14.2
		R&LM_2	24.2	14.3
		R&LM_3	24.4	15
S. theobaldi	[a]PUPC 00/94	P_2	25	13
	[a]GCS 11/19	P_2	25	14
	[a]GCS 11/20	M_1	21.0	15.0
	[a]PUPC 07/167	P_4	23	15.6
	[b]AMNH 29806	M_2	25	15

[a]The referred material is used from Ghaffar [5]
[b]The referred material is used from Colbert [2]

4 Discussion

The body size of *Sivalhippus* is comparatively larger than other hipparionines. The molars are slightly more developed and are not much squariform as *Cormohipparion*. *Sivalhippus* represents higher degrees of hypsodonty than other old world three toed horses. The dentition of *Sivalhippus* has a complex dental pattern. The enamel border is simple and has less bifid to trifid plications but some samples have a complex pattern of plications in pre and post fossettes. Two hypoglyphs are deeply incised as in *S. theobaldi* while hypoglyphs in other species are not as much deeply incised but moderate. The described samples represent all the basic characters of *Sivalhippus*.

The less negative values of $\delta^{13}C$ (average −7.682‰) represent an increase in the intake of C4 grasses in diet as it was the time span when C4 grass lands were expanding in latest Miocene of Pakistan [1]. Open areas were expanding at the expense of closed canopies as represented by the oxygen isotope value (average −8.52‰) but the grass lands were not dominating but at an early age of evolution while oxygen isotope values also show that the water intake behavior of *Sivalhippus* was restricted and they were dependent mainly on their diet for water requirements. In the latest Miocene, the environment was undergoing a change towards open and arid condition but the levels of stress on *Sivalhippus* were moderate but not intense. Increase in HI index shows that these hipparionines were well adapted for harsh vegetation as C4 grasses in latest Miocene.

5 Conclusion

The morphometric, stable isotopic and enamel hypoplasia analysis confirms that the genus *Sivalhippus* lived in a mosaic of wood land and grass land in the latest Miocene. The environment was arid and precipitation was not significant to support higher water supplies, thus the *Sivalhippus* showed a restricted behavior of water intake. In conjunction with increasing C4 grasslands, the hypsodonty was also increased in this genus. Thus it can be hypothesized that one of the factors responsible for increased hypsodonty in *Sivalhippus* was the evolution of C4 grasslands which enabled them to feed on harsh vegetation.

References

1. Barry, J., Morgan, M., Flynn, L., Pilbeam, D., Behrensmeyer, A.K., Raza, S., Khan, I., Badgely, C., Hicks, J., Kelley, J.: Faunal and environmental change in the Late Miocene Siwaliks of Northern Pakistan. Paleobiol. Mem. **28**(3), 1–72 (2002)
2. Colbert, E.H.: Siwalik mammals in the American Museum of Natural History. Trans. Amer. Phil. Soc., n.s. **26**, 1–401 (1935)
3. Domingo, L., Cuevas-González, J., Grimes, S.T., Hernández Fernández, M., López-Martínez, N.: Multiproxy reconstruction of

the paleoclimate and paleoenvironment of the Middle Miocene Somosaguas site (Madrid, Spain) using herbivore tooth enamel. Palaeogeogr. Palaeoclimatol. Palaeoecol. **272**, 53–68 (2009)
4. Fox, D.L., Koch, P.L.: Carbon and oxygen isotopic variability in Neogene paleosol carbonates: constraints on the evolution of the C4-grasslands of the Great Plains, USA. Palaeogeogr. Palaeoclimatol. Palaeoecol. **207**, 305–329 (2004)
5. Ghaffar, A.: Studies on Equids, Cervids and Carnivora from the Siwalik hills of Pakistan. Ph.D. Thesis, University of the Punjab, Lahore, Pakistan (2005)
6. Hussain, S.T.: Revision of Hipparion (Equidae, Mammalia), from the Siwalik Hills of Pakistan and India. Bayer. Akad. Wiss. Abh. **147**, 1–68 (1971)
7. Koch, P.L., Tuross, N., Fogel, M.L.: The effects of sample treatment and diagenesis on the isotopic integrity of carbonate in biogenic hydroxylapatite. J. Archaeol. Sci. **24**, 417–429 (1997)
8. Roohi, G., Raza, S.M., Khan, A.M., Ahmad, R.M., Akhtar, M.: Enamel hypoplasia in Siwalik Rhinocerotids and its correlation with neogene climate. Pak. J. Zool. **47**(5), 1433–1444 (2015)
9. Wolf, D., Bernor, R.L., Hussain, S.T.: A systematic, biostratigraphic, and paleobiogeographic reevaluation of the Siwalik Hipparionine Horse assemblage from the Potwar Plateau, Northern Pakistan. Palaeontogr. A **300**, 1–115 (2013)

The Thar Desert Calcretes: A Proxy for Understanding Late Quaternary Paleoclimate Shifts

Hema Achyuthan

Abstract

In the Thar Desert, India, calcretes occur in several geomorphic environments and have been classified based on their form, induration, chemistry and associations with parent material. These calcretes have been dated from late Neogene-Early Pleistocene (hardpan calcretes) to 5 ka (nodular calcretes). The calcretes consist of $CaCO_3$ (40–75%) with SiO_2, Al_2O_3 and Fe_2O_3 content in decreasing amounts. Integration of multiple data including textural, chemistry and soil micromorphology indicate that the calcrete nodules formed within the dunes are pedogenic in origin while those occurring in the interdunal depressions are largely groundwater formations. Hardpan calcretes formed on various types of bedrocks are geosols and complex in origin. Stable isotope data for the pedogenic calcretes of C and O vary from −3.8 to −0.2‰, and between −6.1 and −1.5‰ for ^{18}O PDB values, groundwater calcretes ($\delta^{13}C$ −2.0 and 2.5‰, and between −5 and −1‰ for $\delta^{18}O$) and hardpan calcretes yield slightly higher $\delta^{18}O$ values (−5.9 to −1.3‰) than the eolian pedogenic carbonates indicating that the calcretes in the desert margin of the Thar Desert was formed near the surface supporting a thin veneer of soil column. The carbon isotope values signify both C3 and C4 vegetation, with increasing C4 vegetation since the late Quaternary period.

Keywords

Late Quaternary • Calcrete • Pedogenic Groundwater • Geosols • Semi-arid to arid conditions

1 Introduction

Carbonates in terrestrial settings form, under a variety of situations, from permanent water bodies such as deep lakes, to permanent sub-aerial conditions (e.g. calcretes and karst), passing by a wide range of environments, including shallow lakes and palustrine environment [1]. Their study provides important data that help to interpret the sedimentary records of many terrestrial environments as well as the determination of the main controls that play an important role in their formation. Calcretes are generally defined as terrestrial, near surface, secondary calcium carbonate accumulation in soil profiles, alluvium, aeolian sand, bedrock and sediments. Calcrete is formed when precipitation exceeds evapo-transpiration. When precipitation exceeds evapo-transpiration, leaching results, forming types of calcium carbonate nodules. Calcretes are thus strongly climate-controlled. Typical water deficits (evapo-transpiration subtracted from precipitation) of <200–600 mm are most favourable for calcrete formation, although it can also form in more humid environments where there is an abundant supply of carbonate. Till date with regard to their formation and age, barring a few publications the calcretes that occur in the eastern margin of the Thar Desert, have not been studied barring a few publications [2–4]. Calcretes occurring within the dune sediments and as hardpan calcretes formed over the bedrock in the eastern margin of the Thar Desert are intriguing as to their formation and source of carbonate as the region receives less than 350–400 mm of annual average rainfall both by the southwest and winter rains, the southwest being dominant. In this paper, a review on the origin of the calcretes with late Quaternary paleoclimatic implications was presented.

2 Materials and Methods

The eastern margin of the Thar Desert, India (Fig. 1) is represented by undulating plains covered by sand sheets, stabilized sand dunes, salt lakes of late Quaternary age with

H. Achyuthan (✉)
Institute for Ocean Management, Anna University, Chennai, 600025, India
e-mail: hachyuthan0@gmail.com

Z. Zhang et al. (eds.), *Patterns and Mechanisms of Climate, Paleoclimate and Paleoenvironmental Changes from Low-Latitude Regions*, Advances in Science, Technology & Innovation, https://doi.org/10.1007/978-3-030-01599-2_13

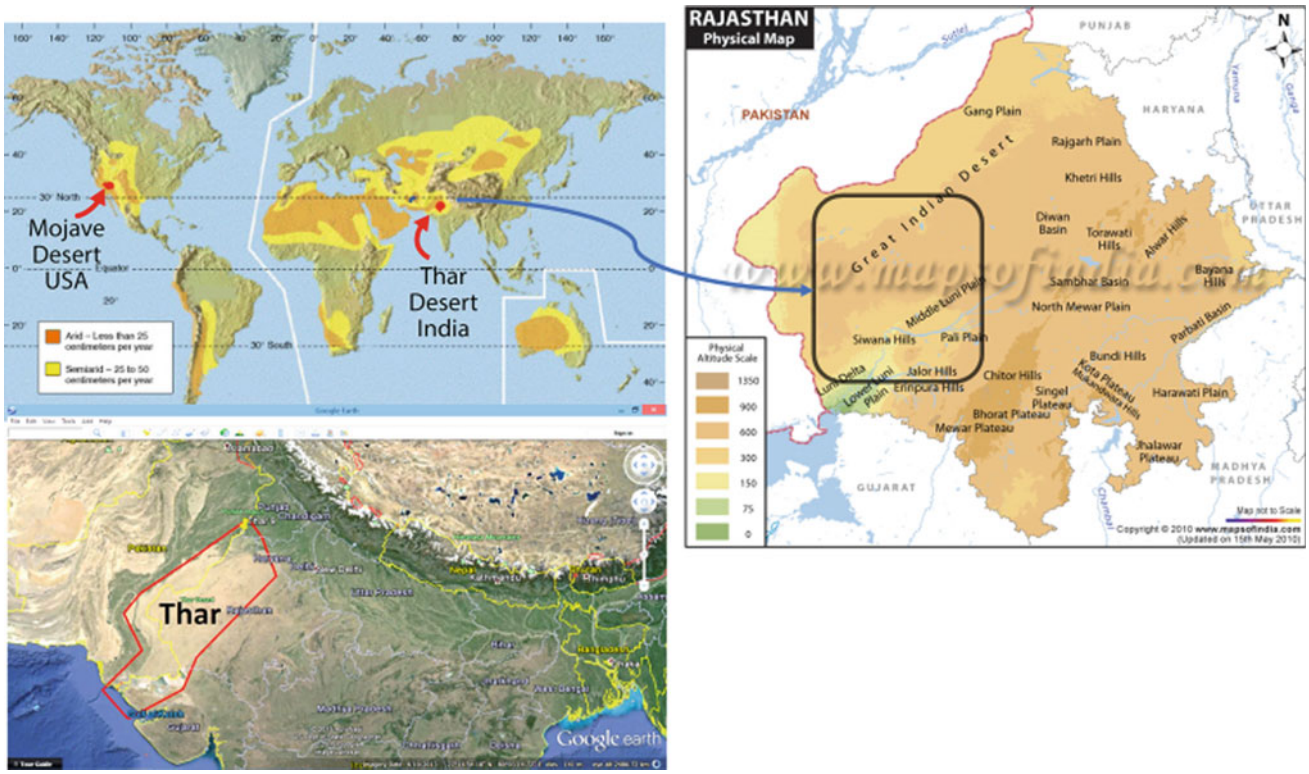

Fig. 1 Location map of the eastern margin of the Thar Desert

isolated granite, granite gneiss, rhyolites and carbonaceous phyllites that occur as monadknocks of Precambrian age, Vindhyan sandstone and Jurassic limestone and sandstone. The desert margin experiences extremes of temperatures with the day time temperature during summer reaching 48–50 °C, whereas the winter is as low as 2–4 °C. The annual rainfall in the area varies from 281 to 503 mm with an average 367 mm. The area can be classified climatically, as semi-arid. The area is sparsely vegetated, and the dunes are covered by shrubby coppice vegetation.

Several dune lithosections range from 2 to 5 m in thickness were trenched and these lithological exposures were studied (Fig. 2) for various parameters such as soil Munsell colours, sediment texture, calcretes types etc. and were closely sampled for textural, soil micromorphology, geochemical analyses and stable isotope studies. Sediment textural analyses were carried out following Carver [5]. 45 calcrete samples were analysed for stable isotopes at the National Geophysical Research Institute, NGRI—Hyderabad. Further, 80 calcrete samples from all the lithosections and hardpan calcretes collected from different sites were thin sectioned and studied under the polarized microscope for soil micromorphology parameters, mineral composition, mineral alteration and weathering features. In the present study, the application of soil micromorphology following the methods put forward by Stoops [6] was adopted.

3 Results

The dune and hardpan calcretes deposits were massive and the stabilised dunes reveal no particular sedimentary structures as they are hardened due to pedogenesis and the calcareous cement. These calcretes have been dated from late Neogene-Early Pleistocene (hardpan calcretes) to 5 ka (nodular calcretes) [2, 3]. The detritus is cemented by calcium carbonate forming the matrix, with clay cutan around the grains. The calcretes formed within the dunes exhibit root pores lined with micritic calcite associated with iron oxide mottling indicating mild pedogenesis as the calcrete is not rich in clays. However, groundwater calcrete displays fibrous calcite (Lublinite) that occurs along with the fibrous calcitic cutans indicating in situ and fast precipitation. Mottles of ferruginous oxides (2–3 um), well rounded and sometimes dispersed within the $CaCO_3$ matrix are distinct. The mottles appear dull orange in colour due to masking of $CaCO_3$ crystals. Calcic grains (60–80 um) within the matrix are well rounded, but at places dissolution of these calcic grains were also noted. Hardpan calcrete displays complex micromorphology textures and features such as several (2–3) micritic rims around the detritus grain, meniscus cement of clear sparry calcite. alveolar structure with root channels indicating both pedogenic and groundwater calcretisation.

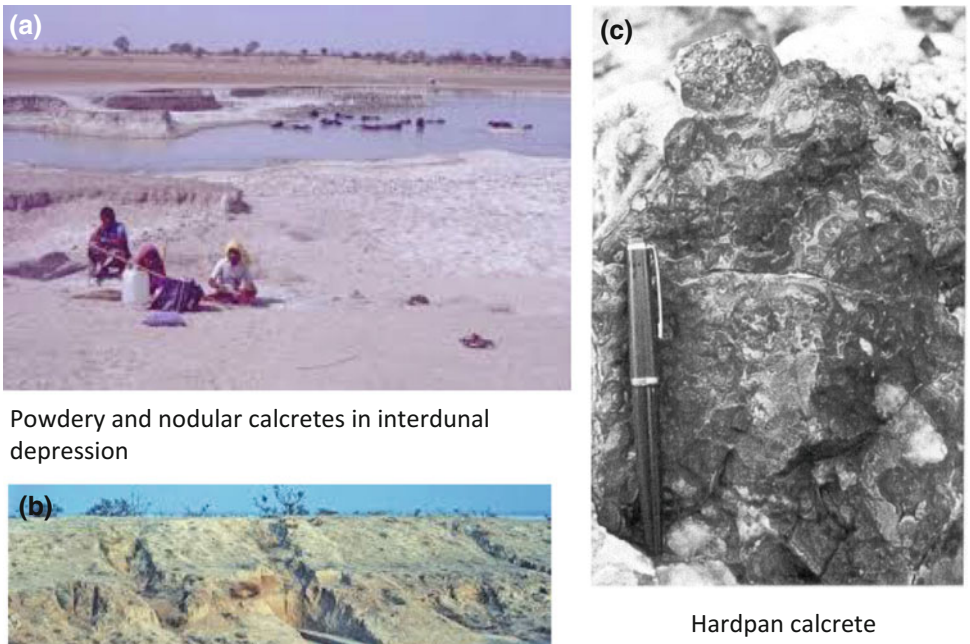

Fig. 2 Types of calcretes that occur in the Thar Desert

Table 1 Geochemistry of calcrete types

Calcrete type	$CaCO_3$ (%)	Stable isotope values
Pedognic carbonates associated with dunes	40–70	^{13}C −3.8 and −0.2‰, and between −6.1 and −1.5‰ for ^{18}O
Groundwater calcretes	48–84	^{13}C −2.0 and 2.5‰, and between −5 and −1‰ for ^{18}O
Hardpan calcretes	42–65	^{13}C 0.3 and 1.5‰, and between −5.9 and −1.5‰ for ^{18}O

Stable isotope data for the pedogenic calcretes of C and O vary from −3.8 to −0.2‰, and between −6.1 and −1.5‰ for ^{18}O PDB values, groundwater calcretes (^{13}C −2.0 and 2.5‰, and between −5 and −1‰ for ^{18}O) and hardpan calcretes yield slightly higher $\delta^{18}O$ values (−5.9 to −1.3‰) than the eolian pedogenic carbonates (Table 1).

4 Discussion

Pedogenic carbonates from the dune sections and several shorter sections including the hardpan calcretes from the Thar Desert, Rajasthan, were analyzed for geochemistry, soil micromorphology and stable isotope to understand the late Quaternary period paleoclimate shifts. Integration of all the data indicate that the pedogenic calcretes is largely composed of well-rounded to sub rounded detritus grains pointing to a long-distance aeolian source of the sediments while the distinguishing feature in the groundwater calcretes is the occurrence of fibrous needle calcite (Lublinite), clear calcic cutans around the detritus pointing to an insitu precipitation of calcite indicating dominant groundwater action. The absence of rootlets, cavity filled by $CaCO_3$ also indicates groundwater activity of calcretisation. Dissolution and re-precipitation of the calcic grains and the presence of mottles indicate short subaerial exposure. Occurrence of

discrete calcic grains (60–80 um) and their dissolution points to dust source.

It is observed that the calcitic coating around the grains occurs more rapidly in semi-arid climates. One of the main reasons for the faster growth rates of carbonates coatings in semi-arid climates is the intensive leaching of carbonate from the upper part of the soil profile or sediment accumulation. The temperature is also found to affect the intensity of $CaCO_3$ accumulation on the detritus in number of ways for example: (i) high temperature promotes evaporation in the soil and increases the concentration of carbonate solution. (ii) $CaCO_3$ solubility in water decreases with growing temperature and a warmer temperature regime favors precipitation of carbonates. The stable $\delta^{13}C$ values show similar values as reported for pedogenic calcretes [2, 3, 7–11]. And this is probably due to the soil derived lighter CO_2 into shallow ground waters [9]. The stable $\delta^{13}C$ data indicate a near surface calcite precipitation.

Geochemical and soil micromorphology data indicate high content of $CaCO_3$ cementing detritus. Carbon isotope results show that C4 biomass (grasses?) has dominated local vegetation for most of the 250,000 years represented by the 16R dune section [3]. The higher 13C values in the dune records correspond to episodes in the strong upwelling and decreased sedimentation rates when compared to the Indian Ocean sediment cores, probably owing to strong Asian Monsoon. The pedogenic calcrete nodules dated to 191,000 years and between 126,000 and ~70,000 years display high % of C4 plants. However, the pedogenic carbonate nodules from 180,000 to 140,000 years and from 13,000 to 26,000 years display lower ^{13}C values consistent with a higher proportion of C3 vegetation.

Stable isotope results show higher % C4 plants that equals high summer rains and a strong monsoon that correlates with the interglacial periods and the early part of the last glacial, which high C3 plants (more winter rain or colder temperatures, a weak monsoon) correlate with glacial maxima. Carbon isotope results show that the C_4 biomass (grasses) has dominated local vegetation for most of the 250,000 years represented by the 16R section longest dune section excavated (19 m trench with Paleolithic tools associated with dune formation) so far. A decrease in $\delta^{18}O$ and $\delta^{13}C$ values during the last interglacial and early glacial periods is noted. The higher $\delta^{13}C$ values in the dune records correlate to episodes in the strong upwelling and decreased sedimentation rates in Indian Ocean cores, probably the result of a strong Asian Monsoon. The high $\delta^{13}C$ values may, therefore, denote the expansion of C_4 vegetation in response to warm, wetter monsoon circulation.

5 Conclusion

In the present study the various types of calcretes from the eastern margin of the Thar Desert was studied for its formation. The calcretes associated with the dunes, interdunal depression and hardpan calcretes were analysed for their chemical composition, soil micromorphology and stable isotopes. The integration of all the data indicates that the calcretes formed within the dunes are pedogenic in formation, while the interdunal calcretes are largely groundwater in origin. The hardpan calcretes reveal a complex action of both pedogenesis and groundwater action. The calcretes are high in $CaCO_3$ content with lower values of SiO_2, Al_2O_3 and Fe_2O_3.

Micromorphological features such as calcicutans, fibrous and needle calcite precipitation around the detritus grain cemented by clear calcite is due to groundwater action, evaporation, evapotranspiration, and precipitation. The micromorphological studies supported by stable isotope data indicate that the process of calcretisation of all the types of calcrete have occurred with a veneer of soil column supporting dominantly C4 grasses in semi-arid climate since the Late Neogene to early Quaternary period and late Quaternary period to recent times.

References

1. Alonso-Zarza, A.M.: Palaeoenvironmental significance of palustrine carbonates and calcretes in the geological record. Earth Sci. Rev. **60**, 261–298 (2003)
2. Achyuthan, H.: Petrologic analysis and geochemistry of the Late Neogene-Early Quaternary hardpan calcretes of western Rajasthan, India. Quatern. Int. **106–107**, 3–10 (2003)
3. Achyuthan, H., Quade, J., Roe, L., Plazcek, C.: Stable isotopic composition of pedogenic carbonates from the eastern margin of the Thar Desert, Rajasthan, India. Quatern. Int. **162**, 50–60 (2007)
4. Dhir, R.P.: Western Rajasthan soils. In: Jaiswal, P.L. (ed.) Desertification and its Control, pp. 102–115. Indian Council of Agricultural Research, New Delhi (1977)
5. Carver, R.E.: Procedures in Sedimentary Petrology. Wiley, New York (1971)
6. Stoops, G.: Guidelines for Analysis and Description of Soil and Regolith Thin Sections. Soil Science Society of America, Madison, WI (2003)
7. Andrews, J.E., Singhvi, A.K., Kailath, A.J., Kuhn, R., Dennis, P. F., Tandon, S.K., Dhir, R.P.: Do stable isotope data from calcrete record late Pleistocene Monsoonal climate variation in the Thar Desert of India? Quatern. Res. **50**, 240–251 (1998)
8. Bajnoczi, B., Horvath, Z., Demeny, A., Mindszenty, A.: Stable isotope geochemistry of calcrete nodules and septarian concretions in a Quaternary 'red clay' paleovertisol from Hungary. Isot. Environ. Health Stud. **42**, 335–350 (2006)

9. Eren, M.: Stable isotope geochemistry of Quaternary calcretes in the Mersin area, southern Turkey—a comparison and implications for their origin. Chem. Erde **71**, 21–27 (2011)
10. Jutras, P.: Climate fluctuations recorded in phreatic and vadose calcretes of the Lower Carboniferous Clyde Sandstone Formation of Machrihanish, Kintyre Peninsula, SW Scotland. Geol. Soc. Lond. **174**, 646–654 (2017)
11. Singh, B.P., Lee, Y.I.I., Pawar, J.S., Charak, R.S.: Biogenic features in calcretes developed on mudstone: examples from Paleogene sequences of the Himalaya, India. Sed. Geol. **201**, 149–156 (2007)

Part IV
Paleoenvironmental Evolution

Using Environmental Isotopes and Krypton-81 to Characterize and Date Continental Intercalaire Paleogroundwater (Southern Tunisia)

Kamel Zouari, Takuya Matsumoto, Rim Trabelsi, and Pradeep Aggarwal

Abstract

In a semi-arid to arid climate region, socio-economic development is mainly dependent on deep groundwater resources. This is the case of the Continental Intercalaire (CI) groundwater which is one of the most important aquifers in the North Western Sahara in Africa. This aquifer system, extending over more than a million of km^2, is mainly confined, poorly recharged but intensely abstracted in Southern Tunisia. Efficient management of this resource relies on accurate data such as recharge/discharge rate and groundwater dynamics. In this study, environmental isotopes (^2H, ^{18}O, ^{13}C, and ^{14}C) were combined with long time lived radio-nuclide (^{81}Kr) to give greater constraint on the groundwater residence time in the CI. Stable isotope signature is depleted compared to the modern rainwater of Sfax station with very low deuterium excess suggesting a paleoclimatic effect. This finding is strongly supported by ^{14}C measurements where most of the analyzed samples are below the detection limit. The used carbon-14 correction models indicate residence times greater than 35 ka. However, the estimated ages range using ^{81}Kr contents are from 150 to 600 kyr, and are clearly much older than the ^{14}C ages, confirming that this method is not suitable for dating CI groundwater.

Keywords

Krypton 81 (^{81}Kr) • Carbon-14 • Noble gas Paleogroundwater • CI Tunisia

1 Introduction

Climate variability and human activity have critical impacts on the sustainability of natural water resources which may lead to the over-abstraction and deterioration of water quality. In the context of climate change and an increasing demand for water, it is essential to understand the origin, the groundwater flow dynamics and the mean residence times for the assessment of the reliability and potential of these resources as a major source of water supply over the medium and long-terms. Radio-isotopes dating of fossil groundwater could further improve the understanding of present and past flow patterns. However, dating of groundwater, particularly on time scales greater than few decades poses problems due to the heterogeneity of the geological and hydrological properties of most aquifers [1, 2]. Under these conditions, the application of inert tracers such as noble gases and radionuclide as Krypton-81, present in very old groundwater are excellent tools to estimate groundwater ages and dynamics [3]. In fact, these radiogenic noble gas isotopes are characterized by long half-life and lack of geochemical interactions.

This paper focused on one of the most important and intensive exploited aquifers in North Western Sahara Aquifer System (NWSAS): the continental Intercalaire extending over large areas of Algeria, Tunisia and also parts of Libyan Desert. The main focus of this investigation was the use of the recently available long-lived radio-nuclides and isotope age tracers for the assessment of groundwater dynamics and age of the Continental Intercalaire aquifer of southern Tunisia.

2 Settings, Sampling and Analysis

The investigated area is located in southern Tunisia and covers Kebili and Tozeur regions. It is limited to the west by the Algerian frontier, to the east by Dahar uplift, to the north

K. Zouari (✉) · R. Trabelsi
Radio-Analysis and Environment Laboratory, ENIS, Sfax University, Sfax, Tunisia
e-mail: kamel.zouari@enis.rnu.tn

T. Matsumoto · P. Aggarwal
Isotope Hydrology Section, International Atomic Energy Agency, Vienna, Austria

Z. Zhang et al. (eds.), *Patterns and Mechanisms of Climate, Paleoclimate and Paleoenvironmental Changes from Low-Latitude Regions*, Advances in Science, Technology & Innovation, https://doi.org/10.1007/978-3-030-01599-2_14

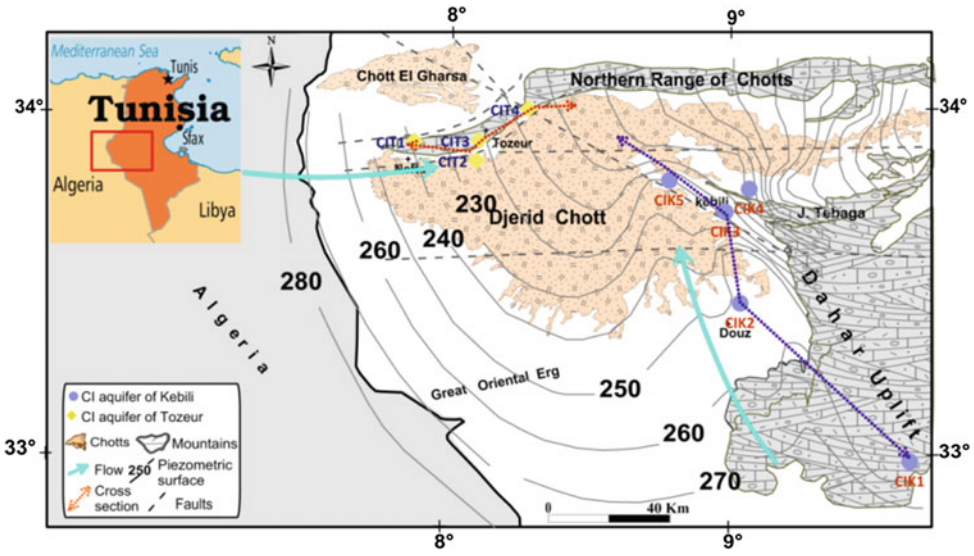

Fig. 1 Location map of the study area showing hydraulic head contour line and sampling points

by the Northern Range of Chotts and to the south by the great oriental Erg (Fig. 1). It is characterized by an arid climate and limited water resources with a mean annual temperature of about 21 °C and precipitation of about 150 mm year^{-1}.

The CI aquifer is made up of middle Jurassic to lower Cretaceous continental formations described as heterogeneous sandy and sandstone units with variable clay contents. The geological sequence of the aquifer consists of several units of detrital sediments separated by clay and gypsum rich strata. The aquifer units are confined by marl and clay layers of Cenomanian age, reaching, in some areas, a thickness of more than 600 m. The CI aquifer is the main resource for water supply. In this research work nine groundwater samples were collected along two flow paths from the main CI hydrogeological formation during February 2015 (Fig. 1) for isotopic and noble gas analyses.

3 Results

3.1 Chemical Composition

The measured conductivity of the groundwater samples ranges from 2.6 to 9.8 ms cm^{-1}. The chemical composition reveals similar water type for all the collected samples with dominance of Na^+–Ca^{2+} and SO_4^{2-}–Cl^- concentrations in both Nefzaoua (Kebili) and Tozeur basins. This chemical pattern could be explained by a water interaction process with the geological formations of the basin (dissolution/precipitation of carbonates and various evaporates) and cation exchange reactions.

3.2 Environmental Isotopes ($\delta^{18}O$, $\delta^{2}H$, ^{14}C, $\delta^{13}C$)

Stable isotopes of the water molecule of CI range from −8.4 to −7.2‰ versus SMOW for $\delta^{18}O$ with a mean value of −8‰, and from −61.5 to −50.3‰ versus SMOW for $\delta^{2}H$. The stable isotope data lie below the local meteoric water line and Global Meteoric water Line [4]. Radiocarbon activities and $\delta^{13}C$ values cover a wide range of values, from 5 to 0.25 pmc and from −10.84 to −7.9‰, respectively.

3.3 Concentration of ^{81}Kr

Concentrations of ^{81}Kr in groundwater samples are expressed in terms of the air-normalized ratio R/R_{air} = [$^{81}Kr/Kr$] sample/[$^{81}Kr/Kr$] air, where R_{air} is the modern atmospheric ratio of 1.10×10^{-12} [5]. The R/Ra ratios of present samples range from 0.16 to 0.28.

4 Discussion

Stable isotopes composition of CI groundwater are all strongly depleted in both ^{18}O and ^{2}H compared to modern Mediterranean rainfall and the shallowest groundwaters by up to 3.5% in ^{18}O. This signature indicates a recharge at higher altitudes or a paleoclimatic effect (recharge under colder climatic conditions than at present). Based on the low ^{14}C activities, the difference between the isotopic composition of CI groundwater and that of present precipitation is caused by a paleoclimatic effect. On the other hand, longer

water residence times enhance equilibration with aquifer carbonate minerals resulting in lower ^{14}C activities and more enriched $\delta^{13}C$ compositions [6]. In fact, the range of $\delta^{13}C$ values is typical of water–rock interaction by the incongruent dissolution of carbonate in recharging meteoric water ($\delta^{13}C$ −22 to −27‰). Based on the different values of pmc, together with the measured $\delta^{13}C$ values, groundwater residence time was calculated using various models [7] taking into account different geochemical processes (carbonate dissolution, soil gas CO_2 dissolution, CO_2 gas-aqueous exchange, calcite, HCO_3 exchange, gypsum dissolution or cation exchange …). These models could be subdivided into: (i) purely chemical mixing, (ii) isotopic mixing and (iii) models of chemical mixing and isotopic exchange. In the present case, only the "Fontes and Garnier Eq." model takes into account major processes occurring in the CI groundwater: gypsum dissolution and Ca/Na cation exchange reactions. The calculated residence times (26–38 ka), correspond to recharge periods of late Pleistocene and exceeds the limits of radiocarbon dating.

Krypton-81 is useful for waters age dating over 50 000 years old and up to approximately 1 Million years [3], greatly exceeding the age range of ^{14}C. The age of ^{81}Kr (t_{Kr}) is calculated by the following equation where R_{air} is the modern atmospheric ratio [5] and λ_{Kr} is 3.03×10^{-6} year^{-1}:

$$t_{Kr} = -\frac{1}{\lambda_{Kr}} \ln\left(\frac{R_{\text{Sample}}}{R_{\text{Air}}}\right)$$

The range of ages estimated for the collected samples is 150–600 kyr, and is clearly much older than the ^{14}C ages, confirming that the ^{14}C method is not suitable for dating the present samples. The lowest residence time is measured close to the aquifer outcrops in the Dahar pointing to a low recharge rate and absence of significant circulation.

5 Conclusion

The Continental Intercalaire (CI) is the largest confined aquifer of NWSAS. The use of environmental isotopes and long-lived radionuclides confirms that CI groundwater is recharged during humid periods of late Pleistocene (150–600 kyr). This information is important for evaluating groundwater dynamics and characterizing the recharge process. This will lead to identify and develop solutions for more effective groundwater management and policy.

References

1. Phillips, F.M.: Chlorine-36. In: Cook, P., Herczeg, A.L. (eds.) Environmental Tracers in Subsurface Hydrology, pp. 299–348. Kluwer Academic Publishers, Norwell, Massachusetts (2000)
2. Love, A.J., Herczeg, A.L., Sampson, L., Cresswell, R.G., Fifield, L. K.: Sources of chloride and implications for ^{36}Cl dating of old groundwater, southwestern great artesian basin, Australia. Water Resour. **36**, 1561–1574 (2000)
3. Sturchio, N.C., Du, X., Purtschert, R., Lehmann, B.E., Sultan, M., Patterson, L.J., Lu, Z.T., Müller, P., Bigler, T., Bailey, K., O'Connor, T.P., Young, L., Lorenzo, R., Becker, R., El Alfy, Z., El Kaliouby, B., Dawood, Y., Abdallah, A.M.A.: One million year old groundwater in the Sahara revealed by krypton-81 and chlorine-36. Geophys. Res. Lett. **31**, L05503 (2004)
4. Craig, H.: Isotopic variations in meteoric waters. Science **133**, 1702–1703 (1961)
5. Du, X., Purtschert, R., Bailey, K., Lehmann, B.E., Lorenzo, R., Lu, Z.-T., Mueller, P., O'Connor, T.P., Sturchio, N.C., Young, L.: A new method of measuring ^{81}Kr and ^{85}Kr abundances in environmental samples. Geophys. Res. Lett. **30**(20), 2068 (2003). https://doi.org/10.1029/2003GL018293
6. Mook, W.G., De Vries, J.J.: Environmental Isotopes in the Hydrological Cycle: Principles and Applications. IHP–V no. 39. UNESCO, Paris (2000)
7. Clark, I.D., Fritz, P.: Environmental Isotopes in Hydrogeology, 328 pp. Lewis Publishers (1997)

Water Column Chemistry of Late Holocene Lake Bafa, Eastern Coast of the Aegean Sea (Turkey)

Özlem Bulkan, Ummuhan Sancar, Wei Wei, Xiaomin Zhu, and M. Namık Çağatay

Abstract

This study represents the preliminary results of the first dataset of diatom and bulk stable carbon organic isotopic ($\delta^{13}C_{org}$) compositions of the sediments collected from Lake Bafa. The aim of this study was to investigate the water column properties of the lake during the Late Holocene, by facilitating salinity and organic matter productivity markers. The isotopic radiocarbon ($\delta^{13}C_{org}$) dating and diatom-faunal analyses were performed for the first time on a variety of sediments from Lake Bafa. They were retrieved from the modern lacustrine basin depo-center, containing the phases of a freshwater lake, an alkaline lagoon and a marine environment respectively. ^{14}C-AMS-dated sediments represent a complete geological archive reflecting the last 2.5 kyr time period, beginning with a depositional phase dominated by marine conditions represented by enhanced salinity ranges and aquatic productivity signals. This stage was followed by a long period (i.e. 1.75–0.8 ka BP) dominated by a lagoonal environment. During the final stage between 0.8 ka BP and recent, fresh water lake conditions in a closed lacustrine system have occurred.

Keywords

Aegean coastal Lake Bafa • Water column chemistry • Stable organic carbon isotopes • Diatom species

Ö. Bulkan (✉)
Department of Surface Waters – Research and Management, Swiss Federal Institute of Aquatic Science and Technology, Kastanienbaum, Switzerland
e-mail: bulkan@istanbul.edu.tr

Ö. Bulkan
Istanbul University-Cerrahpaşa, Avcılar, Istanbul, 34320, Turkey

U. Sancar · M. N. Çağatay
Istanbul Technical University, Istanbul, Turkey

W. Wei · X. Zhu
China Petroleum University, Beijing, China

1 Introduction

Lake Bafa is known to be one of the most significant inland lacustrine systems along the Aegean coastal area of Western Turkey. The modern basin of the lake is 2 m above sea level (masl.) (37° 31′ N, 27° 27′ E) with a maximum water depth of 20 m (Fig. 1a). Previous studies to date have suggested that the Lake Bafa basin was a marine embayment in the southern part of the former Latmian Gulf before the early Holocene and during the late Holocene [1–7]. These studies also revealed that the progradation of the River Büyük Menderes caused an intensive detrital material transportation and accumulation in and around the Lake Bafa basin. We consider that basin as an important sedimentary archive for the understanding of the coastal evaluation of the Aegean Sea eastern coast during the Holocene because it contains important information on the water column characteristics involving a separation phase from residual marine to coastal ecosystem. Diatoms are a large and diverse group of single-celled algae and distributed in several marine and freshwater aquatic ecosystems [8]. Hence, they are potentially very useful for the researchers who aim to determine the rapid changes in aquatic environments. This is the reason why we specifically focused on the diatoms among many other faunas. In this study, we presented the results of our multi-proxy study focusing on the diatom record and isotopic ($\delta^{13}C_{org}$) data in the sedimentary archive of Lake Bafa, which has a potential to give important clues about the temporal changes in the water column chemistry.

2 Materials and Methods

A hammer coring method was used to retrieve a 4.1 m long sediment core (BAF*37*) from the lake depo-center (Figs. 1 and 2). A total of three radiocarbon ages provided from *Cerastoderma glaucum* sp. shells were measured in Beta Analytical Laboratories and calibrated by following the

Z. Zhang et al. (eds.), *Patterns and Mechanisms of Climate, Paleoclimate and Paleoenvironmental Changes from Low-Latitude Regions*, Advances in Science, Technology & Innovation, https://doi.org/10.1007/978-3-030-01599-2_15

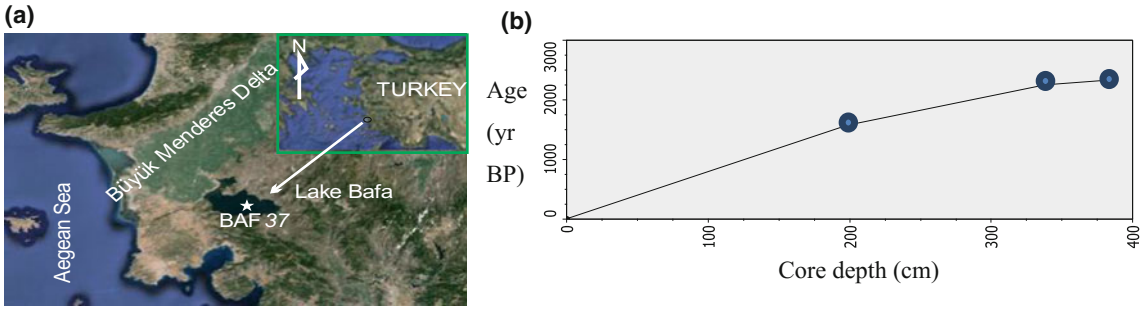

Fig. 1 **a** Location map of Lake Bafa (Google Earth Image); **b** age model for core BAF*37*

methods of Stuiver et al. [9]. Total organic carbon isotopic ($\delta^{13}C_{org}$) measurements were conducted in China University of Petroleum Laboratories. Diatom samples were prepared using a standard method of Renberg [10] and slides were studied using a Nikon type light microscope.

3 Results

We subdivided the sedimentary section of the core BAF*37* into five lithostratigraphical units by taking our sedimentological observations across the core into consideration (e.g. lithology, grain size and fossil records). In order to construct a chronological model, we had three samples dated by ^{14}C method (Figs. 1b and 2). Note that these three samples were specifically taken form the key levels of the sedimentary section. We have organic carbon stable isotopic values determined on 18 samples. These values vary in a range from −23 to −28‰, with an average value of −25‰ (Fig. 2). We determined the characteristic diatom species across the core and divided them into three groups on the basis of the ecosystems they lived in (i.e. marine, brackish and freshwater) (Table 1). We also determined the time dependent changes of their abundance in a variety of ecological conditions along the length of the core sample (Fig. 2).

4 Discussion

Marine specific diatom associations dominate the bottom of the core, corresponding to the period between 1.75 and 2.3 ka BP. Together with relatively higher negative values of $\delta^{13}C_{org}$ (−28‰) from the sediments, this observation indicates the presence of a marine environment with an abrupt increase in salinity and aquatic production signs. Upper in the core (i.e. 0.8–1.75 ka BP period), diatom species which are characteristic of the brackish water environment become abundant. They reflect lagoonal conditions, interrupted by flood events, sourced either from the nearby fluvial prograding delta (e.g. Büyük Menderes) or marine (i.e. Aegean Sea) environments. During the last 800 years, Lake Bafa has been a closed lacustrine system, as indicated by the dominance of fresh water diatom species over brackish ones in the sediments. Relatively more ^{13}C-enriched mean values (−24‰) in these sediments reflect either higher terrestrial organic matter supply from surrounding areas of the lake or enhanced HCO_3^- availability for lacustrine algae within the water column [11].

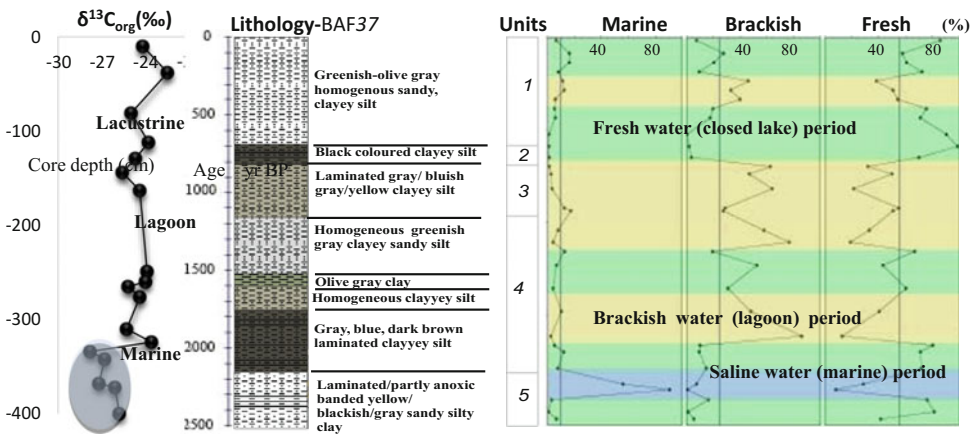

Fig. 2 Lithology, $\delta^{13}C_{org}$ data, percentages of diatoms and marked environmental conditions

Table 1 Diatom species and related environmental signs

Marine water species*	Brackish water species	Fresh water species	
Campylodiscus *limbatus*	Mastogloia *smithii*	Amphora *ovalis*	Gyrosigma *acuminatum*
Coscinodiscus *asteromphalus*	Navicula *peregrina*	Amphora *veneta*	Halamphora *coeffeaeformis*
Dimeregramma *minor*	Rhopalodia *musculus*	Aulocoseira sp.	Mastogloia *albertii*
Diploneis *bombus*	Surrirella *brebissonii*	Cocconeis *placentula* var *euglypta*	Navicula *cassieana*
Diploneis *stroemii*	Thalassiosira *fluviatilis*	Cocconeis sp.	Navicula sp.
Hyalodiscus *subtilis*		Cocconeis *placentula* var *pseudolineata*	Neidium *iridis*
Nitzschia *coarctata*		Cyclotella *ocellata*	Nitzschia *exilis*
Opephora *pasifica*		Cyclotella *rossi*	Nitzschia *palea*
Rhaphoneis *amphiceros*		Cylotella sp.	Planothidium *delicatum*
Synedra *ulna*		Cymbella *cistula*	Pseudostaurosira *brevistriata*
Tabularia *fasciculata*		Epithemia *adnata*	Rhoicosphenia *abbreviata*
Terpsinoe *americana*		Epithemia *sorex*	Rhopalodia *gibba*
Thalassiosira *oestrupii*		Fallacia *pygmaea*	Synedra *famelica*
			Tryblionella *gracilis*
			Gomphonema *truncatum*

*Marine to Fresh water species e.g. Achnanthes *brevipes*, Campylodiscus *clypeus*, Cyclotella *meneghiniana*, Diploneis *smithii*, Tryblionella *punctata* were also observed along the core section. Additional faunal data, e.g. foraminiferal analysis are given in Bulkan et al. [4]

5 Conclusions

The synthesis of a multi-proxy approach provided the following conclusions concerning the water column conditions in Lake Bafa: (1) the water column during the last 800 years indicates the dominance of fresh water (lacustrine) conditions; (2) 0.8–1.75 ka record reflects mainly brackish water (lagoon) chemistry; (3) 1.75–2.5 ka record suggests enhanced salinity and aquatic productivity signals which are consistent with a marine environment.

Acknowledgements We would like to thank the project funds provided kindly by the Tubitak-Ardeb-1001/1002 (P.Nr: 113Y070; P.Nr: 115Y766) and Istanbul University (Bap P.Nr: 28942; P.Nr: 17828). For his valuable constructive comments and suggestions, we would like to thank Prof. Dr. Mehmet Keskin. We thank the ITU-EMCOL team and students, Dursun Acar, Bilgehan Toksoy, Burak Yalamaz and Cansu Demirel for their support to retrieving the core samples or discrete sampling.

References

1. Brückner, H., Müllenhoff, M., Handl, M., van der Borg, K.: Holocene landscape evolution of the Büyük Menderes alluvial plain in the environs of Myous and Priene (Western Anatolia, Turkey). Z. Geomorphol. **127**, 47–65 (2002)
2. Bulkan, Ö., Zhu, X., Wei, W.: Carbon stable isotopic composition of the residual freshwater ecosystems around coastal plain of Great Menderes Delta (Western Anatolia). In: Final Proceedings, 32nd International Meeting of Sedimentology, Marrakech, Morocco (2016)
3. Bulkan, Ö., Zhu, X., Wei, W., Yalamaz, B., Çağatay, M.N.: Organic geochemical characterization of Lake Bafa sediments, accumulated during the last 4500 years (Western Turkey). In: Final Proceedings, 28th International Meeting on Organic Geochemistry, Florence, Italy (2017)
4. Bulkan, Ö., Sancar, Ü., Sarı, E., Kırcı-Elmas, E., Yıldız, T., Çağatay, M.N., Acıpınar, S., Demirel, C., Toksoy, B., Acar, D.: Bafa Gölündeki Holosen İklimsel Değişimlerinin Organik Maddenin Karbon-Hidrojen İzotopik Bileşimi, Lipid Biyolojik İşaretçiler (Uzun Zincirli Alkenon:Lcas) ve Diyatome Kayıtlarına Yansımaları, Final Report, Tubitak, P.Nr.113Y070 (unpublished, in Turkish), 265 pp. (2018)
5. Hakyemez, H.Y., Erkal, T., Göktaş, F.: Late Quaternary evolution of the Gediz and Büyük Menderes grabens, Western Anatolia, Turkey. Quatern. Sci. Rev. **18**, 549–554 (1999)
6. Knipping, M., Müllenhoff, M., Brückner, H.: Human induced landscape changes around Bafa Gölü (Western Turkey). Veget. Hist. Archaeobot. **17**, 365–380 (2008)
7. Müllenhoff, M., Handl, M., Knipping, M., Brückner, H.: The evolution of Lake Bafa (Western Turkey)—sedimentological, microfaunal and palynological results. Coastline Rep. **1**, 55–66 (2004)
8. Round, F.E., Crawford, R.M., Mann, D.G.: The Diatoms: Biology and Morphology of the Genera, p. 747. Cambridge University Press, Cambridge (1990)
9. Stuiver, M., Reimer, P.J., Reimer, R.W.: CALIB 5.0. (Program and Documentation at http://calib.qub.ac.uk/calib) (2005)
10. Renberg, I.: A procedure for preparing large sets of diatom slides from sediment cores. J. Paleolimnol. **4**, 87–90 (1990)
11. Meyers, P.A.: Organic geochemical proxies of paleoceanographic, paleolimnologic, and paleoclimatic processes. Org. Geochem. **27**, 213–250 (1997)

New Reports of Messinian Lago-Mare Episodes from Tunisia: Ostracods and Paleoenvironmental Implications

Rim Temani, Hayet Khayati Ammar, and Francesco Sciuto

Abstract

At the end of the Messinian Salinity Crisis several parts of the Mediterranean Basin were affected by intense continentalization with the deposition of sedimentary facies characterized by brackish to fresh water fauna called Lago-Mare in the lower basin area. In eastern Tunisia, the micropalaeontological analysis performed in two stratigraphical sections sampled on upper Messinian deposits allowed us to identify these sedimentary facies in south Mediterranean regions for the first time. Stratigraphic levels with a high concentration of fresh or brackish water ostracods were identified in two sections and record two contemporary Lago-Mare events. The wadi El Kebir section shows levels dominated by *Cyprideis agrigentina* and *Cyprideis torosa* typical to a lagoon or estuary while the Salakta section presents a very rich ostracod fauna consisting essentially of *Amnicythere propinqua*, *Darwinulina stevensoni*, *Mediocytherideis aff. punctata*, *Ilyocypris gibba* and of very abundant specimens belonging to the genera *Candona* and *Loxoconcha* characterizing a true fresh water environment.

Keywords

Late Messinian • Lago-Mare • Ostracods
Palaeoenvironmental evolution

1 Introduction

After the deposition of the Evaporites related to the Messinian Salinity Crisis (MSC), the breakdown of communication between the Atlantic and Mediterranean sea coupled with the onset of global humid climatic conditions [1, 2] triggered the dilution of the hypersaline Mediterranean waters down to oligomesohaline conditions [3].

According to several authors, after the MSC evaporitic phase, the Mediterranean Sea was transformed into a series of lagoons with reduced salinity. These environmental and facies changes were mentioned as a lago mare event. As a consequence, after the MSC, the hypersaline Mediterranean waters were diluted to brackish conditions and the Paratethyan ostracods were able to spread into the whole Mediterranean area, from east to west, as documented by a number of authors.

Few detailed studies were carried out on the upper Miocene ostracods of Tunisia, especially in the offshore domain (Gulf of Gabes, South Tunisia) [4].

If we except some studies devoted to the Messinian in Tunisia, we need to investigate the Messinian Lago-Mare ostracods as they have received very little attention. This paper is therefore the first attempt to analyze Lago-Mare Messinian ostracods recorded in Eastern Tunisia and interpret their palaeoecologic, palaeoclimatic, and biostratigraphic significance to achieve a palaeoenvironmental understanding of the Lago-Mare deposits in eastern Tunisia.

2 Materials and Methods

Two sections were investigated in details for paleontological analyses focusing on ostracods: the wadi El Kebir (OK) and the Salakta (SAL) sections.

The wadi El Kebir (OK) section outcrops in the eastern side of the wadi El Kebir dam, in the Nabeul region, south eastern part of the Cape Bon Peninsula. It is about 8.5 m thick siliciclastic deposits. It can be divided into two lithostratigraphic units. The first is mostly sandy of 2.5 m thickness. The second level, however, begins with centimetric sandy-clay surmounted by laminated clays interbedded within the sandstone. These deposits correspond to the upper Messinian (Oued el Bir formation).

R. Temani (✉) · H. K. Ammar
The National Office of Mines, 2035 Charguia, Tunisia
e-mail: rim.temani@yahoo.fr

F. Sciuto
Departmento of Biological, Geological and Environmental Sciences, University of Catania, 95129 Catania, Italy

Z. Zhang et al. (eds.), *Patterns and Mechanisms of Climate, Paleoclimate and Paleoenvironmental Changes from Low-Latitude Regions*, Advances in Science, Technology & Innovation, https://doi.org/10.1007/978-3-030-01599-2_16

The Salakta (SAL) section is nearly 10 m thick and is located about 1 km south of Ksour essaf city. The first levels consist of 2 m thick marls and are occasionally silty. Overlying this first level, we observe 3.5 m of biosclastic sand interbedded with centrimetric marls. This sand shows fragments of bivalves and bioturbations in some intervals. Then, 3.5 m thick layer of yellow fine sands containing bioclasts and Pectinids on the top, grading up to calcareous sandstones. The whole is topped by 1 m of green marl containing broken and complete oysters shells and 50 cm of fine sand.

Eighty four samples were prepared, following standard micropalaeontological methods. From each sample, 250 g were washed using diluted hydrogen peroxide for disintegration through standard sieves (63/125/250/500 µm). Residuals were picked out and subjected to detailed taxonomic investigations. SEM micrographs were performed using an LMU Tescan Vega II Scanning Electron Microscope at the Electronic Microscopy Laboratory in the University Catania. The specimens are preserved in the paleontological and sedimentological laboratory, of the geological survey of the National Office of Mines in Tunisia.

3 Results

3.1 Wadi El Kebir Section

The micropalaeontological analyses carried out on the Wadi El Kebir section show well-preserved ostracod faunal records. Our study shows that the lower part of the section from sample OK1 to sample OK19 contains a rich and diversified ostracod fauna that is typical of shallow water marine environments. The association is dominated by *Cytheridea acuminata*; *Paracytheridea triquetra*, *Aurila hesperiae*; *Aurila* spp.; *Loxoconcha* spp.; *Xestoleberis communis*, and *Xestoleberis* spp. The second assemblage (OK20-OK29) shows a very low diversity of ostracods represented mainly by brackish/lagoon species such as *Cyprideis agrigentina* and *Cyprideis torosa* and rare benthic foraminifera with *Elphidium crispum* and/or *Ammonia beccarii*. In the upper and last part of the section, more or less well-preserved ostracods were observed with the restart of the shallow marine association with the abundance of almost the same species of the lower part of the section.

3.2 Salakta Section

The first eight samples gathered from this section show shallow marine ostracod association dominated by *Neomonoceratina interiecta*, *N. laskarevi*, *Acanthocythereis hystrix, Cytheridea acuminata, Occlusacythereis perpusilla*, and *Peteraurila africana*. The upper samples (SAL9 to SAL 17) are characterized by freshwater ostracod assemblages where the main taxa are *Candona* spp.; *Darwinulina stevensoni; Amnicythere propinqua*; *Ilyocypris gibba, Ilyocypris* spp.; *Mediocytherideis (Sylvestra)* aff. *punctata, Mediocytherideis* sp.; *Lepthocythere* spp.; *Callistocythere* sp.; *Loxoconcha perspicua*; *Loxochoncha* spp.; *Phlyctenophora farkasi*. Charophyte gyrogonites (PL.1.H,I) are found in these levels. No ostracods were found in the overlying layers (SAL 18-SAL 21), where most samples are barren. From SAL 22 to SAL 30, the collected ostracods are dominated by *Loxoconcha perspicua*, *Peteraurila africana*, *Cytheridea acuminata*, *Capsacythere sicula*, together with very rare *Candona* spp. and *Darwinulina stevensoni.* The last two samples of the section are barren.

4 Discussion (Paleontology)

Based on previous works, the stratigraphic and geographical features of the six species identified in the Upper Messinian levels where fresh water and/or brackish water ostracods are dominant are shown below.

Cyprideis agrigentina DECIMA 1964, (PL.1.A): is one of the most widespread ostracod that lived in the Paleomediterranean during the latest Messinian Lago-Mare event (5.53–5.33 Ma, CIESM, 2008; 5.55–5.33 Ma), [5, 6]. Messinian of the western and eastern Mediterranean.
Cyprideis ex C. *torosa* group (Jones 1850), (PL.1.B): Italy: Messinian, Quaternary, France: Late Miocene, Tunisia: Pliocene-Pleistocene, Spain: Messinian, Yugoslavia: Pleistocene, Austria: Recent, Turkey: late Miocene -Recent.
Amnicythere propinqua (Livental 1929), (PL.1.C): Mediterranean Basin (Latest Messinian lago-mare event [7], Paratethys: Pliocene and Pleistocene.
Darwinulina stevensoni (Brady and Roberston 1870), (PL.1. D,E): Crete: Upper Serravallian and/or Lower Tortonian. Greece: Upper Pliocene and Upper Pleistocene, Turkey: Widely spread from the Upper Miocene to the Lower Pleistocene.
Mediocytherideis aff. Mediocytherideis (Sylvestra) *punctata* Ligios et al. (2008), (PL.1.F): Italy: late Messinian.
Ilyocypris gibba (Ramdohr 1808), (PL.1.G): France: Upper Miocene, Turkey and Slovakia: Lower Miocene and Pliocene. Its general distribution is Europe, Africa, the Middle East, Central Asia, China, and both North and South America.

The ostracod association found in the two levels of the wadi El Kebir and Salakta sections shows oligotypic character and is certainly comparable with the Lago-Mare ostracod associations reported by many authors for other localities of the Paleomediterranean Basin (Plate 1).

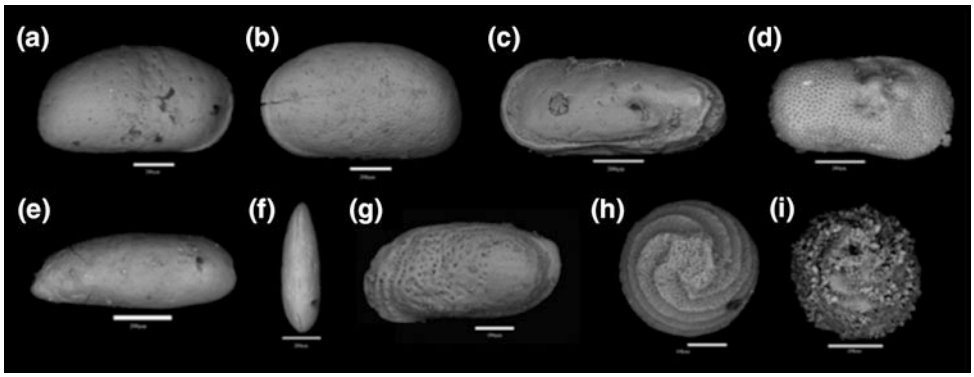

Plate 1 **a** *Cyprideis agrigentina*, **b** *Cyprideis* ex C. *torosa group*, **c** *Amnicythere propinqua*, **d** *Ilyocypris gibba*, **e**, **f** *Darwinulina stevensoni*, **g** *Mediocytherideis aff. Mediocytherideis punctata*, **h**, **i** Charophyte

5 Conclusions

The upper Messinian deposits analyzed in the two sections show a high biological diversity and occurrence of biota having a biostratigraphic and paleoecological significance, leading us to identify two contemporary Lago-Mare events, representing two different environmental conditions.

The first event, identified in the laminated clay interbedded within sandstone (samples OK 20 to OK 29) of Wadi El Kebir section, reveals a strongly reduced diversity; the faunistic association is generally poor or completely barren. The ostracofauna is represented only by species of the genus *Cyprideis* (genera known to thrive under hyposaline and hypersaline conditions) associated with rare benthic foraminifera such as *Elphidium crispum* and/or *Ammonia beccarii*. *Cyprideis, Elphidium*, and *Ammonia* are taxa that can survive low oxygen levels that are common in lagoons or estuaries, where they proliferate [8].

The second Lago–Mare event indentified in the biosclastic sand interbedded with centrimetric marls (samples SAL 9 to SAL 17) of the Salakta section shows a rich freshwater ostracod input and is characterized by the occurrence of *darwinulina stevensoni*, *Amnicythere propinqua* (Livental); *Ilyocypris gibba* and very abundant specimens belonging to the genera *Candona* and *Loxoconcha* associated with Charophyte. This interval most likely records a true fresh water environment.

In the northern side of the studied area, the Lago-Mare biofacies are characterized by a brackish/lagoon environment characterized by the "*Cyprideis* assemblage", whereas, in the southern part, the ostracod assemblage reveals a lacustrine freshwater environment.

References

1. Griffin, D.L.: Aridity and humidity: two aspects of the late Miocene climate of North Africa and the Mediterranean. Palaeogeogr. Palaeoclimatol. Palaeoecol. **182**, 65–91 (2002)
2. Bertini, A.: The Northern Apennines palynological record as a contribute for the reconstruction of the Messinian palaeoenvironments. Sed. Geol. **188–189**, 235–258 (2006)
3. Grossi, F., Cosentino, D., Gliozzi, E.: Palaeoenvironmental reconstruction of the late Messinian lago-mare successions in central and eastern Mediterranean using ostracod assemblages. Boll. Soc. Paleontol. Ital. **47**, 131–146 (2008)
4. Bonaduce, G., Ruggieri, G., Russo, A., Bismuth, H.: Late Miocene ostracods from the Ashtart 1 well (Gulf of Gabés, Tunisia). Boll. Soc. Paleont. Ital. **31**(1), 3–93 (1992)
5. Manzi, V., Gennari, R., Hilgen, F., Krijgsman, W., Lugli, S., Roveri, M., Sierro, F.J.: Age refinement of the Messinian salinity crisis onset in the Mediterranean. Terra Nova **25**, 315–322 (2013)
6. Roveri, M., Flecker, R., Krijgsman, W., Lofi, J., Lugli, S., Manzi, V., Sierro, F.J., Bertini, A., Camerlenghi, A., De Lange, G., Govers, R., Hilgen, F.J., Hübscher, C., Meijer, P.T., Stoica, M.: The Messinian salinity crisis: past and future of a great challenge for marine sciences. Mar. Geol. **352**, 25–58 (2014)
7. Gliozzi, E., Rodriguez-Lazaro, J., Nachite, D., Martin-Rubio, M., Bekkali, R.: An overview of Neogene brackish leptocytherids from Italy and Spain: biochronological and palaeogeographical implications. Palaeogeogr. Palaeoclimatol. Palaeoecol. **225**, 238–301 (2005)
8. Van de Poel, H.M.: Foraminiferal biostratigraphy and paleoenvironments of the Miocene-Pliocene Carboneras-Nijar Basin (SE Spain). Scr. Geol. **102**, 1–32 (1992)

Geochemical Evidences of Paleoenvironmental Changes in Late Quaternary Lacustrine Sediments of the Konya Closed Basin (Konya, Turkey)

Hükmü Orhan, Arif Delikan, Ahmet Demir, Sevinç Kapan, Kemal Olgun, Ayhan Özmen, Ülkü Sayin, Gamze Ekici, Hülya Aydin, and Atike Nazik

Abstract

Important geochemical evidence reflecting Quaternary climatic changes was obtained by evaluating geochemical data from 51 samples and datings from 3 samples by ESR method from sediments of a 7-m-deep trench in Great Konya lake area at the southwest of Adakale village (Konya, Turkey). The geochemical data indicate that the study area was influenced, four times, by a climate having strong precipitation, which caused strong erosion and high detrital input between 25,276 ± 1732-year BP and approximately 50,000-year BP. These periods correspond to climatic changes during the last glacial periods, the warm climate of D-O-2, D-O-5, D-O-6 and D-O-14 events and the cold climate of H2, H3, H4 or H5 and H6 events.

Keywords

Konya Closed Basin • Quaternary climate
Geochemical proxies • Last glacial maximum

1 Introduction

Lacustrine sedimentation is controlled by numerous interacting factors such as climate, tectonic, geomorphology, surrounding vegetation, aquatic biota and recent human activities [1–3].

The Konya Closed Basin is an important basin in central Turkey, in terms of geographic position, Quaternary infills and well-preserved archeological sites (Fig. 1) and has been studied by many researchers [4–7 among others].

The Quaternary sediments in the Konya Closed Basin are represented by the coarse-grained marginal shoreline facies and associated landforms (beach ridges, wave-cut cliffs, etc.) which surround the plain and lake marls and others, mainly fine grained, sediments which locally exceeds 400 m.

Global climate during the last glacial (~120,000–10,000 years before present) period has experienced at least twenty short-lived abrupt and large-amplitude warming shifts called Dansgaard-Oeschger (D-O) events determined in Greenland ice cores. Heinrich events (H) are the second major type of climatic event that occurred mostly in the latter half of the last glacial. They are the coldest intervals between D-O events [8].

The geochemical data obtained from the late Quaternary lacustrine sediments in the Konya Closed Basin have been used to elucidate the climatic changes, weathering regime, redox conditions and lake productivity in the Konya region during the late Quaternary.

This study was supported by the **TUBİTAK project no 114Y237**.

H. Orhan (✉) · A. Delikan · A. Demir
Department of Geological Engineering, Selçuk University, Konya, Turkey
e-mail: horhan@selcuk.edu.tr

S. Kapan
Department of Geological Engineering, Çanakkale 18 Mart University, Çanakkale, Turkey

K. Olgun
DSİ 4. Regional Directory, Konya, Turkey

A. Özmen · Ü. Sayin · G. Ekici
Department of Physics, Selçuk University, Konya, Turkey

A. Özmen · Ü. Sayin
Advanced Technology Research & Application Center, Selçuk University, Konya, Turkey

H. Aydin
Department of Physics, Dokuz Eylül University, Izmir, Turkey

A. Nazik
Department of Geological Engineering, Çukurova University, Adana, Turkey

Z. Zhang et al. (eds.), *Patterns and Mechanisms of Climate, Paleoclimate and Paleoenvironmental Changes from Low-Latitude Regions*, Advances in Science, Technology & Innovation, https://doi.org/10.1007/978-3-030-01599-2_17

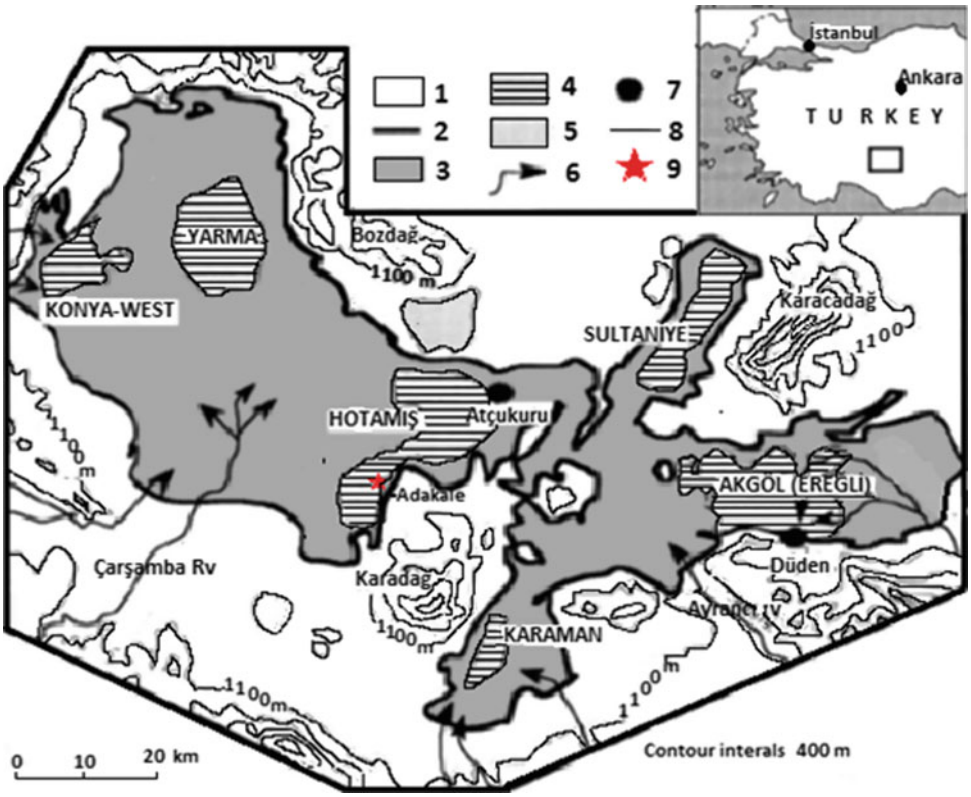

Fig. 1 Map of the Upper Pleistocene Lake systems in the Konya Closed Basin [7]. *1*. Limestone and volcanic basement; *2*. Limit of Pleniglacial paleobeaches and fans; *3*. Extension of Pleniglacial lake; *4*. Approximate extension of Late Glacial and Holocene lakes and marshes; *5*. İsmil dune system (Lake Glacial); *6*. Main surface inflow; *7*. Swallow holes; *8*. Contours; *9*. Sampling site (Adakale)

2 Materials and Methods

51 samples about 10 cm apart were collected from a 7-m deep trench opened near the Adakale village (Konya, Central Turkey). All of these samples were analyzed for their major oxides and trace elements including REEs by inductively coupled plasma emission spectrometry (ICP-ES; major elements) and inductively coupled plasma mass spectrometry (ICP-MS; trace elements including REEs), in the Acme Analytical Laboratory (Vancouver, Canada).

Three highly fossiliferous (Mollusca shells; *Bithnia tentaculate*, *Valvata piscinalis*) samples collected at the depth of 60, 419, and 491 cm from the trench, suitable for ESR dating, were dated.

3 Results

3.1 Detrital Influx Proxies

The Al, Ti and Zr content and the Ca/Al, Ca/Ti, Si/Al, Ti/Al and Sr/Al ratios have been widely used as detrital influx proxies [3, 9]. In a place where the climatic conditions were characterized by strong rainfall, erosion rate and the detrital input to the lakes would be high [10]. The Al, Ti and Zr content of these sediments would be high, while the Ca/Al, Ca/Ti and Sr/Al ratios would be low [2, 3].

Three levels corresponding relatively to high Si, Al, K, Ti and Fe, low Ca contents and high Ti/Al, Rb/Sr and low Si/Ti ratios represent periods of strong rainfall and high detrital input.

3.2 Redox Proxies

The concentration of redox sensitive elements such as U, Th, Mo, Ni, V, Fe and trace element ratios may provide important clues about the paleoredox conditions [9]. Most of the redox-sensitive trace metals tend to be more soluble under oxidizing conditions than under reducing conditions. This behavior makes U, V and Mo, and to a lesser extent certain other trace metals such as Cr and Co, useful as paleoredox proxies [9].

Four levels which are characterized by high Th, Ni, V, Cs and Ce and low Mo contents were identified through the measured section. Samples from these levels were also relatively enriched in SiO_2 and Al_2O_3, which indicated oxic bottom water condition and cold and wet climate.

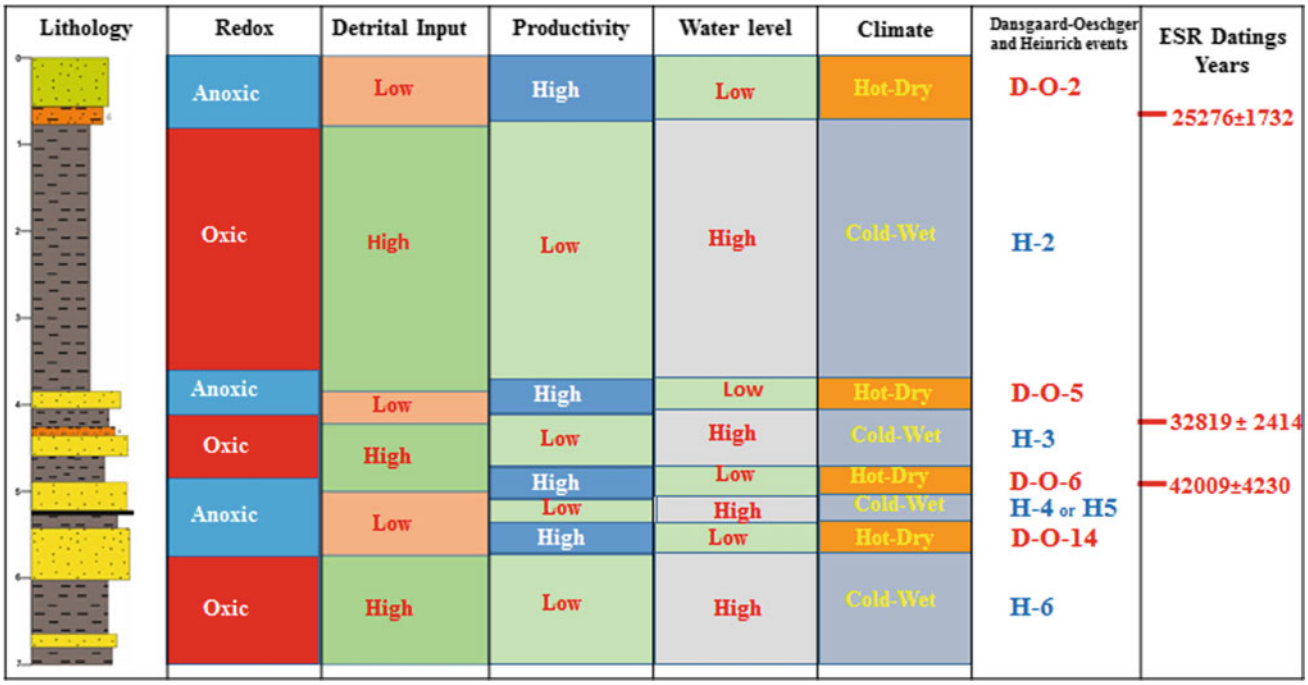

Fig. 2 The interrelation among redox, detrital input, productivity, the climate, water level determined by paleoenvironmental and paleoecological proxies, Daansgard-Oaschger (D-O) and Henrich (H) climatic events

3.3 Paleoproductivity Proxies

Productivity of organisms in a lacustrine environment is controlled by the chemistry, temperature, salinity and turbidity of lake water and terrigenous input. Ni and Cu in sediments were mainly deposited first as organometallic complexes which degraded after deposition [11]. The released Ni and Cu may be incorporated into sediments under reducing conditions. Several proxies such as Cu/Al, Ni/Al, Ca/Al, Ba/Al Si/Ti and Ca/Ti were used to predict the paleoproductivity [11].

Four levels which are relatively depleted in Cu, Ni and Ba and enriched in CaO were determined within the studied samples. These levels represent high productivity periods and a hot and dry climate.

4 Conclusions

The geochemical data show that weathering processes, detrital input, redox conditions, water levels and paleoproductivity in the study area for the last 50 ka fluctuated due to climatic changes. Three periods of high detrital input (high Si+Al+K+Ti+Fe, high Ti/Al, Rb/Sr, low Ca and low Si/Ti), four periods of anoxic conditions (low Mn, Th/U, V/(V+Ni) and high Ni/Co, Mo/Al and V/Cr) and four periods of higher productivity (high Cu/Al, Ni/Al, Ca/Al, Ba/Al Si/Ti and Ca/Ti) were determined. These periods correspond to climatic changes during last glacial periods, the warm climate of D-O-2, D-O-5, D-O-6 and D-O-14 events and the cold climate of H2, H3, H4 or H5 and H6 events (Fig. 2).

Paleoenvironmental and paleoecological interpretations for different levels on the studied samples determined by geochemical proxies are quite compatible with each other and confirm each other (Fig. 2).

References

1. Martín-Puertas, C., Valero-Garcés, B.L., Mata, M.P., Moreno, A., Giralt, S., Martinez-Ruiz, F., Jiménez-Espejo, F.: Geochemical processes in a Mediterranean Lake: a high-resolution study of the last 4,000 years in Zoñar Lake, southern Spain. J. Paleolimnol. **46**, 405–421 (2011)
2. Guimaraes, J.T.F., Sahoo, P.K., Souza-Filho, W.M., Maurity, C. W., Junior, R.O.S., Costa, F.R., Dall'agnol, R.: Late Quaternary environmental and climate changes registered in lacustrine sediments of the Serra Sul de Carajas, south-east Amazonia. J. Quat. Sci. **31**(2), 61–74 (2016)
3. Zhao, J., Jin, Z., Jin, Z., Geng, Y., Wen, X., Yan, C.: Applying sedimentary geochemical proxies for paleoenvironment interpretation of organic-rich shale deposition in the Sichuan Basin, China. Int. J. Coal Geol. **163**, 52–71 (2016)
4. Roberts, N., Black, S., Boyer, P., Eastwood, W.J., Griffiths, H., Lamb, H.F., Leng, M., Parish, R., Reed, J., Twigg, D., Yiğitbaşoğlu, H.: Chronology and stratigraphy of Late Quaternary sediments in the Konya Basin, Turkey: results from the KOPAL project. Quat. Sci. Rev. **18**, 611–630 (1999)
5. Erol, O.: The relationship between the development of the Konya-Karapınar obruks and the Pleistocene Tuz Gölü and Konya

pluvial lakes, Turkey. Deniz Bilim ve Cogr. Enst. Bült. Istanb. **7**, 5–49 (1991). (in Turkish)
6. Kuzucuoğlu, C., Karabıyıkoğlu, M., Parish, R.: The dune systems of the Konya Plain (Turkey) their relation to the environmental changes in Central Anatolia during Late Pleistocene and Holocene. Geomorphology **23**, 257–271 (1998)
7. Fontugne, M., Kuzucuoğlu, C., Karabıyıkoğlu, M., Hatte, C., Pastre, C.F.: From Pleniglacial to Holocene: a ^{14}C chronostratigraphy of environmental changes in the Konya Plain, Turkey. Quat. Sci. Rev. **18**, 573–591 (1999)
8. Rahmstorf, S.: Ocean circulation and climate during the past 120,000 years. Nature **419**, 207–214 (2002)
9. Tribovillard, N., Algeo, T.J., Lyons, T., Riboulleau, A.: Trace metals as paleoredox and paleoproductivity proxies: an update. Chem. Geol. **232**, 12–32 (2006)
10. de Oliveira, S.M.B., Saia, S.E.M.G., Pessenda, L.C.R., Favora, D. I.T.: Lacustrine sediments provide geochemical evidence of environmental change during the last millennium in southeastern Brazil. Chem. Erde **69**, 395–405 (2009)
11. Piper, D.Z., Perkins, R.B.: A modern vs. Permian black shale—the hydrography, primary productivity, and water-column chemistry of deposition. Chem. Geol. **206**, 177–197 (2004)

Reconstruction of Holocene Paleoenvironmental Changes Along Northern Coast of Sfax: Analysis of Foraminiferal Associations

Afef Khadraoui, Jérôme Bonnin, Chahira Zaïbi, and Fekri Kamoun

Abstract

Late Pleistocene-Holocene evolution of El Merdassia sebkha (Sfax Northern coast, Gabes Gulf, Tunisia) was deduced on the basis of the analysis of sediment cores and coastal outcrops. The environmental changes were established by means of foraminifera assemblages, diversity index and biocenotic parameters complemented by sedimentological analyses. A shallow marine environment, rich in warm Senegalese fauna, allowed the deposition of quartz sands in Late Pleistocene age. After an important stratigraphic gap, a major modification of the environmental characters was recognized. The dominance of coastal foraminifera such as *Elphidium crispum*, *Quinqueloculina seminula* and *Ammonia beccarii* coupled with the high values of species richness and the two diversity index (H and E) characterize the settlement of a widely opened lagoon. This lagoon is subjected to the action of the longshore drifts which are responsible for the buildup of sand spit, the closure and the genesis of the present sebkhas. Two transgressive events, overlying the marine Late Pleistocene are dated at 2018–2419 and 1001–1804 a cal BP. Sudden changes, toward 0–502 a cal BP, in the structure populations and sedimentological trend argues in favor of a high energy event and the settlement of a peculiar environment.

Keywords

Foraminifera • Sfax coastline • High energy event
Seal level • Transgression

1 Introduction

Foraminifera are important proxies of sea-level change, salinity and oxygen availability. Their density, species richness and diversity index are influenced by environmental conditions. Fluctuations in salinity, nutrient availability and oxygenation rate are controlling parameters for the relative abundance of foraminiferal assemblages. A great deal of research was achieved in Tunisia on benthic foraminifera from marine, lagoonal and estuarine environments. These authors identified, through the foraminifera taxa, numerous assemblages characterizing each environment and reconstituted the evolution of the Holocene environments. Recently Khadraoui et al. [1] and Zaibi et al. [2] discussed the impact of storms and tsunamis on environmental change and used foraminifera population structure to recognize these extreme events. Accordingly, the main objective of the present study was to: (1) reconstruct the succession of Holocene environmental conditions reflected in foraminifera assemblages and to find a link between these results and sedimentological analyses; and (2) discuss the factors controlling the palaeoenvironmental changes.

2 Settings

The study area corresponds to the northern coast of Sfax and is delimited by Sidi Mansour Cape South and Sebkha El Garra North. A flat topography and semi-diurnal tides, with amplitude ranging from 80 to 150 cm, characterize this area. A detailed morphological analysis shows the succession of three sebkhas, from South to North, namely El Merdassia, El Awebed and El Garra. The El Achaach wadi is observed in the middle part of the area and delimits the sebkhas El Merdassia and El Awebed. The intertidal zone extending to about 300 m in front of El Awebed, is further developed to the South and reaches 1 km. The shores of El Merdassia and

A. Khadraoui (✉) · C. Zaïbi · F. Kamoun
GEOGLOB Laboratory, Faculty of Sciences, Sfax University, BP 1171, 3000 Sfax, Tunisia
e-mail: afefkhadraoui1988@gmail.com

J. Bonnin
EPOC, UMR 5805, Bordeaux University, Allée Geoffroy Saint-Hilaire, 33615 Pessac, France

Z. Zhang et al. (eds.), *Patterns and Mechanisms of Climate, Paleoclimate and Paleoenvironmental Changes from Low-Latitude Regions*, Advances in Science, Technology & Innovation, https://doi.org/10.1007/978-3-030-01599-2_18

El Awebed gulfs are colonized by tight halophile vegetation. However, the slikke is made up of silty sands.

3 Results

To reconstruct the development of the sebkha El Merdessia, three cores sediments are retrieved (C1S, C3, C4) drilled in the area of sebkhas at about 0.5 m above sea level. The cores C1S, C3, C4, are situated at 34°50′16.44″N-10°52′7.71″E; 34°49′55.06″N-10°52′3.81″E and 34°50′47.15″N-10°53′11.85″E respectively. The distribution of foraminifera taxa, coupled with their biocenotic parameters allowed us to distinguish several zones covering the interval Late Pleistocene–Holocene:

Core C3 zones

Zone I, from 131 to 100 cm, made up of Tyrrhenian sands rich in mollusks and lithoclasts and shows the dominance of coastal foraminifera (64%). Several trenches, dug near C3 core and outcrops, show the presence of mollusks dominated by *Cerithium vulgatum* characterized by their high diversity and whose shells ewre filled by silts and *Strombus bubonius.* These mollusks are commonly referred to the Tyrrhenian series, which outcrops in El Awebed coast. **Zone II**, from 100 to 63 cm, built up by coarse sands, 2018–2419 a cal BP in age. It reveals the increase of coastal foraminifera, which reaches 90%. **Zone III**, from 63 to 38 cm, is characterized by a sequence of azoic silts and clays signing an episode of closure (CL) of the previous lagoon and its filling by silts leading thereby to its emersion. **Zone IV**, from 38 to the surface, made up of sands rich in mollusks and Phanerogams, is characterized by the reappearance of lagoonal (52%) and coastal (47%) foraminifera. These parameters reflect the onset of a very shallow littoral environment. From 20 cm to the surface, azoic grey clays and silts, show the settlement of the present sebkha.

Core C1S zones

Zone I, 1001–1804 a cal BP in age, shows the dominance of the lagoonal foraminifera (80%), the high foraminifera species number and the dominance of coastal association (80%) represented by *Haynesina germanica*, *Quinqueloculina laevigata* and *Peneroplis planatus*. **Zone II**, from 64 to 36 cm, is made up of very coarse sands rich in lagoonal bivalvia, gastropoda, charcoal particles and Tyrrhenian lithoclasts. It shows an increase of foraminifera species number and an abrupt enhancement of their density (880 ind./10 g dry sediment). The coastal assemblages reach up to 94%, where *Quinqueloculina seminula* is dominant. **Zone III**, from 36 to the surface, built up of fine sands, is marked by the decrease of species and individual number of microfauna. The lagoonal foraminifera assemblage increases and reaches up to 33%. All these parameters indicate the implementation of a closed lagoon. From 18 to the surface, the disappearance of foraminifera mark the closure of the lagoon and the apparition of the present sebkha.

4 Discussion

The multi-proxy approach allowed us to recognize the events responsible for the evolution of Sfax Northern coastline (Fig. 1).

4.1 Tyrrhenian Sea-Level High Stand, Substage 5e

It reveals the dominance of coastal foraminifera, the high values of species richness and density. Developed during the marine isotopic sub-stage 5e, this event corresponds to a sea-level highstand humid period, which favored terrigenous and silico-clastic sedimentation along most of the Tunisian coastline.

4.2 First Holocene Marine Transgression 2018–2419a Cal BP in Age

This transgression is marked by the increase of coastal foraminifera such as *Elphidium crispum*, *Quinqueloculina seminula* and *Ammonia beccarii*, which reaches 90%. The enhancement of microfauna and diversity index imply a widely open environment subjected to pelagic influences. All these parameters register a marine transgression toward 2018–2419 a cal BP.

4.3 Period of Sand Spits Development, Between 2018–2419 and 1001–1804 a Cal BP)

During this wet period, the increase of the estuarine *Haynesina germanica* indicates the settlement of estuarine influences in relation with the activity of El Achaach wadi. This period favored the erosion of quartz grains and their deposition on the coast. These were subjected to the action of the drift currents, responsible for the build-up of sand spits.

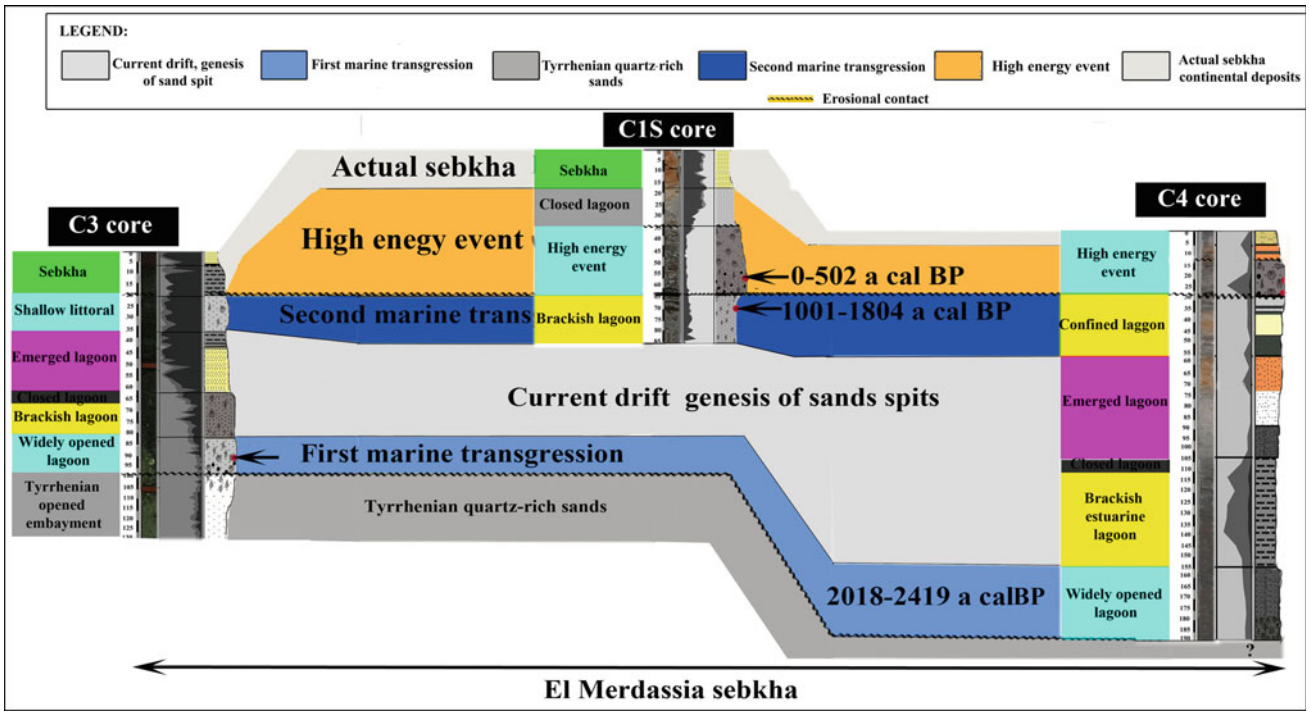

Fig. 1 Stratigraphy of El Merdassia subsurface sediments

4.4 Second Marine Transgression Towards 1001–1804 a Cal BP

This event is characterized by the diversification of coastal foraminifera which denote the settlement of an opened lagoon subjected to pelagic influence, following a marine transgression toward 1001–1804 a cal BP.

4.5 High Energy Extreme Event Towards 0–502 a Cal BP

This event is distinguished by the abrupt enrichment coastal foraminifera and their highest values of species number and density. In addition to the presented core data, the shelly sands outcrops reveal the presence of Tyrrhenian mollusk, such as the dominant *Cerithium vulgatum*, showing a dissolved surface tubercles, and ribs testifying their transport under a turbulent condition.

5 Conclusion

Late Pleistocene-Holocene evolution of El Merdassia sebkha (Northern coast of Sfax) established from the multi-proxy approaches reveals: (i) a sea-level highstand and humid period permitted the deposition of Tyrrhenian quartz-sands in an opened embayment rich in Senegalese mollusks and coastal foraminifera; (ii) Two transgressive events, toward 2018–2419 and 1001–1804 a cal BP in age, permitted the settlement of an opened lagoons evidenced by the high values of microfauna species richness and diversity; and (iii) towards 0–502 a cal BP, a high energy event was recognized by means of a scarce change in population structure and sedimentological trends.

References

1. Khadraoui, A., Kamoun, M., Ben Hamad, A., Zaibi, C., Bonnin, J., Viehberg, F., Bahrouni, N., Sghari, A., Abida, H., Fekri, K.: New insights from microfauna associations characterizing paleoenvironnements, sea level fluctuations and a tsunami event along Sfax Northern Coast (Gulf of Gabes, Tunisia) during the Late Pleistocene-Holocene. J. Afr. Earth Sci. (in press)
2. Zaïbi, C., Kamoun, F., Viehberg, F., Carbonel, P., Jedoui, Y., Abida, A., Fontugny, M.: Impact of relative sea level and extreme climate events on the Southern Skhira coastline (Gulf of Gabes, Tunisia) during Holocene times: ostracodes and foraminifera associations response. J. Afr. Earth Sci. **118**, 120–136 (2016)

Evolution of Korba Lagoon (Cap Bon, Tunisia) During the Last Millennia Based on the Analysis of Foraminiferal Assemblages

Asma Ben Hamad, Chahira Zaïbi, Martin R. Langer, and Fekri Kamoun

Abstract

The quantitative study of foraminiferal associations coupled with geochemical and sedimentological proxies, of a 94-cm sediment core from Korba lagoon (Cap Bon, Tunisia), enabled us to better understand the dynamics of depositional environments and identify different stages of evolution of the lagoon. Three major periods were identified. The first revealed high abundance of foraminifera dominated by lagoonal taxa associated with high TOC, TIC and Ca contents. These parameters marked the settlement of a closed lagoon separated from the open ocean by a sandy bar with high foraminiferal productivity in fine sediments. The second period showed the development of estuarine foraminifera coupled with the appearance of charophyte oogonia in addition to planktonic foraminifera, high Ti and Fe concentrations and dominant coarse fraction. These parameters are indicative of an open lagoon environment with the fluvial inputs. The disappearance of charophyte oogonia and planktonic foraminifera coupled with the enrichment of marine taxa marked the opening of our lagoon to the sea. The progressive modification of foraminiferal association revealed by the increase of lagoonal species and the decrease of estuarine taxa prove the settlement of the present-day lagoon conditions.

Keywords

Korba lagoon • Foraminiferal associations
Palaeoenvironment

A. Ben Hamad (✉) · C. Zaïbi · F. Kamoun
Geoglob Laboratory, Faculty of Sciences, Sfax University, Sokra Road, 3018 Sfax, Tunisia
e-mail: asmabenhmad@live.fr

M. R. Langer
Steinmann Institut für Geologie, Mineralogie und Paläontologie, Rheinische Friedrich-Wilhelms Universität Bonn, Bonn, Germany

1 Introduction

Korba lagoon, situated in northeastern Tunisia, is an elongated, shallow and saline depression belonging to a coastal lagoon system extending between Maamoura and Kelibia (Cap Bon, Tunisia). This system corresponds to a coastal wetland of typical coastal ecosystems of the Cap Bon. It originated in a synclinal depression affected offshore by a directional accident [1]. It extends parallel to the coastline and is separated from the sea by a sandy bar. The latter is interrupted by four main open passes permitting the connection between the lagoon and the sea. The continental and marine water inputs of the lagoon are occasional due to the succession of wet and dry periods. These flows provoked eventual tidal and flood delta conditions.

Our study aimed to reconstruct the different palaeoenvironments of this coastal ecosystem during the last millennium and infer factors controlling the palaeoenvironmental changes. This study involves the analyses of foraminiferal association changes coupled with geochemical and sedimentological features.

2 Materials and Methods

KK9 Core with a length of 94 cm was obtained from the middle part of the lagoon. It occupied a very strategic place affected by both continental and marine water inputs. One half of the core was, described and used for high-resolution X-ray fluorescence (XRF) scanning. Each cm of the other half was continuously sampled. Total organic carbon (TOC) and total inorganic carbon (TIC) concentrations were determined with a DIMATOC 200 (DIMATEC Co.). Grain-size analyses were preceded by a multi-step chemical treatment procedure to remove autochthonous sediment components without altering the clastic material. They were performed using a Saturn DigiSizer 5200 laser particle analyzer. 20 samples were gently washed using 63 and 125 μm mesh sieves. Foraminifera were

Z. Zhang et al. (eds.), *Patterns and Mechanisms of Climate, Paleoclimate and Paleoenvironmental Changes from Low-Latitude Regions*, Advances in Science, Technology & Innovation, https://doi.org/10.1007/978-3-030-01599-2_19

picked, counted and identified. The species identification followed the taxonomical classifications of Cimerman and Langer [2] and Langer and Schmidt-Sinns [3]. The results were standardized to 5 g dry weights in the diagram.

3 Results

3.1 Lithology, Geochemistry and Sedimentology

KK9 core consists of nine different parts (U1 to U9). It is marked by the dominance of sand fraction with an average percentage of 50%. The silt fraction, dominant in U3 and U7, is on average 36% and clay appeared with low values not exceeding 14% and showing its highest values in U1. Ti and Fe, proxies that reflect detrital inputs, are mostly important in the lower part of the core (U1 to U5). Ca ions, related to marine influence or the detrital carbonate, are important in U1, U2 and U7 units. The TOC, representing the content of organic matter, varies between 0 and 1.5% with the highest values in the lower units (U1 and U2) and to the top of the core (U9). TIC also shows important peaks in U1 and U2.

3.2 Distribution of Foraminiferal Associations

The benthic foraminifera are abundant and constitute up to 500 individuals per 5 g of dry sediment. The estuarine taxon *Haynesina depressula* is the dominant benthic foraminifer (41%). It is followed by the lagoonal species *Ammonia tepida* (23%) and the estuarine *Haynesina germanica* (10%). The other taxa do not exceed 26% of relative abundance. The vertical distribution of foraminifera and the numerical abundance of individuals along the KK9 core allowed us to distinguish the following zones (Fig. 1): the lower zone (zone I: 94–70 cm) is marked by a high foraminiferal abundance with the dominance of the lagoonal taxa *Ammonia parkinsoniana* and *Ammonia tepida* (60%). A pronounced change in foraminiferal associations characterized by the development of estuarine taxa, appearance and increase of marine species associated with a reduction of individuals in zone II (90–15 cm). It can be subdivided into two subzones. The first one (IIA: 75–40 cm) is marked by the decrease of lagoonal foraminifera coupled with the dominance of estuarine taxa and the gradual increase of marine species (e.g. *Cibicides advenum* and *Elphidium jenseni*). It recorded the enrichment of planktonic foraminifera probably reworked from Tertiary outcrops. The subzone IIB, 40–15 cm, shows a slight decrease of estuarine species and an increase of marine taxa associated with low abundance. Zone III, 15 cm to the surface, is characterized by the increase of lagoonal association, the decrease of estuarine taxa with low foraminiferal abundance and reduced number of planktonic foraminifera.

4 Discussion

Foraminiferal associations and the sedimentological and geochemical features of the studied levels, revealed the three following periods: **The first one** is marked by the

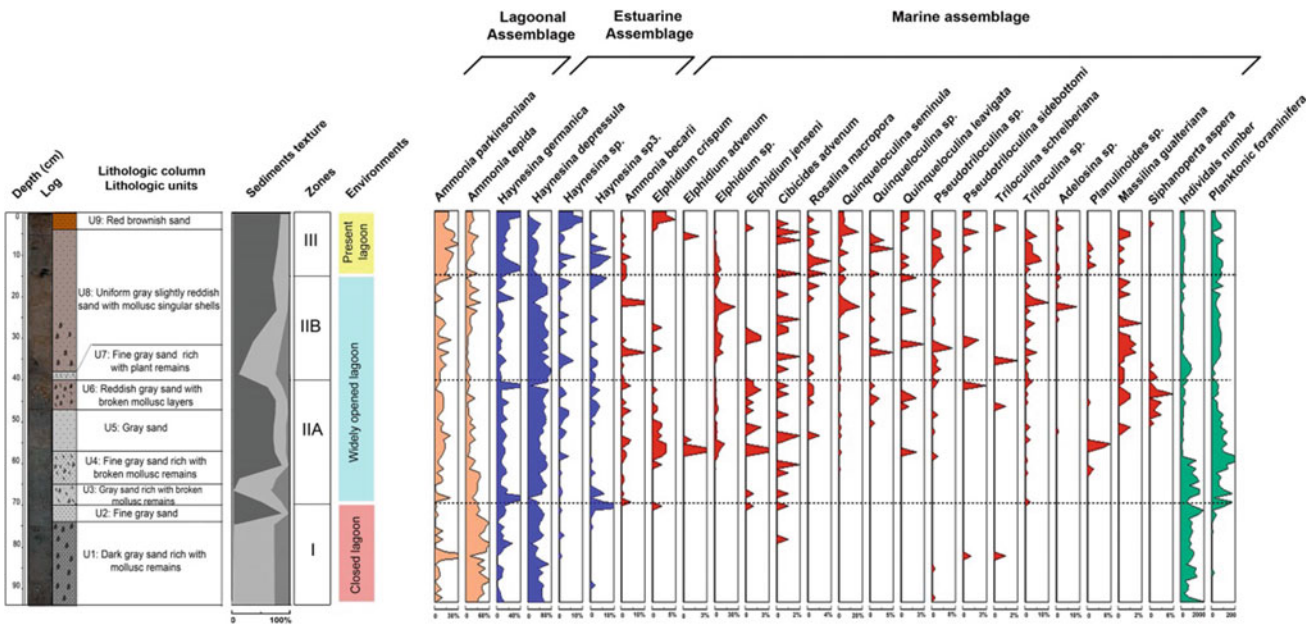

Fig. 1 Log showing lithological columns and units, sediments texture, zones, environments and quantitative vertical distribution of foraminifera (benthic and planktonic) with individuals number along the KK9 core from Korba lagoon

development of lagoonal foraminifera. High TOC (up to 1%) and TIC suggest high productivity supported by high Ca values and high numbers of individual of foraminifera. During this period, a closed lagoon separated from the sea by a sandy bar is indicated. **The second period** is characterized by the dominance of estuarine foraminifera (*Haynesina germanica*, *Haynesina depressula*) with dominance of coarse fraction revealing high energy conditions. This period revealed two environments: The first one is marked by the appearance of charophyte oogonia in addition to planktonic foraminifera associated with the highest values of Ti and Fe. The latter indicates terrigenous components derived from fluvial inputs. This period is followed by an increase of marine foraminiferal associations coupled with the absence of charophyte oogonia, a decrease of planktonic foraminifera and TIC and TOC and an overall increase of Ca. These parameter changes denote an open lagoon environment. **The third period**, which can be dated at 1885 AD [4], is characterized by an increase of lagoonal taxa especially *Ammonia parkinsoniana* with a decrease of estuarine species, planktonic foraminifera and charophyte oogonia. The association changes indicate the establishment of the present-day lagoon conditions. Its existence was also proven by Bouden et al. [1] through the decrease of mollusk shells indicating a relatively confined environment. The increase of TOC in the upper part of the core is probably due to recent anthropic activities (discharges of domestic and agro-industrial wastewater) [5].

5 Conclusions

Korba Lagoon, initially separated from the sea by a sand bar, experienced a gradual opening to fluviatile inflows and the open sea. These fluvial contributions are probably synchronous with the little Ice Age characterized by a colder climate and higher atmospheric humidity as recognized in various Tunisian wetlands. The onset of the present-day lagoonal conditions is indicated by modifications of benthic foraminiferal associations and the reduction of detrital and marine inflow indices.

References

1. Bouden, S., Chaabani, F., Abdeljaoued, S.: Dynamique sédimentaire de la lagune de Korba (NORD-EST de la Tunisie). Quaternaire **20**(2), 227–237 (2009)
2. Cimerman, F., Langer, M.R.: Mediterranean Foraminifera, 119 pp. Slovenska Academia Znanosti in Umetnosti, Ljubljania (1991)
3. Langer, M.R., Schmidt-Sinns, J.: The 100 Most Common Foraminifera from the Bay of Fetovaia, Elba Island (Mediterranean Sea). Monographie im Selbstverlag. Institut für Paläontologie, Universität Bonn, 37 pp, 15 pls (2006)
4. Birks, H.H., Peglar, S.M., Boomer, I., Flower, R.J., Ramdani, M., Appleby, P.G., Bjune, A.E., Patrick, S.T. and Kraïem, M.M. with contributions from Fathi, A.A., Abdelzaher, H.M.A.: Palaeolimnological responses of nine North African lakes in the CASSARINA Project to recent environmental changes and human impact detected by plant macrofossil, pollen, and faunal analyses. Aquat. Ecol. **35**, 405–430 (2001)
5. Bouden, S., Chaabani, F., Abdeljaoued, S.: Caractérisation géochimique des sédiments superficiels de la lagune de Korba (Cap Bon, Nord-Est de la Tunisie). Geo-Eco-Trop **28**(1–2), 15–26 (2004)

Paleoenvironment Evolution of a Paralic System, El Guettiate and Dreïaa Sebkhas (Gulf of Gabès, Tunisia)

Zeineb Gargouri and Kamel Zouari

Abstract

The Holocene sedimentary record of El Guettiate and Dreïaa sebkhas located on the southern littoral of Skhira, Gulf of Gabès in Tunisia is expressed by five deposit units, unconformably overlying the continental clay sediment of the Mio-Pliocene. Sedimentological and palaeontological analyses and ^{14}C dating provide palaeoenvironmental information for the reconstruction of shoreline changes of Skhira-Gabès littoral and the progressive infilling of both sebkhas over the last 10,000 years. The sedimentary package of this cycle starts with the marine transgression between 8770 and 4000 ^{14}C years BP. This oldest unit consists of muddy bioclastic. The following unit is dated 3300 to 1500 ^{14}C years BP and consists of mud and sand. The third unit is dated around 1307 to 558 ^{14}C years BP. It consists of muddy sand. The fourth unit marking the filling of the sebkhas is a continental deposit which is rich in gypsum crystals. The last and fifth units on top of these sedimentary units have a microbial mat environment. The sebkhas under investigation were isolated from the open sea since 558 years BP due to the decrease of the marine influence and the increase of continental influence (clays and silts deposits) under an arid climate. The main factors controlling the Holocene sedimentary dynamics in this paralic system of southern Tunisia are the fluvial inputs, the relative sea level fluctuation and changes in local climate.

Keywords

Sedimentology • Sea level fluctuation • Paleoenvironment
Sebkhas • Shoreline changes • Holocene
Southern Tunisia

1 Introduction

The north-eastern coast of the Gulf of Gabès is characterized by miopliocene deposits forming high cliffs with sand beaches, salt marsh, tidal flat and sebkhas. The latters are separated from the open sea by sandbars and sandy beach deposits. Such coastal sedimentary environments are marginal areas located in the narrow transition zone between the marine and continental domains. Consequently, they are sensitive to even small changes in sea level. The Holocene transgressive episode caused the deposition of large volumes of well-preserved coastal sediments containing marine and lagoonal units in complex stratigraphical sequences. Studying these sequences helps to better understand sea-level changes during the Holocene. In recent decades, several sedimentological studies have been made based on Holocene sea level fluctuations around the Gulf of Gabès [1–6].

The present study is based on the deposits of El Guettiate and Dreïaa sebkhas situated on the north-eastern coast of the Gulf of Gabès (Fig. 1). It aimed at providing additional data on the Holocene sedimentary facies distributions as well as their depositional environments evolution with relation to sea-level fluctuations and inherited morphology.

2 Materials and Methods

Sediment cores were retrieved from 18 boreholes (N1, N2, N3, N4, G0, G1, G2, GR1, GR2, GR3, C2, C3, C4, SG1, SD1, SD2, T1 and T2) along five cross-sections NW–SE (cross-section N) and W–E (cross-section GR and C) in the El Guettiate sebkha and NW–NE (cross-section SD) and

Z. Gargouri (✉)
Laboratoire de Modélisation des Systèmes Géologiques et Hydrologiques (GEOMODELE), LR16ES17, Faculté des Sciences de Sfax, University of Sfax, B.P. 802, 3038 Sfax, Tunisia
e-mail: zeineb.gargouri@enis.tn

K. Zouari
Laboratoire de Radio-Analyses et Environnement, Ecole Nationale d'Ingénieurs de Sfax, University of Sfax, B.P. W, 3038 Sfax, Tunisia

Z. Zhang et al. (eds.), *Patterns and Mechanisms of Climate, Paleoclimate and Paleoenvironmental Changes from Low-Latitude Regions*, Advances in Science, Technology & Innovation, https://doi.org/10.1007/978-3-030-01599-2_20

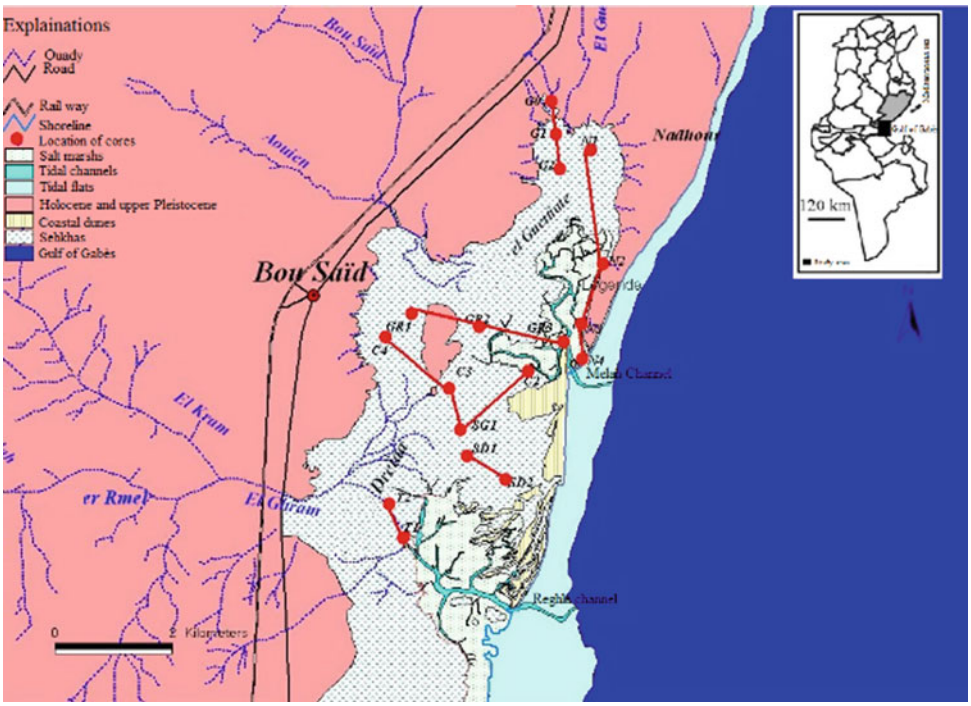

Fig. 1 Localization of study area

SW–SE (cross-section T) in the Dreïaa sebkha (Fig. 1). We collected 252 samples. Each sample underwent sieve dry analysis and silt and clay (smaller than 63 µm) fractions were studied using a laser particle size analyser.

The mineralogical study was based on X-ray diffraction analysis of powders in the case of fresh sediments and of oriented aggregates in the case of clays, using a diffractometer with a cobalt anticathode (CGR 45 tetha). The radiocarbon dating was made on mollusc shells and based on the advocated International Atomic Energy Agency (I.A.E.A.) method called spectrometry by liquid scintillation. Its (^{14}C) measurements were performed by CO_2 β^- counting method.

3 Results and Discussion

The results allowed us to separate five periods in the sedimentological record of Skhira-Gabès coastal evolution. Cores display the same stratigraphy, with five different sedimentary units. For a detailed analysis, we selected core GR2, in the central part of El Guettiate sebkha (Fig. 2).

First period (8770–4000 years BP): this period is characterized by the deposition of the transgressive sedimentary body that accompanied the global Holocene sea level rise. The presence of *Posidonia* fibers and rhizomes indicates a direct marine influence on El Guettiate system since 5660 years BP before it became a confined system. Since 4000 years BP, a growing coastal spit progressed towards the Northeast, progressively isolating El Guettiate lagoon from the sea. This zone, however, has remained constantly connected to the sea by a tidal channel (EL Melah). With regard to Dreïaa sebkha, it has been marked by tidal flats with numerous tidal channels since 8771 years BP.

Second period (3300–1550 years BP): El Guettiate sebkha apparently was still open to the sea by an inlet as it was evident from the presence of marine shells. This situation can be explained by the separation of the lagoon of El Guettiate sebkha from the open sea by a spit. The confinement is much more intense than the one during the preceding period. This semi-closed sebkha was likely "a lagoon, in constant communication with the sea which was then partially closed". The spit progresses essentially towards a North-East direction causing the isolation of the lagoon and the formation of salt marshes Dreïaa.

Third period (1307–558 years BP): during this period, although they show a semi-closed lagoon connected to the sea, the sediments are more confined. The third marine elevation caused a flooding. The salt marshes of Dreïaa are more closed from the open sea, while the sand spitted progress essentially to the South-West direction and the communication with the sea decreased.

Fourth period (after 558 years BP): this period illustrates the lagoon infilling. The reduced communication with the open sea led to the definitive conversion of the lagoon into a coastal sebkha where continental influences were materialized by sand and silt deposits. The Late Holocene dry climate and the associated capillarity evaporation led to the development of gypsum crystals within the uppermost part of the sequence. The causes of this change is materialized by

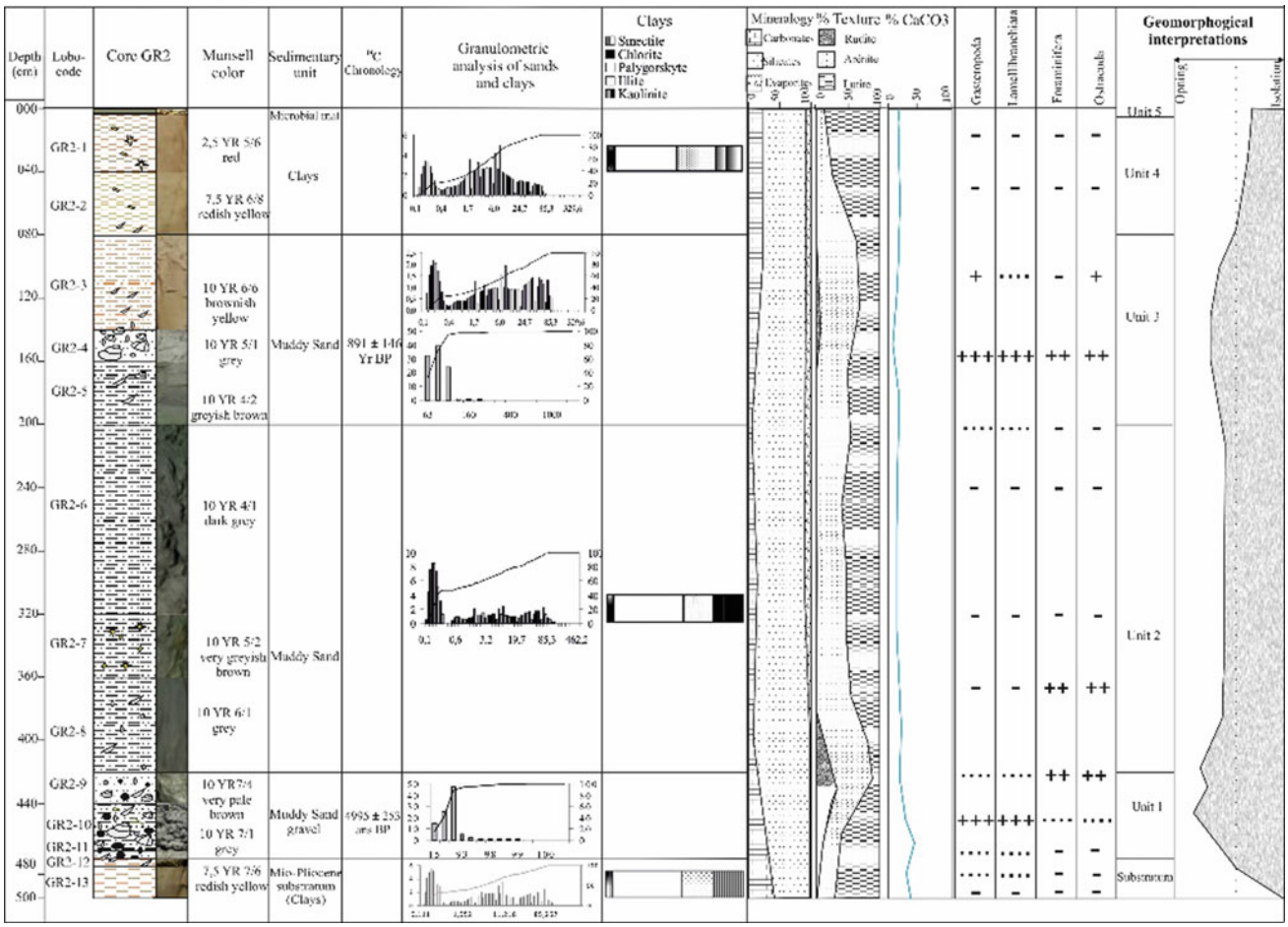

Fig. 2 GR2 core sediment analyses result

the development of confined conditions which are justified by evaporite and palygorskite deposits similar to those developing currently throughout in the Persian Gulf and platform subtidal deposits. These evaporites are associated with continental detrital grains (clay and silt).

Fifth period (actual): the microbial mat horizon within the top of the sequence is limited to the area situated near the channel edges. In the salt marshes of Dreïaa, the eastward expansion of the microbial mat follows the shoreline migration (progradant sedimentary system).

4 Conclusions

The Holocene sedimentary sequences of El Guettiate sebkha on the southern littoral of Skhira, southeastern Tunisia showed bioclastic deposits (marine macro and microfauna) on the bottom and detrital deposits on the top whereas those of the nearby Dreïaa sebkha are more open to the sea with paleo-channel deposits. The installation of sandy spits led to the evolution of the coastline towards the South-Est direction. Besides, the filling up of the lagoons was accompanied with the development of microbial mats.

With respect to the sedimentary sequences, they showed an early diagenes materialized by an early cementing, i.e. the precipitation of the autochthone gypsum. Two principal factors of regional and global nature governed and drove the Holocene sedimentary dynamics in the area of study. In fact, the dry climate of the Late-Holocene and the diagenetic processes (gypsum precipitation) are both indicators of the marine regression during that time. Moreover, the fluctuations of the sea level occurring over all the Mediterranean area during the Holocene have affected the coastal regions morphology.

The paleo-environmental reconstruction of the coastal sector of Skhira-Gabès proved that this area was an open lagoon that became separated from the Mediterranean Sea after *558* ^{14}C years. Our study demonstrates that an integrated paleo-environmental, sedimentological and radiometric approach can be used as an efficient tool for reconstructing shoreline changes and coastal dynamics.

References

1. Jedoui, Y., Kallel, N., Fontugne, M., Ben Ismail, M.H., M'Rabet, A., Montacer, M.: A high relative sea level stands in the middle Holocene of southeastern Tunisia. Mar. Geol. **147**(1998), 123–130 (1998)
2. Lakhdar, R., Soussi, M., Ben Ismail, M.H., M'Rabet, A.: A Mediterranean Holocene restricted coastal laggon under arid climate: case of the sedimentary record of the Sabkha Boujmel (SE Tunisia). Palaeogeogr. Palaeoclimatol. Palaeoecol. **241**, 177–191 (2006)
3. Medhioub, K., Saubade, A.M., Zaouali, J., Guelorget, O., Perthuisot, J.P.: Evolution paléogéographique de la Bahiret el Biban (Sud-Est tunisien) depuis 5000 ans d'après les variations de la malacofaune fossile et quelques données géochimiques, pp. 131–138. Bulletin de la Société géologique de France, Paris (1987) **3**(1), série 8: carte, graph. bibliogr. p. 138, rés. (Fr., Angl)
4. Morhange, C., Pirazzoli, P.A.: Mid-Holocene emergence of southern Tunisian coasts. Mar. Geol. **220**, 205–213 (2005)
5. Zaïbi, C., Carbonel, P., Kamoun, F., Azri, C., Kharroubi, A., Kallel, N., Jedoui, Y., Montacer, M., Fontugne, M.: Évolution du trait de côte à l'Holocène supérieur dans la Sebkha El-Guettiate de Skhira (Golfe de Gabès, Tunisie) à travers sa faune d'ostracodes et des foraminifères. Geobios **44**, 101–115 (2011)
6. Zaïbi, C., Carbonel, P., Kamoun, F., Azri, C., Fontugne, M.: Évolution of sebkha Dreîaa (South-Eastern Tunisia, Gulf of Gabes) during the Late Holocene: response of ostracod assemblages. Rev. Micropaléontol. **55**(2012), 83–97 (2011)

Part V
Spatio-temporal Patterns of Climate Change

Testing for Collective Statistical Significance in Climate Change Detection Studies

Radan Huth and Martin Dubrovský

Abstract

We examined several approaches to detecting statistical significance of trends defined on a grid, that is, on a regional scale. To this end, we introduced a novel simple procedure of significance testing based on counting signs of local trends (sign test), and comparing it with four other approaches to testing collective significance of trends (counting, extended Kendall, Walker, and FDR tests). Synthetic data were used to construct the null distributions of trend statistics and determine critical values of the tests. The application of the five tests to real datasets reveals that outcomes of the tests may differ even though trends are locally significant at the majority of the grid points.

Keywords

Climate change • Significance testing • Collective statistical significance • Temperature • Trend detection

1 Introduction

The question on collective significance of local tests (also referred to as 'global' or 'field' significance), that is, whether the observed number of significant trends (i.e. of rejected null hypotheses) at individual sites may or may not have occurred due to mere chance, has scarcely been posed in climate change detection studies. The reflection and apprehension of the necessity to also account for the collective significance has been weak or even negligible among atmospheric scientists as Wilks [7] points out, although the importance of evaluation of the collective significance has been stressed repeatedly in meteorological and climatological literature [1, 2, 4–7].

This calls for an assessment of trends and their significance on a regional level. It is reasonable to assume that the prevalence of one sign of trends at individual sites is indicative of a high confidence we may have that the trend is not zero, regardless of how large or small the trend magnitude at individual sites is. This study has three objectives: First, we designed a novel method of evaluating significance of trends over a region, which is based on counting signs of local trends. Second, we compared the performance of several tests suitable for evaluating regional-scale significance of trends, including the one we designed. And third, the tests were applied to annual and seasonal mean temperature over the Mediterranean, including substantial parts of Europe, northern Africa, and the Middle East.

2 Statistical Tests and Synthetic Data

The Counting test is a classical test for collective significance [4], the essence of which is that the collective significance is achieved if significance is detected for a sufficiently large number of local tests. Walker test [6] is built on the premise that the local significance can be achieved even if just one of the local tests is sufficiently highly significant. The test based on false detection rate [5, 7] can be viewed of as a generalization of Walker test; the difference is that it takes into account the strength of all local tests significance, not only the most significant one. The extended Kendall test is based on summing the local Kendall statistics over all sites [3]. The test statistic of the sign test that we propose is simply the normalized difference between the number of positive and negative trends.

Null distributions and critical values of the five tests are determined from synthetic data. Data are generated by software tool SPAGETTA (Spatial Generator for Trend Analysis) as a temporal and spatial AR(1) process at a

R. Huth (✉)
Department of Physical Geography and Geoecology, Charles University, Prague, Czechia, Czech Republic
e-mail: huth@ufa.cas.cz

R. Huth · M. Dubrovský
Institute of Atmospheric Physics, Czech Academy of Sciences, Prague, Czechia, Czech Republic

Z. Zhang et al. (eds.), *Patterns and Mechanisms of Climate, Paleoclimate and Paleoenvironmental Changes from Low-Latitude Regions*, Advances in Science, Technology & Innovation, https://doi.org/10.1007/978-3-030-01599-2_21

20×20 grid with a pre-specified local variance and various temporal and spatial autocorrelations. Ten thousand realizations are generated for each combination of temporal and spatial autocorrelation. Critical values for significance at the 5% level are determined as 95% quantiles in the set of the ten thousand values of test statistics (that is, of the null distributions) for the given autocorrelation values. These critical values are then tabulated.

3 Application to Real-World Data

We demonstrate the use of statistical tests on the NCEP/NCAR reanalysis as a real-world example. The grid of 20×20 points with the 2.5° step in both latitude and longitude extends from 22.5 to 70°N and from 0 to 47.5°E. The grid covers the Mediterranean together with adjacent parts of Africa, Europe, and the Middle East. Annual and seasonal mean surface temperatures are analyzed for the period going from December 1960 to November 2010; annual means are calculated for periods starting in December and ending in November for the sake of simplicity. The series length is thus 50 years for all seasons as well as for annual data.

Trends are displayed in Fig. 1. Positive trends obviously and expectedly prevail; in spite of the fact that there are always gridpoints with negative trends in every season and in the annual means. Small and even negative trends concentrate in the southwestern and northeastern edges of the domain (central Sahara and Barents Sea, respectively) throughout the year and over Turkey in all the seasons except for the summer. Such a geographical confinement is suspicious and may be indicative of a problem concealed in the data rather than being a realistic feature.

The test statistics are displayed in Table 1. One can see that the largest number of gridpoints with locally significant positive trends (that is, the largest values of the statistic of the counting test) occur annually and in the summer (85.25 and 82.5% of all gridpoints, respectively), while the significant positive trends are less frequent in the winter (50.5%) and the autumn (55.75%). The share of positive trends is smallest in winter (60%, corresponding to the value of the

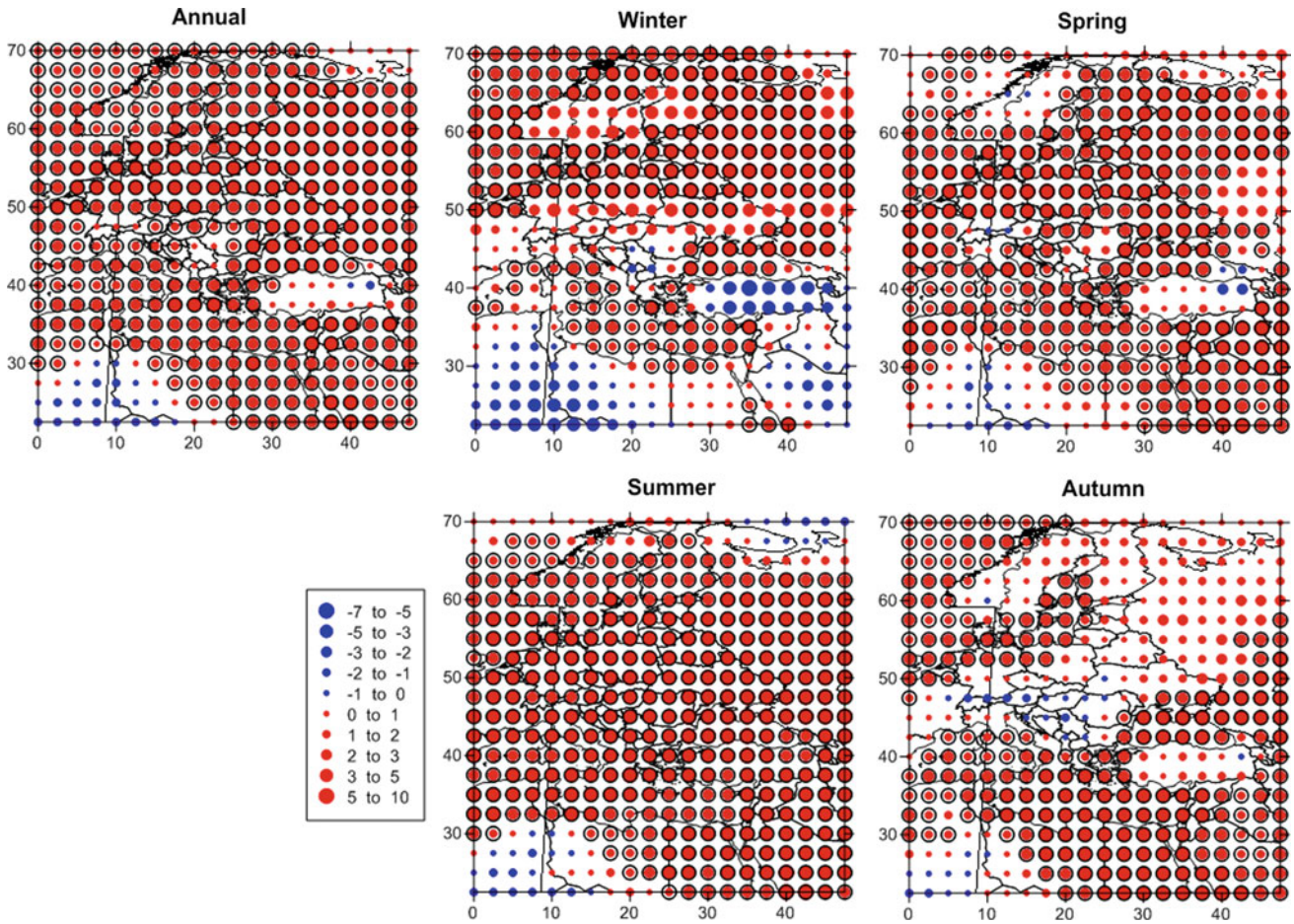

Fig. 1 Temperature trends in NCEP/NCAR reanalysis for all seasons and annually: negative trends in blue, positive trends in red, the size of a circle is proportional to the trend magnitude. Locally significant trends according to t-test are marked by a black circle

Table 1 Test statistics for the NCEP/NCAR temperature

Test	Annual	Winter	Spring	Summer	Autumn	Critical value
Sign	88.5	60.0	87.5	86.0	85.5	98.0
Counting	85.2*	50.5*	69.8*	82.5*	55.8*	30.3
Kendall	5.50*	3.14*	4.03*	5.76*	4.25*	1.63
Walker	0.0*	0.11*	0.0*	0.0*	0.0*	1.61
Fdr	0.0*	0.04*	0.0*	0.0*	0.0*	0.12

Asterisks indicate statistical significance. The critical value determined from the synthetic data is in the last column

statistic of the sign test of 80.0), while it is over 90% in all the other seasons and annually.

By comparing the test statistics with the critical values corresponding to the values of autocorrelations that are representative for the data (last column in Table 1), that is, temporal autocorrelation equal to zero and spatial autocorrelation between neighbouring gridpoints being 0.95, one can see that all the tests except for the sign test indicate that positive trends in all seasons are statistically significant over the entire region, that is, that they are unlikely to have occurred by chance. The counting and fdr tests do not prove significance for the higher autocorrelation values in winter; this can be interpreted so that the trends are near the edge of significance according to these two tests. For Kendall test, the test statistics fall far beyond the critical values, securing a high significance. On the other hand, the sign test suggests that trends are not significant if taken collectively over the entire region in any season even though their majority is positive and locally significant.

4 Conclusions

We compared the performance of five tests for the significance of trends over a region as a whole. The critical values of the tests were developed on a synthetic dataset. The application of the tests to the reanalysis data demonstrated that the tests outcomes may differ: while the sign test does not detect significance of trends in annual and seasonal temperature in Europe and its vicinity in NCEP/NCAR reanalysis, the other four tests do. These tests' different behaviors may reflect the fact that different tests take the data different properties into consideration or may be a manifestation of a different sensitivity of the tests to breaking their assumptions, most notably the equality of both spatial and temporal autocorrelations across the entire analysis domain.

Acknowledgements This study was supported by the Czech Science Foundation, project 16-04676S.

References

1. DelSole, T., Yang, X.S.: Field significance of regression patterns. J. Climate **24**, 5094–5107 (2011)
2. Katz, R.W., Brown, B.G.: The problem of multiplicity in research on teleconnections. Int. J. Climatol. **11**, 505–513 (1991)
3. Khaliq, M.N., Ouarda, T.B.M.J., Gachon, P., Sushama, L., St-Hilaire, A.: Identification of hydrological trends in the presence of serial and cross correlations: a review of selected methods and their application to annual flow regimes of Canadian rivers. J. Hydrol. **368**, 117–130 (2009)
4. Livezey, R.E., Chen, W.Y.: Statistical field significance and its determination by Monte Carlo techniques. Mon. Weather Rev. **111**, 46–59 (1983)
5. Ventura, V., Paciorek, C.J., Risbey, J.S.: Controlling the proportion of falsely rejected hypotheses when conducting multiple tests with climatological data. J. Climate **17**, 4343–4356 (2004)
6. Wilks, D.S.: On "field significance" and the false discovery rate. J. Appl. Meteorol. Climatol. **45**, 1181–1189 (2006)
7. Wilks, D.S.: The stippling shows statistically significant gridpoints. How research results are routinely overstated and overinterpreted, and what to do about it. Bull. Amer. Meteorol. Soc. **97**, 2263–2273 (2016)

Long-Term Variability of Gauged Precipitation Over California and Its Links to Circulation Patterns

Luciano Rodriguez, Cyril Rakovski, Mohamed Allali, and Hesham El-Askary

Abstract

California is an area of diverse topography and has what many scientists call a Mediterranean climate. Various precipitation spatial and temporal patterns exist due to El Niño Southern Oscillation (ENSO) which can cause abnormal precipitation or droughts. As temperature increases due to the rise of CO_2 in the atmosphere, it is rapidly changing the climate of not only California but the world. Using NOAA's hourly precipitation data from rain gauges and modeled data, we performed an extensive analysis (Empirical Mode Decomposition) with SOI, PDO, and AMO to depict ENSO patterns. We found that indices have a stronger relationship with the gauge datasets than the modeled data. Also, SOI has a stronger correlation to the northern regions of California and PDO to the southern. Lastly, AMO shows insignificant correlations in California.

Keywords

Precipitation • Time series • ARMA/ARIMA
Climate • ENSO

L. Rodriguez · C. Rakovski · M. Allali
School of Computational Sciences, Schmid College of Science and Technology, Chapman University, Orange, CA, USA

H. El-Askary (✉)
School of Earth and Environmental Sciences, Schmid College of Science and Technology, Chapman University, Orange, CA, USA
e-mail: elaskary@chapman.edu

H. El-Askary
Center of Excellence in Earth Observing, Chapman University, Orange, CA, USA

H. El-Askary
Department of Environmental Sciences, Faculty of Science, Alexandra University, Alexandria, Moharam Bek, Egypt

1 Introduction

The world's climate is continuously changing. Due to the various coupling of Earth's spheres, there exist many variations of local and regional climate changes. Unfortunately, record keeping of changes in the weather has not been extended over space and time, as well as developing instruments (more locations, scheduled maintenance on existing instruments, and acquiring new and improved gauges) to have accurate measurements to analyze the climate change accurately. Ideally, to have a better understanding of the changes in the climate, one must know and understand the small processes (microclimates) that make up the significant climate changes over many years. Weather, for example, is one of the small changes that affect the climate. Patterns such as drought, precipitation, flash floods, thunderstorms, etcetera will be accurately detected and provide enough warning time for people to mitigate. This paper focused on precipitation analysis using empirical mode decomposition in seven regions of California [3] to correctly map out weather patterns.

The National Climatic Data Center (NCDC) partitioned California into seven distinct climate divisions defined where the topography of California plays a significant role. The alignment of the watersheds, agricultural administrative districts, geographic convenience, and clear judgment of the committee have established the climate boundaries [3]. Figure 1 shows the topography of California with the changes of elevation. Green represents sea level as the color scheme transitions to white to represent higher elevations.

2 Data and Methods

We uses hourly precipitation data for the analysis from National Climatic Data Center and NOAA's Forecast Systems Laboratory (FSL) CD-ROM where there are more than 2500 active stations and 7000 total stations. Most of the data

Z. Zhang et al. (eds.), *Patterns and Mechanisms of Climate, Paleoclimate and Paleoenvironmental Changes from Low-Latitude Regions*, Advances in Science, Technology & Innovation, https://doi.org/10.1007/978-3-030-01599-2_22

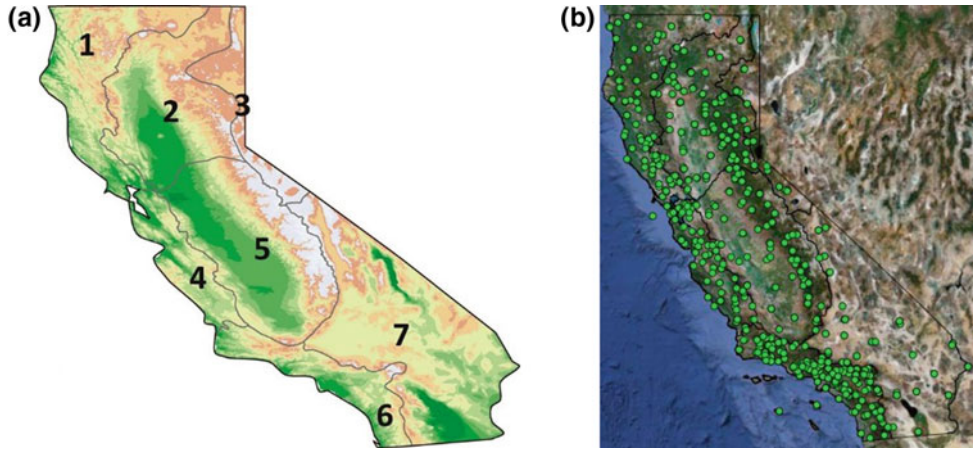

Fig. 1 **a** Seven climate divisions of California where green represents sea level as the color scheme transitions to white to represent higher elevation: 1 North Coast Drainage, 2 Sacramento Drainage, 3 Northeast Interior Basins, 4 Central Coast Drainage, 5 San Joaquin Drainage, 6 South Coast Drainage, 7 Southeast Desert Basin [2]. **b** 735 stations used in the analysis

ranges from 1948 through 1995. However, some stations begin as early as 1900. The hourly data extracted (735 stations from 1948 to 1995) concentrated on California's seven climate divisions as shown in Fig. 1. The data obtained have missing hours, days, and up to a few weeks. Therefore, total precipitation of monthly data was calculated to solve the discontinuous problem by inputting missing values. We arithmetically averaged the multiple stations in each climate division.

Monthly modeled precipitation data from NCDC gridded dataset translated to California's seven climate divisions was used to compare with the rain gauge measurements. The data begins from 1895 through 2013 for all climate divisions. To accurately compare both time series, we cropped the monthly modeled data to the respective timestamp of the gauge data per climate division. Southern Oscillation Index (SOI), Pacific Decadal Oscillation (PDO), and Atlantic Multidecadal Oscillation (AMO) indices were used to reference the correlation between the signals of ENSO to distinguish the differences between modeled and gauge data.

An essential part of the assessment is to know what each component represents. According to Wu et al. [10], they interpret the meaning of each component for SOI only. The first component, c_1, is related to physical phenomena or simply noise in the time series. The second component is known as a semiannual cycle given from the migration of the sun that crosses the equator twice a year. The third component is the annual cycle of Tahiti and Darwin pressures. The fourth component, known as a biennial cycle, is the nonlinear response of the tropical atmosphere to the seasonally-varying force. In addition, it can also be the interaction between South Asian Monsoon and large-scale circulations in the tropics and extra tropics. The fifth and sixth components are considered as an inter-annual mode varying on average 3.3 and 5.9 years, respectively. They represent the oscillations induced by atmosphere-ocean interaction. Components greater than 7 are decadal modes that are possibly related to the atmosphere-ocean interaction of longer timescales. In addition, they are responses of the tropical Pacific to decadal forcing. We discussed the results of such comparison in the later sections.

3 Results

We performed empirical mode decomposition (EMD) on the rain gauge and modeled data sets and SOI, PDO, and AMO indices. The raw datasets have an insignificant relationship with each other, and thus EMD was performed. In the first row of Fig. 2, one can see that the modeled/gauge has almost a zero correlation with SOI, PDO, and AMO as raw datasets. A low correlation is due to the high amount of noise within the datasets. Not surprisingly, the modeled and gauge time series have a high correlation of 0.92, which solidifies a great correspondence amongst the datasets. In the second and third row, one can see there is a much better correlation amongst the time series. The noted correlations are for the strongest correlation among all components and lag times. A positive lag means that the modeled or gauge is ahead by n months. A negative lag means that SOI, PDO, or AMO is ahead by n months. For example, referring to the correlation between the gauge time series and SOI, it has a high correlation of 0.84 with a positive lag of three months. We interpret that the gauge time series is three months ahead of the SOI time series.

Table 1 shows all seven climate divisions with its respective precipitation EMD components compared to the three indices. SOI has a stronger relationship with the

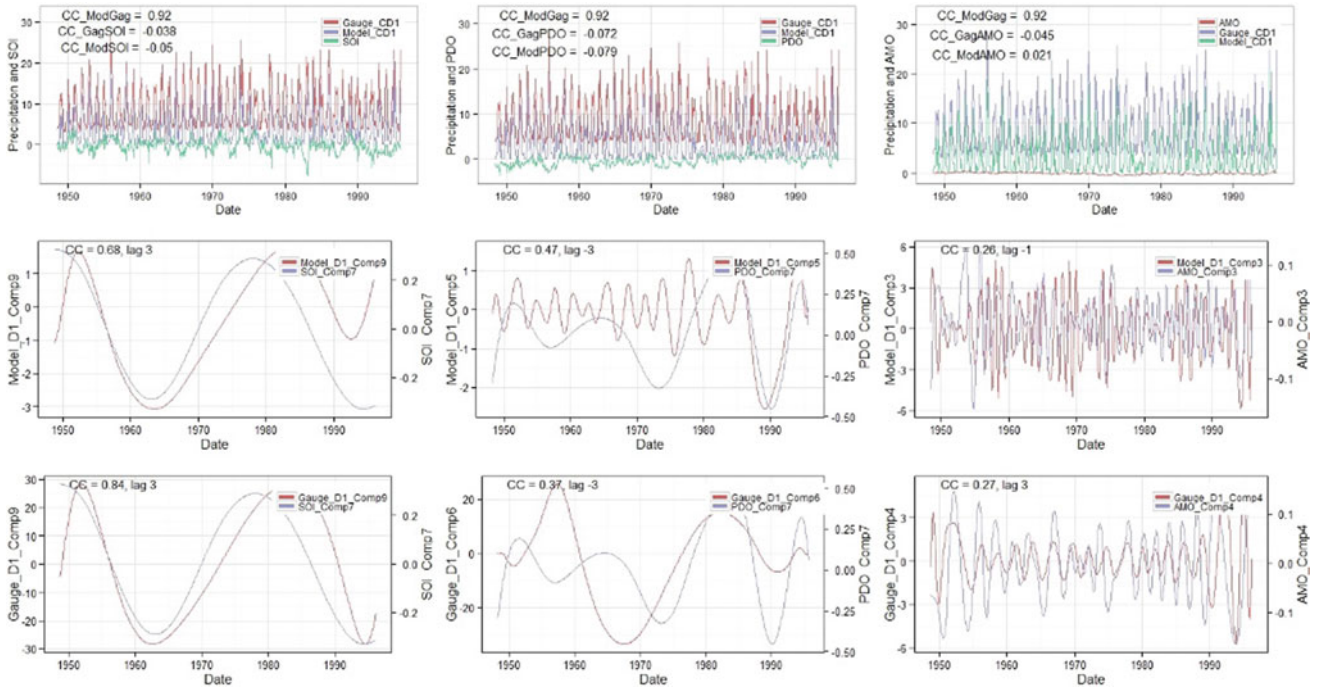

Fig. 2 Climate division 1 EMD correlation between model-based/gauge and SOI/PDO/AMO

Table 1 Precipitation data from modeled and gauged data compared to SOI, PDO, and AMO

	SOI	PDO	AMO
D1_Mod	C9, C7, 0.68, 3	C5, C7, 0.47, −3	C3, C3, 0.26, −1
D1_Gag (112 Stat.)	C9, C7, 0.84, 3	C6, C7, 0.37, −3	C4, C4, 0.27, 3
D2_Mod	C5, C5, 0.23, −3	C7, C9, 0.38, −3	C7, C7, 0.49, 3
D2_Gag (136 Stat.)	C4, C3, 0.08, −1	C6, C7, 0.41, −1	C7, C7, 0.37, −3
D3_Mod	C6, C7, 0.34, −3	C6, C7, 0.49, −3	C4, C4, 0.20, 0
D3_Gag (18 Stat.)	C5, C5, 0.36, 3	C7, C7, 0.51, −3	C6, C4, 0.41, −3
D4_Mod	C10, C6, 0.33, 3	C5, C5, 0.49, 1	C5, C5, 0.32, −3
D4_Gag (97 Stat.)	C9, C7, 0.61, 3	C7, C7, 0.52, −3	C5, C5, 0.36, −3
D5_Mod	C10, C7, 0.44, 3	C7, C6, 0.69, −2	C5, C5, 0.38, −3
D5_Gag (103 Stat.)	C8, C7, 0.45, 3	C7, C7, 0.50, −3	C7, C6, 0.30, 3
D6_Mod	C6, C7, 0.24, −3	C8, C7, 0.49, 0	C7, C5, 0.21, −3
D6_Gag (209 Stat.)	C6, C4, 0.21, 3	C6, C6, 0.53, −3	C4, C4, 0.22, 1
D7_Mod	C7, C7, 0.35, 3	C7, C7, 0.63, 3	C7, C6, 0.29, −3
D7_Gag (60 Stat.)	C7, C7, 0.52, −3	C6, C7, 0.85, 2	C4, C4, 0.21, −3

The first component corresponds to the row (modeled/gauge and Climate Division), the second component corresponds to its respective column (SOI, PDO, or AMO), third is the cross-correlation, and fourth is the lag
The number of stations used for each gauge calculation is in parenthesis

northern climate divisions than the southern climate divisions. Like SOI, the gauge time series typically has a stronger correlation to PDO than the modeled time series. Additionally, PDO has a stronger relationship in the southern climate divisions than the northern ones. AMO has consistently been irrelevant in all climate divisions for both modeled and gauge time series comparisons. The strongest signal is in climate division 2 with a correlation of 0.49 and 0.37 for the modeled and gauge, respectively. These patterns have not been consistent with Trenberth and Shea [9].

4 Discussion

Each index has a different relationship within California's seven climate divisions. The calculation of each index determines this relationship and is the byproduct in each region. The results highlight that in general, the gauge time series has a stronger correlation to SOI. More importantly, SOI has a stronger relationship with the northern climate divisions than the southern ones. This relationship has been seen and reported by McCabe and Dettinger [5] and Redmond and Koch [8]. Moreover, the average rainfall increase from south to north [1] validates the link between SOI and precipitation variability. On the other hand, PDO shows an inverse relationship to SOI as it has a stronger correlation to the southern climate divisions than the northern ones. This inverse relationship is due to the PDO's strong correlation with drought events at low elevations where the majority of southern California desert like terrain exists [4, 6].

As suggested by NOAA [7], AMO is related to droughts in the Midwest and Southwest, but there is no such evidence in the current time frame of this data analysis. It is surprising since AMO has an effect on temperature and precipitation throughout North America and Europe. NOAA and Trenberth and Shea [9] agree that AMO cycle is 60–80 years, where each warm and cold phase may last anywhere between 20 and 40 years. Unfortunately for both cases, the data used in the modeled and gauge time series just about extends NOAA's cycle but is shallow to Trenberth and Shea [9]. It extends to a deeper understanding of the various cycles for each time series, indices, their respective correlation, and EMD components.

5 Conclusions

Forecasting atmospheric hazards using historical precipitation data is what scientist/researchers are attempting to do well enough to be able to avoid catastrophic events. However, the usage is different from researcher and location. Therefore, this study focuses on historical hourly precipitation data to modeled extreme precipitation (mainly related to ENSO). The data consisted of 47 years of daily observation in various regions in California. Our results show the connection and impacts of precipitation with each climate index. SOI has a stronger relationship with the northern climate divisions since they are subtle to precipitation. PDO is strongly related to the southern climate divisions since it correlates with drought/dry conditions that are present in southern California. AMO, on the other hand, had little connection with precipitation in California but may be due to the limited amount of data used in this study. Also, we connected the impact of SOI and PDO to have connections with solar activities that have attributions to ENSO events due to the warming of the oceans. AMO has a connection with Thermohaline Circulation, though little work exists with such association.

References

1. Castello, A.F., Shelton, M.L.: Winter precipitation on the US Pacific Coast and El Niño–southern oscillation events. Int. J. Climatol. **24**(4), 481–497 (2004)
2. El-Askary, H., Allali, M., Rakovski, C., Prasad, A., Kafatos, M., Struppa, D.: Computational methods for climate data. WIRS Comput. Stat. **4**(4), 359–374 (2012)
3. Guttman, N.B., Quayle, R.G.: A historical perspective of U.S. climate divisions. Bull. Am. Meteor. Soc. **77**, 293–303 (1996)
4. Howat, I.M., Tulaczyk, S.: Trends in spring snowpack over a half-century of climate warming in California, USA. Ann. Glaciol. **40**(1), 151–156 (2005)
5. McCabe, G.J., Dettinger, M.D.: Decadal variations in the strength of ENSO teleconnections with precipitation in the western United States. Int. J. Climatol. **19**(13), 1399–1410 (1999)
6. McCabe, G.J., Palecki, M.A., Betancourt, J.L.: Pacific and Atlantic Ocean influences on multidecadal drought frequency in the United States. Proc. Natl. Acad. Sci. **101**(12), 4136–4141 (2004). https://doi.org/10.1073/pnas.0306738101
7. Physical Oceanography Division. (2005, Nov 9). Retrieved May 28, 2016, from http://www.aoml.noaa.gov/phod/amo_faq.php
8. Redmond, K.T., Koch, R.W.: Surface climate and streamflow variability in the Western United States and their relationship to large-scale circulation indices. Water Resour. Res. **27**(9), 2381–2399 (1991)
9. Trenberth, K.E., Shea, D.J.: Atlantic hurricanes and natural variability in 2005. Geophys. Res. Lett. **33**(12), L12704 (2006)
10. Wu, Z., Schnieder, E., Hu, Z.-Z., Cao, L.: The impact of global warming on ENSO variability in climate records. Retrieved from ftp://cola.gmu.edu/pub/ctr/ctr_110.pdf (n.d.)

Sensitivity of IDF Curves to Rainfall Gauge Type

A. S. Al-Wagdany

Abstract

The primary objectives of the study was to evaluate the effect of using tipping bucket rain gauges of different types of computing Intensity-Duration-Frequency Curves. Data were used from two tipping bucket rain gauges installed in an upstream sub basin of Numan catchment in Saudi Arabia. With the help of the probability distribution of Gumbel. Records of gauges for the period 2006–2017 were used to develop IDF curves. Comparison of the resulting IDF curves indicated that the Hydrological Services (HS) gauge produced IDF curves with higher rainfall intensities compared to the Texas Electronics (TEMM) gauge. This can be ascribed to fact that the HS gauge are fitted with a siphon tube which decreases undercatchment in the course of intense rainfall events.

Keywords

Rainfall records • IDF curves • Dual recording rainfall gauges • Arid climate • Saudi Arabia

1 Introduction

Intensity Duration Frequency (IDF) curves represent the relation between intensity, duration, and frequency of rainfall. Reviewing and updating IDF curves is necessary since they are usually utilized to design hydrologic and hydraulic structures. IDF curves can be developed from the data of a recording rain gauge through utilizing a frequency analysis procedure.

Using rainfall gauges with different specifications can affect the recorded values of intensity, duration, and return period of rainfall events. The estimation of the probable effects of using different types of rain gauges is an effective approach to face the risk in vulnerable urban areas.

The construction of IDF curves requires a rainfall data with fine temporal resolution that are usually unavailable particularly in arid regions. Daily rainfall data are commonly available. Therefore, daily rainfall disaggregation model is usually used to generate rainfall data at shorter time steps to develop IDF curves. Fortunately, rainfall data with very fine temporal resolution (5 min) are available and were used in the current study.

Several researchers analyzed the rainfall data to develop IDF curves or produce rainfall hyetographs in arid regions. This includes the works of Al-Khalaf [1], AlHassoun [2], Elsebaie [3], Awadallah and Younan [4] Sherif et al. [5], Elfeki et al. [6].

2 Materials and Method

In the present study, 5 min rainfall data, collected from a recording rainfall measurement station equipped with double tipping bucket rain gauges were used. These data are currently available for a 12-year period (2006–2017). The first rain gauges were produced by Texas Electronics (TEMM) while the second were obtained from Hydrological Services (HS). This rainfall station was installed to monitor precipitation in the upper catchment of Numan basin in 2006. Detailed descriptions of the dual rainfall station and the purpose of the various experiments were given in Al-wagdany [7].

The followed procedure in this investigation is summarized hereafter:

1. Collection of rainfall records of both HS and TEMM gauges;
2. Extraction of maximum rainfall depths for the different durations;
3. Carrying out rainfall frequency analysis for each rainfall duration.

A. S. Al-Wagdany (✉)
Department of Hydrology and Water Resources Management, King Abdulaziz University, P. O. Box 80208 Jeddah, 21589, Saudi Arabia
e-mail: awagdani@yahoo.com

Z. Zhang et al. (eds.), *Patterns and Mechanisms of Climate, Paleoclimate and Paleoenvironmental Changes from Low-Latitude Regions*, Advances in Science, Technology & Innovation, https://doi.org/10.1007/978-3-030-01599-2_23

4. Construction of IDF curves from both rainfall data sets.
5. Comparison of the resulting IDF curves.

The first step in the IDF analysis is to extract rainfall events of different durations from the observed rainfall records. In the current study, maximum rainfall depths were extracted for each 5 min starting from 5 to 210 min. The IDF curves construction needs that a frequency analysis be carried out to fit annual extreme data to a probability distribution. Two approaches may be followed to perform such frequency analysis. The first, consists in using an empirical plotting position method to compute the exceedance probabilities from the observed rainfall records. The second is to fit a theoretical Extreme Value (EV) distribution to the observed rainfall data. This theoretical distribution is then used to extract values of rainfall intensity and duration corresponding to specific exceedance probabilities.

In the current study, the theoretical Extreme Value (EV) Distribution approach was adopted. In this investigation, Gumbel Extreme Value I distribution was used since it is the most commonly used probability distribution for extreme rainfall data. According to Watt et al. [8] Gumbel probability distribution Type I can be expressed as:

$$X_T = X + K_T S \tag{1}$$

where X and S are the mean and the standard deviation of the observed rainfall records. The frequency factor, K_T for a specific return period T, can be estimated as:

$$K_T = \frac{-\sqrt{6}}{\pi}\left[0.5772 + \ln\left(\ln\left(\frac{T}{T-1}\right)\right)\right] \tag{2}$$

When using this procedure, the frequency factors corresponding to given return periods are first computed using Eq. (2). Then, the mean and standard deviation are computed for each duration. Finally, Eq. (1) is used to compute the rainfall depth and hence the intensity associated with each return period.

3 Results and Discussion

The HS and TEMM gauging period continued for 12 years. For each duration, the maximum annual rainfall values were extracted from the raw data of HS and TEMM gauges. Then, the mean and standard deviations of these values were computed. Tables 1 and 2 show statistics of annual extreme rainfall depths for durations from 5 to 210 min for HS and TEMM gauges, respectively.

Gumbel distribution methodology was used to compute the IDF curves for both rainfall gauges. In Fig. 1, a comparison between derived IDF curves from rainfall data of HS and TEMM rain gauges for four different return periods is presented. From Fig. 1 and Tables 1 and 2, it is clear that the observed maximum precipitation depth and intensity for the HS gauge are always higher than those of the TEMM gauge. These differences range from about 23% for maximum rainfall depth at 5 min duration to about 10% at the 210 min rainfall durations.

4 Conclusions

This study utilized short duration rainfall data from dual tipping-bucket gauges (TEMM and HS) to develop IDF curves of an arid area in the west of Saudi Arabia. HS gauge recorded higher values of precipitation depths as well as intensity compared to the TEMM gauge. This can be attributed to the fact that HS gauge is equipped by a siphon tube which allows a fixed amount of cached water to reach each bucket, reducing undercatchment during intense rainfall (Al-Wagdany [7]. In rainfall investigations which utilized values of extreme rainfall depths or intensity, it is recommended to correct the rainfall data collected by TB rain gauges that are not equipped with siphon mechanism. The correction process can be carried out by using a correction factor such as that recommended by Al-Wagdany [7].

Table 1 Values of annual maximum rainfall depth, mean and standard deviation for HS gauge

Time	Max.	Mean	S.D.	Time	Max.	Mean	S.D.
5	12.9	8.0	2.5	110	53.3	31.7	12.5
10	22.3	13.0	4.5	115	53.3	31.8	12.5
15	27.2	16.0	5.7	120	53.3	31.8	12.5
20	31.0	18.8	6.4	125	53.3	31.8	12.5
25	34.0	21.2	6.8	130	53.3	31.8	12.5
30	34.8	22.4	7.2	135	53.3	31.8	12.5
35	35.3	23.8	7.6	140	53.3	31.9	12.5
40	37.6	25.5	8.6	145	53.3	31.9	12.5
45	40.9	26.5	9.3	150	53.3	31.9	12.5
50	41.2	27.3	9.9	155	53.3	32.0	12.5
55	46.7	28.4	10.9	160	53.3	32.0	12.5
60	49.3	29.1	11.6	165	53.3	32.1	12.5
65	51.0	29.8	12.3	170	53.3	32.1	12.5
70	52.1	30.4	12.9	175	53.3	32.1	12.5
75	52.3	30.6	13.0	180	53.3	32.2	12.5
80	52.6	30.7	13.1	185	53.3	32.4	12.4
85	52.6	30.9	13.0	190	53.3	32.6	12.3
90	52.8	31.1	12.8	195	53.3	32.6	12.3
95	53.1	31.2	12.6	200	53.3	32.7	12.3
100	53.1	31.4	12.4	205	53.3	32.7	12.3
105	53.1	31.5	12.5	210	53.3	32.7	12.3

Table 2 Values of annual maximum rainfall depth, mean and standard deviation for TEMM gauge

Time	Max.	Mean	S.D.	Time	Max.	Mean	S.D.
5	10.5	6.7	1.9	110	48.3	29.3	11.9
10	17.5	11.2	3.6	115	48.3	29.3	11.9
15	22.0	14.2	4.8	120	48.3	29.4	11.8
20	25.7	16.9	5.5	125	48.3	29.4	11.8
25	28.2	19.2	5.8	130	48.3	29.4	11.8
30	29.1	20.5	6.0	135	48.3	29.4	11.8
35	30.2	21.9	6.7	140	48.3	29.4	11.8
40	37.6	23.5	8.0	145	48.3	29.4	11.8
45	40.9	24.4	8.8	150	48.3	29.4	11.8
50	41.2	25.1	9.5	155	48.3	29.5	11.8
55	42.0	26.0	10.3	160	48.3	29.5	11.8
60	44.3	26.6	10.8	165	48.4	29.6	11.8
65	46.1	27.2	11.2	170	48.4	29.6	11.8
70	47.0	27.8	11.8	175	48.4	29.7	11.8
75	47.3	28.1	12.1	180	48.4	29.8	11.8
80	47.6	28.3	12.3	185	48.4	29.9	11.8
85	47.8	28.4	12.3	190	48.4	30.0	11.8
90	48.0	28.6	12.2	195	48.4	30.1	11.7
95	48.1	28.7	12.1	200	48.4	30.1	11.7
100	48.2	28.9	11.9	205	48.4	30.2	11.8
105	48.3	29.1	11.8	210	48.4	30.3	11.8

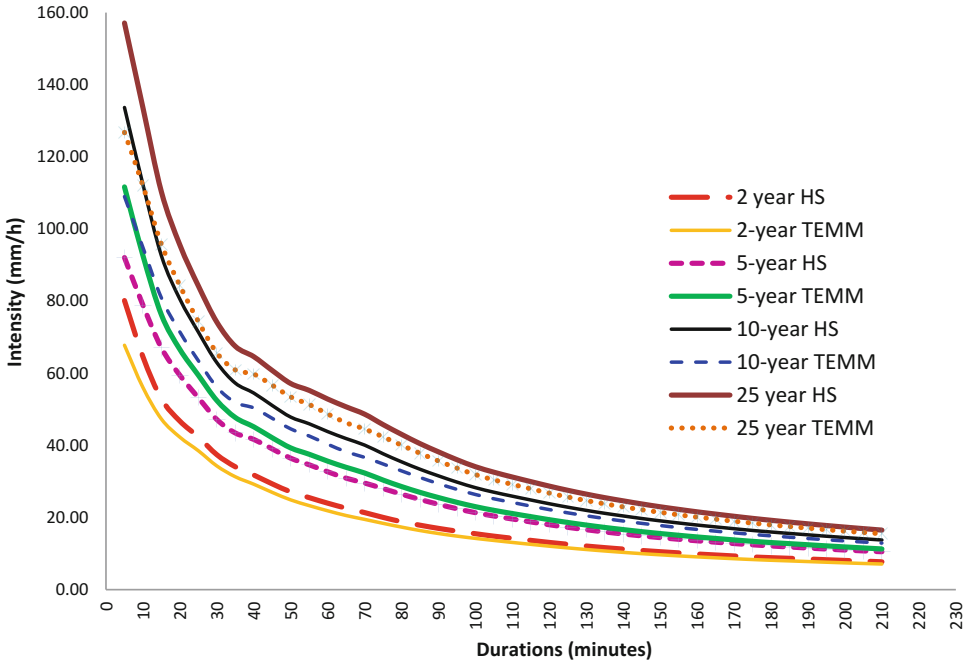

Fig. 1 IDF curves for HS and TEMM gauges

References

1. Al-Khalaf, H.A.: Predicting short-duration, high-intensity rainfall in Saudi Arabia. M.S. Thesis, Faculty of Graduate Studies; King Fahad University of Petroleum and Minerals, Dahran (K.S.A) (1997)
2. AlHassoun, S.A.: Developing an empirical formulae to estimate rainfall intensity in Riyadh region. J. King Saud Univ. Eng. Sci. (2011)
3. Elsebaie, I.H.: Developing rainfall intensity-duration-frequency relationship for two regions in Saudi Arabia. J. King Saud Univ. Eng. Sci. **24**, 131–140 (2012)
4. Awadallah, A.G., Younan, N.S.: Conservative design rainfall distribution for application in arid regions with sparse data. J. Arid. Environ. **79**, 66–75 (2012)
5. Sherif, M.M., Almulla, M., Shetty, A., Chowdhury, R.K.: Analysis of rainfall, PMP and drought in the United Arab Emirates. Int. J. Climatol. **34**(4), 1318–1328 (2014)
6. Elfeki, A.M., Ewea, H.A., Al-Amri, N.S.: Development of storm hyetographs for flood forecasting in the Kingdom of Saudi Arabia. Arab. J. Geosci. **7**, 4387–4398 (2014)
7. Al-Wagdany, A.S.: Inconsistency in rainfall characteristics estimated from records of different rain gauges. Arab. J. Geosci. **9**(5), 1–10 (2016)
8. Watt, W.E., Lathem, K.W., Neill, C.R., Richard, T.L., Rousselle, J.: Hydrology of Floods in Canada: A Guide to Planning and Design. National Research Council of Canada (1989)

Structural Characteristics of Precipitation in Jordan

Fayez A. Abdulla and Abdulelah Al-Qadami

Abstract

In this paper, the structure characteristics of rainfall time series were studied based on the consistency, randomness, trend, and goodness of fit tests. For this purpose, thirty-two climatic stations distributed over Jordan were selected with fifty-two years' time series. The time series analysis indicates consistent and evidence of randomness in data series at 1 and 5% significance level with the exception of two stations time series. Mann-Kendal trend tests indicates free trend in all the stations at 95% confidence level with the exception of six stations which have a negative trend.

Keywords

Precipitation • Randomness • Consistency
Trend analysis • Jordan

1 Introduction

Water resources engineers are responsible for the design of an optimum water management and distribution plan and the related activities over the region of interest. Precipitation is considered as one of the significant and viable components of water resources and the only renewable water source especially in the arid and semi-arid areas. Jordan is an arid and semi-arid country that suffers from water resources scarcity and vulnerability due to the insufficient amount of rainfall and groundwater over-pumping to maintain human, agricultural, and industrial needs. Furthermore, Jordan received huge numbers of refuges from the neighboring countries mainly Syria, Iraq, Libya, and Yemen because of the political conflicts, which has put more stress on the demand of fresh water [1].

The importance of precipitation as a significant input factor with high variability and uncertainty for all water resources indicates the necessity of studying the precipitation statistical characteristics. Studying the structural characteristics of hydrological and metrological variables, especially precipitation, is necessary for climate change and hydrological modelling studies. Precipitation is considered one of the most important input variables for the modelling process. The input data set should be free of trend, out of discontinuity and the best fitted probability distribution function should be determined. The fundamental characteristics of annual precipitation have not been investigated properly, which is the reason for the study of its structural characteristics.

2 Study Area and Methodology

The data used in this study consists of series of daily rainfall covering the rainy seasons from October to May. Only stations with good records were used (for at least 30 years). In this study, the precipitation data were checked for missing information then filled using the Normal Ratio method. Accordingly, thirty-two stations were selected for this study (Fig. 1). Fifty-three years of rainfall time series starting from January-1960 and ending in December-2013 were used in this study.

Annual rainfall data characteristics were investigated using different statistical tests including randomness, consistency, trend existence and goodness of fit to the probability distribution functions. The non-parametric randomness run test is used to detect the time series departure in randomness. This test represents whether the data series passes the randomness test or not in the form of statistics Z at a given significance level. Z test statistic value for each station records were compared with respect to the null hypothesis test at 99% $Z_{0.01} = \mp 2.57$ and 95% $Z_{0.05} = \mp 1.96$ [2]. The consistency or inconsistency of the data series were tested using the double mass curve. In this method the rainfall data series cumulative in each station was plotted against the average cumulative of all the stations. The Sequential version of Non-parametric Mann-Kendall trend test was used for detecting the monotonic

F. A. Abdulla (✉) · A. Al-Qadami
Jordan University of Science and Technology, 2210 Irbid, Jordan
e-mail: fabdulla@just.edu.jo

Z. Zhang et al. (eds.), *Patterns and Mechanisms of Climate, Paleoclimate and Paleoenvironmental Changes from Low-Latitude Regions*, Advances in Science, Technology & Innovation, https://doi.org/10.1007/978-3-030-01599-2_24

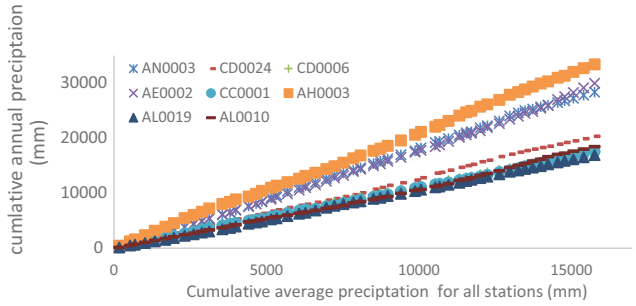

Fig. 1 Double mass curves of annual precipitation data series (Consistent one only)

positive or negative trend of the data set [3]. Finally, the best fit probability distribution function of each data set was determined based on Chi-square, which compares the observed relative frequency with the theoretical relative frequency method [4]. Six probability distributions were chosen for frequency analysis of the data series records including normal, log-normal, log-normal (3P), gamma (3P), generalized extreme value and log-Pearson.

3 Results

3.1 Consistency

Fifty-three years of data series for each station were examined for their consistency using double mass curve method. Consistent, low consistent and inconsistent time series were found as a result of this curve. For the limitation of space only consistent precipitation time series were plotted.

3.2 Randomness

The non-parametric randomness run is used to decide whether the data series is from a random process. In general, the run test is based on the run. A run is defined as a consecutive sequence of increasing or decreasing values. The length of the run depends on the number of increasing or decreasing values. The probability of the run is independent. Whether the (i + 1) value is larger or smaller than the Ith values follows a binomial distribution. Table 1 summarizes the results of all rain gauge stations based on randomness run test.

3.3 Trend

The Non-Parametric sequential version of Mann-Kendall trend test was performed for all the stations time series. From the null hypothesis of Mann-Kendall trend test, the values of test statistics Z of each station time series were compared to the test statistics Z_α at the confidence levels with $\alpha = 0.01$ (99% confidence level) and with $\alpha = 0.05$ (95% confidence level). The results are shown in Table 2.

Table 1 Randomness run test results of total annual rainfall for all the stations

Station ID	Z	Station ID	Z	Station ID	Z	Station ID	Results
AL0059	−0.27	DA0002	1.1	CF0007	0	CD0003	−3.30**
CD0006	0	DA0007	−1.92	AD0021	1.65	AL0010	1.1
CD0010	0	G0009	−1.1	AH0003	0	CA0002	−1.65
DB0002	0	F0002	0	AL0053	−1.65	H0001	0.84
CF0001	−3.02**	AL0018	1.65	AL0066	−1.1	F0011	1.65

*Sign indicates significant randomness at 95% confidence level and **sign indicates significant randomness at the 99% confidence levels

Table 2 Trend tests of total annual precipitation

Station ID	Z	Station ID	Z	Station ID	Z	Station ID	Z
AN0003	−0.46	F0001	−2.80**	CC0001	0.4	AL0035	3.66**
CD0024	−0.28	AE0002	−2.35**	CD0011	−1.92	AL0055	3.57**
AD0019	−1.41	AD0032	1.54	ED0002	2.05*	AL0019	0.92
AL0059	−1.78	DA0002	−1.04	CF0007	−0.92	CD0003	−2.51**
CD0006	0.34	DA0007	−5.11**	AD0021	1.92	AL0010	2.06*
CD0010	−1.02	G0009	−1.62	AH0003	−0.16	CA0002	−1.84
DB0002	−0.86	F0002	−2.28*	AL0053	1.25	H0001	−0.63
CF0001	−2.72**	AL0018	−0.1	AL0066	3.35**	F0011	−0.87

*Sign indicates significant trends at 95% confidence level and **sign indicates significant trends at the 99% confidence level

4 Discussion

Eight out of 32 rainfall data series are consistent which means there is no break points in the slope of the double mass curve line between the cumulative annual rainfall of each station with the average cumulative annual rainfall of all the stations. Six rainfall stations show low consistency with one or two break points in the slope. The other 18 data series are inconsistent because they have more than two break points in the line slope.

The time series of all stations accept the null hypothesis of the randomness run test at the two confidence intervals 99 and 95% except for two stations time series CF0001 (GhorEs-Safi st.), and CD0003 (El-Muwaqqarst.) which exceeded the Z values at the two confidence levels. Mann-Kendall trend tests results indicate that there are some stations with an obvious significant trend in the total annual precipitations. For instance, H5 Evap station has decreasing trends at the 95% confidence level whereas, RasEn-Naqb, DeirAlla have increasing trends at the 95% confidence level, while GhorEs-Safi, Um El-Quttein, Irbid Agr.Station, Feedan, El-Muwaqqar have decreasing trends at the 99% confidence level whereas KhirebitEs-Samra, Baq'a, WadiDhuleil Nursery have increasing trends at the 99% confidence level. On the other hand, 15 stations have a cooling decrease trend whereas 6 stations have cooling increase trend of the total annual precipitations.

5 Conclusions

More than half of the selected rain gauge station time series are inconsistent, 8 are consistent and 6 are increased. Evidence of randomness in the data series at 1 and 5% significance level is found with exception of two stations time series. H5 Evap. station had a significant decreasing trend at the 95% confidence level. Data series point out the existence of increasing and decreasing trends. RasEn-Naqb, Deir-Alla have increasing trends at the 95% confidence level. GhorEs-Safi, Um El-Quttein, Irbid Agr. Station, Feedan, El-Muwaqqar have decreasing trends at the 99% confidence level. Khire bitEs-Samra, Baq'a, Wadi Dhuleil Nursery revealed increasing trends at the 99% confidence level. A slightly decreasing trend is detected for 15 stations whereas the other 6 stations' trends are increasing.

References

1. Dahamsheh, A., Aksoy, H.: Structural characteristics of annual precipitation data in Jordan. Theor. Appl. Climatol. **88**(3–4), 201–212 (2006)
2. Wald, A., Wolfowitz, J.: On a test whether two samples are from the same population. Ann. Math. Stat. **11**(2), 147–162 (1940)
3. Sneyers, R.: Climate chaotic instability: statistical determination and theoretical background. Environmetrics **8**(5), 517–532 (1997)
4. Cochran, W.G.: The χ^2 test of goodness of fit. Ann. Math. Stat. **23**(3), 315–345 (1952)

The Shift of the Atmospheric Circulation Patterns and Its Impacts on Western Mediterranean

Mohammed-Said Karrouk

Abstract

Cumulating ocean-atmospheric energy caused by global warming has resulted in the reversal of the energy balance towards the poles. This situation is characterized by a new ocean-continental thermal distribution: this new surplus energy balance imposes a "New Atmospheric Circulation" predominantly meridian, and a "New Water Cycle" characterized by the intensity of evaporation, extreme precipitation, and a different rain distribution pattern: it is the actual "Warmed New Climate". Thanks to satellite observation and daily monitoring of meteorological conditions for more than ten years, we have observed that the positive balance has shifted more towards the poles, mainly in the northern hemisphere. Subtropical anticyclones are strengthened and have extended to high latitudes, especially over the Atlantic Ocean. This situation creates global peaks strengthened in winter periods, and imposes on cosmic cold (The cosmic cold settles in winter around the poles when the energy balance is extremely deficient.) the deep advection toward the south under the form of planetary valleys "Polar Vortex" [Barnes in Geophys. Res. Lett. 40(17):4734–4739, 2013; Francis and Vavrus in Geophys. Res. Lett. 39(6), 2012; Lindsey in Polar vortex brings cold here and there, but not everywhere. NOAA, 2014 1–3]. This situation imposes a pronounced ripple on the jet stream and installs a Meridian (The circulation is along a meridian, north/south and south/north.). Atmospheric Circulation (MAC) in winter, which brings the warm tropical air masses to reach the Arctic Circle, and cold polar air masses to reach Western Mediterranean. This situation creates unusual atmospheric events, characterized by "extreme" conditions: excessive heat at high latitudes, accompanied by heavy rains and floods, as well as cold at low latitudes and the appearance of snow in the Sahara!

Keywords

New climate • Extreme rainfall • Western Mediterranean • Morocco • MAC

1 Introduction

Since the eighties of the last century, climatological research has made a great scientific advance in the field of prediction, and the variability and evolution of different climatic parameters began to be clearer! [4].

But today, mainly since 2005, certainly because of the oceanic thermal accumulation, and the displacement of climatic zones towards the poles in selective forms[1]; climatic events do not evolve according to the usual and expected rhythms: atmospheric circulation, precipitations, temperatures, seasonal phenomena, etc. These events are experiencing a new spatial and temporal evolution and distribution, which characterize the global "New Climate".

In this new situation, the Western Mediterranean, located in a climate transition zone, has been fully affected by the "New Climate". Usually, the atmospheric response to major climatic events (ENSO) in this region such as "El Niño" was characterized by the installation of the NAO positive index, stability and drought, due to the dominance of the zonal atmospheric circulation in winter. On the other hand, in episode "La Niña", it was the negative index of the NAO and the meridian circulation that prevailed [5], and precipitation became abundant.

Since the beginning of this century, flood-causing weather events qualified as "exceptional!" have continued to occur in the Western Mediterranean and elsewhere, with

M.-S. Karrouk (✉)
FLSH Ben M'Sick, Department of Geography, LCEAT, CEREC, Hassan II University of Casablanca, Rue Tarik Bnou Ziad, Mers Sultan BP 9167, Casablanca, Morocco
e-mail: cerec@univh2m.ac.ma; climdev.morocco@gmail.com

[1]More pushed in oceans than above the continents.

Z. Zhang et al. (eds.), *Patterns and Mechanisms of Climate, Paleoclimate and Paleoenvironmental Changes from Low-Latitude Regions*, Advances in Science, Technology & Innovation, https://doi.org/10.1007/978-3-030-01599-2_25

an increasingly high recurrence, prompting scientists to wonder about the "new" hydro-thermal operation mode of the climate system inducing torrential rains, as well as other effecting on environments and societies.

The latest event was the October and December 2016 flood disaster in the Laayoune region in Southern Morocco, which was especially due to the unusual return of the rains in a region considered dry and Saharan.

2 Data and Methods

The data used in this research derive, according to their categories, from the following services:

Synoptic maps NOAA's hemispheres: NCEP/DFC, and European maps from Aktion "Wetterpate", Institute for Meteorology FU Berlin, Met Office and Deutscher Wetterdienst (DWD).

Geopotential maps Hemispheric and European maps obtained through the website wetterzentrale.de: ECMWF, GFS, GPDM 500 and 850 hPa, ground pressure 1015 hPa, Precipitations (mm), Temperatures 2 m from the ground (°C).

Meteorological data National Meteorological Office of Morocco (DMN).[2]

The methodology used is purely geographical; that of observing, analyzing, confronting and restoring. It is therefore observed events, which we tried to analyze by the various maps mentioned above. The daily observation period extended from 1990 to 2016 (25 years).

3 The New Meridian Atmospheric Circulation (MAC) and Its Effects on Floods and Drought in Western Mediterranean

3.1 "Normal" Atmospheric Circulation

This hemispheric circulation was characterized by the extreme seasonal tilting of the zonal and meridian atmospheric systems. The former prevailed in the cold season when the energy gradient was high between deficit and surplus areas, so that fast air flows were organized from west to east, thus separating the cold and warm zones at the front north of the Mediterranean region. The latter prevailed in the warm season when the energy gradient was low, and the slower flows undulated, taking a north–south and south–north meridian shape, thus establishing an intense activity of latitudinal energy transfer between the various regions of the mid-latitudes.

During the cold season, the subtropical Azores anticyclone pushed the flow from West to North, thus protecting/disfavoring the North African and Iberian region from polar front disturbances. This has imposed the droughts, quite normal under these conditions, which have characterized the secular Man/Space links[3] since the dawn of time in this region. But from time to time, when the tails of the polar disturbances reached our region, precipitation was back, which has always ensured the renewal of water resources in this region of the world.

It is these thermo-energetic conditions that have ensured the stability of the atmospheric circulation as we knew it in the twentieth century, and on the basis of which the scientific literature and engineering of this field as well as all human socio-economic structures have developed.

3.2 "Current" Atmospheric Circulation

Nowadays, we notice since the end of the last century, a new planetary thermo-energy distribution, characterized by the widening of the intertropical hot zone and its displacement towards the poles, mainly above the oceans [6]. This has led to the shrinking of the polar cold zone, and its invasion of continents, especially in the cold season [7].

This situation imposes a new hemispheric atmospheric circulation predominantly meridian. The western flows, forced to bypass the subtropical high pressure pushed to the poles, are found to be able to once again bypass intrusive subpolar depressions deep to the confines of the subtropical zones [8]. This leads to a succession of deep planetary waves: hot and stable ridges follow cold valleys and disturbances throughout the region of North Africa and Western Europe. The latter is characterized by brief and severe winter storms (2010, 2012) caused by blockage by the subtropical oceanic high pressure. While the Western Mediterranean countries are undergoing cold low pressure intrusions that give abundant rainfall at the meridian shear flow, or a cold frost if this shear is over the Atlantic, otherwise it is the daytime heat and the night cold if the anticyclonic ridge caps North Africa, or in any case, its western part.

The question of alternating peaks/heat valleys/freshness[4] imposes very active hydro-thermal interactions, which are manifested by an exceptional violence given the excess of the latent energy balance and the atmospheric humidity that accompanies it; This explains the torrential rains and floods

[2]Obtained directly from the DMN, or indirectly from other partners.

[3]Local geographical and cultural context.

[4]Low temperature.

of recent years, as well as the significant damage that results, especially in the autumn season [6].

Thus, in September/March 2008/2009 (La Niña phase), and December/February 2009/2010 (El Niño phase), the global valley installed on the European continent and North Africa, makes the Western Mediterranean conditional on 'exceptional' moisture accompanied by floods throughout the region [8].

These atmospheric conditions are "New", and put North Africa under the influence of moisture; this can minimize the effects of drought, desertification and water stress, if one adapts well to the new climate regime.

In these new conditions, the processes and mechanisms of drought and moisture become different, and undergo a successive alternation in time and space, and therefore, we witness a new distribution mode of the humidity in Western Mediterranean space [6], characterized by its brevity on the one hand, and its severity on the other, hence the need for reflection on the fate of water resources and their impacts in the Western Mediterranean countries.

These new atmospheric conditions alternate floods and droughts in the Western Mediterranean: the deep valleys in autumn and winter cause torrential rains and floods; this was the case of the floods of October 2008 in Tangier[5] (North Morocco), January/February 2010 in the Gharb region[6] (north, Fig. 1), November 2010 in Casablanca[7] (centre), November 2014 in Guelmim[8] (south, Fig. 2).

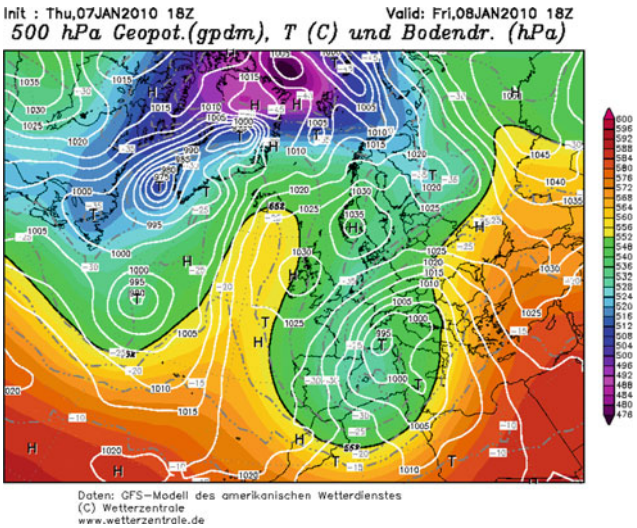

Fig. 1 Status of January 07, 2010 (Wetterzentrale)

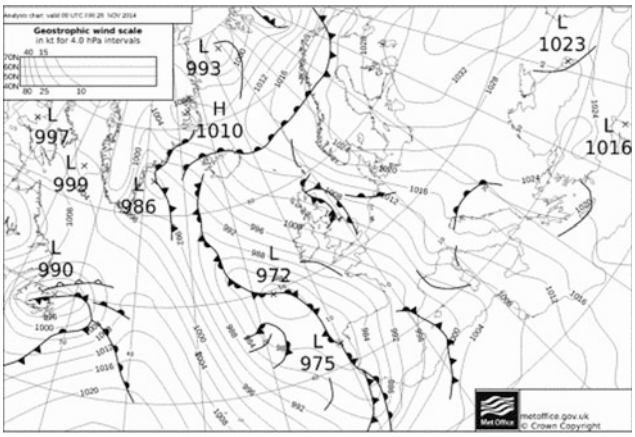

Fig. 2 Status of November 28, 2014 (Met Office)

4 Conclusion

These events, and other similar ones: floods caused by extreme rainfall of El Attaf, Ain Defla and M'sila in October 2007, Ghardaïa in October 2008, Algiers in October 2015 (Algeria), Tunis in October 2007, Sfax 2009 (Tunisia), Andalucía (Spain) in December 2010, the Var (France) in June 2010, Genoa (Italy) in November 2011, … etc., as well as many cases of extreme rainfall causing floods, should be considered as reference laboratory cases for the simulation of future situations, and integration into development plans in the future.

[5]Rainfall of 199.5 mm and 10 million m^3 of water in 5 h. Never seen!!! Absolute national record, (DMN).

[6]Submersion of 168,000 ha, of which 135,000 in the Gharb region, displacement of 22,000 inhabitants, cutting of several roads and railroads.

[7]This is unheard of in the economic capital of Morocco. In a single night, a first in the history of Casablanca, a peak of 178 mm of rain fell, half a year amount of rain (DMN).

[8]The depression of this storm (Xandra) reached the surprising value of 975 hPa on November 28, 2014 (Met Office). The human and material damage caused by this flood is impressive: people have died, roads destroyed, dams overwhelmed, farming destroyed, infrastructure dilapidated; it was a catastrophe.

References

1. Barnes, E.A.: Revisiting the evidence linking Arctic amplification to extreme weather in midlatitudes. Geophys. Res. Lett. **40**(17), 4734–4739 (2013)
2. Francis, J.A., Vavrus, S.J.: Evidence linking Arctic amplification to extreme weather in midlatitudes. Geophys. Res. Lett. **39**(6) (2012)
3. Lindsey, R.: Polar Vortex Brings Cold Here and There, But Not Everywhere. NOAA, 10 Jan (2014)
4. Karrouk, M.S.: Climate change and its impacts in Morocco. In: Mellouki, A., Ravishankara, A.R. (eds.) Regional Climate Variability and Its Impacts in the Mediterranean Area. NATO Science Series: IV: Earth and Environmental Sciences, vol. 79. Springer, Dordrecht (2007). https://doi.org/10.1007/978-1-4020-6429-6

5. Kennedy, C., Lindsey, R.: How is the Polar Vortex Related to the Arctic Oscillation? NOAA, 20 Jan (2014)
6. Karrouk, M.S.: New Planetary Energy Balance, Ocean-Atmosphere Interaction and Their Effects on Extreme Events in North Atlantic. EGU, Vienna (2016)
7. Wallace, J.M., et al.: Global warming and winter weather. Science **343**, 729–730 (2014)
8. Karrouk, M.S.: "New Climate" New Atmospheric Events and "New Climate Risks": The Case of Morocco. American Geophysical Union Fall Meeting, San Francisco (2015)

Recent Rainfall Variability in the South-West Mediterranean Region and Links with Teleconnection Patterns

Sabrina Taibi, Imane Messelmi, Mohamed Meddi, and Mohamed Amine Feddal

Abstract

Rainfall variability of Northern Algeria was analyzed over nine synoptic stations of the National office of meteorology during the period 1950–2017. Statistical tests of Mann-Kendall and Pettitt were applied to detect a significant trend and break over monthly and annual rainfall series. Stations located at the West side of the study area showed a significant decrease of annual rainfall during December, April and May while September and November recorded an increase of rainfall over the study period. Atmospheric circulation patterns affect the rainfall variability, that is why six climate indices were correlated to mean rainfall using spearman coefficient correlation. Annual rainfall series characterized by long period of drought are significantly correlated with El Nino southern oscillation (ENSO) and East Atlantic oscillation (EA). At the seasonal scale, East Atlantic oscillation and Mediterranean oscillation (MO) are the most dominant circulation modes, particularly during wet seasons.

Keywords

Rainfall variability • Atmospheric circulation • Climate indices • Algeria • Mediterranean basin

1 Introduction

In a context of climate change, the scientific community is increasingly interested in climate variability at global and regional scales since the last century. More studies highlighted a negative trend of rainfall variability since the mid seventies in Spain [1], Italy [2], Greece [3], Morocco [4] and Tunisia [5]. In Algeria, some studies analyzed the rainfall variability over different regions of Northern Algeria; most results show a significant decrease of rainfall since the mid seventies in the Northwestern part of Algeria [6–9]. Many authors associated the rainfall variability of the Mediterranean basin to atmospheric circulation principally North Atlantic Oscillation (NAO) and Mediterranean oscillation (MO) which affect significantly the winter rainfall [10–13]. Correlation with El Nino Southern Oscillation (ENSO) has been found in the Northwestern part of Algeria at the annual scale [6, 14], while seasonal rainfall seems to be correlated with NAO and MO [14].

The present work aimed to study the rainfall variability of Northern Algeria over the period 1950–2017 and link it with teleconnection patterns at the annual and monthly scale. The climate indices used in this study are: East Atlantic Oscillation (EA), Mediterranean Oscillation (MO), North Atlantique Oscillation (NAO), Western Mediterranean oscillation (WeMO), Atlantic oscillation (AO) and El Nino Southern Oscillation (SOI).

2 Methods

Mann–Kendall test was used to detect a significant trend in the mean rainfall variability, when Pettitt's test was applied to detect a significant average change and the date of break over main rainfall series.

To analyze correlation between rainfall variability and climate indices, the Spearman coefficient correlation was used.

Statistical tests were applied at 5% significant level.

S. Taibi (✉) · I. Messelmi
Department of Water and Environment Sciences, University of Saad Dahlab, Blida, Algeria
e-mail: taibisabrina86@gmail.com

M. Meddi
National High School of Hydraulic (ENSH), Blida, Algeria

M. A. Feddal
National High School of Agronomy (ENSA), El Harrach, Algiers, Algeria

Z. Zhang et al. (eds.), *Patterns and Mechanisms of Climate, Paleoclimate and Paleoenvironmental Changes from Low-Latitude Regions*, Advances in Science, Technology & Innovation, https://doi.org/10.1007/978-3-030-01599-2_26

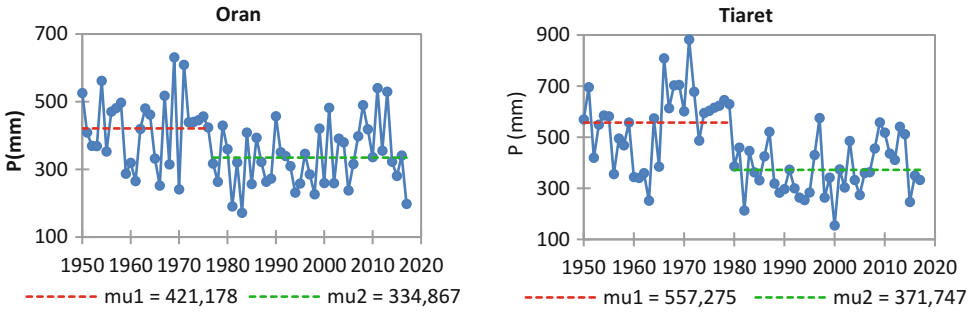

Fig. 1 Trend of annual rainfall variability at Oran and Tiaret stations according to Pettitt's test

3 Results

3.1 Rainfall Variability Analysis

The analysis of annual rainfall variability over the period 1950–2017 showed a downward trend in the western part of the study area (Fig. 1) while the stations located at the Eastern part were stationary. A break point was observed between 70s and 80s and rainfall deficit recorded about 20–33%. At seasonal scale, rainfall recorded a decrease of about 40% in December and about 50% in April and May, while a rainfall increase was observed in November at the same stations.

3.2 Links Between Rainfall and Climate Indices

The relation between annual rainfall and climate indices showed a significant negative correlation with SOI and EA, only with the stations that recorded a significant decrease of rainfall (Table 1). At the seasonal scale, significant negative correlations were observed with EA, MO and NAO, EA was a more dominant mode in the Mediterranean fringe of the study area while MO dominated the rainfall variability of Inland region of Northern Algeria (Table 1). The strongest coefficients correlations are observed from December to March (0.3–0.5). The western Mediterranean oscillation (WeMO) and Atlantic oscillation (AO) are not correlated with rainfall variability of Northern Algeria.

4 Discussion

An analysis of the mean rainfall variability in nine synoptic stations of Northern Algeria using Mann-Kendall and Pettitt's test showed a significant downward trend in the northwestern region between the 70s and 80s associated to the decrease of rainfall in December, April and May, while, stable rainfall patterns were observed in the eastern region. The search for a relationship between rainfall and circulation indices is based on correlations between mean rainfall (averaged signal) and each of the NAO, SOI, MO, AO, EA and WeMO circulation indices. Inter-annual variability of rainfall is linked with ENSO and EA. Strong anomalies of El Nino affect the global climate, and cause a reduction of rainfall in the Mediterranean basin. This circulation mode is partly responsible for long drought periods observed in Northwestern Algeria. The East Atlantic pattern is the second prominent mode of low-frequency variability over the North Atlantic, and appears as a leading mode in all months [15]. The EA pattern exhibits very strong multi-decadal variability in the 1950–2004 records, with a negative phase prevailing during much of 1950–1976, and the positive phase occurring during much of 1977–2004 [15]. The EA positive phase corresponds to a negative trend of annual rainfall.

At the seasonal scale, significant correlations were observed with NAO, MO and EA. The EA pattern is structurally similar to the NAO, and consists of a north-south dipole of anomaly centers spanning the North Atlantic from east to west [15]. The effect of EA on mean rainfall variability of the Mediterranean region has not been analyzed by others authors, unlike MO which was considered by a lot of authors as an important regional mode of atmospheric circulation that affects the rainfall variability of the Mediterranean basin [16–18] and is strongly correlated in winter with NAO [13]. Taibi et al. [14] analyzed relationship between seasonal rainfall variability of northern Algeria and SOI, NAO, MO and WeMO index. They found no significant correlation with stations located in the Eastern region of study area. However, the present study highlighted a significant negative correlation between two stations of the North-East (Annaba, Constantine), and EA index. To confirm this result more stations of the Eastern region should be studied.

5 Conclusions

This work aimed to analyze the recent mean rainfall variability of northern Algeria and its potential links with atmospheric circulation. A decrease of annual rainfall was observed in the western part of the study area which is

Table 1 Spearman coefficient correlation between mean rainfall and climate indices (only significant correlations are presented for each station)

C.I.	J.	F.	M.	A.	M.	J.	Jt.	Aug.	Sep.	Oct.	Nov.	Dec.	An.
Algiers													
EA	0.03	**−0.34**	−0.12	**−0.34**	**−0.28**	**−0.30**	0.02	0.09	**−0.26**	−0.21	−0.13	−0.17	−0.05
MO	**−0.52**	**−0.44**	**−0.44**	−0.12	−0.17	−0.02	0.10	−0.18	**−0.47**	**−0.36**	**−0.45**	−0.21	−0.06
NAO	−0.22	**−0.30**	**−0.32**	−0.10	−0.23	−0.01	−0.07	−0.08	**−0.45**	−0.05	−0.19	−0.02	−0.14
Chlef													
EA	−0.04	**−0.33**	−0.21	**−0.39**	**−0.31**	**−0.32**	−0.08	−0.09	−0.14	−0.17	−0.10	**−0.24**	−0.20
MO	**−0.54**	**−0.50**	**−0.48**	−0.16	−0.17	−0.08	0.01	−0.20	**−0.38**	**−0.28**	**−0.59**	−0.23	−0.18
NAO	**−0.25**	**−0.39**	**−0.38**	−0.12	−0.20	0.02	−0.05	0.10	**−0.38**	0.11	**−0.29**	0.01	−0.07
Annaba													
EA	−0.11	**−0.52**	−0.19	−0.07	**−0.49**	−0.10	0.00	−0.08	−0.18	−0.09	−0.13	−0.18	−0.03
MO	−0.17	−0.12	−0.05	0.10	−0.22	**−0.30**	−0.12	−0.11	−0.13	−0.04	0.11	−0.06	−0.12
NAO	0.01	−0.18	0.04	**0.30**	−0.14	−0.12	0.01	0.08	−0.16	0.21	0.15	0.13	0.07
WeMO	**0.26**	−0.02	0.01	0.17	−0.08	−0.05	−0.23	**−0.36**	0.00	0.14	0.08	0.23	−0.07
constantine													
EA	−0.05	**−0.44**	−0.23	−0.20	**−0.33**	−0.13	−0.03	−0.08	**−0.36**	−0.17	−0.20	−0.13	**−0.31**
MO	−0.14	−0.18	−0.13	0.16	−0.24	−0.21	−0.07	0.02	**−0.28**	−0.07	0.03	−0.02	−0.22
NAO	0.00	−0.18	0.09	0.13	−0.17	0.01	0.08	0.21	**−0.35**	0.12	0.10	0.21	−0.04
WeMO	**0.36**	−0.05	0.02	0.12	−0.23	−0.10	−0.13	−0.02	−0.04	−0.01	**0.26**	**0.33**	0.06
Setif													
EA	0.05	−0.21	0.06	−0.10	−0.21	−0.10	−0.09	0.01	−0.22	−0.04	**−0.38**	−0.11	0.08
MO	**−0.44**	0.02	−0.05	0.18	0.10	−0.11	0.10	0.07	**−0.27**	0.10	**−0.42**	**−0.35**	−0.13
NAO	−0.14	−0.11	0.00	−0.01	−0.19	−0.07	0.14	0.19	**−0.43**	0.08	−0.15	0.00	−0.01
WeMO	0.21	−0.12	0.14	**−0.34**	**−0.32**	−0.04	−0.12	0.00	−0.06	−0.08	−0.12	0.23	**−0.25**
Jijel													
EA	−0.16	−0.21	−0.10	**−0.27**	−0.15	−0.07	0.13	0.06	−0.09	−0.20	−0.07	−0.22	−0.09
WeMO	**0.27**	0.16	0.08	0.02	−0.03	−0.07	−0.03	0.19	−0.09	0.11	0.13	**0.33**	0.00
Oran													
EA	−0.04	**−0.42**	−0.23	**−0.40**	−0.17	−0.19	0.07	−0.02	−0.20	−0.18	−0.19	**−0.31**	**−0.40**
MO	**−0.44**	**−0.32**	**−0.38**	−0.16	−0.17	−0.17	−0.17	**−0.33**	−0.23	**−0.40**	**−0.45**	**−0.28**	−0.12
NAO	−0.17	**−0.26**	**−0.29**	−0.05	−0.13	−0.16	0.07	−0.06	−0.14	−0.09	−0.15	−0.04	0.03
SOI	0.15	0.01	0.19	0.10	0.00	0.08	−0.23	−0.07	−0.14	−0.13	0.02	0.14	**0.33**
WeMO	−0.04	**−0.30**	−0.21	−0.12	**−0.26**	−0.13	−0.14	**−0.33**	−0.20	−0.22	−0.12	0.08	0.10
Tiaret													
EA	0.07	0.08	**−0.24**	−0.22	−0.07	**−0.33**	**−0.29**	**0.24**	0.08	−0.17	−0.16	0.02	**−0.36**
MO	**−0.44**	**−0.30**	**−0.26**	−0.04	0.02	−0.09	0.15	−0.12	**−0.25**	**−0.27**	0.01	−0.10	**−0.35**
WeMO	**0.25**	**0.27**	−0.01	0.10	0.21	0.21	0.20	−0.04	**−0.28**	−0.23	0.07	0.03	0.21
Mascara													
MO	**−0.44**	0.02	−0.05	0.00	−0.08	−0.12	0.10	0.14	−0.18	**−0.55**	**−0.42**	**−0.35**	−0.13
NAO	**−0.25**	−0.01	0.04	−0.20	−0.11	−0.01	0.08	0.03	−0.14	−0.17	−0.10	−0.10	−0.10
WeMO	0.18	−0.16	0.07	−0.16	0.00	−0.19	−0.03	0.02	**−0.30**	**−0.25**	−0.10	−0.04	−0.17

Significant correlations are in Bold at 5% significant level

associated to El Nino as global mode of atmospheric circulation and positive phase of EA. The seasonal rainfall variability is affected by both EA and MO that are considered as regional mode of atmospheric circulation.

North Algeria is considered as semi-arid region and water availability is becoming weaker. Thus, the assessment and monitoring of rainfall variability is important. Links with teleconnection patterns allows predicting rainfall variability according to the most dominant mode of atmospheric circulation.

References

1. Sinoga, J.D.R., Marin, R.G., Murillo, J.F.M., Galeote, M.A.G.: Precipitation dynamics in southern Spain: trends and cycles. Int. J. Climatol. **31**, 2281–2289 (2011)
2. Longobardi, A., Villani, P.: Trend analysis of annual and seasonal rainfall time series in the Mediterranean area. Int. J. Climatol. **30**, 1538–1546 (2009)
3. Feidas, H., Noulopoulou, Ch., Makrogiannis, T., Bora-Senta, E.: Trend analysis of precipitation time series in Greece and their relationship with circulation using surface and satellite data: 1955–2001. Theor. Appl. Climatol. **87**, 155–177 (2007)
4. Benassi, M.: Drought and climate change in Moroco. Analysis of precipitations field and water supply. Options. Mediter. sér. A **80**, 83–86 (2001)
5. Kingumbi, A., Bargaoui, Z., Hubert, P.: Investigation of the rainfall variability in central Tunisia. Hydrol. Sci. J. **3**, 493–508 (2005)
6. Meddi, M., Assani, A.A., Meddi, H.: Temporal variability of annual rainfall in the Macta and Tafna catchments, Northwestern Algeria. Water Resour. Manage **24**, 3817–3833 (2010)
7. Meddi, M., Talia, A.: Pluviometric regime evolution in the North of Algeria. Arab. Gulf J. Sci. Res. **26**, 152–162 (2008)
8. Bekkoussa, B., Meddi, M., Jourde, H.: Forçage climatique et anthropique sur la ressource en eau souterraine d'une région semi-aride: cas de la plaine de Ghriss (Nord-Ouest algérien). Sécheresse **18**, 173–184 (2008)
9. Taibi, S., Souag, D.: Regionalization of drought in Northern Algeria using a standardized precipitation index (1936–2010). In: Ferrari, E., Versace, P. (eds.) From Prediction to Prevention of Hydrological Risk in Mediterranean Countries , 4th International Workshop on Hydrological extremes MEDFRIEND Group, University of Calabria; EdiBios, Cosenza, Italia, pp. 169–182 (2011)
10. Xoplaki, E., Gonzalez-Rouco, J.F., Luterbacher, J., Wanner, H.: Wet season Mediterranean precipitation variability: influence of large-scale dynamics and trends. Clim. Dyn. **23**, 63–78 (2004)
11. Lopez, J., Frances, F.: Influence of the North Atlantic oscillation and the western mediterranean oscillation in the maximum flow events in Spain. In: International Workshop Advances in Statistical Hydrology, May 23–25 2010 Taormina, Italy (2010)
12. Brandimarte, L., Di Baldassarre, G., Bruni, G., D'Odorico, P.: Montanari A: Relation between the north-atlantic oscillation and hydroclimatic conditions in mediterranean areas. Water Resour. Manage **25**, 1269–1279 (2011)
13. Dünkeloh, A., Jacobeit, J.: Circulation dynamics of Mediterranean precipitation variability 1948–98. Int. J. Climatol. **23**, 1843–1866 (2003)
14. Taibi, S., Meddi, M., Mahé, G., Assani, A.: Relationships between atmospheric circulation indices and rainfall in Northern Algeria and comparison of observed and RCM-generated rainfall. Theor. Appl. Climatol (121) 2015: https://doi.org/10.1007/s00704-015-1626-4
15. Noaa, http://www.cpc.ncep.noaa.gov/ (2018/04/29)
16. Kutiel, H., Maheras, P., Guika, S.: Circulation indices over the Mediterranean and Europe and their relationship with rainfall conditions across the Mediterranean. Theor. Appl. Climatol. **54**, 125–138 (1996)
17. Douguédroit, A.: Que peut-on dire d'une oscillation méditerranéenne? In: Alcoforado, M.J. (ed.) Climate and Environmental Change, Evora, pp. 135–136 (1998)
18. Maheras, P., Xoplaki, E., Kutiel, H.: Wet and dry monthly anomalies across the Mediterranean Basin and their relationship with correlation, 1860–1990. Theor. Appl. Climatol. **64**, 189–199 (1999)

Regionalization of Precipitation in Jordan

Abdulelah Al-Qadami and Fayez A. Abdulla

Abstract

This study aimed to cluster the temporal and spatial precipitation of the Hashemite Kingdom of Jordan. Rainfall data for a period of 53 years (1960–2013) at 32 stations representing the whole country was used. The clustering process was conducted temporally and spatially using the Ward's linkage method of Agglomerative Hierarchical Clustering (AHC). The study revealed three groups of months which are, rainy months group (December–March), moderately rainfall months group (April–November) and dry rainfall months group (May–October). Spatially, the country consists of four homogeneous groups based on the root mean square of standard deviation (RMSSTD). The first and the second clusters include the northern part of Jordan characterized by high rainfall intensity, whereas the third group includes the southern part of Jordan and the last cluster represents the Badia and desert of Jordan country.

Keywords

Precipitation clustering • Optimal clusters
Ward's algorithm • Jordan

1 Introduction

Currently, the clustering analysis is receiving a great deal of attention in the hydrological studies to get the optimal benefit from all available dataset in the locations with shortage of data. Precipitation events are characterized by high variability and complex distribution spatially and temporally. A precipitation occurrence is estimated by a stochastic approach known as frequency analysis. The estimated precipitation from the frequency distributions applied in several hydrological and water resources management studies such as, flood analysis, downscaling research, water infrastructure design, drought analysis, etc.

Hydrologist and water resources engineers face a problem in finding a full record for long return period needed to develop a frequency analysis which enables them to represent the real variability of local precipitations [1]. This urges to use the neighbor's stations with similar statistics to cope these encountered problems. This technique assigns sites to homogeneous regions (clusters) based on climatic variables called regionalization. This paper aimed to study the spatial and temporal clustering analysis of precipitations regimes in Jordan based on AHC techniques.

AHC Hierarchical clustering techniques are frequently used algorithms such as Ward's algorithm, Average linkage algorithm, and regional linkage algorithm, used in regionalization studies of climatology and hydrology. Hierarchical methods produce a series of consecutive partitions, each corresponding to a different number of clusters. In the beginning, each single object of data series is assigned a cluster, for N number of data series there is an N number of clusters. Successive merging operations between the clusters are then performed until there is only a single cluster containing all the N objects [2, 3].

2 Study Area and Methodology

Study area and data: Jordan is recognized as a semi-arid region, and has a climate ranging from Mediterranean to Arid with approximately 93% of the country receiving less than 200 mm of precipitation annually. The bulk amount of precipitation falls in the winter season (i.e., between October and May) [4, 5]. This study relied on 53-year rainfall data (1960–2013) from 32 selected rainfall stations.

Methodology The well-known Hierarchical clustering analysis (Ward's method) was used in this study. The method is described below.

A. Al-Qadami · F. A. Abdulla (✉)
Jordan University of Science and Technology, 2210 Irbid, Jordan
e-mail: fabdulla@just.edu.jo

Z. Zhang et al. (eds.), *Patterns and Mechanisms of Climate, Paleoclimate and Paleoenvironmental Changes from Low-Latitude Regions*, Advances in Science, Technology & Innovation, https://doi.org/10.1007/978-3-030-01599-2_27

In this method N is the number of stations with elements (n_x, n_y, n_z, … , N) and M is the number of years with elements (x_1, x_2, x_3, … , x_m), (y_1, y_2, y_3, … , y_m), …,etc. For each time series, we calculate the mean $\bar{x}$ and variance σ_x^2 using the below equations:

$$\bar{x} = \frac{1}{M}\sum_{i=1}^{N} x_i \tag{1}$$

$$\sigma_x^2 = \frac{1}{M-1}\sum_{i=1}^{N}(x_i - \bar{x})^2 \tag{2}$$

where x_i, y_i are the mean spatial value of the variables of interest- in this study precipitation and temperature over each spatial region (stations) at time *i*.

For the first two time series, we calculate the similarity using Pearson's correlation *r*

$$r_{x.y} = \frac{1}{M-1}\sum_{i=1}^{M}\left(\frac{x_i - \bar{x}}{\sigma_x}\right)\left(\frac{y_i - \bar{y}}{\sigma_y}\right) \tag{3}$$

where σ_x, σ_y are the standard deviation of the time series x and y respectively.

The, we compute the dissimilarity between all regions $N \times N$ based on their mean time series x and y using Pearson correlation distance,

$$d_{x.y} = 1 - r_{x.y} \tag{4}$$

We assign each station to one cluster and merge the most similar pair of clusters then update distances between the new clusters and the others using an update formula of Ward's method of clustering, the update formula is written as follows

$$d_{x\cup y.z} = (n_x + n_z)d_{x.z} + (n_y + n_z)d_{y.z} - n_z d_{x.y} \tag{5}$$

Steps e and f are repeated until all clusters are merged into one cluster representing the full region of study [6].

The optimum number of clusters found form the dendrogram based on the vertical heights should be checked for its accuracy by some other reliable methods. The Root Mean Square Standard Deviation (RMSSTD) was used for this purpose.

$$RMSST = \sqrt{\frac{\sum_{k=1}^{P}\sum_{i=1}^{N}\sum_{j=1}^{M}(x_{kij} - \bar{x}_{kj})^2}{N}} \tag{6}$$

where P is the number of clusters, N is the number of elements (gauging stations) in each cluster, M number of variables (months), x_{kij} j-th month at the i-th gauging station in the k-th cluster $\bar{x}_{kj}$ average value of the i-th gauging station at the j-th month in the k-th cluster [7].

3 Results and Discussion

3.1 Temporal Analysis (Months Clusters)

Rainy months were grouped together based on precipitation characteristics using Ward's method and resulted in three clusters (Fig. 1). The first cluster includes four consecutive months (December–March) named rainy months group, while the second group of moderate rainfall months, involves April and November. The last cluster represents May and October which are known as low rainfall months.

3.2 Spatial Analysis

Based on the results of the temporal analysis, the clustering analysis of the rainfall gauge stations were established for each cluster separately. The optimal number of clusters of precipitation in Jordan was determined using RMSSTD.

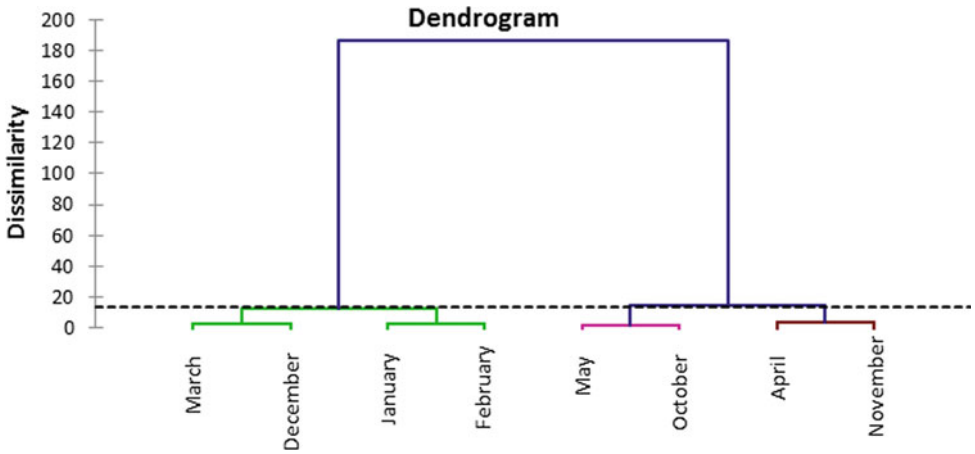

Fig. 1 Dendrogram of temporal time series (months) clusters

RMSSTD was calculated in different cut levels (clusters) in the dendrogram as shown in Fig. 2. When similar clusters are being merged early in the process, the dissimilarity distances are small, and they increase gradually as the clustering proceeds. The process can be stopped just before these distances become larger. The RMSSTD results indicated that the optimal number of clusters is four clusters. The final proposed optimal Jordan precipitation clusters map and their elements (rainfall stations) was estimated based on the Ward's algorithm (Fig. 3). Regarding the spatial analysis, two clusters located in the northern and western parts of Jordan. The third area involves the

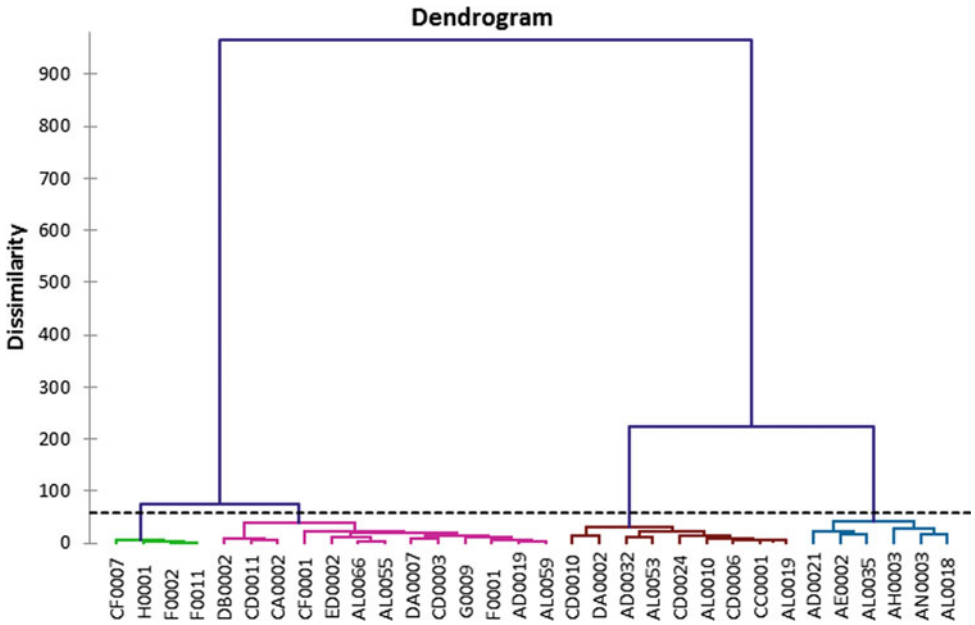

Fig. 2 Dendrogram of all rainfall stations included in this study

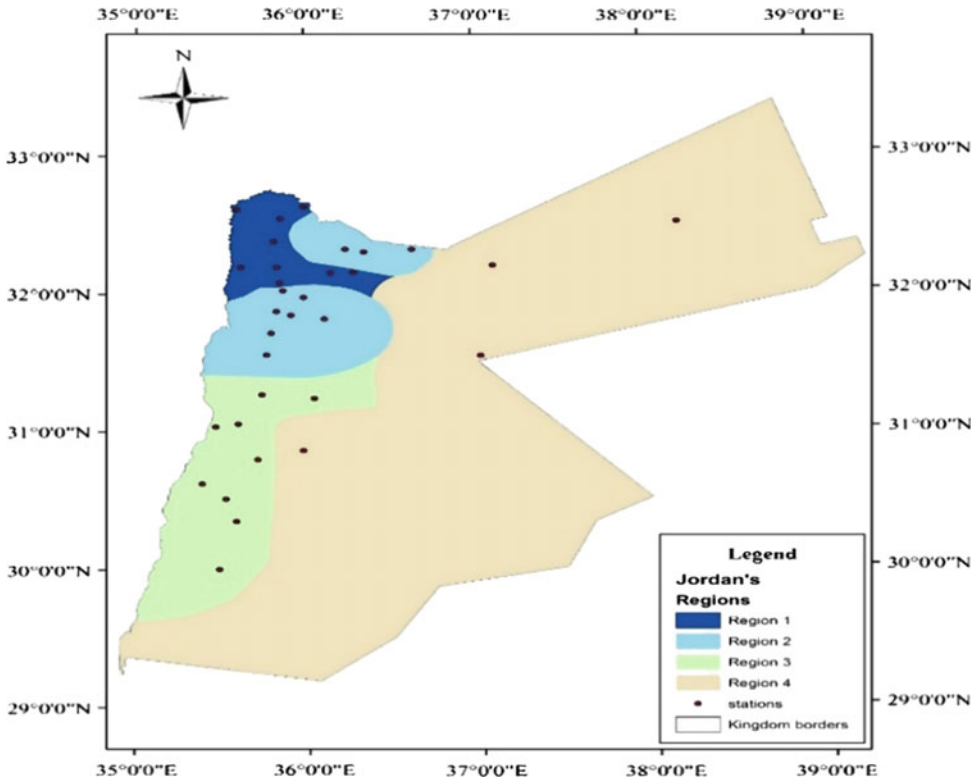

Fig. 3 Homogenous precipitation regions of Jordan based on rainy months group

southern part of Jordan. The last region covers the eastern part of the country.

4 Conclusions

Agglomerative hierarchical clustering analysis was performed for the temporal time series (monthly precipitations) using Ward's linkage method to classify the homogeneous months. Three groups of months resulted from this analysis: December–March group called rainy months, April–November group called moderate rainfall months and the dry rainfall months involving May–October. The RMSSTD was used to identify the optimal number of clusters. It indicated four regions as the optimal number of homogeneous precipitation clusters in Jordan. Ward's linkage method of clustering was used to determine the clusters of Jordan precipitation regions. Rainy months (December–March) was chosen as the best representative temporal group of the country. Depending on the optimal number of clusters, the Ward's clustering method and rainy month groups, the country was clustered into three regions.

References

1. Chin, D.A.: Water-Resources Engineering, 3rd edn, p. 960. Pearson, Upper Saddle River (2012)
2. Ward Jr., J.H.: Hierarchical grouping to optimize an objective function. J. Am. Stat. Assoc. **58**(301), 236–244 (1963)
3. Badr, H.S., Dezfuli, A.K., Zaitchik, B.F., Peters-Lidard, C.D.: Regionalizing Africa: patterns of precipitation variability in observations and global climate models. J. Clim. **29**(24), 9027–9043 (2016)
4. Al-Qinna, M.I., Hammouri, N.A., Obeidat, M.M., Ahmad, F.Y.: Drought analysis in Jordan under current and future climates. (Author abstract) (report). Clim. Change **3**, 421 (2011)
5. Hammouri, N., El-Naqa, A.: Drought assessment using GIS and remote sensing in Amman-Zarqa basin, Jordan. Jordan J. Civ. Eng. **1**(2), 142–152 (2007)
6. Badr, H.S., Zaitchik, B.F., Dezfuli, A.K.: A tool for hierarchical climate regionalization. Earth Sci Inf., 1–10, (2015)
7. Shahana Shirin, A.H., Thomas, R.: Regionalization of rainfall in Kerala state. Procedia Technol. **24**, 15–22 (2016)

Correlation Between NAO and Radio Refractive Index Over Africa

Joseph Dada, Adekunle Titus Adediji, Kayode Adedayo, and Moses Ajewole

Abstract

The pathway of a propagated radio waves is partly determined by the refractive index of the atmosphere through which the waves traverse. The radio refractive index is in turn governed by the variations in the meteorological parameters while the Northern Atlantic Oscillation (NAO) has been found to influence temperature and precipitation patterns. This study investigated the correlation between NAO and radio refractive index over Africa using 30 years data of daily meteorological parameters and NAO, spanning from 1981 to 2010. Rainforest and Desert climate recorded the highest (>290 N-units) and the lowest (<200 N-units) radio refractive index, respectively. The correlation is observed to be generally weak (−0.2 to 0.2).

Keywords

NAO • Radio • Refractive index • Correlation Meteorological

1 Introduction

Northern Atlantic Oscillation (NAO) is one of the most prominent and recurrent patterns of atmospheric circulation variability that dictates climate variability from the eastern seaboard of the United States to Siberia and from the Arctic to the subtropical Atlantic [1]. NAO is the most important mode of atmospheric variability over the North Atlantic Ocean, and plays a major role in weather and climate variations over the North Eastern America, the North Atlantic and the Eurasian continent [2].

NAO influences temperature and precipitation patterns and was recently shown to be behind any significant fraction of climatic anomalies observed on either side of the Atlantic [3]. The recent trend of the NAO was due to an extra-tropical response to changes in tropical sea-surface temperature (SST) [4] and another involving stratospheric changes [5]. Similarly, [6] has shown that both NAO positive and negative phases promote a windy westerly flow in Northern and Southern Europe respectively.

The atmosphere is one of the channels through which information is transmitted in the form of electromagnetic waves from one point to the other on the earth's surface. The wave's speed, amplitude, and direction of propagation depend on numerous atmospheric variables (temperature, moisture, pressure and so on). Changes in these variables cause variation in the wave's speed and propagation direction which then result in a change of refractivity, N which in turn affects the radio signal. Radio refractivity, N is related to refractive index, n by [7]

$$N = (n - 1) \times 10^6 \tag{1}$$

In terms of the atmospheric variables and for radio frequencies up to 100 GHz, the refractivity can be expressed as;

$$N = 77.6\frac{P}{T} + 3.75 \times 10^5 \frac{e}{T^2} = N_{dry} + N_{wet} \tag{2}$$

where T is temperature (K), e is water vapour (hPa) and P is pressure (hPa) [8].

The refractivity can also be expressed in terms of the dry component N_{dry} and wet component N_{wet} (Eq. 2) [9]. N_{dry} accounts for 70% of the refractivity value while its variation

J. Dada (✉)
Department of Physical and Chemical Sciences, Elizade University, P.M.B 002 Ilara-Mokin, Ondo State, Nigeria
e-mail: babatunde.dada@elizadeuniversity.edu.ng

J. Dada · A. T. Adediji · K. Adedayo · M. Ajewole
Department of Physics, Federal University of Technology, P.M.B 704 Akure, Ondo State, Nigeria
e-mail: kadediji@futa.edu.ng

K. Adedayo
e-mail: kbadedayo@futa.edu.ng

M. Ajewole
e-mail: oludare.ajewole@futa.edu.ng

Z. Zhang et al. (eds.), *Patterns and Mechanisms of Climate, Paleoclimate and Paleoenvironmental Changes from Low-Latitude Regions*, Advances in Science, Technology & Innovation, https://doi.org/10.1007/978-3-030-01599-2_28

is determined by N_{wet} [10, 11]. Water vapour mostly influences the refractivity followed by a change in temperature [12] while a change in pressure influences refractivity much less than that of temperature [13].

The strength of a linear relationship between two variables is measured by a correlation coefficient, r. A correlation can only indicate the presence or absence of a relationship, not the nature of the relationship. Spearman and Pearson correlation defines the range for a perfect linear relationship as $-1 \leq r \leq +1$. The positive and negative relationship between the variables are represented by +1 and −1 respectively [14]. Correlation of 0 implies zero linear relationship not zero relationship between the two variables. The correlation coefficient (r) can be expressed as

$$r = \frac{1}{n-1}\sum\left(\frac{x-\bar{x}}{S_x}\right)\left(\frac{y-\bar{y}}{S_y}\right) \quad (3)$$

where x, y are the variables, $\bar{x}$, $\bar{y}$ are the mean value of the variables and S_x, S_y are the standard deviation of the variables [15].

Having known that NAO influences precipitation and temperature patterns of a location, hence, the knowledge of the relationship between refractivity and NAO is vital in planning communication network systems. No research publication has specifically studied the relationship (correlation) between NAO and Radio refractive index over Africa or how NAO directly or indirectly affect the radio refractive index. This can help mitigate against communication impairments and hence plan for better communication network systems over Africa.

2 Methodology

The data set of NAO from the archive of National Oceanic and Atmospheric Administration (NOAA) and daily reanalysis of metrological data (Temperature, Pressure and Dew point) from the European Centre for Medium-Range Weather Forecasts (ECMWF) (ERA-Interim), spanning from 1981–2010 on the grid of 0.25 × 0.25 were used for this work. Locations with no statistical significance (*P*-value >0.05) were not considered. Equations (3) and (2) were used to compute the linear relationship between the two quantities and the refractivity respectively. The dew point temperature was converted to relative humidity and subsequently to water vapour e by the expression;

$$H = 100 - 5(t - t_d) \quad (4)$$

$$e = H \times \frac{6.1121\exp\left(\frac{17.502t}{t+240.97}\right)}{100} \quad (5)$$

where t, t_d, and H are the ambient temperature (°C), dew point temperature (°C), and Relative humidity (%) respectively [8, 16].

3 Results

See Figs. 1 and 2.

4 Discussion

The mean distribution of refractivity over Africa (Fig. 1) indicates highest refractivity values in the rainforest, the coastal and 35% of the savanna region closer to the

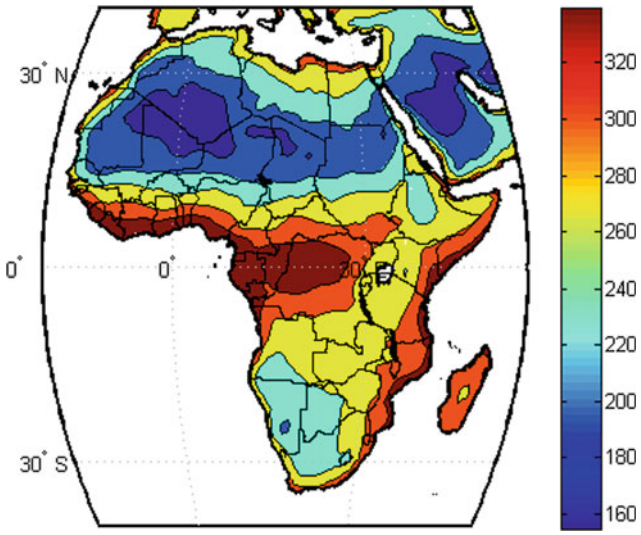

Fig. 1 Distribution of mean value of refractive index over Africa

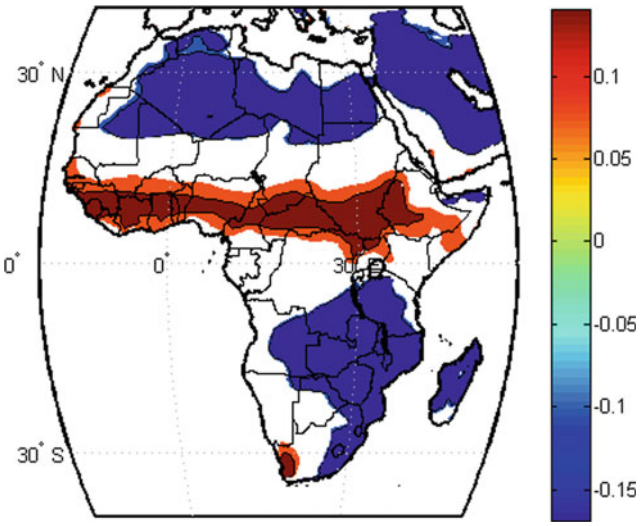

Fig. 2 Correlation between NAO and radio refractive index over Africa

rainforest region (>290 N-units) which can be linked to the presence of high precipitation, temperature and large water vapor content in the atmosphere of the coastal regions. The larger path of the savanna region accounts for the refractivity values in the range of 250–280 N-units, this could be related to the low precipitation received by the region.

The steppe climatic region show a relative low value of refractivity (200–250 N-units) which can be a result of the precipitation that is below potential evapotranspiration of the region. Little precipitation, high pressure and high temperature account for the lowest refractivity (160–200 N-unit) value recorded at the desert region.

The correlation between the refractivity and NAO for locations with the evidence about the statistical significance ($P < 0.05$) of the association between the variables is shown in Fig. 2. The correlations were found to be in the range −0.2 to 0.2. Rainforest and Mediterranean show a weak positive correlation with the range of 0.1–0.15. The Desert region shows a weak negative correlation in the range of −0.15 to 0.1.

5 Conclusions

The distribution of mean refractivity values and the correlation between NAO and Refractivity was carried out in this study. The results show that refractivity over Africa ranges from 150–340 N-units. The highest value (>290 N-units) was recorded at the rainforest climatic region and the lowest at the Desert region (<200 N-units). The correlation is observed to be generally weak (−0.2 to 0.2).

References

1. Hurrell, J.W., Kushnir, Y., Ottersen, G., Visbeck, M.: An Overview of the North Atlantic Oscillation. American Geophysical Union, pp. 1–35 (2003)
2. Greatbatch, R.J.: The North Atlantic Oscillation (2000)
3. Beniston, M., Jungo, P.: Shifts in the distributions of pressure, temperature and moisture and changes in the typical weather patterns in the Alpine region in response to the behavior of the North Atlantic Oscillation. Theor. Appl. Climatol. **42**(71), 29–42 (2002)
4. Hoerling, M.P.: Tropical origins for recent North Atlantic climate change. Science **292**(5514), 90–92 (2001)
5. Baldwin, M.P.: Stratospheric harbingers of anomalous weather regimes. Science **294**(5542), 581–584 (2001)
6. Jerez, S., Jimenez-Guerrero, P., Montávez, J.P., Trigo, R.M.: Impact of the North Atlantic oscillation on European aerosol ground levels through local processes: a seasonal model-based assessment using fixed anthropogenic emissions. Atmos. Chem. Phys. **13**, 11195–11207 (2013)
7. Agbo, G.A.: Tropospheric refractivity dependence on atmospheric weather condition in Jos-Nigeria. J. Basic Phys. Res. **2**(2), 1–6 (2011)
8. Ogunjo, S.T., Fuwape, I.A., Oluyamo, S.S., Rabiu, A., Dada, J.B.: Dynamics of vertical profile of radio refractivity. In: Annual Conference of African Geophysical Society, Abidjan, Cote d'Ivoire (2017)
9. Raju, C.S., Saha, K., Thampi, B.V., Parameswaran, K., Suresh, R. C.: Empirical model for mean temperature for Indian zone and estimation of precipitable water vapor from ground based GPS measurements. Ann. Geophys. **25**(9), 1935–1948 (2007)
10. Hall, M.P.M.: Effect of the troposphere on radio communication. Pete Peregrins Ltd., U.K (1979)
11. Willoughby, A.A., Aro, T.O., Owolabi, I.E.: Seasonal variations of radio refractivity gradients in Nigeria. J. Atmos. Solar-Terr. Phys. **64**, 417–425 (2002)
12. Adediji, A.T., Ajewole, M.O., Ojo, J.S., Ashidi, A.G., Ismail, M., Mandeep, J.S.: Influence of some meteorological factors on tropospheric radio refractivity over a tropical location in Nigeria. MAUSA 123–128 (2015)
13. Adediji, A.T., Ajewole, M.O.: Vertical profile of radio refractivity gradient in Akure South-West Nigeria. Prog. Electromagn. Res. C **4**, 157–168 (2008)
14. Fuwape, I.A., Ogunjo, S.T., Dada, J.B., Ashidi, G.A., Emmanuel, I.: Phase synchronization between tropospheric radio refractivity and rainfall amount in a tropical region. J. Atmos. Solar-Terr. Phys. **149**, 46–51 (2016)
15. Samprit, C., Hadi, A.S.: Simple Linear Regression. Wiley, New York, pp. 21–45 (2006)
16. Mark, G.: The relationship between Relative humidity and the dew point temperature in moist air. Am. Meteorol. Soc. J. **86**(2), 225–234 (2005)

Convective Cloud Climatology Over Indian Tropics and Nearby Regions Using Multi-spectral Satellite Observations

Anoop Kumar Mishra, Mohammd Rafiq, Sagarika Chandra, and Nagaiyavedu Adalarasu Sivarajan

Abstract

Extreme precipitation and severe weather conditions often result in flash floods, Glacier Lake outburst floods (GLOFS), landslides and other disasters. These extreme events are linked with convective clouds. Convective clouds form the major energy transport in the troposphere and are responsible for the latent heat transfer in the atmosphere. Hydrologic cycle and atmospheric circulations are often included in these systems. We have used multispectral observations from Meteosat-7 at Thermal Infra Red (TIR) channels (11 and 12 μm) and water vapor absorption channel (6.7 μm) for the detection of convective clouds. The convective cloud climatology was developed over Indian tropics using this approach. The convective cloud climatology developed from the present approach was validated against Tropical Rainfall Measuring Mission (TRMM) Precipitation Radar (PR) data and the Indian Meteorological Department (IMD) data. The results show a correlation coefficient (cc) of 0.79 and Root Mean Square Error (RMSE) of 2.61 (%) against rain gauge based observations of convective clouds.

Keywords

Convective clouds • Tropics • Precipitation • Disasters

1 Introduction

Convective cloud systems are brighter on the upper surface and comparatively darker below with almost a horizontal base. These clouds can go beyond freezing point to develop ice crystals, ice pellets, snowflakes or super cooled water droplets or the combination of all. 30–40% of signals are from these convective clouds in Inter Tropical Convergence Zone (ITCZ) and they are vital in controlling the earth's climate by exchanging moisture and heat from earth to the atmosphere [1]. Observational networks have very limited record of convective clouds. Active remote sensors like radars have been used to observe these clouds. However their coverage is also very limited. An indirect technique using remote sensing observations in Thermal Infrared (TIR) and Visible (VIS) frequencies have been utilized to detect these clouds [2]. As cirrostratus and cirrocumulus clouds are in contact with deep convective clouds having cloud tops below −35 °C [3] it is difficult to discriminate between deep convective clouds and cirrus clouds. To eliminate the convective and stratiform clouds Anagnostou and Kummerow [4] developed a technique using SSM/I 85 GHz brightness temperature. The technique was improved by Hong et al. [5]; however, these techniques cannot differentiate the cirrus with deep convective clouds.

The advance in space science provides a better resolution radar system with the launch of Tropical Rainfall Measuring Mission (TRMM) which can interact with cloud structures. Many researchers documented its usage in detecting convective clouds and storms in tropics. The narrow swath of PR and poor temporal resolution of the TRMM limit its usage in identifying most of the convective clouds that last for few days. Convective clouds during South-West Monsoon season over the Indian region were identified and net cloud radiative forcing at the top of atmosphere was examined using data from Earth Radiation Budget Experiment (ERBE) [6]. Convective clouds were identified and used for estimating rainfall over India from Kalpana data at 11 μm observation [7]. Sengupta et al. [8] studied structural evolution of clouds using Multiangle Imaging Spectro Radiometer (MISR)-derived cloud fraction over Indian CTCZ. Multi-spectral observations at 6.7 and 11 μm were used from Meteosat data to identify convective clouds and estimate rainfall over Indian land and oceanic region. The present study focused on

A. K. Mishra (✉) · M. Rafiq · S. Chandra · N. A. Sivarajan
Centre for Remote Sensing and Geoinformatics, Sathyabama Institute of Science and Technology, Chennai, 600119, Tamil Nadu, India
e-mail: emidamls6@gmail.com

M. Rafiq
e-mail: mohammadrafiq@kashmiruniversity.net

Z. Zhang et al. (eds.), *Patterns and Mechanisms of Climate, Paleoclimate and Paleoenvironmental Changes from Low-Latitude Regions*, Advances in Science, Technology & Innovation, https://doi.org/10.1007/978-3-030-01599-2_29

developing convective cloud climatology using multispectral observations at split window channels (near 11 and 12 μm) and water vapour absorption channels (near 6.7 μm) from Meteosat 7 data over India and adjacent oceanic regions. Results were compared with observations (reflectivity-based threshold) from Precipitation Radar (PR) on-board Tropical Rainfall Measuring Mission (TRMM).

2 Study Area and Data Sets

The study area is illustrated in Fig. 1. It extends from 30°S to 50°N and 50°E to 120°E including the Indian land and nearby oceanic regions (Fig. 1). India has 29 states and 7 union territories. Its land surface area covers over 3,287,590 km^2. With more than seven thousand kilometers of coastline, it is surrounded by Arabian Sea, Bay of Bengal and the Indian Ocean.

For the present study, we used Meteosat 7 data of Meteosat First Generation (MFG). The multispectral observations in Thermal Infrared (TIR) 10.5–12.5 μm and Water vapour (WV) 5.7–7.1 μm were used.

For comparison purposes of our results, the reflectivity factor from level 2 Rain Characteristics Product (TRMM Product 2A25) was used in this study (https://disc.gsfc.nasa.gov/). For the validation of our results, we also used rain gauge based precipitation products from IMD.

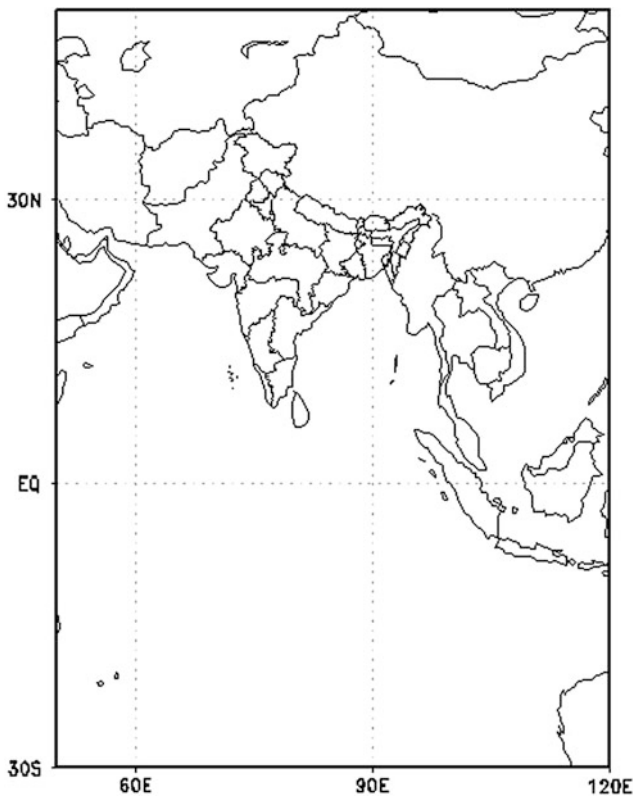

Fig. 1 Study area

3 Methodology

We followed an approach developed by Adler and Negri [9] to remove cirrus clouds and identify the convective ones. A slope parameter S_P and a temperature gradient T_G were computed for each local temperature minimum. These values are given as:

$$T_G = T_{avg} - T_{min} \quad (1)$$

$$S_P = 0.568\ (T_{min} - 217) \quad (2)$$

where;

T_{min} is the local minimum temperature (derived from TIR channel, 11 μm) T_{avg} is the mean temperature of the 6 pixels surrounding the current pixel. A large T_G is associated with convective clouds and a small value indicates a weak gradient and thus detects the cirrus clouds. Convective clouds with overshooting tops were identified using difference of 11 and 6.7 μm channels. Such convective clouds are known to play an important role in the interaction and exchange between troposphere and stratosphere. Simultaneous observations of these clouds in the infrared window region (11 μm) and the water vapour absorption band (6.7 μm), reveal that the equivalent brightness temperature in the latter is larger than that of the former. Negative differences ($TB_{11} - TB_{6.7}$) are associated with convective clouds with overshooting tops.

Using the above-mentioned approach, convective clouds are identified. The convective clouds occurrence (in %) is calculated by dividing the total number of convective pixels by the total number of pixels Observations from PR (2A23) were also used to detect the convective clouds for comparison purposes with present approach of convective cloud detection from Meteosat data. We used a 40 dBZ threshold (reflectivity) for detecting convective clouds.

There is strong relationship between precipitation extremes and cloud top temperature. Lau and Wu [10] investigated the climatological characteristics of tropical rain and cloud systems over Tropics using brightness temperature (TB) data from Visible and Infrared Scanner (VIRS) and precipitation data from Tropical Rainfall Measuring Mission (TRMM) Microwave Imager (TMI) and Precipitation Radar (PR) on-board TRMM. It was found that the Top 10% heavy precipitation may be associated with convective clouds. The precipitation spectrum obtained from IMD rain gauge based product was divided into 10 bins.

4 Results and Discussion

Different case studies have been carried out to monitor the convective clouds over the Indian region and nearby oceanic regions. One of the case studies is presented below for brevity.

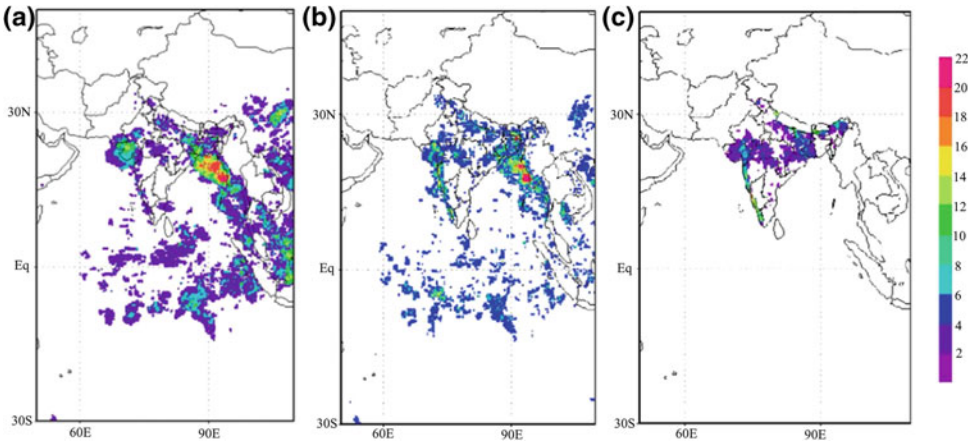

Fig. 2 Fraction of convective clouds (%) from **a** present technique, **b** from PR observations, **c** from rain gauge based IMD product during July 2007. Units are in percentages

For this case study, we have identified multiple convective events in July 2007 over the Bay of Bengal (~90°E, 14°N) and the Western part of the Indian region (~73°E, 19°N).

Figure 2 shows the convective clouds occurrence (%) over the study area. These convective systems brought heavy rainfall over the Bay of Bengal and Western Ghats. Few localized convective systems over India Ocean can also be identified. It can be inferred that a maximum of 24% convective clouds (from Fig. 2b) occur over the Bay of Bengal which matches with the observations from the present technique (Fig. 2a). The convective systems over Bengal and Bangladesh cause heavy flooding over these regions. Similarly, convective clouds occurrences over Western Ghats are also comparable to those produced by the present technique and that of Radar observations. Scattered convective systems over Mumbai, Central India and North-eastern parts of the Indian region can also be observed from the present technique. These observations are consistent with those derived from ground based rain gauges (Fig. 2c).

5 Conclusions

Satellite-based multispectral observations were used to detect convective clouds over India and nearby Oceanic regions. A case study of convective clouds during 2007 has also been discussed. The performance of the technique was evaluated with space based radar observations onboard of the TRMM and the rain gauge-based observations from IMD. Our results reveal that the present technique is able to monitor the coverage of convective clouds efficiently. The adopted approach in the present study to monitor convective clouds is crucial given the limitation of station and radar data and sampling errors associated with microwave sensors. The proposed methodology in the present algorithm finds application in operational contexts where MFG, Meteosat Second Generation (MSG), and Meteosat Third Generation (MTG) data are available in almost real time.

References

1. Liu, G., Curry, J.A., Sheu, R.S.: Classification of clouds over the western equatorial Pacific Ocean using combined infrared and microwave satellite data. J. Geophys. Res. **100**, 13811–13826 (1995)
2. Hall, T.J., Haar, T.H.V.: The diurnal cycle of west Pacific deep convection and its relation to the spatial and temporal variations of tropical MCSs. J. Atmos. Sci. **56**, 3401–3415 (1999)
3. Luo, Y., Krueger, S.K., Mace, G.G., Xu, K.M.: Cirrus cloud properties from a cloud-resolving model simulation compared to cloud radar observations. J. Atmos. Sci. **60**, 510–525 (2003)
4. Anagnostou, E.N., Kummerow, C.: Stratiform and convective classification of rainfall using SSM/I 85-GHz brightness temperature observations. J. Atmos. Ocean. Technol. **14**, 570–575 (1997)
5. Hong, Y., Kummerow, C., Olson, W.S.: Separation of convective and stratiform precipitation using microwave brightness temperature. J. Appl. Meteorol. **38**, 1195–1213 (1999)
6. Simpson, J., Halverson, J., Pierce, H., Morales, C., Iguchi, T.: Eyeing the eye: exciting early stage science results from TRMM. Bull. Am. Meteorol. Soc. **79**, 1711 (1998)
7. Mishra, A.K.: Estimation of heavy rainfall during cyclonic storms from microwave observations using nonlinear approach over Indian Ocean. Nat. Hazards **63**(2), 673–683 (2012)
8. Sengupta, K., Dey, S., Sarkar, M.: Structural evolution of monsoon clouds in the Indian CTCZ. Geo Res. Lett. **40**, 5295–5299 (2013)
9. Adler, R.F., Negri, A.J.: A satellite technique to estimate tropical convective and stratiform rainfall. J. Appl. Meteor. **27**, 30–51 (1988)
10. Lau, K.M., Wu, H.T.: Climatology and changes in tropical oceanic rainfall characteristics inferred from Tropical Rainfall Measuring Mission (TRMM) data (1998-2009). J. Geo Res. **116**, D17111 (2011)

Analysis of Trend and Variability in Time Series of Extreme Daily Temperature of Abu Dhabi City (UAE)

Nishi Bhuvandas

Abstract

Trend identification plays a significant role in climate change studies to make future predictions about possible consequences on the urban environment, agriculture, water availability, etc. The Variation of Extreme Temperature intensity is observed in many regions all over the globe as an outcome of abrupt changes in climate. Keeping in mind the non-stationary climate conditions, it is essential to incorporate potential future changes in climatological studies. In the present study, the statistical parameters and the variability in time series of extreme daily temperature were analyzed using Generalized Extreme Value (GEV) distribution and its suitability has been examined by superimposing onto Gringorten plotting positions. The trend analysis of extreme daily temperatures was carried out using an innovative trend template proposed by Şen [7] and non-parametric Mann-Kendall (MK) trend test. The trend detection and variability of extreme daily temperature of Abu Dhabi City station, UAE was also carried out in this study. 34 years of temperature data were used for the analysis. Also, the extreme daily temperatures time series were checked for their serial correlation.

Keywords

Abu Dhabi city • Climate variability • Extreme daily temperature • Generalized extreme value • Trend analysis

1 Introduction

The time series analysis is a major tool to detect the trend in climatic parameters under changing climatic conditions. According to the methodology followed by Yue et al. [7, 8] serial correlation coefficient of the extreme time series was checked. The IPCC [5] states that climate change has intensified the hydrological cycle. Various non-parametric tests are widely used to test for the existence of trends in the time series data [3]. Amongst these tests, the Mann-Kendall (MK) test is invariably used to examine the trend. Şen [6] presented an innovative trend analysis methodology on the basis of portioning the time series derived from a given time series on a Cartesian coordinate system. For the analysis of the magnitude and frequency of extreme events, Generalized Extreme Value (GEV) distribution is invariably used. Of these, extreme rainfall is most commonly modeled using Extreme Value Type I (EVI) distribution [1]. Cunnane [2] had studied various plotting position methods using the criteria of unbiasedness and maximum variance, for data distributed according to the Extreme Value Type I distribution (or Gumbel distribution), the Gringorten formula (b = 0.44) was found to be the best.

Abu Dhabi is the capital and the largest of the UAE's seven emirates constituting an area of 972 km^2. It has an arid hot climate with low precipitation, the summer months being from June through September with extremely hot and humid climate with maximum temperatures. The location of the observed temperature data is of Abu Dhabi city station with coordinates 24° 25′ 58.8″N and 54° 39′ 3.6″E. The present study used a 34-year period data starting in 1983 to 2016. The extreme one—daily temperature for every year is extracted from the CRU (Climate Research Unit) dataset and used in this study. The goal of this study was to explore extreme temperature characteristics for Abu Dhabi city which can be put to use in order to construct future climate scenarios.

2 Methodology

Statistical Parameters: Standard deviation, Coefficient of variance, Coefficient of skewness of the time series data were calculated to measure the variability with respect to the

N. Bhuvandas (✉)
PO Box 36293 Abu Dhabi, UAE
e-mail: nishibhuvandas@gmail.com

Z. Zhang et al. (eds.), *Patterns and Mechanisms of Climate, Paleoclimate and Paleoenvironmental Changes from Low-Latitude Regions*, Advances in Science, Technology & Innovation, https://doi.org/10.1007/978-3-030-01599-2_30

Table 1 Statistical parameters of time series data

Station	Statistical parameters				
	Mean	Standard deviation	Coefficient of variance	Skewness	Mann Kendall (*P*)
Abu Dhabi city	47.6	0.85	0.017	0.30	0.96

mean value, spread of data from its mean and the degree of asymmetry of the time series around its mean respectively as given in [1]. The statistical parameters computed for the data set used in the present study are shown in Table 1.

Trend Analysis: *Innovative trend analysis*—In the present study, observed extreme annual temperature data are used to detect the trends. The innovative methodology proposed by Şen [6], applicable to any time series irrespective of their sample size, serial correlation structure and non-normal probability distribution functions, has been used. *Mann-Kendall trend test*—The MK test is a nonparametric trend test that involves the ranks for each element in the data series and uses the statistical hypothesis testing method to analyse the trend. The standardized test statistic is computed as per [8].

Generalized Extreme Value Distribution: Extreme value theory provides the statistical framework to make inferences about the probability of very rare or extreme events. In the present study, the extreme value type I (EVI) distribution was modeled using EVI distribution [1].

Gringorten plotting position: According to Cunnane [2], for the data distributed according to EVI distribution, Gringorten formula (b = 0.44) is more suitable. The plotting position formula used is in accordance with Chow et al. [1].

Serial Correlation: The serial correlation coefficient and lag-one auto correlation coefficient were computed according to Yue et al. [8] to check if the data are independent at 10% significance level.

3 Results and Discussion

For the independent sample data without trend, the probability *P* value of the MK statistic *S* should be equal to 0.50. For the sample data with a large positive trend the *P* value should be closer to 1.0, whereas a large negative trend should yield a *P* value closer to 0.0, [8]. The MK test statistic (*Z* value) for extreme daily temperature time series at Abu Dhabi city was calculated to be 1.88. The *P* value (Table 1) is more than 0.5, which indicates a statistically significant upward trend. The serial correlation between the data set was checked and was not found to be auto correlated and hence to use it for further statistical analysis pre-whitening is a pre requisite. The highest value of the daily maximum temperatures was observed to be 49.4 °C. The statistical parameters like mean, standard deviation, coefficient of variance and coefficient of skewness were also worked out for the time series as shown in Table 1.

From Fig. 1, it is observed that the time series of extreme daily temperature at Abu Dhabi city is following an increasing trend. In Fig. 2, all of the scatter points are at the increasing

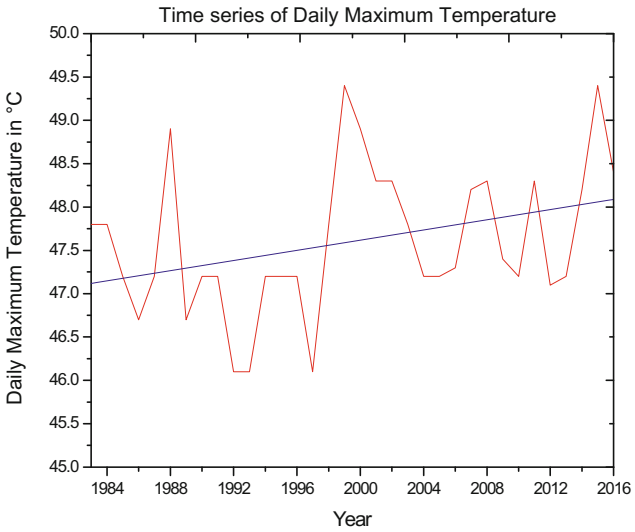

Fig. 1 Time series of daily maximum temperatures at Abu Dhabi city

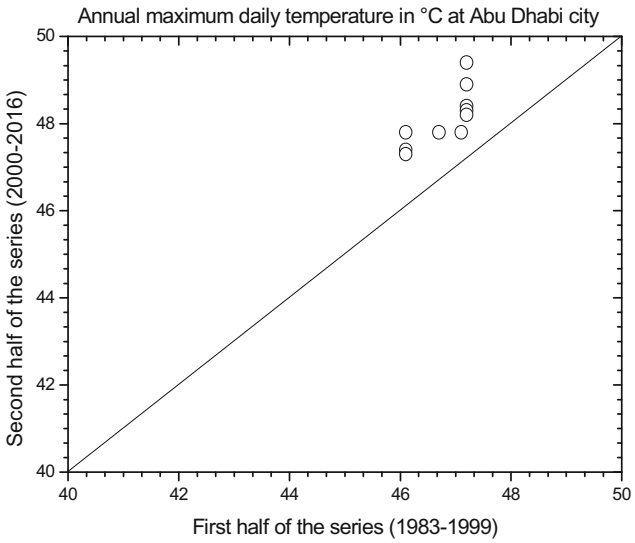

Fig. 2 Innovative trend analysis of daily maximum temperatures at Abu Dhabi city

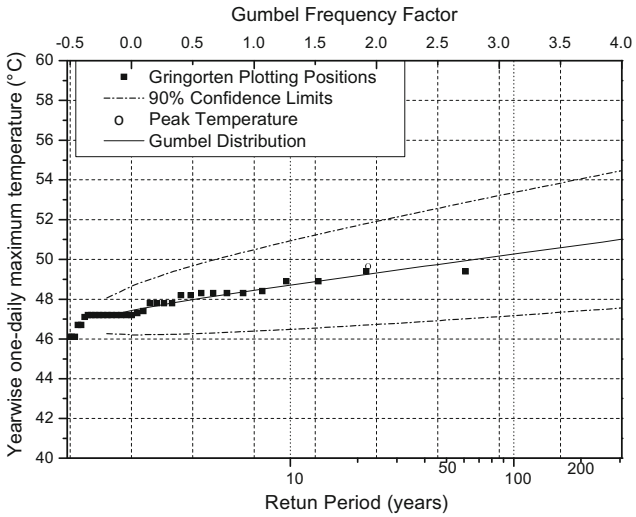

Fig. 3 Extreme value distribution at Abu Dhabi city

trend area above 1:1 line with extreme temperature values depicting an all-time increasing trend which could be a long time effect of global warming at the station. The peak value observed during the period taken into consideration 49.4 °C which has an average return period of approximately 41 years.

The Generalized Extreme Value (GEV) distribution, type I also known as EVI was fitted to the data as per the steps followed by Huang [4] as shown in Fig. 3. Also, the Gringorten plotting positions are used to examine the suitability of EVI distribution by superimposing them on the fitted distribution. The fitted distribution, its 90% confidence limits and corresponding Gringorten plotting positions are shown in Fig. 3. It can be seen that they are well within 90% confidence limits of EVI distribution.

4 Conclusion

The extreme climatic events can leave adverse impacts on the environment and society. The present study showed that at Abu Dhabi city station magnitude of the extreme temperatures has a strong increasing trend. The innovative trend analysis also indicated a significant increasing trend for the higher data values. The EVI distribution was fitted to obtain the extreme temperature for different return periods. A better understanding of the various issues associated with climatic variability can be obtained by trend analysis with respect to future climate scenarios.

References

1. Chow, V.T., Maidment, D.R., Mays, L.W.: Applied Hydrology. Tata McGraw-Hill, New York (1988)
2. Cunnane, C.: Unbiased plotting positions—a review. J. Hydrol. **37**, 205–222 (1978)
3. Douglas, E.M., Vogel, R.M., Kroll, C.N.: Trends in floods and low flows in the United States: impact of spatial correlation. J. Hydrol. **240**, 90–105 (2000)
4. Huang, Y.: Rapid flood risk assessment using GIS technology. Int. J. River Basin Manag. **7**(1), 3–14 (2010)
5. IPCC: Climate change 2007: impacts, adaptation and vulnerability. In: Parry, M.L., Canziani, O.F., Palutikof, J.P., van der Linden P.J., Hanson, C.E. (eds.) Contribution of Working Group II to the Fourth Assessment Report of the Intergovernmental Panel on Climate Change, Cambridge University Press, Cambridge, UK, 976pp (2007)
6. Şen, Z.: An innovative trend analysis methodology. J. Hydrol. Eng. **17**(9), 1042–1046 (2012)
7. Yue, S., Pilon, P., Cavandis, G.: Power of Mann-Kendall and Spearman's rho test for detecting monotonic trends in hydrological series. J. Hydrol. **259**, 254–271 (2002)
8. Yue, S., Pilon, P., Phinney, B., Cavandis, G.: The influence of autocorrelation on the ability to detect trend in hydrological series. Hydrol. Process. **16**, 1807–1829 (2002)

Black Carbon Aerosol Characteristics and Its Radiative Effect in Xuzhou City, China

Mengdie Xie and Wei Chen

Abstract

Based on the measurement of the concentration and aerosol optical depth of black carbon aerosol during April 27, 2014 to August 1, 2016, in Xuzhou city, China, the black carbon aerosol temporal variability and its impact on the atmospheric radiative forcing were studied. The mean black carbon aerosol mass concentration during the measurement period was 2.278 ± 1.551 μg/m^3 and demonstrated significantly seasonal variation with two peaks occurring in spring and winter. Simulating the radiative forcing of the black carbon aerosol by a radiative transfer model-6S code, it revealed that black carbon aerosol radiative forcing at the surface varies between about −0.37 to −15.24 W/m^2, which represents a considerable amount of cooling to the surface.

Keywords

Black carbon aerosol • Radiative forcing • Xuzhou city

1 Introduction

Black carbon aerosol is a key kind of carbonaceous aerosols in the atmosphere. Due to its porosity and adsorption of pollutants on its surface, a large number of black carbon aerosol particles can significantly reduce the atmospheric visibility [1]. At the same time, since black carbon aerosol can absorb solar radiation strongly, its climatic effects have been paid much attention recently [1–7].

M. Xie
College of Global Change and Earth System Science, Beijing Normal University, Beijing, 100875, China

W. Chen (✉)
School of Geoscience and Surveying Engineering, China University of Mining and Technology, Beijing, 100083, China
e-mail: chenweibnu@126.com

Sources of black carbon aerosol can be classified as natural sources (e.g. volcanic eruptions) and anthropogenic sources (e.g. fossil fuel combustion). Xuzhou city in China is an important base of the supply to the national coal energy in China. There are many large-scale coal mines [8]. Therefore, assessing black carbon aerosol and related effects in Xuzhou (China) is necessary for local and regional environmental change.

2 Data and Method

Xuzhou is a major city in Jiangsu province, China (see Fig. 1) and is positioned the city as a region of coal mining and heavy industry.

The black carbon aerosol concentration of the 6th band in Xuzhou city were measured every 5 min by Magee Scientific Aethalometer during 27 April 2014 to 1 August 2016. The method of smoothed moving average was applied to reduce the impacts of some days with too much missing values.

The black carbon aerosol radiative forcing (ΔF) can be estimated by [2, 3]

$$F = \pi * L \quad (1)$$

$$\Delta F = F_B - F_0 \quad (2)$$

where,

- L is apparent radiance,
- F is net radiative fluxes.
- F_B is the net radiative fluxes with black carbon aerosol at the surface.
- F_0 is the net radiative fluxes without black carbon aerosol at the surface

Apparent radiance (L) is simulated by feeding various parameters of black carbon aerosol optical (e.g. Aerosol Optical Depth (AOD) and surface albedo) into the 6S code, which is a basic RT code used for the calculation of lookup

Z. Zhang et al. (eds.), *Patterns and Mechanisms of Climate, Paleoclimate and Paleoenvironmental Changes from Low-Latitude Regions*, Advances in Science, Technology & Innovation, https://doi.org/10.1007/978-3-030-01599-2_31

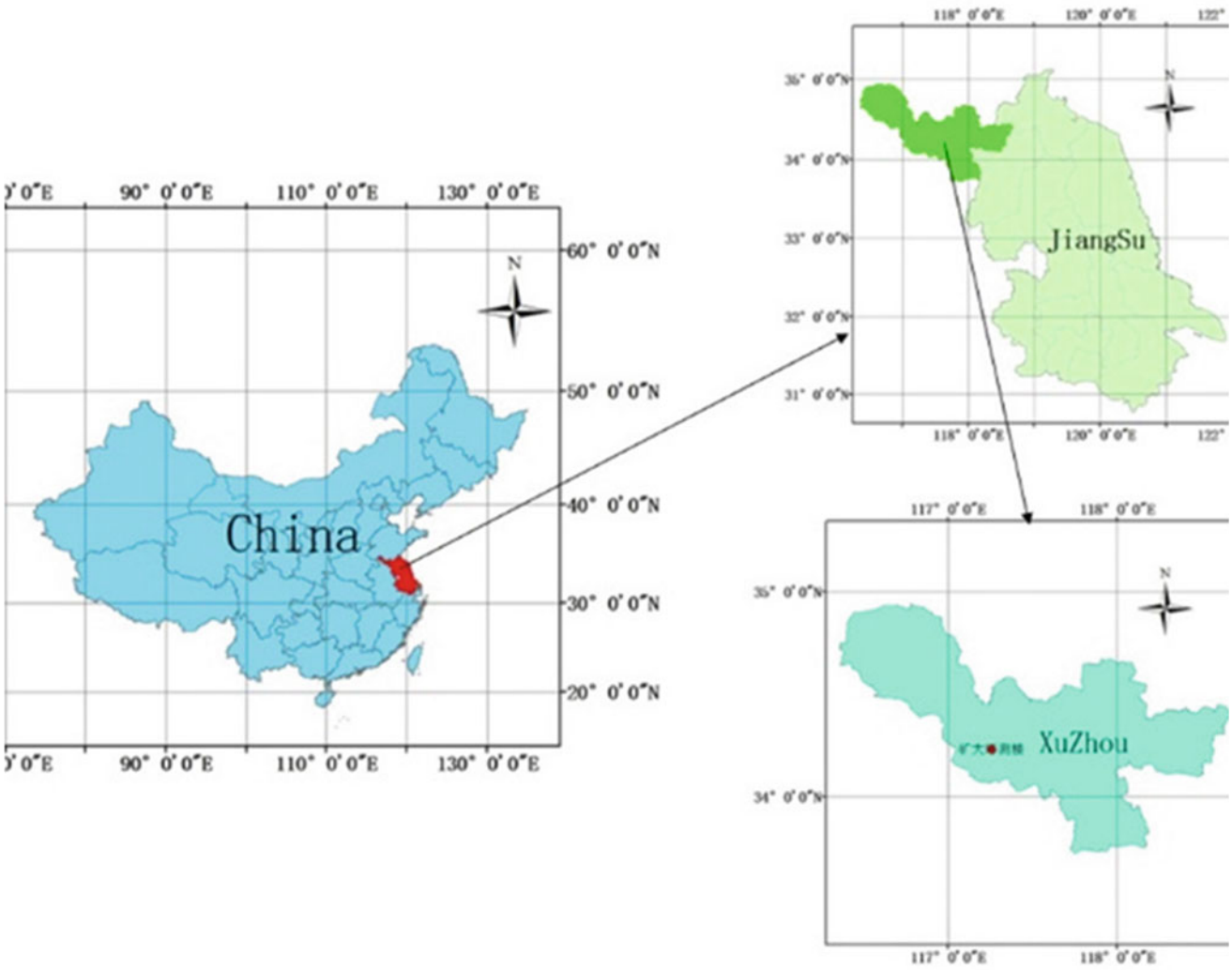

Fig. 1 The location of measurement region

tables in the MODIS atmospheric correction algorithm [4]. The black carbon AOD of bands at 550 nm is interpolated by the AOD data of bands 675 and 500 nm, downloaded from the Xuzhou station in AERONET (Aerosol Robotic NETwork, https://aeronet.gsfc.nasa.gov/).

3 Results

3.1 Seasonal Variation of Black Carbon Aerosol Concentration

During April 27, 2014 to August 1, 2016, the daily mean black carbon aerosol concentration varied between about 0.034–11.642 μg/m^3 (Fig. 2). Among eight main significant peaks in black carbon aerosol concentration, seven peaks occurred in winter and spring, while only one peak occurred in summer (Fig. 2). The seasonal variation of black carbon aerosol concentration has two significant peaks in spring and winter. Especially, in the winter of 2015, the daily black carbon aerosol concentrations varied in a boarder range than those in other observed seasons (Fig. 3).

3.2 Radiative Forcing Caused by Black Carbon Aerosol

Simulating the radiative forcing of the black carbon aerosol in Xuzhou city, China, by a radiative transfer model-6S code, it revealed that the radiative forcing of black carbon aerosol at the surface varies between about −0.37 to −15.24 W/m^2 (Fig. 4). It means that black carbon aerosol can cooling the surface in Xuzhou. The maximal radiative forcing occurs during 9:00 to 10:00.

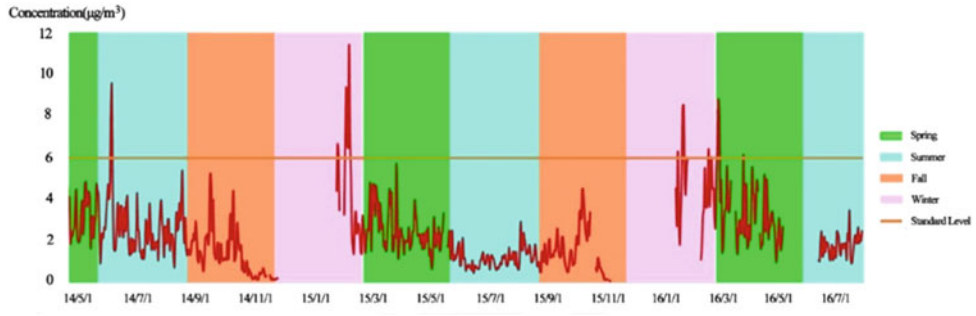

Fig. 2 Daily mean concentration of black carbon aerosol in Xuzhou

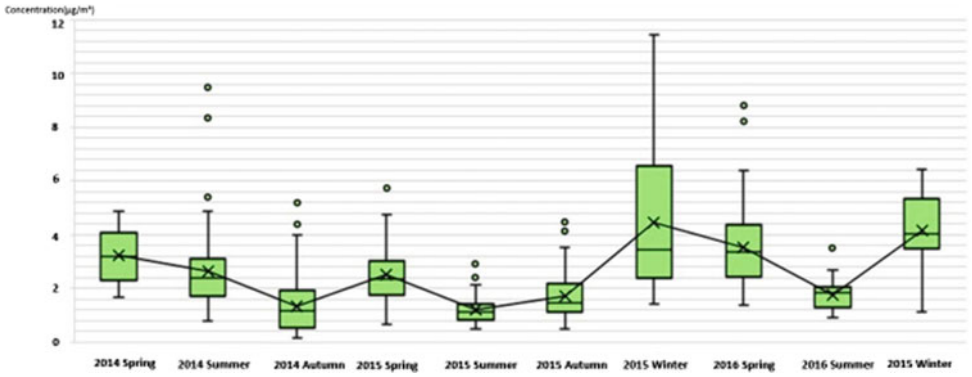

Fig. 3 The seasonal variation of black carbon aerosol concentration in Xuzhou

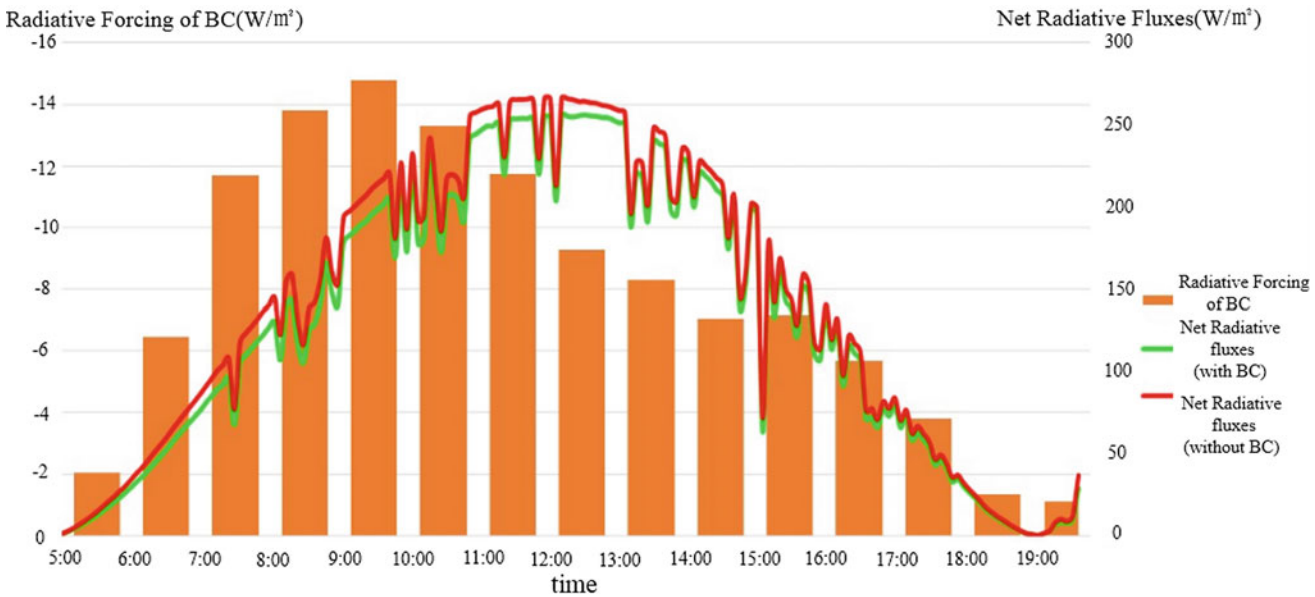

Fig. 4 Radiative forcing of black carbon aerosol (BC) at the surface

4 Discussion and Conclusions

The black carbon aerosol average concentration in Xuzhou (China) during the measurement period (during April 27, 2014 to August 1, 2016) was 2.278±1.551 μg/m^3. Its temporal variability demonstrated that significant peaks mainly occurred in winter, which was caused by the burning of coal for heating. Simulating results of the radiative forcing show that in Xuzhou, black carbon aerosol can lead to a cooling effect for the surface. Comparing with the measurement of black carbon aerosol concentration over main megacities in China: Nanjing (6.7 ± 4.6 μg/m^3) [1], Chongqing (4.86 ± 2.37 μg/m^3) [5], Lanzhou (1.568 μg/m^3) [6], Beijing (6.5 ± 7.3 μg/m^3), Hebei (9.6 ± 8.4 μg/m^3) [7], it is clear that black carbon concentration in Xuzhou is lower than most of megacities in China.

Acknowledgements This research is partially supported by National Key Science Programme for Global Change Research 2015CB953602.

References

1. Jun, F., et al.: Study radiative forcing black carbon aerosol suburban Nanjing Environmental Research Chinese. Climat. Environ. Res. **18** (05), 662–670 (2013)
2. Zhao, W., et al.: Algorithm analysis of 6S Radiation Model and its application in MODIS atmospheric correction. J. Shaanxi Meteorol. **2006**(05), 34–37 (2006)
3. Srivastava, A.K., et al.: Black Carbon Aerosol Characteristics and Its Radiative Impact over Nainital: A High-Altitude Station in the Central Himalayas. Journal of the Institute of Engineering **8**(03), 1–10 (2011)
4. Guangyu, S., et al.: The radiative and climatic effects of atmospheric aerosols. Chin. J. Atmos. Sci. **32**(4), 826–840 (2008). (in Chinese)
5. Jie, Z., et al.: Concentration characteristics of black carbon aerosol and its impact factors in Chongqing core area. Chin. J. Environ. Eng. **10**(02), 805–810 (2016)
6. Lei, Z., et al.: Property of black carbon concentration over outskirts of Lanzhou, Northwest China. China Environ. Sci. **31**(08), 1248–1255 (2011)
7. Xiao, Z., et al.: Characteristics of black carbon aerosol in Beijing and surrounding areas in 2006–2012. China Powder Sci. Technol. **21**(04), 24–29 (2015)
8. Lixin, W., et al.: Analysis to Xuzhou aerosol optical characteristics with ground-based measurements by sun photometer. Chin. Sci. Bull. **61**(20), 2287–2298 (2016)

Part VI

Sea Level Variability: Past, Present and Future

On the Long-Term Mediterranean Sea Level Variability

Mahdi Haddad and Antonio Bonaduce

Abstract

The present study focuses on the long term variability of Mediterranean Sea level variability. 14 long series of tidal heights were considered in this study to find out the long term trends in the sea level along the Mediterranean shores using Mann-Kendall test and Sen's slope estimator. One advantage of Mann-Kendall test is that the data do not need any particular distribution. The second advantage of the test is its low sensitivity to abrupt breaks (change-points) in the time series. Sen's method uses a linear model to estimate the slope of the trend (change per unit time). The identified yearly trends using these tests for more than fifty years of data point clearly and unequivocally towards the same conclusion that is the Mediterranean Sea level has risen since the end of the 19th century.

Keywords

Sea level • Tidal heights • Trend • Mann-Kendall test • Sen's slope

1 Introduction

Originally, tide gauges were deployed for navigation and tidal prediction. Their scope has expanded considerably from coastal engineering and coastal management to climate change, of which sea level is an essential parameter. Currently, the Permanent Service of Mean Sea Level (PSMSL) established in 1933, is responsible for the collection, publication, analysis and interpretation of sea level data from the global network of tide gauges. The most widely used application based on PSMSL's data is the global and regional sea level rise and variability. The PSMSL data set is the main source of information on long term changes in global sea level during the last two centuries. The data have been used intensively in studies such as those of Intergovernmental Panel on Climate Change (IPCC) [1].

In this study, we aimed to provide a description of the secular trend of the Mediterranean Sea level changes from the longest possible tidal gauge series. To this end, the series of monthly values of sea level, provided by the PSMSL, were analyzed for monotonous increasing or decreasing trends using the non-parametric Mann-Kendall test [2–4] and Sen's method for slope estimates [4, 5].

2 The Data

The study of the trend of sea level variability does not necessarily require direct manipulation of hourly tide gauge data. Indeed, the mechanism for calculating the average hourly data for one month or one year filter the fluctuations of short period observed in tide gauge records, that they are of irregular nature (storm waves, tidal waves …) or periodical (diurnal, tidal waves, tides …). The time series of monthly or annual averages are consequently suitable for the investigation of the sea level secular variations. In the framework of this study, we chose to analyze the available monthly averages sea level series with more than 50 years of measurements: Tarifa (Spain), Algeciras (Spain), Malaga (Spain), Marseille (France), Genova (Italy), Venezia (Punta Della Salute) (Italy), Trieste (Italy), Rovinj (Croatia), Bakar (Croatia), Split Rt Marjana (Croatia), Split—Gradska Luka (Croatia), Dubrovnik (Croatia), Alexandria (Egypt) and Ceuta (Spain). The corresponding monthly tidal heights series were obtained from Internet site of the PSMSL. These data are of the "RLR" (Revised Local Refers) category; in other words, those which underwent the battery of test, controls and processing aiming at checking the continuity and local stability of the tide gauge reference [6, 7].

M. Haddad (✉)
Centre of Space Techniques, 1 Avenue de Palestine.
BP 13, 31200 Arzew, Oran, Algeria
e-mail: haddad_mahdi@yahoo.fr; mhaddad@cts.asal.dz

A. Bonaduce
Mercator Océan, Toulouse, France

Z. Zhang et al. (eds.), *Patterns and Mechanisms of Climate, Paleoclimate and Paleoenvironmental Changes from Low-Latitude Regions*, Advances in Science, Technology & Innovation, https://doi.org/10.1007/978-3-030-01599-2_32

Table 1 Descriptive statistics of used tide gauge

Station	Latitude (°)	Longitude (°)	Data range	Obs.	Missing data
Tarifa	36.008600	−5.602600	1943–2016	880	50
Algeciras	36.116669	−5.433333	1943–2002	711	127
Malaga	36.712700	−4.415460	1944–2013	840	149
Marseille	43.278801	5.353860	1885–2016	1583	48
Genova	44.400000	8.900000	1884–1997	1368	297
Venezia	45.433333	12.333333	1909–2000	1104	65
Trieste	45.647361	13.758472	1875–2016	1704	230
Rovinj	45.083300	13.628300	1955–2014	714	3
Bakar	45.300000	14.533333	1930–2013	1008	132
Rt Marjana	43.508333	16.391667	1952–2011	716	8
Gradska Luka	43.506700	16.441700	1954–2014	730	0
Dubrovnik	42.658300	18.063300	1956–2014	708	7
Alexandria	31.216667	29.916667	1944–2006	755	33
Ceuta	35.892400	−5.315890	1944–2016	874	28

The descriptive statistics of tidal data for the 14 selected stations are given in Table 1.

3 Results

The classical Mann-Kendall test is used to test if there is a trend in the sea level time series. Table 2 gives the summary of the obtained results of this test for the 14 sea level time series. The null hypothesis H_0 for the Mann-Kendall test is that there is no trend in the series. The three alternative hypotheses H_a are that there is a negative, non-null, or positive trend. It can be seen from Table 2 that, with the exception of Split Rt Marjana series $(p = 0.263)$, the obtained p values for the remaining data are lower than the fixed significance level $(\alpha = 0.05)$, one should reject the null hypothesis H_0, and accept the alternative hypothesis H_a. We can conclude that there are significant positive trends in our sea level series $(S > 0)$.

Usually, the slope for linear trend is estimated by the least squares estimate. However this method is very sensitive to outliers and is only valid when there is no serial correlation. Here, we use the more robust method of Sen to estimate the sea level variability rate (mm per year). Table 3 gives the summary of the obtained Sen's slopes for the considered 14 tidal heights series. The mean sea level secular trends and its standard deviation of the residual variability estimated by the PSMSL for the quasi-equivalent range of sets of data are given for comparison and validation purposes. These secular trends are obtained using a time series decomposition procedure based on the Generalized Gauss Markov Model, that allows extracting the linear trend, the seasonal component made up of an annual and a semi-annual cycle and the noise component from the time series [7].

The Sen's slopes, in Table 3, indicate that all the series presenting significant trends are increasing, proving, if it is still necessary, the rise of the Mediterranean sea level during the previous century. The differences between the slope values estimated by the PSMSL and from the use of the Sen's approach range from 0.01 to 0.77 mm/year in absolute values. The maximal value of 0.77 mm/year observed for Split Rt Marjana time series, where the null hypothesis H_0 is accepted: there is no significant trend in this series (see, Table 2). The following important value of 0.37 mm/year assigned to Malaga series can be related to the accuracy of the slope value provided by the PSMSL (standard deviation of 0.66 mm/year).

4 Conclusions

The main purpose of this study was to highlight, on the basis of statistical tests, the significant secular changes of the Mediterranean sea level, through the analysis of historical tide gauge records. In this framework, 14 long tide gauge monthly series selected from the Permanent Service of Mean Sea Level (PSMSL) database were used. The search for the presence of trends within these series was carried out using the Mann-Kendall test and Sen's slope estimator. The obtained results show that the Split Rt Marjana series is the only one which does not exhibit a significant trend. The other 13 series showing significant trends are increasing.

Table 2 Man-Kendall trend test

Station	Mann-Kendall statistic S	Var S	*p* value	Risk to reject the null hypothesis H_0 while it is true (%)
Tarifa	77,957.000	63,644,155.667	<0.0001	<0.01
Algeciras	11,249.000	22,185,786.333	0.017	1.69
Malaga	39,630.000	36,737,888.667	<0.0001	<0.01
Marseille	503942.000	402,249,772.000	<0.0001	<0.01
Genova	211,644.000	136,684,412.667	<0.0001	<0.01
Venezia	230,566.000	124,801,981.333	<0.0001	<0.01
Trieste	407,832.000	356,190,664.667	<0.0001	<0.01
Rovinj	33,495.000	40,018,652.333	<0.0001	<0.01
Bakar	80,595.000	74,816,433.000	<0.0001	<0.01
Rt Marjana	7043.000	39,514,591.000	0.263	26.25
Gradska Luka	44,872.000	43,310,978.000	<0.0001	<0.01
Dubrovnik	58,345.000	38,354,886.333	<0.0001	<0.01
Alexandria	61,332.000	41,903,860.667	<0.0001	<0.01
Ceuta	59,598.000	67,392,980.000	<0.0001	<0.01

Table 3 Seasonal Sen's slope and PSMSL estimated slope

Station	Data range	Sen's slope (mm/year)	PSMSL Data range	PSMSL slope (mm/year)	PSMSL Std. slope (mm/year)	Diff. (mm/year)
Tarifa	1943–2016	1.25	1944–2015	1.06	0.38	0.19
Algeciras	1943–2002	0.29	1944–2001	0.40	0.24	−0.11
Malaga	1944–2013	1.08	1944–2012	0.71	0.66	0.37
Marseille	1885–2016	1.25	1885–2015	1.32	0.13	−0.07
Genova	1884–1997	1.23	1884–1996	1.18	0.07	0.05
Venezia	1909–2000	2.41	1909–2000	2.47	0.26	−0.06
Trieste	1875–2016	1.30	1875–2015	1.29	0.10	0.01
Rovinj	1955–2014	0.79	1956–2014	0.89	0.27	−0.10
Bakar	1930–2013	1.00	1930–2013	1.19	0.27	−0.19
Rt Marjana	1952–2011	0.44	1953–2011	-0.33	0.54	0.77
Gradska Luka	1954–2014	0.95	1955–2014	1.11	0.46	−0.16
Dubrovnik	1956–2014	1.38	1956–2014	1.65	0.45	−0.27
Alexandria	1944–2006	1.78	1944–2006	1.80	0.24	−0.02
Ceuta	1944–2016	0.71	1945–2015	0.62	0.22	0.09

After detecting the presence of significant and monotonic trends, the annual rates of sea level variability were estimated using the non-parametric seasonal Sen's approach. These estimated rates are fully consistent with those estimated by the PSMSL. The overall estimated annual rates indicate a very clear increase in the sea level along the Mediterranean shores.

References

1. Intergovernmental Panel on Climate Change (IPCC): Climate Change 2013: The Physical Science Basis. www.climatechange2013.org (2013), last accessed 2017/07/17
2. Mann, H.B.: Nonparametric tests against trend. Econometrica **13**, 245–259 (1945)
3. Kendall, M.G.: Rank Correlation Methods. Griffin, London (1975)
4. Hirsch, R.M., Slack, J.R., Smith, R.A.: Techniques of trend analysis for monthly water quality data. Water Resour. Res. **18**(1), 107–121 (1982)
5. Sen, P.K.: Estimates of the regression coefficient based on Kendall 'S tau. J. Am. Stat. Assoc. **63**, 1379–1389 (1968)
6. Holgate, S.J., Matthews, A., Woodworth, P.L., Rickards, L.J., Tamisiea, M.E., Bradshaw, E., Foden, P.R., Gordon, K.M., Jevrejeva, S., Pugh, J.: new data systems and products at the permanent service for mean sea level. J. Coastal Res. **29**(3), 493–504 (2013)
7. Permanent Service for Mean Sea Level (PSMSL) Homepage, http://www.psmsl.org, last accessed 2017/07/17

Impacts of Relative Sea Level Change and Sedimentary Dynamic on an Historic Site Expansion Along the Coast Between Sfax and Jebeniena, Tunisia

Mohamed Kamoun, Afef Khadraoui, Asma Ben Hamad, Chahira Zaïbi, Martin R. Langer, Nejib Bahrouni, Mohamed Ben Youssef, and Fekri Kamoun

Abstract

New data evaluating the relative sea level changes and sedimentary dynamics along the coast of Tunisia are presented. Data are inferred from archaeological sites of Punic-Roman age located between Ras Boutria (Jebeniena) and El Awebed (Sfax). New results are based on high-resolution micropalaeontological, sedimentological and geochemical analyses of several sediments cores coupled to new ^{14}C datings. The coast of Jebeniana (Ras Boutria historic site) recorded the first marine transgression, overlying the quartz sand Tyrrhenian deposits, 2210 a BP in age. This transgression, also recognized in Sfax coast, revealed by the dominance of lagoonal ostracod associated to coastal and marine taxa, allows the settlement of an open lagoon. It reveals also, a high value of species number and a reduced density. The pelagic influences are augmented by the high marine geochemical elements concentrations such as the chloride (Cl) and the sulfur (S). The increase of the brackish ostracod mark the settlement of a closed lagoon toward 768 a BP. The enrichment of the sediment in quartz grains coupled with the action of the current drift authorized the build-up of sandy spits and the genesis of the lagoon that preserve a rich assemblage of euryhaline ostracods and mollusks species. This process was probably responsible of the obstruction of the historic Boutria harbor and the abandon of the historic city.

Keywords

Ras boutria • El awebed • Ostracods • Foraminifera Holocene

1 Introduction

Tunisia coast is marked by a diversity of wet lands more or less eccentric compared to the current coast. These environments have acquired a configuration determined by the neotectonic [1], the variation of the sea level [2] and the sedimentary dynamic [3]. Two generations of wetlands can be distinguished. The first one is intracontinental completely circumscribed to the Pleistocene such as sebkha Al Kalbya [4] and the second bordering on the shore and communicates occasionally with the sea [3]. These wetlands, which are very sensitive, have recorded during historic times climatic changes, human activities such as construction harbors and watershed development. These ecosystems have become very vulnerable to different factors. The aim of this work is to provide new analysis and interpretation on the relative sea level changes and sedimentary dynamic since the last 2 ka. The archaeological features of the investigated sites are briefly discussed; readers are referred to specific archaeological publications.

2 Geomorphologic Settings

The Jebeniena coast, including the Ras Boutria lagoon is characterized by specific geomorphological units from West to East: (1) several archaeological ruins; (2) a developed intertidal zone with a quartz-rich substratum; (3) a lagoons separated from the sea by a system of current sandy spits

M. Kamoun (✉) · A. Khadraoui · A. B. Hamad · C. Zaïbi
F. Kamoun
Laboratory GEOGLOB, Faculty of Sciences, Sfax University, BP 1171 Sfax, Tunisia
e-mail: med23km@yahoo.fr

M. R. Langer
Steinmann Institut Für Geologie, Mineralogie Und Paläontologie, Rheinische Friedrich-Wilhelms Universität Bonn, Bonn, Germany

N. Bahrouni
Geological Survey, National Office of Mines, 24, Rue de L'Energie 2035 La Charguia, B.P. 2151080 Tunisie, Tunis Cedex, Tunisia

M. B. Youssef
Water Researches and Technologies Center of Borj Cedria, Borj Cedria, Tunisia

Z. Zhang et al. (eds.), *Patterns and Mechanisms of Climate, Paleoclimate and Paleoenvironmental Changes from Low-Latitude Regions*, Advances in Science, Technology & Innovation, https://doi.org/10.1007/978-3-030-01599-2_33

denoting a southern longshore drift. This lagoon is opened to the sea under tidal influences, especially during the high tides by channels, which penetrate into the schorre and the slikke.

3 Results

3.1 Jebeniena, Ras Boutria Coast

The variation of ostracods along the core BT1 (Fig. 1) allowed us to distinguish the successive zones: **Zone I**, from 130 to 100 cm and 2210 a BP in age, is characterized by the presence of brackish, lagoonal, coastal and marine ostracod taxa. It shows also, a high values of ostracod species richness, equitability and Shannon index and low density revealing a well-structured population. **Zone II**, from 100 to 50 cm, is marked by the enrichment of brackish ostracods, containing the two euryhaline species *Cyprideis torosa* and *Loxoconcha elliptica,* and lagoonal one. However, the coastal and marine taxa depletion is associated to the high values of density. The zone II is also characterized by the decrease of marine geochemical elements such as sulfur (S) and chloride (Cl) well represented in the previous zone. Nevertheless, the detrital element, silicon (Si) and Titanium (Ti) give high concentration. **Zone III**, from 50 cm to the surface, is marked by the dominance of brackish ostracod association represented by *Cyprideis torosa* and the depletion of lagoonal, coastal and marine associations. It shows also the decrease of the density and species richness of ostracodes.

3.2 Sfax, El Awabed Coast

The variation of ostracods taxa along the core C3 allowed us to distinguish the successive zones: **Zone I**, from 131 to 100 cm, shows the dominance of the brackish euryhaline taxa *C. torosa*. Several trenches digging near C3 show the presence of a Senegalese mollusks commonly mentioned in Tyrrhenian series. **Zone II**, from 100 to 83 cm, 2595 ± 30 a BP in age, records the appearance of coastal, marine and lagoonal ostracod associated to brackish one. **Zone III**, from 83 to 63 cm, is marked by the enrichment and the dominance of the brackish ostracod (100%). This zone reveals also the abundance of quartz grains, coupled with the dominance of the brackish *C. torosa,* which suggest their continental origin. **Zone IV**, from 63 to 38 cm, made up of silts and clays without fauna. **Zone V**, from 38 to 20 cm, the dominant brackish *Cyprideis torosa* is associated to the lagoonal and to the coastal ostracodes. To the top of the zone, the brackish taxa become poor and the lagoonal and coastal taxa grow. **Zone VI**, is characterized by the absence of ostracods and mollusks, which sign the settlement of the present sebkha.

4 Conclusion

We produced the Holocene evolution of the Sfax and Jebeniena coasts. (i) a transgressive event toward 2200 a BP, evidenced by the high values of ostracodes species richness and the diversity of ostracod and mollusk associations;

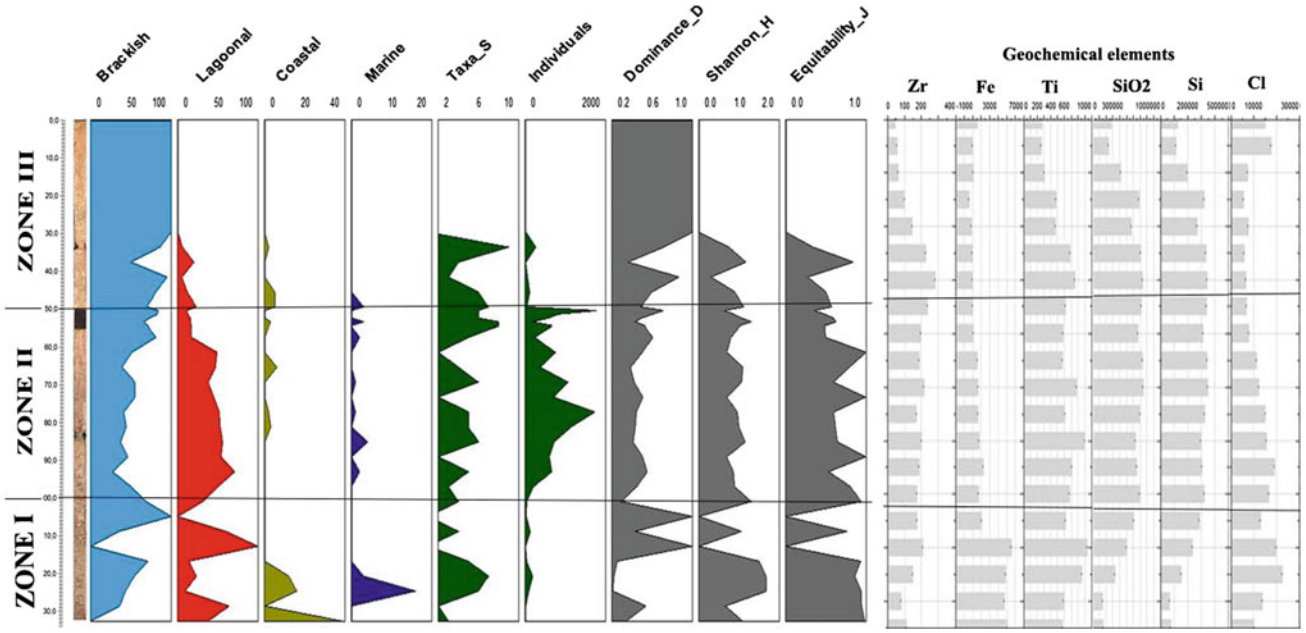

Fig. 1 Quantitative vertical distribution of ostracods with species and individuals number, diversity indices D, H and E and geochemical elements along the core BM1

(ii) the enrichment of brackish ostracods associated to the high values of density and to the reduction of the diversity sign the settlement of closed lagoon at boutria coast; (iii) the dominance of brackish ostracods mark a more closed lagoon. The action of the long shore drift authorized the build-up of sandy spits and the genesis of the lagoon. This process was probably responsible of the obstruction of the historic Boutria harbor and the abandon of the historic city.

References

1. Bahrouni, N., Bouaziz, S., Soumaya, A., Ben Ayed, N., Attafi, K., Houla, Y., El Ghali, A., Rebai, N.: Active deformation analysis and evaluation of earthquake hazard in Gafsa region (Southern Atlas of Tunisia). J. Seismolog. **18**, 235–256 (2013)
2. Anzidei, M., Antonioli, F., Lambeck, K., Benini, A., Soussi, M., Lakhdar, R.: New insights on the relative sea level change during holocene along the coasts of Tunisia and western Libya from archaeological and geomorphological markers. Quat. Int. **232**, 5–12 (2011)
3. Zaïbi, C., Kamoun, F., Viehberg, F., Carbonel, P., Jedoui, Y., Abida, A., Fontugny, M.: Impact of relative sea level and extreme climate events on the Southern Skhira coastline (Gulf of Gabes, Tunisia) during Holocene times: Ostracodes and foraminifera associations response. J. Afr. Earth Sci. **118**, 120–136 (2016)
4. Boujelben, A., Lebreton, V., Karray, M.R.: Dynamique lacustre Holocène dans la sebkha al Kalbiyya (Tunisie centre orientale). **28**, 239–245 (2017)

Sedimentary Dynamic and Sea Level Variation Along Hachichina Coast (Sebkha Ras Younga, Gulf of Gabes, Tunisia) During Holocene: Response of Ostracods and Foraminifera Assemblages

Khaoula Ben Khlifa, Chahira Zaïbi, Jérome Bonnin, and Fekri Kamoun

Abstract

Several cores retrieved from Ras Younga Sebkha, (Hachichina coast, Gulf of Gabes), are subjected to a micropalaeontological and sedimentological study. The analysis of ostracods and foraminifera coupled with statistical approach (Correspondence analysis) are used in order to reconstruct the evolution of Holocene environment related to climatic and hydrodynamic forcing. The foraminifera and ostracods association present in the sediments core, allowed us to identify the different steps of the genesis of the Sebkha Ras Younga. Four major steps were distinguished: (i) the first one, corresponding to an estuarine lagoon, is characterized by the dominance of brackish ostracods association and reduced values of the diversity index (H) and (E); (ii) the second one, marked by the enrichment of marine, lagoonal, and shallow water ostracods and shallow water foraminifera and high values of (H) and (E) index, indicate the settlement of an opened lagoon toward 5105 a BP; (iii) the enhancement of lagoonal ostracods, associated to the increase of the individuals number mark the settlement of a closed lagoon related to the genesis of sand spit under the action of longshore currents; (iv) the last step, characterized by the absence of microfossil, corresponds to a more closed lagoon evolving into the current Sebkha.

Keywords

Sebkha • Ostracods • Foraminifera • Holocene

1 Introduction

During the last decade, ostracods and foraminifers are used as indicators for the reconstruction of the Holocene paleoenvironment evolution caused by anthropological or natural forcing. The main climatic and sea level variations have been reconstructed based on quantitative and qualitative distributions of ostracods and foraminifera populations and sedimentological features. In Tunisia, the Holocene coastal environments are found to be lagoon and brackish-lagoon. These environments include Lake of Tunis, Ariana sebkha [1], Ghar El Melh lagoon, Ichkeul Lake, Sliman lagoon El Melah and El Guettiate and Dreiia sebkhas [2]. This study represents a continuity of a previous research dealing with ostracods associations [2]. Its main objectives are (1) to reconstruct the different palaeoenvironments which succeeded from 5000 a BP, and to determine the factors controlling paleoenvironmental changes, (2) to describe and compare the morphological evolution of the differents sebkhas, and (3) to understand the mechanisms of their evolution and provide future evolution scenarios within a global context.

2 Settings

Hachichina coast, including Ras Younga Sebkha, shows five zones (Fig. 1): (1) a land which is characterized by the presence of several archaeological sites; (2) a supratidal zone, with developed sebkhas, surrounded by windy dunes; (3) a developed intertidal zone subdivided into slikke and schorre; (4) two lagoons separated from the sea by a system of current sandy spits denoting a southern and northern longshore drift. These lagoons are open to the sea under tidal influences, especially during the high tides by channels, which penetrate into the schorre and the slikke.

K. B. Khlifa (✉) · C. Zaïbi · F. Kamoun
Laboratory GEOGLOB, Faculty of Sciences of Sfax, Sfax University, BP 1171 Sfax, Tunisia
e-mail: Khaoula.benKhlifa@yahoo.com

J. Bonnin
Laboratory EPOC UMR 5805 CNRS, Bordeaux University 1, Avenue Des Facultés, 33405 Bordeaux, Talence Cedex, France

Z. Zhang et al. (eds.), *Patterns and Mechanisms of Climate, Paleoclimate and Paleoenvironmental Changes from Low-Latitude Regions*, Advances in Science, Technology & Innovation, https://doi.org/10.1007/978-3-030-01599-2_34

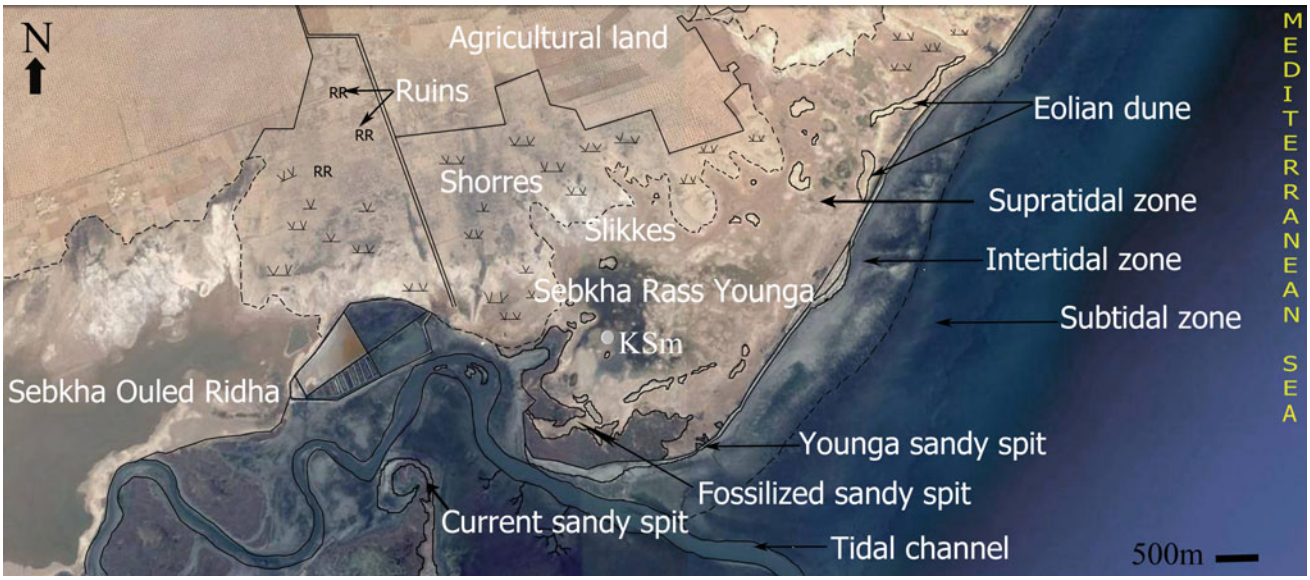

Fig. 1 The different zones of the Hachichina coast

3 Results

The variation of benthic foraminifera and ostracods along the core KSm allowed us to distinguish the following zones: Zone I, from 330 to 270 cm, characterized by high values of foraminifera species richness (5–19 species) and low abundance (546 individuals/10 g dry sediments), is marked by the dominance of lagoonal foraminifera association (76%) followed by coastal one (24%). The ostracods are represented by the brackish association (56%) containing the two euryhaline species *Cyprideis torosa* (40%) and *Loxoconcha elliptica* (60%). Zone II, from 270 to 100 cm, shows a high value of species richness (9–19 species) and an increase of the density (2500 individuals/10 g dry sediments). The enhancement of the coastal association (63%), which contains the dominant *Ammonia beccari* and *Quinqueloculina seminula*, characterize this zone, is associated to the reduction of the lagoonal association (37%). Zone II is also characterized by the enhancement of marine ostracods (31%), represented by *Cushmanidea elongata* (31%), *Semicytherura incongruens* and *Carinocythere carinata*, coupled to the coastal association (14%). H and E indices of foraminifera and ostracods progressively increase, reaching the highest values of the core. Zone III, from 100 to 40 cm, is marked by a decrease in the density and species richness of foraminifera. This zone shows the increase of the lagoonal taxa *Ammonia parkinsoniana* (17%) and *Ammonia tepida* (24%). In addition, the lagoonal ostracods represented by *Xestoleberis aurantia* (50%) and *Leptocythere fabaeformis* (6%) are dominant. The reappearance of the brackish species at the top of this zone indicates the evolution of the environment towards the closure. This zone is also marked by the reduction of the density values, species richness and diversity indices H and E of ostracods. All these parameters indicate a poorly structured population and reveal the settlement of a lagoonal environment evolving toward closure following the probable installation of a sandy spit. Zone IV, from 40 cm to the surface, is distinguished by the absence of foraminifera, ostracods and mollusks, which reveals the actual sebkha.

4 Discussion

Four phases can be distinguished during the Holocene at the Sebkha Ras Younga (Fig. 2):

Phase 1 is characterized by the dominance of brackish ostracods and reduced values of the diversity index (H) and (E). The richness of sediments in the brackish species *Loxoconcha elliptica*, showing high energy and estuarine environments, indicate the settlement of a lagoonal environment subjected to estuarine influences. Phase 2 is marked by the development of coastal and marine ostracods associated to marine molluscs, which indicate the settlement of a lagoon more opened to the sea. This evolution could be a consequence of marine transgression toward 5105 a BP. Phase 3, characterized by the reappearance of the species *Cyprideis torosa* and *Loxoconcha elliptica* and by the impoverishment of the marine-coastal species, indicates the installation of a closed lagoon following the probable genesis of a sandy spit. Phase 4 is distinguished by the absence of microfossil and macrofossil, which reveals a closed lagoon evolving into the current Sebkha.

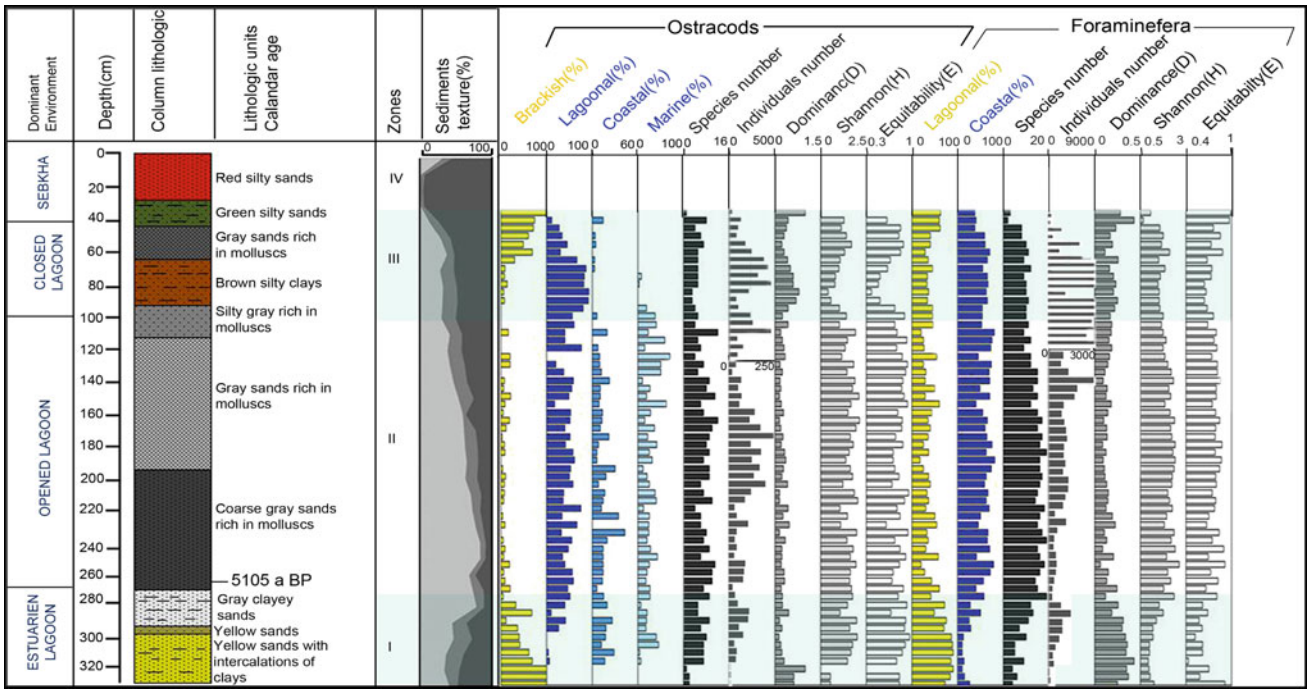

Fig. 2 Evolution of ostracods and foraminifera assemblages, biocenotic parameters, dominance, species richness and individuals number along KSm core

5 Conclusion

The evolution of the Sebkha Ras younga is established from the micropalaeontological and sedimentological study of the sediments present in one collected drill core. This evolution, from an estuarine environment to the present sebkha going through an opened lagoon, seems to be linked to the hydrographic setting of the sebkha and of the Ouadrane Wadi outlet discharging in the Hachichina coast.

References

1. Carbonel, P.: Les ostracodes et leur intérêt dans la définition des écosystèmes estuariens et de plateforme continentale. Essais d'application à des domaines anciens. Mémoire l'Institut Géologie Bassin d'Aquitaine **11**, 350 (1980)
2. Zaïbi, C., Kamoun F., Viehberg, F., Carbonel, P., Younes Jedoui, Y., Abida, H., Fontgny, M.: Impact of relative sea level and extreme climate events on the Southern Skhira coas line (Gulf of Gabes, Tunisia) during holocene times: ostracodes and foraminifera associations' response. (2016)

New Experimental Low Cost Technique of Sea-Level Monitoring: Toward a Sea-Level Monitoring for All

Yacine Hemdane, Mohamed Bouhmadouche, Bachir Hamadache, and Mohamed Aounallah

Abstract

In this paper, we proposed a new low cost technique of sea-level observation and monitoring inspired by the classical Tide Pole (Tide Staff). The results obtained by our proposed High Frequency Rotational Tide Gauge (RTG_{HF}) are promising. They show that RTG_{HF} is very adapted to an agitated environment and is able to measure high and low frequencies oscillations (waves/swells, infragravity waves, seiches, meteotsunamis, tsunamis, tides, sea-level change, etc.). Contrary to modern tide gauges, where a measure is given with intermediate methods (pressure, ultrasonic, radar, bubbler, laser, etc.), this proposed solution is based on direct reading of sea-level movement with a precision of 1 mm and sampling rate of more than two readings per second (2 Hz). RTG_{HF} uses a rotational floated patented system (Hemdane in Algerian Patent. N° DZ Patent: 9539. Echelle de marée cylindrique codifiée/houlographe à lecture directe et automatique des oscillations marines de hautes fréquences, [1]) (Algerian Patent) where levels coded in barcodes. It is important to emphasize the existence of systems using barcode technology for water level measurement. To the best of our knowledge, some patents describe solutions through barcodes for no or less agitated water environments and groundwater (still water) (CN 201628523 U. Intelligent Barcode ruler, [5], CN 202024806 U. Underground water level observation device, [6]). On the other hand, thanks to its innovative rotational system (Hemdane in Algerian Patent. N° DZ Patent: 9539. Echelle de marée cylindrique codifiée/houlographe à lecture directe et automatique des oscillations marines de hautes fréquences, [1])—which is very adapted to wave induced orbital motions (alternating crest/through)—RTG_{HF} adapts to high frequencies characterizing an oceanographic environment (strong and perpetual agitations induced especially by waves). Therefore, our proposed solution based on a rotational system that allows the detection of high frequencies and thus makes it very suitable for marine and coastal environments. In addition, RTG_{HF} operates without stilling well, and all high frequency oscillations are easily detected. Moreover, its low cost can make this technique very accessible for generalization of sea level observation. Then, RTG_{HF} could help to better understand and monitor sea-level movement and thereby reduce coastal risks.

Keywords

Tide gauge • Sea-level monitoring • Rotational system and wave induced orbital motions • High frequency oscillations • Tide pole

1 Introduction

Relative and sudden sea-level rise are a major challenge faced by vulnerable coastal populations and facilities. Hence, tide gauges are used to detect any abnormal increase or decrease in sea level in view to reduce their impact on coastal communities [2]. However, the high cost of these devices makes their generalization difficult, especially on coasts at risk.

The objective of this work was to propose an accessible technique of sea-level observation and monitoring. We presented here the first results of High Frequency Rotational Tide Gauge (RTG_{HF}) tests carried out in an open air harbor area.

Inspired by classical Tide Pole—which remains the only instrument providing direct reading and the correct

Y. Hemdane (✉) · M. Bouhmadouche
Laboratoire Géo-Environnement, Faculté Des Sciences de La Terre, Géographie et Aménagement Du Territoire, Université Des Sciences et de La Technologie Houari Boumediene, BP 32, El-Alia, Algiers, Algeria
e-mail: yacinehemdane@gmail.com

B. Hamadache · M. Aounallah
Office National de La Météorologie (Météo-Algérie), Dar El Beïda, Algeria

Z. Zhang et al. (eds.), *Patterns and Mechanisms of Climate, Paleoclimate and Paleoenvironmental Changes from Low-Latitude Regions*, Advances in Science, Technology & Innovation, https://doi.org/10.1007/978-3-030-01599-2_35

measurement of sea-level as noticed by IOC [3] and SHOM [4]—Rotational High Frequency Tide Gauge (RTG_{HF}) develops classical Tide Pole into a new generation of tide staff (Tide Pole). Indeed, Tide Pole is considered as the basic reference of water level observation. However, the greatest disadvantage of this instrument is the impossibility of human observers to continuously check the levels given by this instrument. In addition, the accuracy of Tide Pole measurements depends closely on observers especially during stormy sea conditions (i.e., presence of waves and harbor oscillations). In these conditions, high frequency oscillations make the direct reading of levels very difficult by human observers. Consequently, errors can easily occur and accuracy becomes decimetric or greater.

2 Methods

Contrary to modern water level gauges where the measurement is given with intermediate methods (pressure, ultrasonic, radar, bubbler, laser, etc.), RTG_{HF} is based on direct reading of sea-level movement with a precision of 1 mm (or less) and a sampling rate of more than two direct readings per second (2 Hz). These characteristics are sufficient for sea level measurement. However, the sample frequency and accuracy can be increased according to desired objective. Moreover, RTG_{HF} can be installed quickly and easily (see Fig. 1a).

RTG_{HF} tests were performed for short periods to observe the performance of our proposed sea-level monitoring solution in an open air harbor area. RTG_{HF} uses a rotational system where the levels are coded in barcodes. It is important to emphasize the existence of systems using the barcode technology for measurement of water levels. However, to the best of our knowledge, some patents describe solutions through barcodes for no or less agitated water environments and groundwater (calm water) where for instance pulley/counterweight and/or stilling well (orifice, filter and chamber) are used (i.e. [5, 6]). On the other hand, thanks to its innovative rotational system [1]—which is very adapted to wave induced orbital motions (alternating crest/through)—RTG_{HF} adapts to high frequency oscillations characterizing the oscillation of an oceanographic environment (i.e., waves/swell, harbor oscillations, seiches and tsunamis), and consequently levels and high frequency oscillations are read very easily [2].

3 Results

The results obtained by RTG_{HF} solution are promising (see Fig. 1). Sea-level oscillations are easily measured with a precision of 1 mm and sampling rate of more than about three direct readings per second (about 3 Hz). The first results obtained show that the proposed solution easily detects waves. Thanks to the patented rotational system [1], characterizing our proposed high frequency sea-level monitoring, the peaks of high frequencies are well detected by RTG_{HF}. In addition, the device structure resists very well to induced forces especially by waves. A detailed observation of sea level record obtained by RTG_{HF} shows that signal is continuous with no interruption in the sea level reading. During these short tests, we recorded waves with maximum heights of about 30 cm. Finally, the cylindrical shape of device makes it resistant to wind (see Fig. 1a).

4 Discussion

Sea-level oscillations are easily measured with a precision of 1 mm and a sampling rate of more than about three direct readings per second (about 3 Hz). The results show that RTG_{HF} is very adapted to the oceanographic environment and is able to measure the high frequencies oscillations. Indeed, its innovative rotational system adapts to wave-induced orbital motions (alternating crest/through). Then, RTG_{HF} adapts to high frequencies characterizing an oceanographic environment. On this point, RTG_{HF} gives a detailed profile of waves. Hence, it is important to emphasize the importance of high frequency waves in measuring and monitoring the risk of marine submersion (storm surges). In addition, RTG_{HF} operates without stilling well, and all high frequency oscillations are easily detected (see Fig. 1b). Indeed, the orifice (and chamber), act as a mechanical low-pass filter that eliminates high frequency wave action [7]. Although results are promising, more tests need to be conducted to improve the performance of our proposed instrument. This technique still has some limitations or difficulties especially on macrotidal coasts where high tide requires high installations. In addition, a new study underway to estimate the period necessary for the maintenance of our instrument especially against biofouling.

5 Conclusions

These preliminary results show that our proposed solution is promising. Thanks to the innovative rotational system, RTG_{HF} adapts to wave induced orbital motions (alternating crest/through). Then, RTG_{HF} adapts to high frequencies characterizing an oceanographic environment. In addition, RTG_{HF} could help in sea level measurement and monitoring by making sea level monitoring possible for all. Although the results are promising, more tests are necessary to improve performance of the proposed technique for sea-level observation and monitoring. These tests will allow

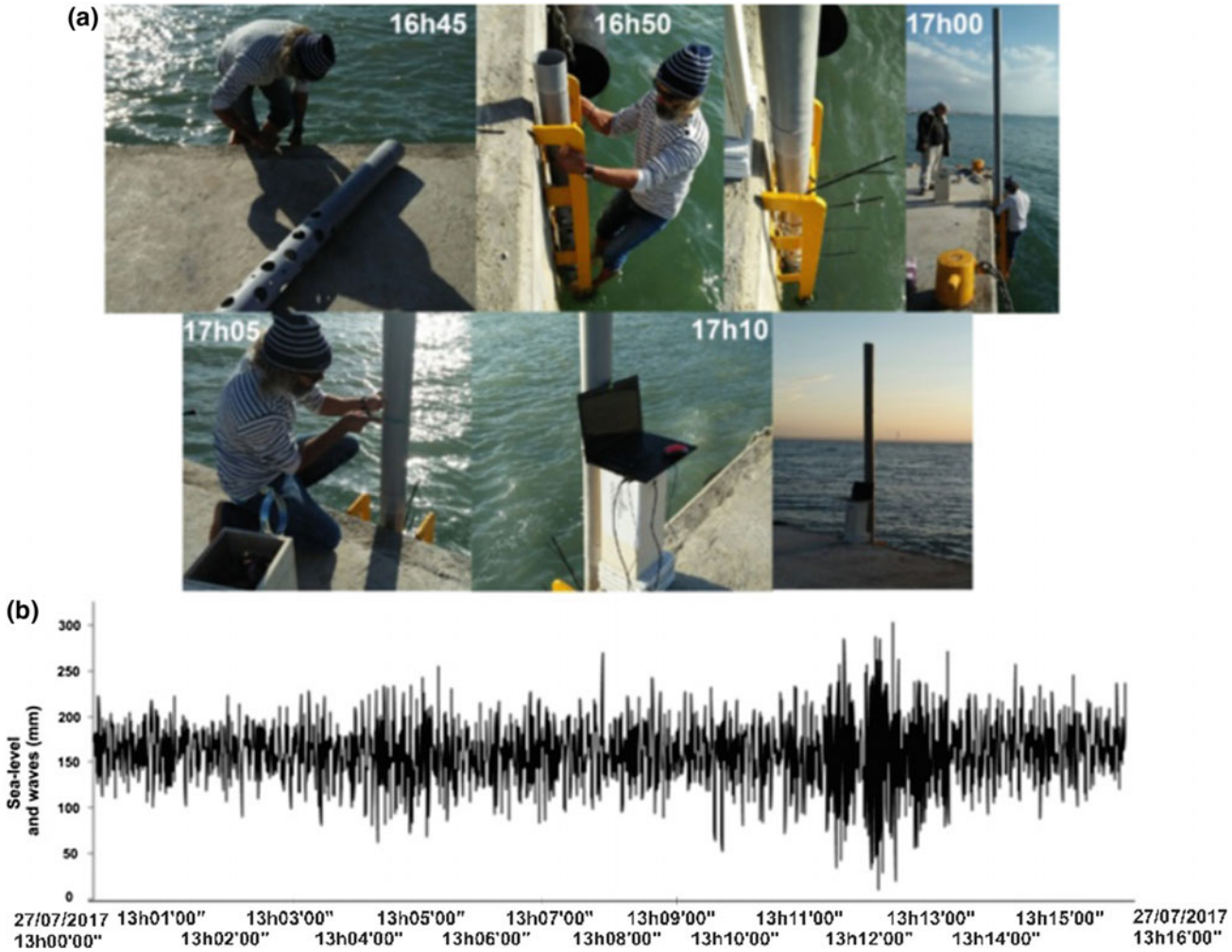

Fig. 1 **a** Less than 1 h for RTG_{HF} installation. **b** Example showing 16 min of sea-level recording obtained by RTG_{HF}. Thanks to rotational system, high frequency oscillations are easily detected [8]

estimating the period necessary for the device maintenance especially against biofouling. Moreover, more tests are necessary to increase performance and durability of this proposed solution. Finally, it would be interesting to compare our instrument against other instruments to check the results given by different methods of sea level recording.

References

1. Hemdane, Y.: Algerian Patent. N° DZ Patent: 9539. Echelle de marée cylindrique codifiée/houlographe à lecture directe et automatique des oscillations marines de hautes fréquences (2016)
2. Hemdane, Y., Bouhamadouche, M., Atroune, F., Meghraoui, M.: Very low cost high frequency tide gauge: the Rotary Tide Gauge—Tsunamis, meteotsunamis/seiches, harbor oscillations, waves/swell and tide observations. Final meeting 6th–8th April 2017—Mallorca, Baleares. Assessment, strategy and risk Reduction for Tsunamis in Europe (2017)
3. http://unesdoc.unesco.org/images/0014/001477/147773e.pdf
4. http://refmar.shom.fr/documentation/instrumentation/echelle-de-maree
5. CN 201628523 U: Intelligent barcode ruler. https://worldwide.espacenet.com/publicationDetails/biblio?CC=CN&NR=201628523U&KC=U&FT=D
6. CN 202024806 U: Underground water level observation device. https://patents.google.com/patent/CN202024806U/en?oq=cn+202024806+u
7. Hannah. J.: The difficulties in using tide gauges to monitor long-term sea level change. International Federation of Surveyors. Article of the Month. July 2010. https://www.fig.net/resources/monthly_articles/2010/july_2010/july_2010_hannah.pdf
8. Tests carried out with the help of RECIFS association (Tamentfoust. Alger)

Part VII
Climate Change Impacts and Migration Schemes

Economic Impact of Sand and Dust Storms on the Oil Sector in Kuwait

Ali Al-Hemoud and Safaa Al-Awadhi

Abstract

There is a lack of published research on sand and dust storms (SDS) impact on the economy worldwide, and particularly in Kuwait. The economic performance of the oil sector in Kuwait during sand and dust storms was evaluated during 2009–2017. Kuwait SDS events restrict or delay oil explorations and drillings, production and operations, marine transports and other associated activities. It was found that a total of 129 SDS events occurred between the years 2001 and 2016. All of these activities and disruptions imposed costs on the oil sector economy and, based on actual data provided from both Kuwait Oil Company (KOC) and Kuwait Gulf Oil Company (KGOC), estimates were made for both the time delay and the annual costs of SDS to the economy. For the nine-year period, from 2009 to 2017, the total time delay was estimated to be 14,941.15 h, while the annual estimated cost was 489,993 KD due to restrictions in multiple oil operations, of which 56% (276,087 KD) was attributed to exploration and drilling activities. One of the challenges identified in this study is the lack of data, economic or physical, in some sectors of the economy, thus the 489,993 KD (equivalent to 70,000 KD per year) would represent only the minimum cost imposed on the Kuwait economy by SDS events.

Keywords

Sand and dust storms • Oil sector • Economic impact Kuwait

1 Background and Introduction

Kuwait, like many countries in western Asia and the Middle East, is subject to sand and dust storms (SDS) throughout the year. Many of the SDS events that impact Kuwait come from the northwestern part of the country, and transport sand and dust from close neighboring countries, specifically Iraq and Saudi Arabia. Nonetheless, many SDS sources and trajectories to Kuwait come from other countries, including Iran, Turkey, and Egypt [1–3].

Research on the economic impacts of SDS is relatively limited, and national level analysis is virtually non-existent. Huszar and Piper [4] studying the off-site costs of wind erosion in New Mexico, USA estimated the total costs at $466 million, with the majority of the costs borne by households for interior and exterior cleaning and landscaping repair. The economic impact of SDS also depends on the level of economic activities within the affected countries [5]. SDS containing associated pollens, radionuclide, mineral and trace metal elements were also linked to the socioeconomic effects of DSD in Kuwait [6]. Meibodi et al. [7] estimated that the total cost of SDS on Iran and Iraq economies to be around $1 billion and $1.4 billion, respectively.

2 Method

SDS data were collected from two major Kuwait oil companies, namely: Kuwait Oil Company (KOC) for nine years (2009–2017) and Kuwait Gulf Oil Company (KGOC) for five years (2011–2015) related to the total estimated cost and the non-productive lost time for all SDS events. The data were analyzed using Microsoft Excel and later graphed and summarized.

A. Al-Hemoud (✉) · S. Al-Awadhi
Crisis and Decision Support Program, Environment and Life Sciences Research Center, Kuwait Institute for Scientific Research, 13109 Safat, Kuwait
e-mail: ahomood@kisr.edu.kw

Z. Zhang et al. (eds.), *Patterns and Mechanisms of Climate, Paleoclimate and Paleoenvironmental Changes from Low-Latitude Regions*, Advances in Science, Technology & Innovation, https://doi.org/10.1007/978-3-030-01599-2_36

3 Results

3.1 Sand and Dust Storm Events

Figure 1 shows the number of Kuwait SDS events that occurred between 2001 and 2016. The total number frequency during this 16-year period was calculated to be 129 SDS events with an average of 8 SDS events per year. The highest SDS events occurred during 2008 (23 SDS) and the lowest was recorded during 2002 (only 1 SDS).

3.2 Estimated Cost and Lost Time for KGOC Due to SDS

The estimated cost and lost time for KGOC during 2011–2015 is shown in Fig. 2. The maximum estimated cost (64,689 KD) was found to be for the year 2015, while the minimum estimated cost was for the year 2012 (50,871 KD).

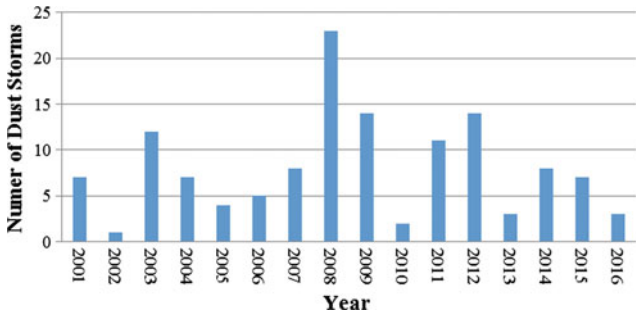

Fig. 1 Number of SDS events in Kuwait (2001–2016)

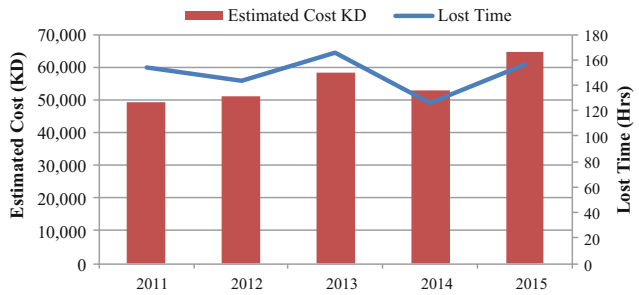

Fig. 2 Estimated cost and lost time for KGOC (2001–2015)

As for the lost time, it was found that 2013 had the maximum amount of lost time (165 h), while the minimum lost time was for the year 2014 (127 h).

3.3 Estimated Cost and Lost Time for KGOC and KOC

Table 1 details the lost time and estimated costs for both KGOC and KOC operations. The KGOC data analysis shows that the total amount of lost time affected the exploration and drilling activities, and was equivalent to 746 h costing the oil sector economy a total loss of 276,087 KD between the years 2011 and 2015.

As for KOC, the deep drilling and completion operations, rig operations, and field operations incurred a total cost of 213,906 KD with a total of 602.75 lost hours for the eight-year period from 2009 to 2016. Other major activities within KOC such as production, excavation and transportation, drilling and technology, painting, project management, health and environment, and port operations have suffered from SDS events with a total lost time of 13,592.4 h between the years 2010–2017. The cost estimation for the lost time, however, was not calculated. The total estimated cost for both companies, KGOC and KOC, was equal to roughly half million KD (489,993 KD) as a minimum with a total amount of lost time of 14,941.15 h.

4 Discussion

SDS events have detrimental effects on the oil drilling and production activities in Kuwait. There are eight oil companies in Kuwait with various operations, ranging from drilling, production, processing and export. Only two companies, KGOC and KOC, which have adequate records of loss data related to SDS events contributed to this study. The total estimated cost of SDS events on Kuwait's economy during a nine-year period (2010–2017) was calculated to be roughly half a million KD (equivalent to $1.5 million) with a lost time of about 15,000 h, as a minimum. A single SDS event may last from 15 min to over 24 h, and as a result different economic impacts are incorporated. The results of this study were presented in the thirteenth session of the conference of parties (COP-13) that was held in Magnolia during 4–16 September, 2017.

Table 1 Lost time and estimated cost for the KGOC and KOC

Sector	Year	Lost time (h)	Estimated cost (KD)
KGOC			
Exploration and drilling	2011	154	49,420
	2012	143	50,871
	2013	165	58,195
	2014	127	52,912
	2015	157	64,689
Subtotal		746	276,087
KOC			
Deep drilling and completion operations	2015–2016	32.5	18,525
Rig operation	2010–2015	468.25	161,786
Field operations	2009–2015	102	33,595
Subtotal		602.75	213,906
Production	2010–2017	9854.4	N.A.
Excavation and transportation	2016	52.5	N.A.
Drilling and technology	2015-2017	205	N.A.
Painting	2014	231	N.A.
Project management	2010–2014	328.5	N.A.
Health and environment	2010–2016	2091	N.A.
Port operation	2016	830	N.A.
Subtotal		13,592.4	N.A.
Grand total (KGOC + KOC)		14,941.15	489,993

5 Conclusion

The objective of this study was to assess the economic impact of SDS events on Kuwait oil sector economy. The total cost of SDS events during a nine-year period (2009–2017) was estimated at half a million KD (equivalent to $1.5 million) with a lost time of about 15,000 h, as a minimum. To measure the SDS impact on the economy of Kuwait more accurately, it would be necessary to undertake a more comprehensive analysis utilizing surveys, interviews, and international records covering the entire spectrum of production and service sectors.

References

1. Al-Dousari, A., Doronzo, D., Ahmed, M.: Types, indications and impact evaluation of sand and dust storms trajectories in the Arabian Gulf. Sustainability **9**, 1526 (2017)
2. Cao, H., Amiraslani, F., Liu, J., Zhou, N.: Identification of dust storm source areas in West Asia using multiple environmental datasets. Sci. Total Environ. **502**, 224–235 (2015)
3. Yassin, M.F., Almutairi, S.K., Al-Hemoud, A.: Dust storms backward Trajectories' and source identification over Kuwait. Atmospheric Research (2018)
4. Huszar, P.C., Piper, S.L.: Estimating the off-site costs of wind erosion in New Mexico. J. Soil Water Conserv. **41**, 414–416 (1986)
5. Al-Hemoud, A., Al-Sudairawi, M., Neelamanai, S., Naseeb, A., Behbehani, W.: Socioeconomic effect of dust storms in Kuwait. Arab. J. Geosci. **10**, 18 (2017)
6. Al-Dousari, A.M., Aba, A., Al-Awadhi, S., Ahmed, M., Al-Dousari, N.: Temporal and spatial assessment of pollen, radionuclides, minerals and trace elements in deposited dust within Kuwait. Arab. J. Geosci. **9**, 95 (2016)
7. Meibodi, A.E., Abdoli, G., Taklif, A., Morshedi, B.: Economic modeling of the regional polices to combat dust phenomenon by using game theory. Proc. Econ. Financ. **24**, 409–418 (2015)

Spatial and Temporal Variations of Bare Land in Beijing, China: A 30-Year Analysis

Yating Chen and Aobo Liu

Abstract

Bare land can be used as an indicator of urbanization. It can be accurate, fast, and low-cost to acquire the distribution and temporal-spatial variations of bare land with remote sensing technology. Over the last 30 years, the rapid urbanization processes of Beijing may have introduced bare land in urban areas. In this study, we take advantage of high-spatial resolution Landsat archive with long-term record to extract the bare land areas in Beijing. Then the temporal-spatial evolution of bare land area in winter and summer for 16 districts and 4 functional zones of Beijing are analyzed. We find that the bare land area in Beijing was reduced by about 600 km^2 between 1987 and 2016. Changes in bare land are caused by the urban development process. Bare land is mainly distributed in new urban development zone and ecological conservation zone. Finally, we proposed some suggestions for controlling the bare land in winter, which would help to mitigate environmental hazard such as dust emission and soil loss caused by exposed bare land.

Keywords

Bare land • Dust source • Beijing • Landsat

1 Introduction

Bare land includes non-vegetated farmland, unhardened land (not covered by buildings or roads), dried up river valley, construction site, etc. The climate in Beijing is characterized by semi-humid warm temperate continental monsoon climate, which is hot and rainy in summer, cold and dry in winter. The surface soil will be exposed during the dormancy period of covered vegetation, thus led to a potential source of PM_{10} emissions. Exposed soil under natural conditions is prone to erosion by strong winds, which cast irreversible impacts on regional environment, such as land degradation and air pollution [1]. Therefore, the distribution of bare land and its temporal-spatial changes are of great significance to regional ecological construction and the improvement of environmental protection strategies in Beijing.

In this study, Beijing is divided into four functional zones based on the development plan (Fig. 1). We will take advantage of high-spatial resolution Landsat archive with long-term record to identify and estimate the main types, areas, and distribution of bare land in Beijing. Then the temporal-spatial variations of bare land area during the past three decades and the evolution patterns behind are analyzed, followed with some relevant suggestions for controlling the exposed soil in suburbs.

2 Materials and Methods

In order to characterize the spatial-temporal variation of bare land, Landsat remote sensing data are used to identify bare soil area from 1987 to 2016. In order to reduce the impact and interference of the cloud, cloud cover was restricted to a maximum of 15%. Based on Bands 1–5 for Landsat 7 and bands 2–6 for Landsat 8 (Table 1), the enhanced bare soil index (EBSI) [2] is extracted by bare soil index (BSI), modified normalized difference water index (MNDWI) and the soil adjusted vegetation index (SAVI).

3 Results and Discussion

We fitted the overall changes in bare land area of Beijing during the past 30 years, with linear and cubic polynomial regressions (Fig. 2). The linear function shows that the bare

This research is supported by National Key Science Programme for Global Change Research 2015CB953602.

Y. Chen (✉) · A. Liu
College of Global Change and Earth System Science, Beijing Normal University, 100875 Beijing, China
e-mail: chenyt2016bnu@gmail.com

Z. Zhang et al. (eds.), *Patterns and Mechanisms of Climate, Paleoclimate and Paleoenvironmental Changes from Low-Latitude Regions*, Advances in Science, Technology & Innovation, https://doi.org/10.1007/978-3-030-01599-2_37

Table 1 Spatial data sources used in this research

Data	Time of observation	Spatial resolution (m)	Number of images[a]
Landsat-5 (TM)	1987.01 ~ 1999.06	30	68
Landsat-7 (ETM+)	1999.07 ~ 2003.04	30	21
Landsat-5 (TM)	2003.05 ~ 2011.07	30	53
Landsat-7 (ETM+)	2011.08 ~ 2013.04	30	9
Landsat-8 (OLI)	2013.05 ~ 2016.12	30	24

[a]Cloud cover was restricted to a maximum of 15%

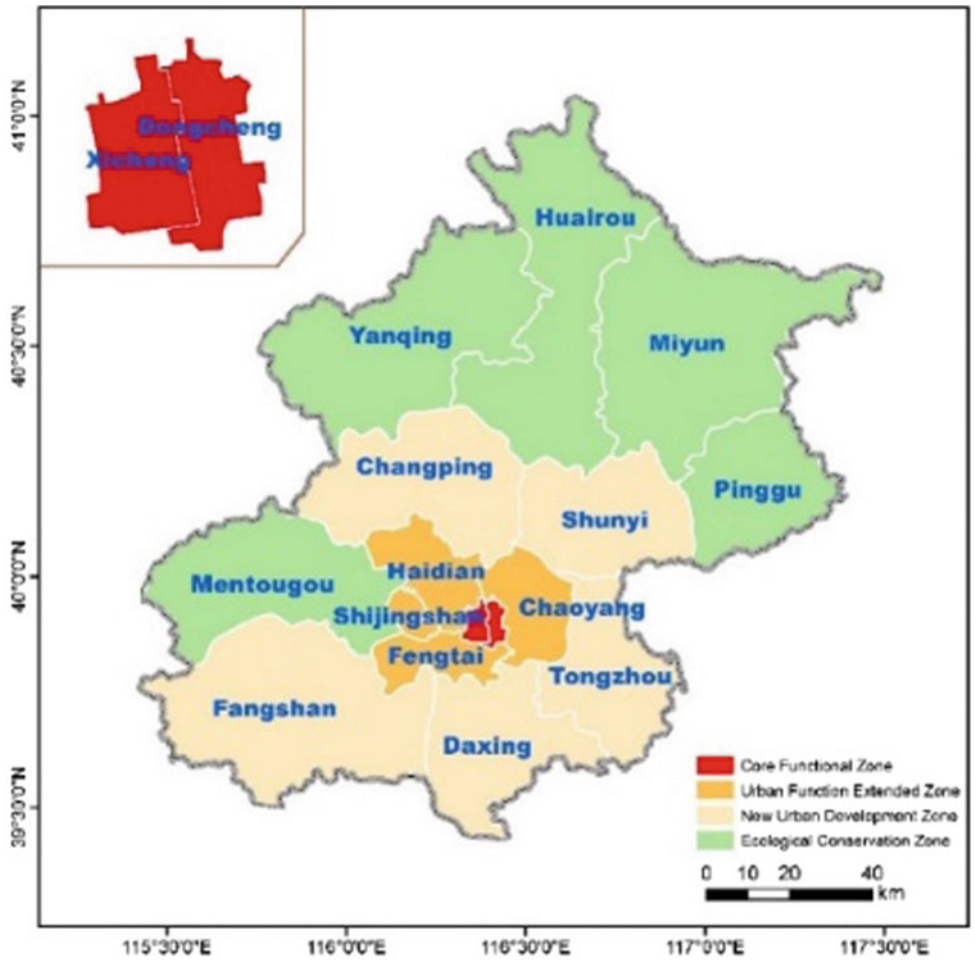

Fig. 1 Sixteen districts in Beijing

land area has a slight decreasing trend, decreasing by approximately 177 km^2 per decade. According to R^2, the cubic-polynomial model fits better than the linear model (R^2 = 0.82 vs. 0.38). The cubic-polynomial function shows that the bare land area decreases slightly between 1987 and 1996, and increase slightly between 1997 and 2006, then decrease obviously between 2007 and 2016.

Figure 3 shows the overall change of the bare distribution for the past three decades. The overall extent of bare land decreases, and the newly added bare area is mainly concentrated in the urban function extended zone (see Fig. 3a). Rapid urbanization in Beijing may a main driver for the

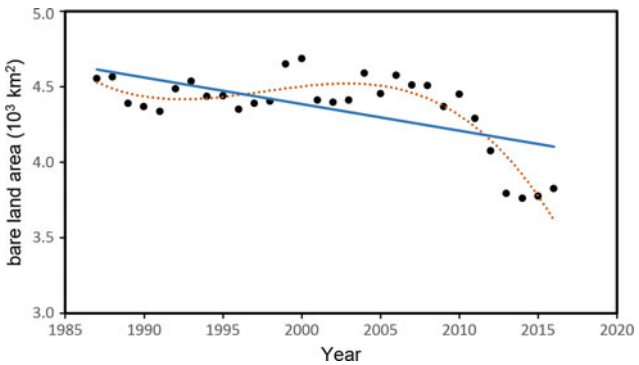

Fig. 2 Change of bare land area in the winter of 1987–2016

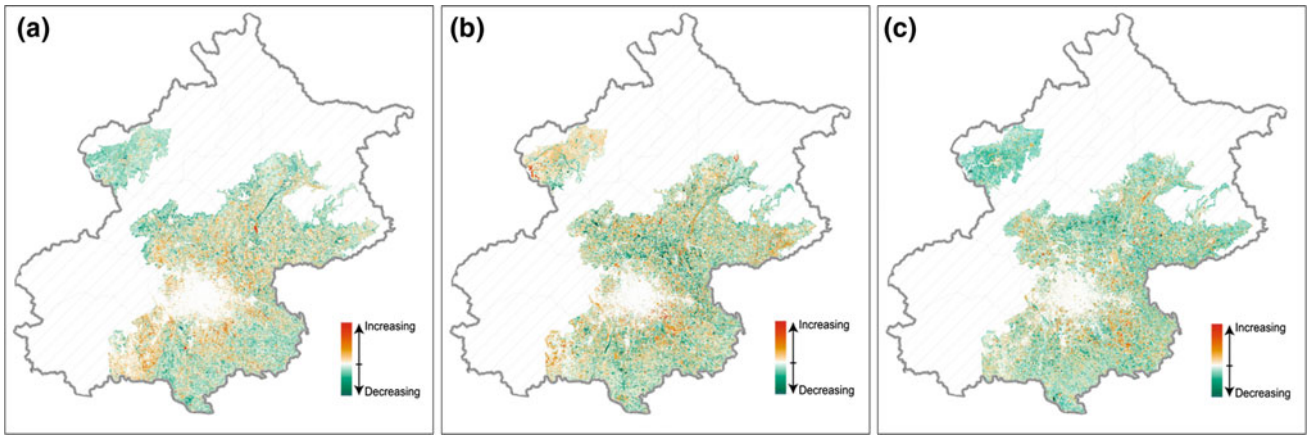

Fig. 3 Change trend in bare land area of Beijing **a** from 1987 to 1996, **b** from 1997 to 2006, and **c** from 2007 to 2016

increasing of bare land area, between 1997 and 2006, the increase in bare areas is mainly due to the development of the Yanqing Plain in the northwest, and the development of the central urban area shows a spread tendency. In 2007, the *2006–2020 Beijing Land Use Planning* began to be implemented through the establishment of ecological conservation zone which helped build a green ring around the city, the plain farmland ecosystem and the mountainous ecological barrier circle. These strategies resulted in a significant reduction in bare land area in the following decade.

In 2016, the bare land area in Beijing reached 3992.1 km^2 in winter and 360.2 km^2 in summer, accounting for 25.1 and 2.3% of total area of Beijing. The bare land area demonstrate a significant seasonal variation, which mainly caused change of vegetation coverage and agricultural activities (e.g. paddy fields fallow periods after harvesting). Seasonal bare land is mainly distributed in the outskirts.

In the core functional zone, there are extremely few bare land area and almost no season change because of its high level of urbanization. In the urban function extended zone,

Table 2 Area of bare land in winter and summer (2016) over different districts in Beijing

Functional region	Districts	Area of districts (km^2)	Bare land area in winter (km^2)	Bare land area in summer (km^2)	Seasonal difference winter-summer (km^2)
Core functional zone	Dongcheng	42.6	0.6	0.6	0.1
	Xicheng	48	0.4	0.4	0.0
Urban function extended zone	Chaoyang	430.5	87.7	19.3	68.5
	Haidian	414.7	80.7	7.1	73.6
	Fengtai	299.2	51.7	8.6	43.0
	Shijingshan	90.6	6.8	1.3	5.5
New urban development zone	Daxing	1013	615.7	49.8	565.9
	Tongzhou	878.2	548.9	74.9	474.0
	Changping	1298.2	305.8	23.2	282.6
	Fangshan	1959.8	198.9	11.4	187.5
	Shunyi	988.9	638.8	73.5	565.3
Ecological conservation zone	Mentougou[a]	1369.1	5.2	1.3	3.9
	Pinggu	915.5	391.9	39.7	352.2
	Miyun	2135.9	396.5	19.4	377.0
	Huairou	2063.7	164.0	9.0	154.9
	Yanqing	1945.8	498.6	20.7	477.9
Total	Beijing	15893.6	3992.1	360.2	3632.0

[a]Ecological conservation zone like Mentougou district has large-scale forest land coverage

the bare land area accounted for 18.4% in winter and 3.0% in summer Because landscape plants seasonally exposed in winter. In new urban development zone, the bare land area is 37.6% in winter and 3.8% in summer. This significant seasonal difference is due to relatively high proportion of cultivated land in the suburbs. In the farmland around Beijing suburbs, cultivated soils are left to be bare in winter and in a highly erodible condition for a relatively long period from harvest of crops in late September to sowing in late April the following year [3]. In the ecological conservation zone, the bare land area is 17.3% in winter and 1.1% in summer. These zone has large area of forest, thus has the smallest proportion of exposed area in Summer (Table 2).

4 Conclusions and Discussion

Over the past three decades, the bare land area in Beijing was reduced by about 600 km^2 ($\sim$13%) between 1987 and 2016. Since future changes of bare land in Beijing are closely related to urban planning, economic development and management policies, it is suggested to promoting the planting of drought-resistant and evergreen vegetation in bare land. At the same time, in order to mitigating negative environmental impacts of bare land, it is suggested to take dust control measures in farmland which would help to lower local atmospheric particulate emissions and improve air quality.

References

1. Hoffmann, C., Funk, R., Reiche, M., et al.: Assessment of extreme wind erosion and its impacts in inner Mongolia, China. Aeolian Res. **3**(3), 343–351 (2011)
2. Wu, Z., Zhao, S.: A study of enhanced index-based built-up index based on landsat TM imagery. Remote. Sens. Land Resour. (2012)
3. Zhang H, Wang X, Zhang J., et al.: Investigation and distributions of the bare lands among gardens and greenbelts in winter within the 5th Ring of Beijing. Science of Soil & Water Conservation, 2017

Appraising Climate Change and Its Influence on Glaciers of South Asian Himalayan Region

Sheikh Saeed Ahmad, Javeria Saleem, and Marria Ghalib

Abstract

Climate change is currently a perilous phenomenon that has deleterious economic, social and environmental impacts. Climatic fluctuations directly affect the hydrology of an area, which in turn plays a significant role in the economy of any country. In South Asia, Himalayan glaciers shrinkage at high elevated areas is more pronounced at unprecedented rates causes major change in seasonal freshwater flow regimes. Therefore, the present study is aimed at reviewing and analyzing the cryosphere dynamics of Himalayan region of South Asia. Glacier retreat has resulted in the increase of the number and size of glacial lakes at exposed end moraines; resulting in glacial lake outburst floods (GLOFs). Nepal and Bhutan are two hot spot areas for Glacier retreat. It is predicted that climate change will continue to proceed, temperature will rise globally in the same way. Thus, there is a need to articulate a coordinated strategy to deal effectively with water management issues and risk of GLOFs events.

Keywords

Climate change • Himalayan glaciers • Deglaciation South Asia

1 Introduction

Climate change affecting glacier fed flow regimes have straight repercussions of freshwater availability and subsequently irrigation and potential power generation [1]. Global warming driven deglaciation resulted in increased incidents of glacial avalanches, flood outbursts, landslides and slope instability. Moreover, direct and indirect implications of glacial retreat altered floodplain patterns and channels accompanied by change in water supply. South Asian high mountains are considered as water tower of Asia due to their vital role as feeders of some of the chief rivers in South Asia [2]. Water resources in the Himalayan region are susceptible to the effect of glaciated masses on its hydrology. Seasonal storage of water in snow and ice acts to delay the timing of runoff. Glacial retreat consequently has a substantial impact on water availability and timing of water availability [3]. This article aimed at analyzing the results of the current research to have a thorough outlook of existing status of cryosphere in South Asian Himalayan region.

The climate of the Himalayan region (South Asia) is principally categorized by strong meridional temperature gradient between the subcontinent of India and high mountains of the Himalayan range. The climatic system of this region is strongly influenced by three circulation systems; Indian Summer Monsoon, Western Disturbances and the East Asian Monsoon. Furthermore, Himalayan region has strong temperature contrast ranging between annual mean temperature below 0 °C over high mountains and over 20 °C in lower plains [4]. Synergistic interactions between circulating systems and the Himalayan range, escalated by elevation, leads to contrasting precipitation gradient in Nepal–Bhutan in the East, accompanied by an even stronger gradient from the Himalaya into the Tibetan Plateau. The eastern glaciers are therefore monsoon influenced, whereas those to the west are chiefly winter accumulating.

2 Climate Change Induced Variations

Change of glacier systems by means of climate change will subsequently affect the water availability [5]. Upstream frozen reserves of Yellow, Yangtze, Indus, Ganges and Brahmaputra basin are affected substantially by climate change. Additionally, livelihood of more than 1.4 Billion people is dependent on these basins. Melt water is exceptionally vital for the Indus basin, important for Brahmaputra

S. S. Ahmad (✉) · J. Saleem · M. Ghalib
Fatima Jinnah Women University, Rawalpindi, 46000, Pakistan
e-mail: drsaeed@fjwu.edu.pk

Z. Zhang et al. (eds.), *Patterns and Mechanisms of Climate, Paleoclimate and Paleoenvironmental Changes from Low-Latitude Regions*, Advances in Science, Technology & Innovation, https://doi.org/10.1007/978-3-030-01599-2_38

basin and a moderately important role for Yellow, Ganges and Yangtze rivers [3].

2.1 Glacier Shrinkage/Deglaciation and Snow Depletion

Climate change has also been reflected in the glacial environment of Himalayan region where recession of glaciers has increased since the 1970s [6]. Chinese Glacier inventory has reported that Chinese glaciers are retreating at high pace with 5.5% shrinking with approximate loss of around 3000 km^2 of snow. It has been predicted that if climate fluctuations persisted in the same way, approximately 67% of the glacier would be recessed by 2050 and all would disappear by 2100 [7]. One of the fastest retreating glacier is Imja glacier where retreat rate was 42 m/year from 1962 to 2000. After 2000 the retreat rate has increased to 74 m/year [6]. The glacier retreat has also been observed in the case of Indian glaciers [8]. Climate change can adversely influence water resources of Nepal. Chief water source of Nepal is summer monsoon precipitation and melting of the reserve of glaciers in the Himalayan highlands [9]. Significant evidence of warming has been found with an average trend of 0.06 °C per year that more pronounced during winters. The increasing temperature has resulted in rapid shrinking of the majority of glaciers in Nepal [10]. Glacial environment of Pakistan has also faced retreat especially Siachen, Baltoro, Raikot due to interaction between warmer atmosphere and frozen water reserves.

Climate change patterns have significantly reduced the glacial mass and enhanced glacier retreat rates. Recent trends validate Bhutan and Nepal to be a hotspot for glacier retreat and loss.

2.2 Glacial Runoff and GLOFs

From all climatic projections it has been observed that the glacier area has shrunken dramatically [11]. Runoff has increased in spring whereas in the months of July and August, a significant decrease in runoff has been recorded [12]. Glacier lake outburst is the leading cause of floods in the South Asian scenario. South Asia is among the most vulnerable regions for floods due to Glacier Lake outbursts [13]. Flooding in this region is initiated by substantial precipitation during monsoon season further aggravated by glacier melting causing heavy water influx. Pakistan, Bangladesh and India are at risk due to the high frequency of severe floods. Climatic variability caused extreme floods, but their frequency is controlled by climate change in South Asia [14] (Table 1).

3 Conclusions

If the global temperature continued to rise in a similar trend as predicted due to climate fluctuations and variations, then it would further amplify the deglaciation, glacial lake outburst and snow cover depletion. Drift related dynamic processes would aggravate the situation to a more complex level for decision makers and policy planners. Furthermore, the global temperature may put a burden on south Asian flow regimes and results in intensification of floods. Climatic change prediction models contain a certain degree of uncertainties; therefore, efforts should be made to integrate multi model downscaling and improved data spanning for climatic predictions.

Table 1 Climate change and predicted hydrological response

River	Basin area (km^2)	Glacial melt in river flow (%)	Climate change indicators	Reference
Indus	1,081,718	44.8	Profound increase in rainfall and river flow	[15]
Ganges	1,016,124	9.1	Minor increase in rainfall	[16]
Yangtze	1,722,193	18.5	Increased precipitation, no significant change in runoff; frequent floods	[17]
Yellow	944,970	1.3	Significantly decreased runoff; no significant change in precipitation	[18]
Brahmaputra	651,335	12.3	Increased runoff; no significant change in precipitation	[19]

References

1. Sorg, A., Bolch, T., Stoffel, M., Solomina, O., Beniston, M.: Climate change impacts on glaciers and runoff in Tien Shan (Central Asia). Nat. Clim. Change **2**(10), 725 (2012)
2. Immerzeel, W.W., Van Beek, L.P., Bierkens, M.F.: Climate change will affect the Asian water towers. Science **328**(5984), 1382–1385 (2010)
3. Rabatel, A., Francou, B., Soruco, A., Gomez, J., Wagnon, P.: Current state of glaciers in the tropical Andes: a multi-century perspective on glacier evolution and climate change. The Cryosphere **7**(1), 81 (2013)
4. Wiltshire, A.J.: Climate change implications for the glaciers of the Hindu Kush, Karakoram and Himalayan region. The Cryosphere **8** (3), 941–958 (2014)
5. Wilson, A.M., Gladfelter, S., Williams, M.W., Racoviteanu, A.: High Asia: the international dynamics of climate change and water security. J. Asian Stud. **76**(2), 457–480 (2017)
6. Bolch, T., Kulkarni, A., Kaab, A., Huggel, C., Paul, F., Cogley, J. G., Bajracharya, S.: The state and fate of Himalayan glaciers. Science **336**(6079), 310–314 (2012)
7. Yao, T., Pu, J., Lu, A., Wang, Y., Yu, W.: Recent glacial retreat and its impact on hydrological processes on the Tibetan Plateau, China, and surrounding regions. Arct. Antarct. Alp. Res. **39**(4), 642–650 (2007)
8. Dobhal, D.P., Mehta, M., Srivastava, D.: Influence of debris cover on terminus retreat and mass changes of Chorabari Glacier, Garhwal region, central Himalaya, India. J. Glaciol. **59**(217), 961–971 (2013)
9. Upreti, B.N., Dhakal, S., Bhattarai, T.N., Adhikari, B.R., Bajracharya, S.R., Yoshida, M.: Climate change impact on glacier retreat and local community in the Langtang Valley, Central Nepal. J. Dev. Innov. **1**(1), 45–59 (2017)
10. Shrestha, A.B., Aryal, R.: Climate change in Nepal and its impact on Himalayan glaciers. Reg. Environ. Change **11**(1), 65–77 (2011)
11. Casassa, G., López, P., Pouyaud, B., Escobar, F.: Detection of changes in glacial run-off in alpine basins: examples from North America, the Alps, central Asia and the Andes. Hydrol. Process. **23** (1), 31–41 (2009)
12. Huss, M., Farinotti, D., Bauder, A., Funk, M.: Modelling runoff from highly glacierized alpine drainage basins in a changing climate. Hydrol. Process. **22**(19), 3888–3902 (2008)
13. Aggarwal, S., Rai, S.C., Thakur, P.K., Emmer, A.: Inventory and recently increasing GLOF susceptibility of glacial lakes in Sikkim, Eastern Himalaya. Geomorphology **295**, 39–54 (2017)
14. Mirza, M.M.Q.: Climate change, flooding in South Asia and implications. Reg. Environ. Change **11**(1), 95–107 (2011)
15. Singh, P., Kumar, V., Thomas, T., Arora, M.: Changes in rainfall and relative humidity in river basins in northwest and central India. Hydrol. Process. **22**(16), 2982–2992 (2008)
16. Nepal, S., Shrestha, A.B.: Impact of climate change on the hydrological regime of the Indus, Ganges and Brahmaputra river basins: a review of the literature. Int. J. Water Resour. Dev. **31**(2), 201–218 (2015)
17. Su, B., Huang, J., Zeng, X., Gao, C., Jiang, T.: Impacts of climate change on streamflow in the upper Yangtze River basin. Clim. Change **141**(3), 533–546 (2017)
18. Zhang, Y., Su, F., Hao, Z., Xu, C., Yu, Z., Wang, L., Tong, K.: Impact of projected climate change on the hydrology in the headwaters of the Yellow River basin. Hydrol. Process. **29**(20), 4379–4397 (2015)
19. Milliman, J.D., Farnsworth, K.L., Jones, P.D., Xu, K.H., Smith, L. C.: Climatic and anthropogenic factors affecting river discharge to the global ocean, 1951–2000. Glob. Planet. Change **62**(3–4), 187–194 (2008)

World Population: Its Connection with Climate Variations

Alexey V. Byalko

Abstract

The world population data were analyzed from 1 AD to 2015 whereas those related to temperature variations of the Northern Hemisphere they were studied from 1 AD to 1979. Possible data errors were estimated. The hyperbolical behavior of the world population was evaluated by approximation of its inverse function. The population index was introduced as the relative difference between the inverse numerical data and its parabolic approximation. The index happens to be a bounded function; its average value is close to zero; its error level seems to be nearly uniform. The index describes variations of the world population in the past. The population index was compared with the North Hemisphere temperature variations. During the last millennia, the climate warming seems to stimulate the world population growth while its cooling leads to decrease this growth and even to decrease the population number. However, the population response to temperature variations occurred with a significant delay of about 100 years. Possible reasons for this delay were discussed against the background of known historical events and analyzed by the Hurst method. The historical analysis and the revealed climate—population correlation could give a principal possibility to forecast the world population behavior approximately up to 2080. However, the actual forecast appears to be reliable to the years 2060–2065 only.

Keywords

World population • Approximations • Climate changes Correlations

1 Introduction

Humanity is a unique biological species. Its number grew anomalously fast, close to the hyperbolic law. There are no other examples of hyperbolic growth in biology. But recently, another dangerous feature has arisen: humanity has been able to change the environment so much that this has led to a climate warming. That is why it is of interest to compare the population and climate behaviors in the past.

In the middle of the last century, Heinz von Foerster (1911–2002) first observed that the number of mankind $N(t)$ increases with a reasonable accuracy according to the hyperbolic law asymptotically tending to infinity [1]. Such a dependence obeys the differential equation $dN/dt = N^2/K$ where K is some constant with dimension of people-times-year. The solution of this equation is $N(t) = K/(t_0 - t)$, where t_0 is the moment of asymptotic infinity. Comparison with the data on the population number known in the middle of the last century gave Foerster the value of the limiting time t_0 equal to the year 2026.9 ± 5. Naturally, when approaching this limit, deviations from hyperbolic growth should have increased.

A long time after the appearance of Forster's idea, deviations from the hyperbole have become noticeable and the data on the past world population were refined. An extensive literature arose on this subject, and we can mention articles and books [2–6] and specially those of Kapitza [7, 8]. The authors of these works have offered reasonable explanations for the hyperbolic behavior of mankind population. However, since there is no possibility to verify these theories by an experiment or some independent model, it is difficult to treat them other than interesting social hypothesis. In this paper, we did not discuss this topic; instead we proposed a mathematically simple method for studying the population dynamics in the past. Its result is a time-varying population index which can help for further research, in particular, for comparison purposes between this index and the climate changes in the past and possibly for establishing predictions for the future.

A. V. Byalko (✉)
Landau Institute for Theoretical Physics RAS, Moscow, Russia
e-mail: alexey@byalko.ru

A. V. Byalko
Priroda Journal, Moscow, Russia

Z. Zhang et al. (eds.), *Patterns and Mechanisms of Climate, Paleoclimate and Paleoenvironmental Changes from Low-Latitude Regions*, Advances in Science, Technology & Innovation, https://doi.org/10.1007/978-3-030-01599-2_39

2 Sources and Methods

We studied the world population time dependencies $N(t)$ for the time span from 1 AD to the present taken from different sources [9–11]. The World Bank Data [9] are taken as the most representative while the others were used for error estimates.

The inversion of hyperbolic dependence becomes a linear function of time. Thus, it is reasonable to study the time dependence of inverse world population number $N(t)^{-1}$ [12]. This value is proportional to the Earth area per one person. The parabolic approximation of the inverse population number calculated by the method of least squares is

$$A(t) = 0.04053(t - t_0) - 7.1310^{-7}(t - t_0)^2. \quad (1)$$

Here $t_0 = 2063 \pm 5$, which is sufficiently greater than the Foerster and Kapitza results.

Let us calculate a relative difference $I_{WP}(t)$ between the actual inverse population $N^{-1}(t)$ and its parabolic approximation $A(t)$:

$$I_{WP}(t) = N(t)^{-1}A(t)^{-1} - 1. \quad (2)$$

The result happens to be a bound function: $-0.3 < I_{WP}(t) < 0.6$; its average value $\langle I_{WP}(t)\rangle \approx 0$ happens to be close to zero. Moreover, if possible errors of $N(t)$ are taken into account, then correspondent deviations from $I_{WP}(t)$ happen to be nearly uniform. Therefore, the function $I_{WP}(t)$ could be useful as a characteristic measure for intensity of population changes. For this reason, we called it the world population index.

3 Results

Let us compare the population index curve with the moved averaged climate data of the Northern Hemisphere [13] from 1 AD to 1979. Both functions have a set of consequent maxima and minima (Table 1).

During the first millennium AD there was no great temperature and population index deviations; both were inside their error levels. The first significant temperature maximum occurs in the eleventh century; it is called the Medieval Climate Optimum. The correspondent maximum of population arose rather soon: the growing density of population was a possible cause of twelfth–thirteenth centuries crusades.

Next temperature minimum of 1297 was followed by the Great Hunger of 1315 and the "black death" plague caused a significant population decrease. A slow recovery happened only 150 years after minor warming in the beginning of the fifteenth century.

A deep temperature minimum of the sixteenth–seventeenth centuries is known as the Little Ice Age. The consequent population minimum happened nearly at the end of seventeenth century.

4 Discussion

The average time lag between temperature and population changes occurs to be equal to 105 ± 23 years. At first glance, such a delay seems to be too large to be a cause for population changes. However, there are some reasons.

First. Climate changes do not immediately lead to observable changes of life conditions. A human society needs some period to accumulate wealth in the case of growing temperature and good harvest. Contrary, in the case of cold climate or sudden pandemic the life expectancy is long supported by accumulated wealth spending. Such accumulation periods may last about 50 years. It is only after that the birth rate begins either to grow in the case of climate warming or decrease after cooling. The analysis of long memory situations can be achieved by the mathematical method proposed by Hurst and Mandelbrot [14].

Second. Changes of the world population do not occur simultaneously with the birth rate changes. They are also delayed by the life expectancy estimated at about two

Table 1 Temperature and population index extremes

Extremes	Temperature, year AD	Population, year AD	Time delay, year
Max 1	1102	1165	63
Min 1	1297	1430	103
Max 2	1412	1561	149
Min 2	1589	1686	97
Max 3	1779	1900	121
Min 3	1821	1918	97

generations. The sum of these two delays can explain the time differences in Table 1.

5 Conclusions

Through history, cooling was treated as a "bad" event while warming was "good". This is no longer true nowadays. At present there is a sharp contradiction between unprecedented climate warming and the population index decrease caused by approaching the asymptotical limit t_0. There is no historical example for such a growing discrepancy.

As we have seen the population numbers inertia is about the life expectancy. It means some reasonable predictions of human population in principle can be achieved up to the year 2080. However, the actual forecast occurs to be reliable up to 2060–2065 only. The Paris climate agreement made a climate prognosis up to the end of the current century. However, the world population changes including its possible decrease may occur rather earlier. The future of humanity seems to be unstable.

References

1. von Foerster, H., Mora, P., Amiot, L.: Doomsday: Friday, 13 November, A.D. 2026. At this date human population will approach infinity if it grows as it has grown in the last two millennia. Science **132**, 1291–1295 (1960)
2. Pollard, J.H.: Mathematical Models for the Growth of Human Populations. Cambridge University Press, Cambridge (1973)
3. May, R.: Chaos and dynamics of biological populations. Dynamic chaos. Proc. R. Soc. Lond. A **413**(1844), 27–44 (1987)
4. Cohen, J.: How Many People Can the World Support? Norton, New York (1995)
5. Haub, C., Yanagisita, M.: World Population Data Sheet. Population Reference Bureau, Washington (1995)
6. McLaren, D.: Population growth—should we be worried? Popul. Environ.: J. Interdiscipl. Stud. **17**(3), 243–259 (1996)
7. Kapitza, S.P.: World population growth as a scaling phenomenon and the population explosion. In: Rosen, L., Glasser, R. (eds.) Climate Change and Energy Policy. AIP, New York (1992)
8. Kapitza, S.P.: Population Growth, Sustainable Development and the Environment. World Culture Report. Culture, Creativity and Markets. UNESCO (1998)
9. World Bank Data: https://datacatalog.worldbank.org/search/datasets?search_api_views_fulltext_op=AND&query=world+population. Accessed 21 Dec 2017
10. Worldometers Homepage: http://www.worldometers.info/. Accessed 11 Feb 2018
11. WikipediA: https://en.wikipedia.org/wiki/World_population. Accessed 21 Mar 2018
12. Byalko, A.V., Kauffman, G.B.: Predicting our global future. Chem. Educ. **17**, 195–202 (2012)
13. Moberg, A., Sonechkin, D.M., Holmgren, K., Datsenko, N.M.: Highly variable Northern Hemisphere temperatures reconstructed from low- and high-resolution proxy data. Nature **433**, 613–617 (2005)
14. Graves, T., Gramacy, R., Watkins, N., Franzke, C.: A brief history of long memory: Hurst, Mandelbrot and the road to ARFIMA, 1951–1980. Entropy **19**, 437–458 (2017)

Groundwater Resources Sustainability in Africa Under a Climate Change Scenario: Knowledge Gaps and Needs

Ahzegbobor P. Aizebeokhai, Kehinde D. Oyeyemi, and Adebola E. Adeniran

Abstract

Climate change induced effects on surface-water resources in Africa have been widely reported. However, characterising climate change effects on groundwater resources in the continent is largely complicated due to uncertainty and multi-scale heterogeneity in climate models. Thus, there is need to evaluate groundwater resources availability and sustainability in the continent under climate change scenario. This paper is an assessment of sustainable development and management of groundwater resources in Africa in relation to climate change. Current knowledge gaps and needs on climate change effects on groundwater resource availability and sustainability in Africa are presented.

Keywords

Climate change • Groundwater resource Sustainability • Knowledge gaps • Africa

1 Introduction

Africa is a large continent with over 30 million km^2 land mass characterized by a wide variety of climate systems ranging from equatorial humid, through seasonally-arid tropical to sub-tropical Mediterranean-type climates. Annual precipitation is estimated at about 20,360 km^3 with a continent wide average of about 700 mm per annum [1]. Groundwater is the primary source of drinking water in most parts of Africa, especially in rural settlements which constitute over 60% of the population [2]. The development of groundwater resources in most parts of Africa is indiscriminate and uncontrolled due to weak or inadequate legislations for the regulation of abstraction and management of the resources, as it is the case in most developing nations.

The vulnerability of surface-water resources to climate change has been widely recognized. Obviously, climate change has important implications for groundwater availability and sustainability, but linking climate change to changes in groundwater systems is complex. The complexity is further exacerbated by population growth and anthropogenic activities due to its increasing threat on groundwater availability and sustainability in the continent. Population growth correlates with groundwater withdrawals, and thus declining groundwater levels, deteriorating quality and associated socio-economic problems; this will further threaten groundwater availability and sustainability. Thus, the need for sustainable management of groundwater resources taking climate change effects into consideration has become inevitable. The present paper is an assessment of groundwater resource availability and sustainability in Africa under climate change scenario; current knowledge gaps and needs are presented.

2 Climate Change and Groundwater Systems

Groundwater occurrence depends on a number of factors including geomorphology, geology and rainfall. These factors determine the availability, accessibility, quality, reliability and sustainability of groundwater. Groundwater may occur as basement or basin aquifers; basement aquifers are notoriously complex, spatially variable localized and confined to weathered and fractured zones of the low permeability igneous and metamorphic rocks. Geophysical techniques are used for an efficient characterization of basement aquifers. Basement rocks are extensively distributed throughout Africa.

Climate projections for the twenty-first century indicate a significant increase in global average temperature resulting in changes in evapotranspiration and precipitation patterns

A. P. Aizebeokhai (✉) · K. D. Oyeyemi · A. E. Adeniran
Applied Geophysics Group, College of Science and Technology, Covenant University, Ota, Nigeria
e-mail: philips.aizebeokhai@covenantuniversity.edu.ng

Z. Zhang et al. (eds.), *Patterns and Mechanisms of Climate, Paleoclimate and Paleoenvironmental Changes from Low-Latitude Regions*, Advances in Science, Technology & Innovation, https://doi.org/10.1007/978-3-030-01599-2_40

(both in the frequency and intensity). There is a considerable uncertainty in climate prediction for Africa. Under medium-to-high green house emission, most models agree on: increased average air temperature; decreased annual rainfall in the northern Sahara and southern Africa; increased annual rainfall in the Ethiopian Highlands; and increased variability of rainfall events both in frequency and intensity, with increasing frequency of extreme events (droughts and floods). Mean warming observed for the twentieth century over the continent is 0.5 °C per decade [3], with significant increased in the last three decades, and is projected to increase by 3–4 °C between 2080 and 2099 than that observed between 1980 and 1999. Increased variability in precipitation is observed in most parts of the continent with drying trends in most of the Sahel. Projected changes in precipitation are less certain than those for temperature, particularly in the Sahel and West African coast. Variability of rainfall events is projected to increase. The already observed mean annual rainfall varies considerably, from near-zero in some parts of the Sahara to about 10,000 mm in the Gulf of Guinea.

2.1 Climate Change Effects on Groundwater Sustainability

Climate change has continued to modify precipitation and evapotranspiration patterns; any change in precipitation and evapotranspiration patterns will directly and/or indirectly affect groundwater availability and sustainability. These changes will directly cause shifts in soil moisture deficits, surface runoff and recharge. Increased evapotranspiration will reduce runoff, soil moisture content and net recharge, with indirect effects on groundwater availability and sustainability. Variation in rainfall patterns will generally affect recharge. This depends on a number of factors including timing, intensity and duration of rainfall in relation to temperature, soil-vegetation conditions and land use.

Estimating recharge and groundwater potential over much of Africa is relatively difficult due to lack of spatial and temporal data. Aquifers with low permeability and limited storage occupy most parts of the land mass (Fig. 1). The continent may be broadly divided into three rainfall (Fig. 2) and/or recharge zones: <200 mm annual rainfall with little or no current recharge; 200–500 mm rainfall with about 5% (25 mm) contributing to recharge annually depending on timing and intensity of rainfall events; and >500 mm annual rainfall with significant recharge (5–10% or 25–50 mm per annum) in most years. This over simplification is based on the available studies. Increased knowledge of recharge mechanisms and aquifer responses to rainfall is required for a more confident extrapolation across the continent.

In regions with <200 mm annual rainfall, groundwater withdrawal will increase, and is not actively replenished through natural recharge. The decreasing recharge will lower the water-table or reduce storage, and thus reduce the base flow to surface-water bodies. Groundwater sustainability in these areas is likely to be threatened by climate change effects [2, 4]. In regions where annual rainfall is between 200 and 500 mm, recharge and abstraction is expected to be balanced; but sufficient recharge may not occur in some years. Any reduction in annual rainfall or changes in the frequency and intensity of rainfall events may cause wells or boreholes failure. Shallow aquifers will particularly be affected in areas with prolonged droughts. In regions with >500 mm annual rainfall, recharge is likely to occur in most years; any reduction in rainfall may not affect recharge significantly but prolonged droughts may cause widespread failure.

3 Sustainable Management Strategies

Groundwater withdrawals have major implications for groundwater sustainability. The effects of abstraction may take a long period before they become evident in many aquifers. Thus, studies are required to understand the effects and support sustainable groundwater management that tends to be neglected. Groundwater resource sustainability is based on water balance or conservation law built on the concept of safe yield: the rate of abstraction over an indefinite period that can be maintained without producing negative effects. This implies limiting pumping to the amount that may be safely harvested without lowering the water-table and/or deteriorating groundwater quality.

Under a climate change scenario, there should be concerted efforts to improve the evaluation of groundwater potential, recharge estimation and quality assessment at national, regional and continent wide scale. Groundwater observatories for long term monitoring should be established across the continent to set up baseline conditions for determining spatial

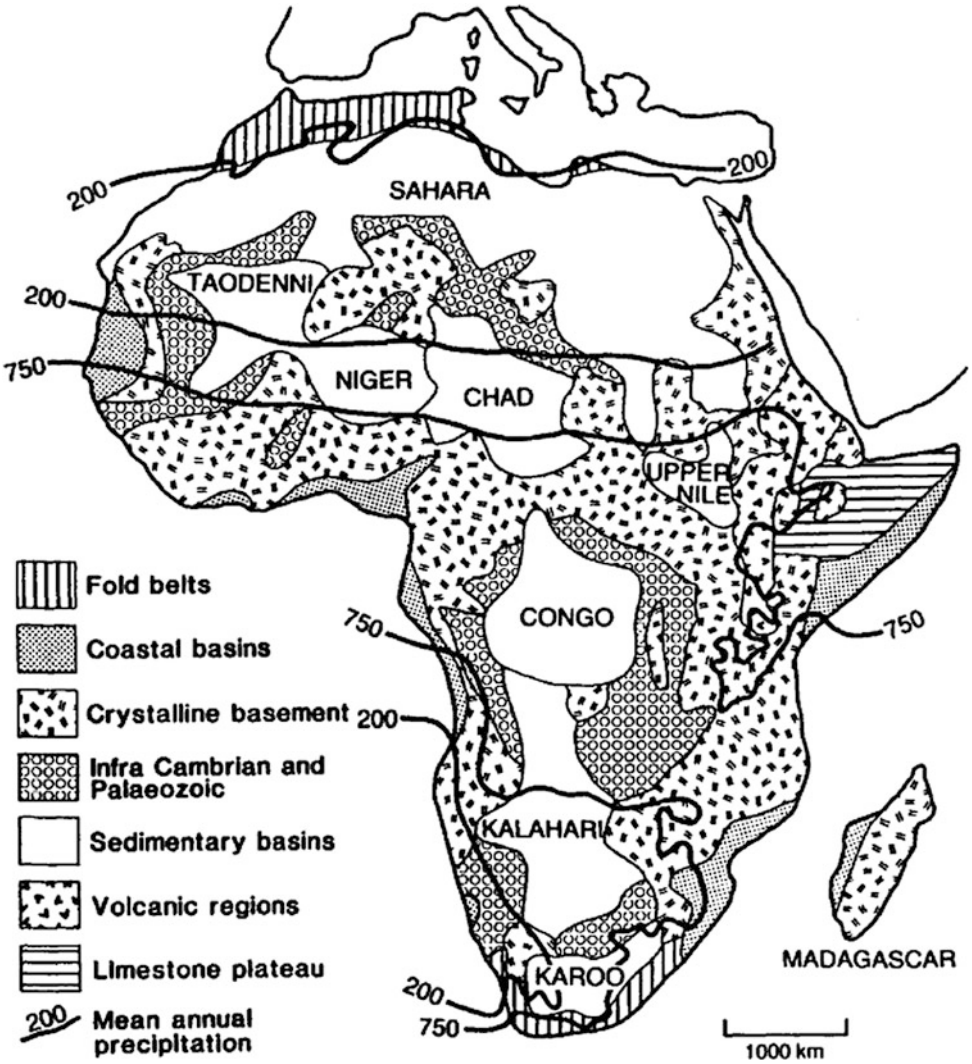

Fig. 1 Groundwater regions in Africa [3]

and temporal variability. Right policies to regulate groundwater abstraction and management should be formulated and implemented. Conjunctive use of surface-water and groundwater resources should be adopted, especially in areas where fresh water resources are already stressed.

4 Knowledge Gaps and Needs

There are huge knowledge gaps and needs in the continent regarding groundwater availability and sustainability in relation to climate change. Climate change effects on groundwater resources are not usually considered while making management decisions. Climate change adaptation should be integrated into water sector policies, planning and management. Studies on groundwater resource evaluation and sustainability, together with the response of groundwater systems to climate change effects, in the continent are relatively scarce. A comprehensive study of groundwater systems is required at local, national, regional and continent wide scale. The responses of principal aquifers to climate change effects should be evaluated on inter-annual to multi-decadal time scale. Numerical models for assessing groundwater response to climate change effects should be developed. Trends in groundwater quality that can be linked to climate change effects should equally be assessed. Also, techniques to predict and control the effects of climate change on groundwater system should be developed.

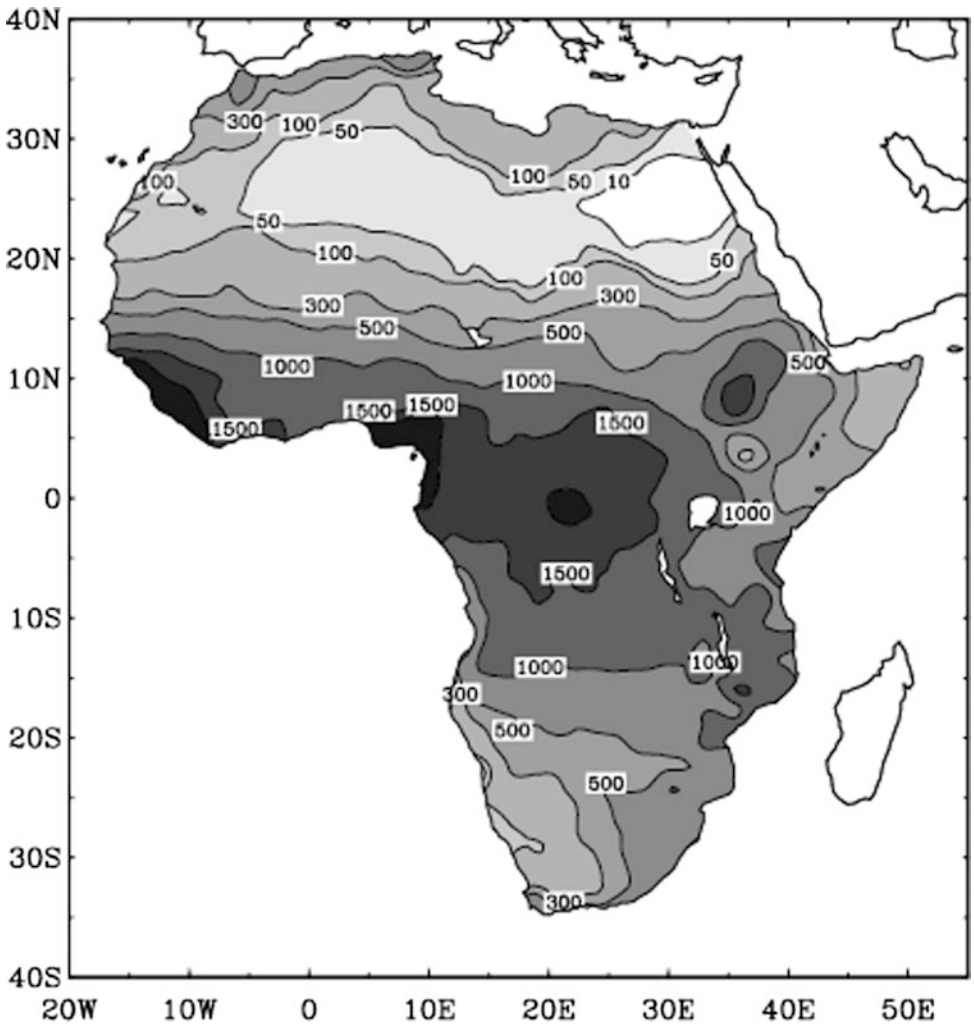

Fig. 2 Mean annual rainfall (mm) distribution over Africa [1]

5 Conclusions

Groundwater resources sustainability in Africa is not only complex but very sensitive. Collective responsibility is required to achieve a sustainable management of the resource. A multi-disciplinary action is required for a continuous monitoring and assessment of the resources. Groundwater may still be substantially affected by climate change even if the present rates of withdrawals do not increase. An appropriate legislation is required to bring useful reforms towards sustainable management of the resource. The populace should be educated on the need for a sustainable utilization of the resource as well as its protection from pollution and contamination.

Acknowledgements Covenant University management is appreciated for providing the conference support.

References

1. Nicholson, S.E.: Climate and environment changes in Africa during the last two centuries. Clim. Res. **17**, 123–144 (2001)
2. Calow, R., MacDonald, A.: What will climate change mean for groundwater supply in Africa. Background note prepared for Overseas Development Institute and British Geological Survey, 8 pp. (2009)
3. Hulme, M., Doherty, R., Ngara, T., New, M., Lister, D.: African climate change: 1900–2100. In: Desanker, P. (ed.) Africa and Global Climate Change. CR SPECIAL 8. Clim. Res. **17**, 145–168 (2001)
4. Fan, Y., Li, H., Miguez-Macho, G.: Global patterns of groundwater table depth. Science **339**, 940–943 (2013)

Adaptation Strategies and Resilience to Climate Change for Warm, Dry-Summer Continental Climate in Iran

Gholamreza Roshan, José A. Orosa, Ángel M. Costa, and Rebeca Bouzón

Abstract

In order to access the process of supply and demand of the energy needed by human settlements to provide thermal comfort in Iran, one warm, dry-summer continental climate station was selected with regard to the recommendations of bioclimatic design for the two periods of 1986–2015 and 2020–2050 was studied. In order to provide bioclimatic solutions, Givoni's correction chart was used in this study. Also, the output of the CanESM2 general circulation model was downscaled using a multi-station metacentric resonance imaging method called SKNN so as to achieve the local values of two components of daily mean of minimum and maximum temperatures and relative humidity in upcoming periods. It should be noted that this study was carried out based on RCP2.6 greenhouse gas emission lines of the fifth report of the Intergovernmental Panel on Climate Change. The findings of this study showed that in all the studied stations, the trend of temperature increase over the coming decades is not unexpected. This will reduce the use of heating strategies and increase the use of different cooling strategies. Also, according to observational and simulated data, it was found that the most important recommendation for the bioclimatic design for these stations is the Internal Gains solution. Finally, the outputs of this research are expected to be used in the area of energy risk management and land use with the global warming approach in Iran.

Keywords

Future climate • Greenhouse gas emissions
Climate responsive design • Energy consumption
Thermal comfort • Iran

G. Roshan (✉)
Department of Geography, Golestan University, Gorgan, Iran
e-mail: r.rowshan@yahoo.com

G. Roshan · J. A. Orosa · Á.M. Costa · R. Bouzón
Energy and Propulsion Research Group, University of a Coruña, ETSNyM Paseo de Ronda 51, Riazor, 15011 A Coruña, Spain

1 Introduction

The Fifth Assessment Report of the Intergovernmental Panel on Climate Change (IPCC) states that climate change is definitely taking place Worldwide. Between 1906 and 2014 the global temperature has increased with 0.56 to 0.92 °C. Despite the uncertainty of future climate scenarios, the IPCC report predicts a temperature increase between 1.1 and 6.4 °C until the end of this century compared to the temperatures in the period of 1980–1999 [1]. The effects of climate change on the built environment and humans recommend the urgency to study, analyze and implement climate change adaption measures at the building scales. Residential buildings in Iran are the largest part of Iran's building stock and are operating in free running mode or rely on personalized heating systems. Therefore, there is a need that buildings provide sufficient protection against heat and avoid as much as possible dual (heating and cooling) active systems. The protection of inhabitants from the climate change impact requires revising passive and bioclimatic design strategies across the country. The climate change adaptation should start by investigating future climate scenarios and prepared climate change weather files. This study builds on previous studies that aimed to define design guidelines and recommendations for urban settlement in Iran [2, 3]. The overarching aim of this study was to improve our understanding of climate change impact and enhance the decision making process of architects and building engineers.

2 Materials and Methods

In order to assess the supply and demand process of the energy needed by human settlements to provide thermal comfort in warm, dry-summer continental climate in Iran, Firoozkooh meteorological station was selected for study taking into account the recommendations of bioclimatic

Z. Zhang et al. (eds.), *Patterns and Mechanisms of Climate, Paleoclimate and Paleoenvironmental Changes from Low-Latitude Regions*, Advances in Science, Technology & Innovation, https://doi.org/10.1007/978-3-030-01599-2_41

design for the two periods of 1986–2015 and 2020–2050. Firoozkooh is located north-east of Tehran, in the middle of Alborz Mountains. It has a warm, dry-summer continental climate where the average coldest month is below 0 °C (32 °F), the average temperature of the warmest month is below 22 °C (71.6 °F) and at least four months averaging above 10 °C (50 °F). In order to provide bioclimatic solutions, Givoni's correction chart was used. The study of Roshan et al. [4] defined 17 design strategies associated with 17 climatic zones in Iran. Also, in order to achieve the local values of two components of daily mean of minimum and maximum temperatures and relative humidity in upcoming periods, the output of the CanESM2 general circulation model was downscaled using a multi-station metacentric resonance imaging method called SKNN. Kim et al. [5] proposed a cluster-based imputation method to simulate the missing values of DNA micro-array data that is called Sequential K-Nearest Neighbor (SKNN) algorithm. This method separates the dataset into two complete and incomplete sets with and without missing values, respectively. The data in an incomplete set are imputed by the order of missing rate that is the missing values are ranked from the fewest number of missing values. Starting with the fewest number of a missing value, it is filled by the weighted mean value of corresponding column of the nearest neighbor of the corresponding row in a complete set. Then taking into account the first imputed value, the process is repeated until all the missing values are imputed. It should be noted that this study was carried out based on RCP2.6 greenhouse gas emission lines of the fifth report of the Intergovernmental Panel on Climate Change. The results of RCP2.6 scenarios were used in order to examine the effects of climate change in the coming decades on different cooling and heating strategies and their results were compared to the current period.

3 Results

Firoozkooh Station is one of the limited stations in Iran that has no need for cooling solutions in the course of the year and these conditions are observed for both observational and simulated periods. What is striking, however, is that according to data from 1986 to 2015, the most important strategy for providing comfort inside buildings was the use of Passive Solar Heating + Humidification with 15% of the frequency of data. For the coming decades, RCP2.6 scenario shows that the main heating bioclimatic recommendation is to use Internal Gains to provide indoor comfort. On the other hand, the use of Passive Solar Heating + Humidification is introduced as the second bioclimatic solution for providing indoor comfort. However, with regard to climate change, the overall RCP scenario' averages used in this study are indicative of a 4% reduction in this zone for decades to come. In some of the bioclimatic recommendations, Qazvin station is is remarked to be similar to Firoozkooh. For the coming decades, the frequency of using Direct and Indirect Evaporative Cooling + High Thermal Mass + Night Ventilation and Direct and Indirect Evaporative Cooling is also almost zero. Interestingly, the observational data show that the most frequent occurrence of data for this station is, respectively, Internal Gains and Passive Solar Heating. In what follows, the findings of Hamedan station were studied. At this station, the most important source of indoor comfort factor is the use of Conventional Heating bioclimatic recommendation, or Conventional Heating, with 21.5% of data frequency. Although this pattern has been repeated for the future, the overall average of the results of RCP2.6 scenario indicates a 2% frequency reduction for the occurrence of this zone. It should be noted that the use of most of the solutions to provide cooling conditions at this station has not been effective, although demand for cooling energy in the coming decades will increase slightly (Fig. 1).

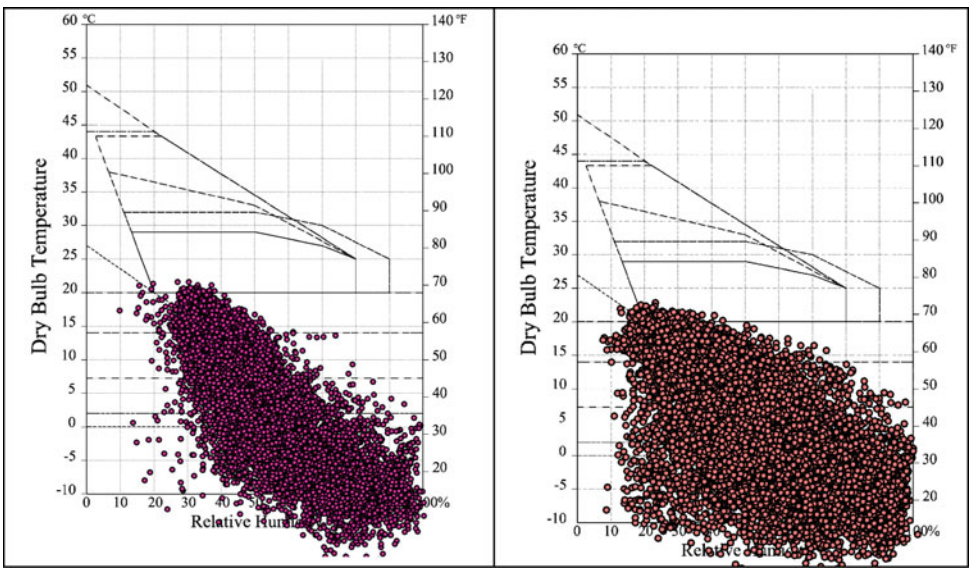

Fig. 1 The distribution of bioclimatic conditions for the current (left) and future (right) periods

4 Discussion and Conclusion

The study results highlight the importance of raising the awareness of the building sector regarding global warming and the cooling needs increase in buildings. The study findings should be extended to investigate the implication of climate change on outdoor microclimate. Therefore, it can be concluded that the occurrence of global warming into Firoozkooh will be accompanied by temperature rise which will reduce the use of heating strategies and increase the use of different cooling strategies. Also, the use of Internal Gains Bioclimatic Recommendation as one of the important strategies for the present and future architecture of buildings in Firoozkooh is recommended. Finally, it is suggested that the effects of global warming on the basis of different models of general circulation of atmospheres be simulated in subsequent studies for Firoozkooh. Using the outputs of these models, different bioclimatic indices and models will be evaluated. Finally, depending on the results that overlap with the different models, the main bioclimatic solutions can be presented in order to adapt and reduce the effect of global warming on the consumption of Indoor heating and cooling energy to provide thermal comfort.

References

1. Stocker, T.F., Qin, D., Plattner, G.K., Tignor, M., Allen, S.K., Boschung, J., Midgley, P.M.: Fifth assessment report of the intergovernmental panel on climate change. In: The Physical Science Basis (2013)
2. Roshan, GhR, Ghanghermeh, A.A., Attia, S.: Determining new threshold temperatures for cooling and heating degree day index of different climatic zones of Iran. Renew. Energy **101**, 156–167 (2016)
3. Attia, S.: Regenerative and Positive Impact Architecture: Learning From Case Studies (2017)
4. Roshan, G.R., Farrokhzad, M., Attia, S.: Defining thermal comfort boundaries for heating and cooling demand estimation in Iran's urban settlements. Build Environ **121**, 168–189 (2017)
5. Kim, K.-Y., Kim, B.J., Yi, G.S.: Reuse of imputed data in microarray analysis increases imputation efficiency. BMC Bioinf. **5**, 160. https://doi.org/10.1186/1471-2105-5-160

Building Energy Consumption and Carbon Dioxide Emissions in a Small Region with a Warm and Semi-humid Climate Type (Iran)

Gholamreza Roshan, José A. Orosa, Ángel M. Costa, and Rebeca Bouzón

Abstract

In this study future climate change effects on energy demand and related carbon dioxide emissions of a dominant building brigade on the southern coast of Iran was obtained based on one station called Ahvaz. One of the main obtained results was the increase in temperature and relative humidity for the coming decades showing that due to the increasing average annual temperature during the 2060s, the number of discomfort warmer days will increase. Considering the studied area climatic type, a decrease in the heating energy demand is not so important when compared to the significantly increased demand for cooling energy, which will lead to further increase in carbon dioxide emissions. Therefore, it is recommended that energy risk management be considered, and bioclimatic solutions of building design be used to solve this expected issue.

Keywords

Climate change • Energy consumption
Carbon dioxide emissions • Building thermal simulation • Iran

1 Introduction

Around one-third of global greenhouse gas (GHG) emissions are produced by buildings. This value is expected to double by 2050 if no action is taken (UNEP, 2015). Half of the world's population lives in cities, a share that is likely to reach 70% in 2050. Buildings account for more than 40% of global energy use, and approximately 30% of energy-related GHG emissions [1]. According to the statistics published by Tavanir Organization in 2015, the construction sector accounted for 40% of the total energy consumption in Iran, of which 33% was spent on heating and cooling of inside the buildings [2]. In 2009, Iran's total greenhouse gas emissions from energy consumption peaked at 528.6 million tons of carbon. Findings from the World Environment Organization indicate that 90% of the source of carbon dioxide pollution in Iran is energy [1] and it is expected that carbon dioxide emissions will double if the same trend continues up to 2030. In spite of this, Iran is ranked as the 9th largest carbon dioxide producer in the world, which can be easily noticed when considering Iran's contribution to carbon dioxide emissions internationally.

2 Materials and Methods

In this study, one station on Iran's southern coast, called was investigated. According to Tahbaz and Jalilian [2], from an architectural point of view, Iran is divided into eight climatic classes. Ahvaz is located in the Southern beaches and islands climate zone, characterized by warm and semi-humid summers and relatively modest winters. Meteonorm, as a powerful software for producing climatic data, has a strong climatic database, which serves as a source for the input of radiation data and other climatic data in building simulation. Meteonorm has also been able to produce other meteorological data, such as precipitation, wind speed, relative humidity and radiation. It is also capable of producing future climate change data predictions based on the 4th IPCC Special Report on Emission Scenarios (SRES-AR4), considering three emission scenarios of A2, A1B and B1 with the approximate carbon dioxide equivalent concentrations of 1250, 850 and 600 ppm in 2100, respectively relying on a simple autoregressive model used to generate realistic monthly time series [3]. In this paper, version 7.2 of Meteonorm software was used to produce climatic data to simulate the energy requirements of indoor buildings. Due to

G. Roshan (✉)
Department of Geography, Golestan University, Gorgan, Iran
e-mail: r.rowshan@yahoo.com

G. Roshan · J. A. Orosa · Á.M. Costa · R. Bouzón
Energy and Propulsion Research Group, University of a Coruña, ETSNyM Paseo de Ronda 51, Riazor, 15011 A Coruña, Spain

Z. Zhang et al. (eds.), *Patterns and Mechanisms of Climate, Paleoclimate and Paleoenvironmental Changes from Low-Latitude Regions*, Advances in Science, Technology & Innovation, https://doi.org/10.1007/978-3-030-01599-2_42

the specific format of input data for building simulator software, these data are hourly and daily over the 24 h.

In order to model for building energy consumption and carbon dioxide emissions of Ahvaz's settlements, we presented these subjects using the current period (1961–1990) and future periods (2020, 2040 and 2060) data on the basis of the A2 scenario.

Building energy simulation can help to study the energy flows. In this study, the Design Builder software was used for energy analysis in residential buildings in Ahvaz in accordance with different construction details. According to Table 1, the construction details were applied for the modeled building.

3 Results

In this part of the study, the findings of the relative humidity pattern changes for the study period have been analyzed. Based on the average output of relative humidity of the environment, it was determined that for Ahvaz, the maximum monthly average relative humidity belongs to the 2060s and the minimum monthly average relative humidity belongs to the observation period. For the study station, the increase of annual relative humidity for the 2060s as compared to the current decade (1961–1990) was calculated to be 6.56%. Therefore, the annual average relative humidity in the 2060s will be 66%. At Ahvaz, considering the simulated

Table 1 Constructional details of case studies

Construction	Details		Thickness (m)	U-value (W/m^2 K)	R-value (m^2 K/W)
	Materials	Thickness (m)			
External wall	Brickwork, outer leaf	0.02	0.28	0.488	2.049
	Cement plaster	0.02			
	Brick-aerated	0.1			
	MW stone wool	0.5			
	Brick-aerated	0.1			
	Cement plaster	0.02			
	Gypsum plastering	0.02			
Internal Wall	Gypsum plastering	0.02	0.18	1.335	0.749
	Cement plaster	0.02			
	Brick-aerated	0.1			
	Cement plaster	0.02			
	Gypsum plastering	0.02			
Roof	Cast concrete	0.05	0.255	0.913	1.095
	MW stone wool	0.25			
	Cast concrete	0.15			
	Cement plaster	0.01			
	Gypsum plastering	0.02			
Floor	Ceiling tiles	0.01	0.181	0.356	2.812
	Cement plaster	0.01			
	Cast concrete	0.05			
	EPS expanded polystyrene	0.091			
	External rendering	0.02			
Window (with wooden frame)	Generic PYR B CLEAR	0.006	0.25	1.931	–
	Air	0.013			
	Generic PYR B CLEAR	0.006			
External door	Wooden flush panel hollow core door		0.042	2.5	0.4
Internal door	Solid hardwood door		0.042	2.557	0.391

temperature inside the building, it was observed that none of the study stations had cold conditions and that, based on the four study periods, it is observed that the condition of thermal discomfort has an upward trend. So, in the current period (1961–1990), there is the need for cooling energy for an average of 194 days a year, while for the 2060s it is expected to increase to 230 days. According to these results, it is observed that the number of indoor comfort days, relying only on the component temperature, is decreasing. The results for the Bushehr station show that, based on the thermal thresholds of the outdoor temperature component, the number of days with cold discomfort condition was 135 days per year for the base period, but due to global warming, this number is expected to decrease to 101 days per year for the 2060s. On the other hand, due to the upward trend in the number of days with thermal discomfort, it has increased from 192 days in the base period to 220 days in the 2060s. An interesting point is that, merely based on the temperature component it is remarked that the number of comfort days per year for the base period is only 39 days, and it is expected to increase slightly for the decades to come. Thus, the number of comfort days is expected to rise in the 2060s to reach 45 days. One of the most important parts of this study was to examine the effect of global warming on the amount of energy demand in the cooling and heating space sectors. At Ahvaz, a decreasing trend for the space heating energy was obtained. Regarding the outputs for the current period (1961–1990), it is determined that the amount of heating energy was 4763.6 kWh/m^2 per year, followed by a decrease for the years of 2020, 2040, and 2060, with the values of 3581, 2799 and 2045 kWh/m^2 respectively. In other words, a comparison between the present period and the 2060s shows that the need for heating energy in the 2060s will decrease by 2718 kWh/m^2 (Fig. 2). On the contrary, the demand for space cooling energy will increase whereas the minimum need in the base period recorded the value of 8609 kWh/m^2 a year. This figure is expected to increase by 1233 kWh/m^2 by the 2060s to reach 9842 kWh/m^2 (Fig. 1).

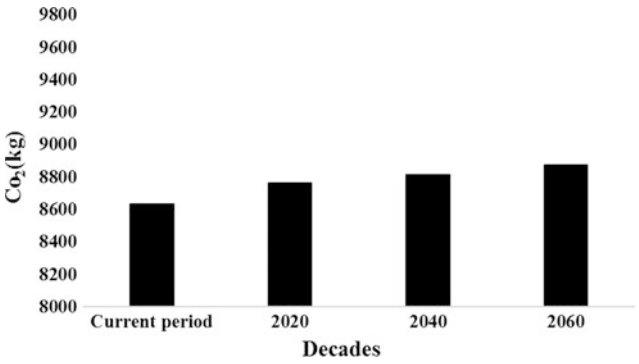

Fig. 2 Assessing the effect of anticipated climate change on carbon dioxide emissions of simulated construction type

It was clearly established that, in all the study periods, the amount of heating energy demand was decreasing and the demand for cooling energy was increasing. Our results show that the carbon dioxide emissions will increase for Ahvaz over the whole studied time span. However, it was 8825 kg in total per year in the base period (1961–1990), but having added another 798 kg per year by the 2060s it would reach 9623 kg.

4 Discussion and Conclusion

Relying on the effect of global warming on the bioclimatic thresholds, the results of this study show that the pattern of comfort and discomfort will change dramatically with its clear effects on the thermal comfort and energy consumption in buildings. In particular, a number of cold discomfort days is declining reducing the demand for heating energy but it increases the demand for cooling energy in the hot season with a related elevated carbon dioxide emission is expected to. What is more, the demand for heating energy is not particularly large throughout the year, and the decline of demand in the next decades will not have much impact on the energy consumption pattern of the settlements.

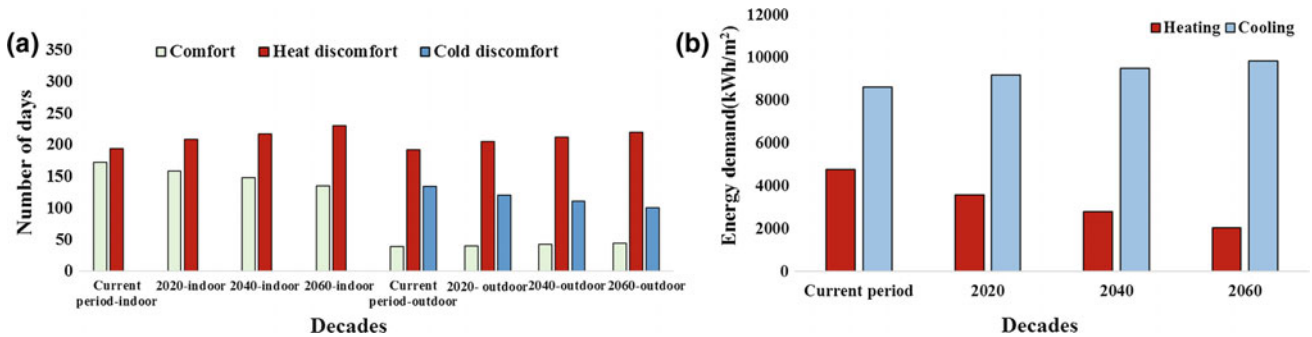

Fig. 1 Modeling the effect of global warming on thermal comfort (indoor and outdoor) (**a**) and on energy demand for space cooling and heating (**b**)

Eventually, with a stronger global warming, it is expected that this climate will follow a common pattern, but with a slight difference in detail.

References

1. UNDP (United Nations Development Program).: Department of Environment. Iran Second National Communication to United Nations Framework Convention on Climate Change (UNFCCC). National Climate Office, Department of Environment. Tehran (2010)
2. Tahbaz, M., Jalilian, S.: Architectural Design Principal Compatible with Climatic Conditions of Iran. Shahid Beheshti University Press, Tehran (2008)
3. Nik, V.M., Coccolo, S., Kämpf, J., Scartezzini, J.-L.: Investigating the importance of future climate typology on estimating the energy performance of buildings in the EPFL campus. Energy Procedia **122**, 1087–1092 (2017)

Climate-Driven Migration Assessment of Southwestern Coast of Bangladesh

Iftekharul Anam Saikat, Nabila Nawshin, and M. Tauhid Ur Rahman

Abstract

Water and soil salinity is one of the serious problems of the coastal region of Bangladesh. It affects production of crops, human heath, fisheries etc. Around 13% of the total urban population live in coastal zones and of these, more than 75% live in Asia. The objective of this study was to assess the coastal salinity over the years of Bagerhat and Satkhira, two south-western districts of Bangladesh. The soil and water salinity data of these areas was collected over 2000–2009 period. The Landsat TM image of these areas were analyzed by GIS. Key Informant Interviews (KII) and field sample collection was also accomplished. Here the data from 2000–2009 were analyzed and revealed that soil and water salinity increased over this period (2000–2009). A landsat image of 2016 (Fig. 1) was developed and showed that there was a decrease in vegetation and bare land.

Keywords

Water salinity • Soil salinity • KII (Key Informant Interviews) • Landsat TM image • Environmental migration

I. A. Saikat · N. Nawshin (✉) · M. Tauhid Ur Rahman
Military Institute of Science and Technology, Mirpur Cantonment, Dhaka, 1216, Bangladesh
e-mail: 201511095@student.mist.ac.bd

Z. Zhang et al. (eds.), *Patterns and Mechanisms of Climate, Paleoclimate and Paleoenvironmental Changes from Low-Latitude Regions*, Advances in Science, Technology & Innovation, https://doi.org/10.1007/978-3-030-01599-2_43

1 Introduction

Bangladesh has one of the highest population densities in the world, with a population of 160 million living within 57,000 mile^2. Of those 160 million people, 4 million lack safe water. As Satkhira and Bagerhat are two coastal districts of Bangladesh, they are suffering the most due to water and soil salinity hazards [1, 2].

Sea water contains high salt content. Due to the tidal effect, the sea salt is drawn-in from the sea into the fresh water aquifers. So the contents are gradually increasing due to this repeated tidal behavior [1].

Salinity intrusion has various effects on human health and climate. Many people suffer directly due to the increasing salinity in the water. It also hampers the crops growth and reduces production. The cultivatable land is decreasing which results in human migration due to job preferences [3].

2 Materials and Methods

The Landsat TM of Shymnagar and Mongla Upazila showed the topographic change in 2016. These secondary data were analyzed to compare the salinity, temperature and

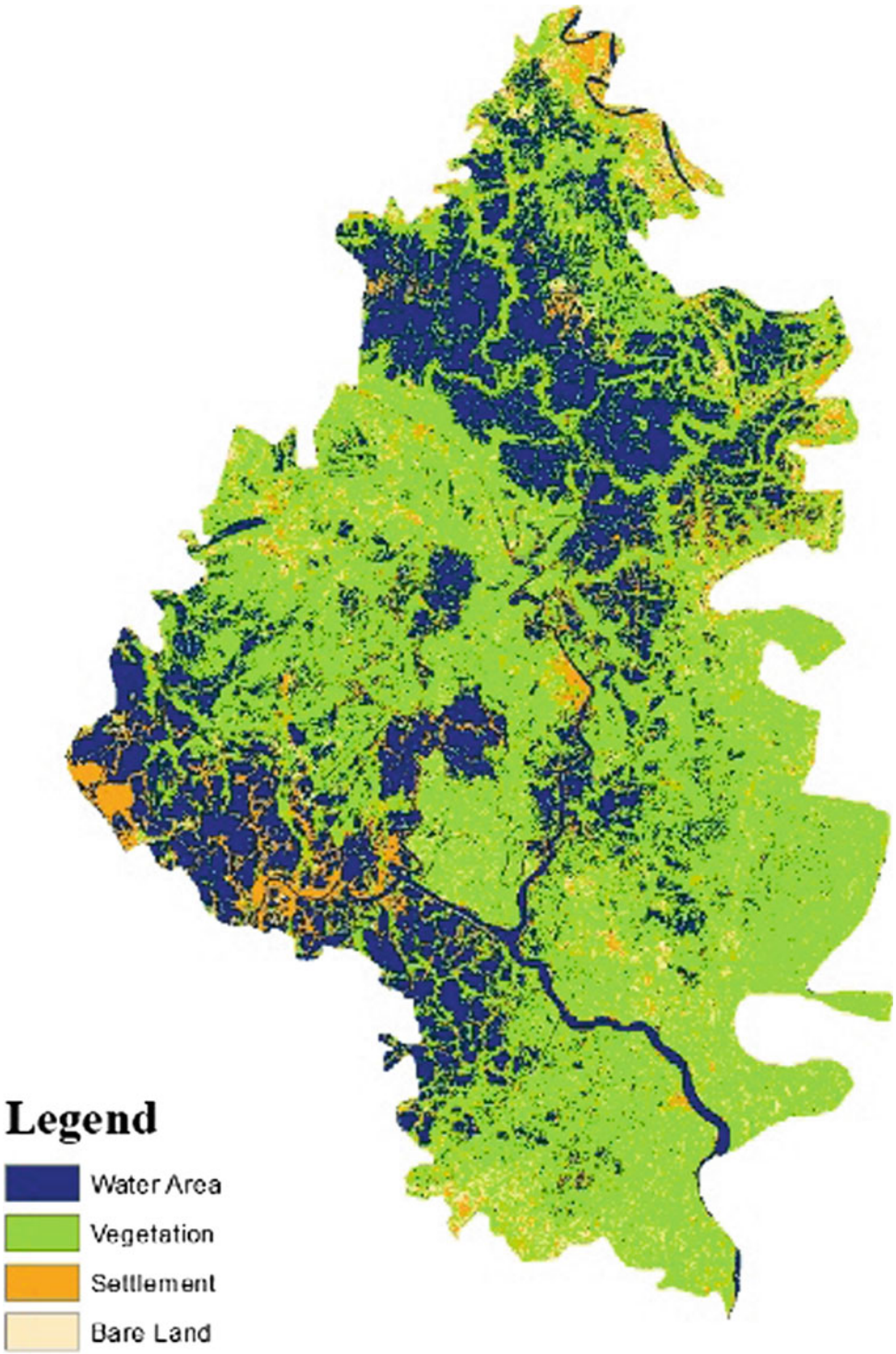

Fig. 1 Landsat image of Bagerhat (2016)

other climate effects from 1973 to 2017. The analysis was also achieved by collecting the soil and water salinity and testing the characteristics like pH, electrical conductivity (EC), total dissolved solids (TDS), chloride concentration (Cl^-) in the laboratory. Key Informant Interviews (KII) of chairman, teacher, religious teacher, and elderly people was taken on field.

3 Results

See Figs. 1 and 2.

From the analysis of the primary and secondary data, it is observed that soil salinity of the south-western coast has gradually increased from 1973 to 2009 (Figs. 3, 4 and 5).

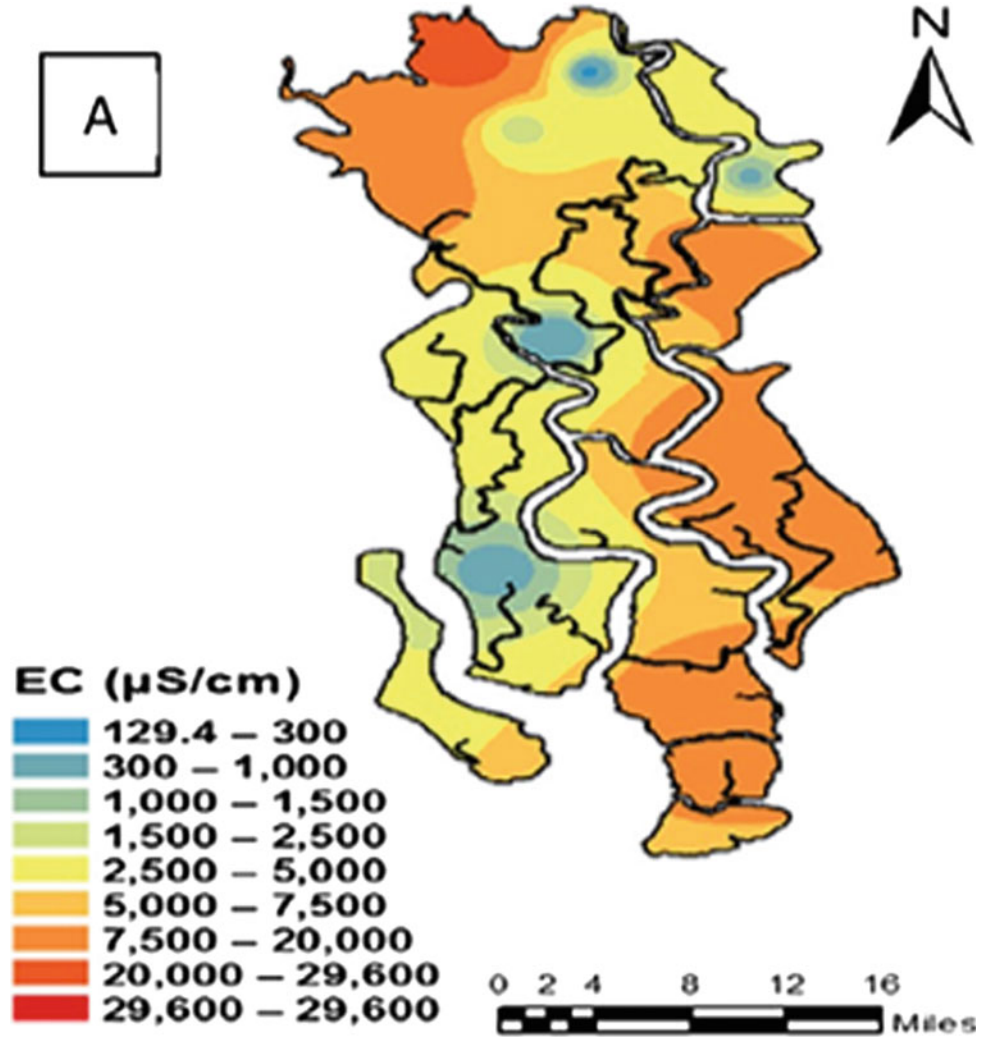

Fig. 2 Spatial distribution of water quality in Satkhira

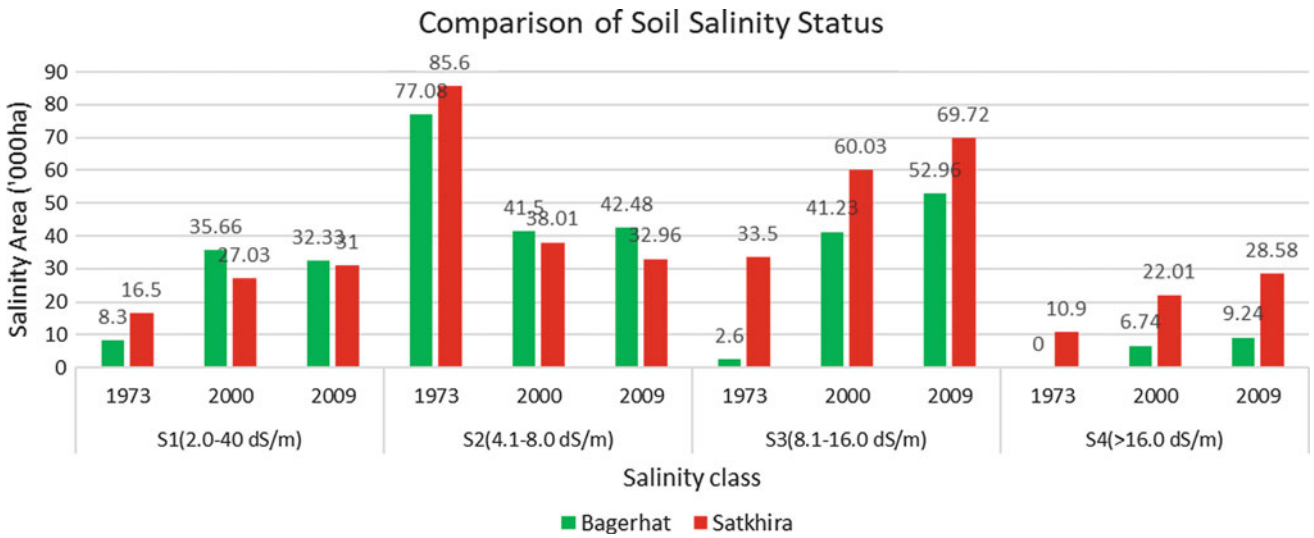

Fig. 3 Comparison of soil salinity over the 1973–2009 period in Bagerhat and Satkhira

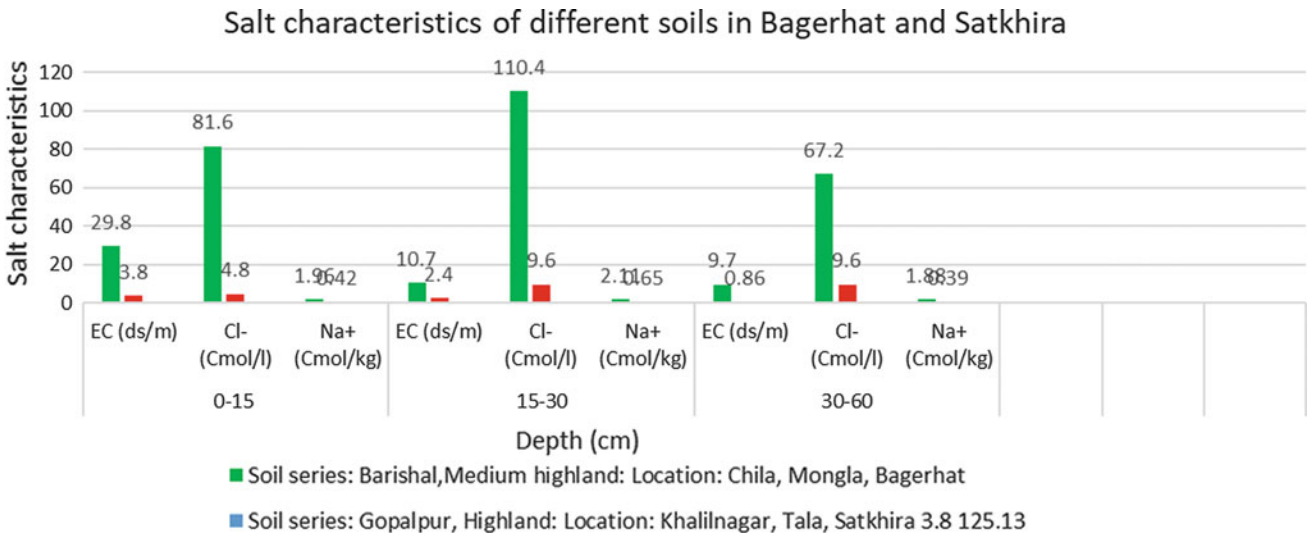

Fig. 4 Salt characteristics of soil in different depths in Bagerhat and Satkhira (2009)

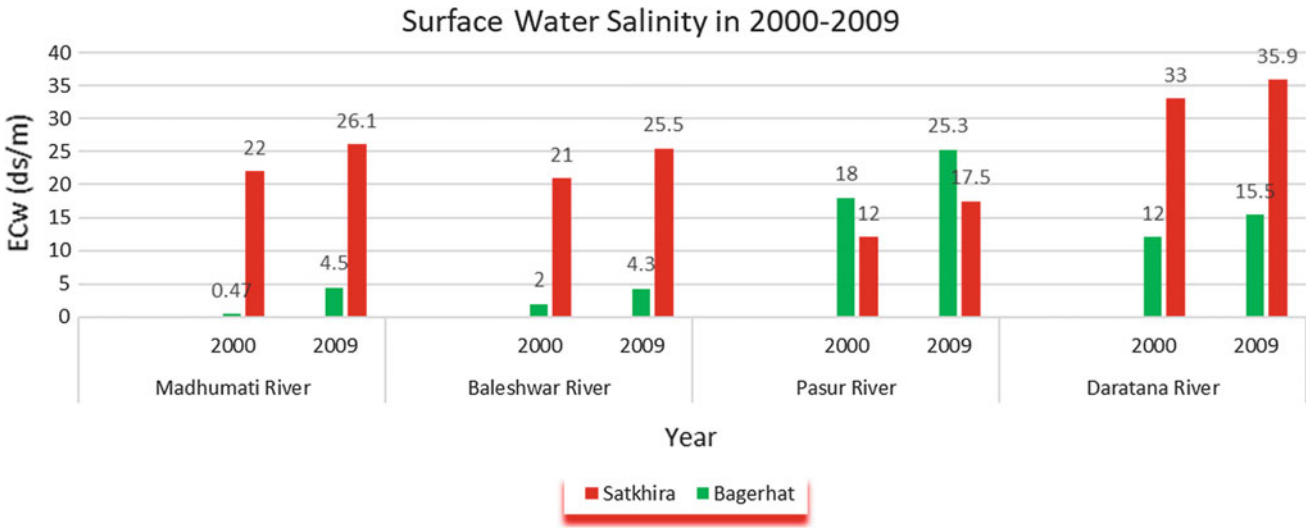

Fig. 5 Surface water salinity over 2000–2009 in Bagerhat and Satkhira

4 Discussion

The findings from the study revealed that salinity affects the lives of coastal people both directly and indirectly. Surprisingly all the data shown in the result from 2000 to 2009 shows that soil and water salinity has increased enormously. Due to lack of data sources we had to rely on past data till 2009. It can be interpreted from the graphs that soil salinity has increased over 2000–2009. Surface water salinity change has been showed with some river data. We developed an image of Bagerhat district in Arc GIS of the year 2016 (Fig. 1). It has hampered the crop growth and increased surface temperature thus changing the vegetation, more bare land Agriculture based profession is decreasing. Force migration has become noticeable due to water and food scarcity. The salinity condition of Satkhira district in 2016 is shown in Fig. 2. It helps us to make a relation between our analysis of 2009 and 1016.

The findings of this study matches with the study of other previous researchers on different districts [3]. So the best possible solution is to look for new hybrid crops

(salt tolerant), salt filtration with new techniques and spread mass awareness to coastal water use to avoid diseases. Research on this aspect should be continued in the future.

5 Conclusions

Bangladesh with her huge population is suffering the most in coastal areas. The crops, fisheries, human heath everything is at risk. The root cause lies in water and soil salinity. Overall, this study suggests that soil and water salinity significantly effects human migration. It also reveals that the living standard of these people is going down, their heath is at risk. So the only solution lies in Hybrid crops, salt water treatment, storage of fresh water and so on. If preventive measures are implemented most of the problems will be eradicated.

References

1. Ali, A.: Climate Change Vulnerability and Adaptation in Asia and the Pacific, vol. 92, pp. 171–179. Kluwer Academic Publishers, Manila, Philippines (1996)
2. Tareq, S., Rahman, M., Islam, A., Baddruzzaman, A., Ali, M.: Evaluation of climate-induced waterlogging hazards in the south-west coast of Bangladesh using geoinformatics. Environ. Monit. Assess. **190**, 230 (2018)
3. Rahman, M., Rasheduzzaman, et al.: Assessment of fresh water security in coastal Bangladesh: an insight from salinity, community perception and adaptation. Ocean Coast. Manag. **137**, 68–81 (2017)